A FREQUENCY DOMAIN APPROACH TO THE ANALYSIS AND OPTIMIZATION OF VALVE SPRING DYNAMICS

by

Andreas Schamel

A Doctoral Thesis

Submitted in partial fulfilment of the requirements
for the award of
the Degree of Doctor of Philosophy
in the Department of Transport Technology
Loughborough University

1993

Dedication

To

My Wife Verena
and my children
Debora, Jessica and Sidney

For their patience and encouragement throughout the work

Acknowledgments

I would like to take this opportunity to thank all colleagues who participated in the work presented in this thesis. Particularly thanks are due to R.C. Innes, P.Phlips, H. Körfgen, W. Herrmann, J. Tucker, R. Ernst, D. Utsch and J. Hammacher.

I also would like to thank the management of Forward Engine Engineering at Ford for the support of this project. Special thanks are due to J. Meyer, B. Wallbrück and G. Schwertfirm.

Last not least I wish to express my appreciation for the time and effort spent by Dr. T. J. Gordon. His guidance and hints, as well as interesting discussions on the subject, were essential for the successful and timely completion of this work.

Andreas Schamel

October 1993

Table of Contents

Table of Figures

1

Abstract

In this thesis a method is derived and presented, for the efficient analysis of the steady state response of dynamic systems with time variant properties. The method is especially attractive for the simulation of the steady state response of lightly damped systems with low numbers of degree of freedom which are forced by a periodic excitation. A major feature of the method is that the system non-linearities can be successfully modelled as time variant properties.

An ideal application for this approach is the calculation of the dynamic response of a modal model for progressive valve springs in the frequency domain. The solution method is explained and derived using this example. The differences, drawbacks, and advantages are assessed by comparison with both a linear modal model and a discrete time-domain model; correlation with actual measurement is also shown.

The extreme efficiency of the method allows its application in a more general study of the dynamic properties of valve springs. This analysis is initially discussed and examined using statistical methods. Then the frequency domain solution method is employed to perform an automatic optimization of the spring frequency characteristic for a 16 valve prototype engine application.

The spring design obtained from this study has been manufactured and the resulting hardware is discussed. The measured response of this hardware is compared with simulation results for the same configuration, verifying the findings from the statistical investigation and the optimization.

Finally open issues and further envisaged work in the area of damping mechanisms in valve springs and manufacturing issues are discussed and an approach for the next steps to take is outlined.

2

Introduction

This section will give an introduction into the subject of the work presented in this thesis. For this purpose a brief review of the available literature is given and the current state of the art in valve spring analysis is looked at. Based on this background the aims of this work and the motivation to carry it out are introduced and discussed.

4-stroke engines play a dominant role in todays automotive applications. One of the most critical issues during their design, whether they are gasoline or diesel operated, is the design of the valvetrain. Especially in passenger cars the demand is for higher and higher engine speeds. The main reason for this is to get higher specific power output from a given engine displacement. Recently, fuel economy has also provided motivation for small displacement, large speed range engines, since they offer a friction advantage at most of the operating points. In all cases the engine performance is directly affected by the valvetrain design and the valve timing. In principle, engine performance, durability, and noise create conflicting design demands for the valvetrain. For engine performance, a high volumetric flow is required, and as a consequence rapid valve opening and closing, is demanded. In terms of durability and NVH one would seek minimal forces being applied in the operation of the valves. In practice a compromise has to be found between these conflicting demands.

In the past this compromise was commonly achieved by extensive engine development work. Currently, a number of factors lead to the demand for a more efficient solution.

- Competition among manufacturers requires shorter hardware development cycles.
- Fuel economy and emission regulations form legal requirements, which are at the border of todays technology.
- Consumer demands increase from year to year in terms of performance, fuel efficiency, and noise and vibration.

The requirement is clearly for more upfront engineering at a stage where no hardware is available. To cope with the situation, one must employ predictive computer tools to develop an early understanding and analysis of a proposed engine design. Such tools have a wide range of application in the engine design. For example engine performance is predicted using gas exchange simulation tools, which can be based on 1 to 3 dimensional flow calculations. Friction models are used to estimate the losses in the engine. Finite element analysis is applied to check the structural integrity of cylinder block, cylinder head

and individual components. Flow predictions are employed to optimize water and oil pump performance. The list is virtually endless and develops more and more as methods and computer hardware improve.

A range of computational support for engine design has traditionally been applied to the valvetrain configuration; cam lift profile design was carried out even in the early days of digital computers. An early and important approach to design cam profiles was published by Dietrich Kurz (1954), which basically defined a cam profile out of two trigonometrical functions, combined with a polynomial section for the opening and the closing flanks. Although this cam design approach has limited design flexibility, it represents the first published approach for a steady acceleration characteristic of the cam profile. Subsequent a lot of discussion on so called "jerk free" cam design was published (e.g. Mook 1986, Bensinger 1968), but today these arguments are really a mere theoretical discussion with very limited practical value.

Analytically derived cam/valve lift laws have been used to calculate and analyse a wide range of aspects in the valvetrain. Standard applications are the calculation of kinematic properties of the valvetrain, quasi static forces, Hertzian stresses, entraining oil film velocity and others (Mettig 1973). These analysis techniques were important in the past and some remain useful. But as the requirements for the valvetrain have increased, failures arose which could not easily be explained. It became apparent that dynamic effects have a major influence, giving loads and stresses in the valvetrain drastically above the levels predicted from kinematic or quasi static analysis.

This has led to the world-wide development of a range of analytical and numerical tools for the analysis and simulation of valvetrains. Most of this work employs lumped mass models of varying degree of detail. Some authors have concentrated on the influence of single components in the valvetrain like the hydraulic lash adjuster element or the camshaft (Koster 1975, Netherlands; Yoshikatsu *et al* 1983, Japan; Kreuter *et al* 1987, Germany; Yusaka *et al* 1991, Japan; Mews *et al* 1992, Germany; Porot *et al* 1993, France). Others have taken a less dedicated approach to fine detail but analyse more the full valvetrain as an interacting system (Nagaya 1989, Japan; Akiba *et al* 1988, Japan; Bakaj 1988, Germany; Phlips *et al* 1889, Germany; Phlips *et al* 1991, Germany). Again other studies concentrate more on the application of the models towards valvetrain simulation and optimization rather than on the analysis of the models themselves (Lianchun *et al* 1991, China; Jeon *et al* 1988, USA; Assanis *et al* 1990, USA; Seidlitz 1990, USA)

As far as the valve spring is concerned, the range of modelling is wide. Among the models are:

- Static spring representation (e.g. Chan and Pisano 1986)
- Discrete models, with three or more degrees of freedom for the spring
- Discrete models with 1 degree of freedom per coil where some of them take coil interference into account and others do not (e.g. Priebsch *et al* 1992, Bakaj 1988)
- Discrete 3 dimensional models with up to a 100 masses to represent the spring (e.g. Lin and Pisano 1989)
- Finite element three dimensional models (Dojong *et al* 1990)
- Modal models based on the wave equation for simple linear springs (e.g. Priebsch 1992, Phlips *et al* 1989)

In a very early paper (Hussmann 1937) the spring is described by the wave equation with a velocity proportional damping term. The problem of how to model damping mechanisms is discussed there, and unfortunately not much advancement has taken place since. The solution technique used by Hussmann is very similar to the modal model presented by Phlips *et al* (1989), which will be discussed in more detail later on. However one has to keep in mind that in 1937 the problem had to be solved analytically and by hand calculations. Thus Hussmann solves each isolated harmonic of the cam profile and plots the frequency response curve over engine speed. The total solution is then obtained by graphical superposition of the single responses. The most interesting part of this work is that it is not restricted to the calculation of the response; Hussmann extends his methods towards the design of cam profiles to avoid spring vibrations. For this purpose he gives examples of cam accelerations which have no contribution in some of the critical Fourier coefficients in a given speed range. The limiting factor of this approach is that it can only deal with linear springs. Furthermore the cam design proposals are not adequate for modern high performance engines. However his direct approach to the optimization of cam profiles for reduced spring vibrations goes beyond even recent spring design guides (Associated Spring 1987, Scherdel 1987); here the simple proposal is made, to keep the cam harmonics above the 9th to 12th very small, that is to design a spring with a natural frequency above the 9th to 12th harmonic at maximum engine speed.

While Hussmann concentrates more on the changes to the cam profile, some authors have tackled the spring design more directly. For example Hoschtalek (1955) makes design proposals for the spring according to the guide line that the spring should have a natural frequency above or equal to the 11th harmonic of the profile at maximum operating speed of the engine. Again there is the shortfall that only linear springs are considered, and for modern engines it is also nearly impossible to design springs which obey this requirement. In addition the 11th harmonic does not give a very meaningful limit since a modern aggressive cam event can have quite substantial amplitudes above the 11th harmonic.

A large amount of work has also been published on the dynamics of the rest of the valvetrain, handling the valve spring only as a sub model with more or less limited attention. An extensive review of this literature is given by Chen (1973).

A sequence of more recent papers on the isolated static and dynamic analysis of valve springs has been published by Lin and Pisano (1987,1988,1989). They derive a very general description for the differential geometry of helical springs and for the solution of their dynamic response. The drawback is that the derived equations require very detailed information on the spring which in practice is difficult to obtain. But if an extremely accurate representation of a fully variable spring design with largely varying pitch and diameter of the spring is required, the equations derived by Lin and Pisano represent a valuable description.

At first sight the large range of different spring models is surprising. To understand this, the function of the spring must be considered, and also how spring models are related to valvetrain models.

The fundamental purpose of the valve spring is to provide the required forces to keep the valvetrain parts in contact during the valve operation. Apart from specialised cases (desmodromic actuation) valvetrain components can only transmit compression forces. As a consequence a spring has to provide the required forces for the valvetrain deceleration. The forces required for this function depend on many factors. The operating speed range of the engine together with the oscillating masses of the valvetrain and the employed cam profile determines the theoretically required force. In addition valvetrain and spring vibrations increase the theoretical force requirement. Tolerances in the spring manufacturing and assembly of the valvetrain further increase the required level of static spring force.

A second function of the valve spring is to provide the forces required to keep the valve closed when the cam event is over. The level of the force needed for this purpose again depends on various factors; one is the force resulting from the pressure difference across the valve. This can be quite small for naturally aspirated engines, but may be very large for turbo charged engines or truck engines where the exhaust pressure is used as a wear free vehicle brake. Further aspects for the spring preload force are loads resulting from the force created by hydraulic lash adjuster elements and camshaft base circle run out; here again an important factor is also the amount of vibration in the spring, which reduces the theoretical static preload.

In the analysis later on, for the purpose of optimization, it will be necessary to find mathematical objective measures to quantify the springs ability to provide the required forces to serve these functions.

Unfortunately the force level of the spring does not only desired properties and functions of the spring. The spring force also critically determines the friction level of the engine. In addition it also determines the durability of the engine at low engine speeds. Since at low speeds the spring force is not counteracted by inertia forces, the cam tip is subjected to large Hertzian stresses at idle speed. As a result of this, the optimal spring design is not simply to increase the spring load until it meets all force requirements. The final spring design has to be a compromise, which takes friction and durability also into account.

To establish this compromise several routes can be taken. The particular route chosen determines the type of analytical model required. If one starts at the most simple case of a low steady speed engine, it appears sufficient to analyse the valvetrain by means of a quasi static model, where the spring is treated as a static spring. For passenger car engines this is not sufficient. It is well known that in high revving engines dynamic effects significantly alter the results from a quasi static analysis (Phlips *et al* 1989, Chan *et al* 1986) and as a consequence dynamic models are required. But the level of modelling detail required depends on the aims of the study. If the aim is to get a coarse idea what the magnitude of the dynamic force magnification is compared to the quasi static analysis, a very simple valvetrain model with a small number of degrees of freedom for both the valvetrain and the spring is sufficient. It is this type of analysis that justifies the simple spring models found in literature.

As the demands for the accuracy of the prediction increase, the required detail of the models for the valvetrain and the valve spring increases too. For such detailed models there are again many possibilities available. In a conventional two valve engine, with limited

spring installation envelope, there is little point in putting too much effort into the modelling of a purely linear spring, since there would be no possibility of making significant changes to the spring design. For cases like this, a simple linear modal analysis is therefore sufficient, and it is more sensible to focus effort on the modelling of the remaining valvetrain components, and in the optimization of the cam profile.

At the other end of the spectrum is the extreme case of a racing engine where the springs survival critically depends on the damping of the vibrations caused by driving the spring extremely close to solid height, essentially leaving no space for any vibrations at maximum valve lift. To analyse such a case it is necessary to have a spring model which takes the effect of coil closure into account. This results in a numerically demanding discrete spring model with high local frequencies.

As a further extension to the modelling of the isolated spring, it is possible to take into account secondary vibration effects like spring bending. Such analysis can give more precise results for the material stresses. For this type of detailed analysis, which may be required for life prediction of the spring, a full three dimensional model is clearly needed.

All such levels of modelling are considered in the literature mentioned above, and all can be seen as state of the art for their specific application. However it will be shown that for the purpose of this work they all lack specific properties.

The aim of this study is the optimization of valvetrains by analytical and numerical methods with the main emphasis on the valve spring dynamic response.

The natural choice with the availability of todays computer capacity to fulfil this aim is a formal parameter optimization approach, and indeed such methods have recently been used for the optimization of the response of a full valvetrain. This was carried out by optimizing the valvetrain excitation, the cam profile (Hussmann 1992, Ernst *et al* 1992). Optimal control approaches have also been used for the same purpose (Ernst *et al* 1993). However it turns out that although these methods allow one to improve the vibrations of the valvetrain fundamental mode, their potential to improve the valve spring response is very limited. This is basically since the valve spring base frequency is so low that it is excited by the low harmonics of the cam profile. Any reduction in these low harmonics tends to be in strong conflict with the main objective of a valvetrain, to provide an efficient gas exchange. This fact suggests that to improve the spring response, the spring design itself should be optimized.

In current practice this is attempted by traditional engineering methods. Typically for a new engine more than a dozen spring alternatives may be manufactured and tested before a satisfactory solution is obtained. However this process is time consuming, expensive and not always successful. Furthermore it is very unlikely that this method results in any truly optimal spring design. This is not only because the hardware being tested is unlikely to include the optimal design; more important is the fact, that in a pre-hardware stage the possible spring designs are heavily restricted by the available spring installation envelope. Clearly a formal optimization tool would help to improve on these early decisions.

For this formal optimization a suitable model of the spring is required. To make the choice for this model two aspects have to be considered.

It is likely that the model has to be solved many times, especially if the number of optimization parameters is large and the evaluation of the objective function requires more than one solution of the model at a time. In the present case it will be seen that both conditions apply. Clearly this suggests a very efficient model like the simple modal one mentioned above.

The second aspect is the ability of the model to reflect the real spring response accurately enough. For a linear valve spring this might be possible to some degree by the modal model mentioned, but for progressive springs this is not true. Modern valve springs rely on the detuning of the excitation and the system frequencies to limit the vibrations. This is achieved by a varying coil pitch spacing, causing a change of the active spring portion with lift and as a consequence a variation of the spring frequency. This effect can clearly be modelled by discrete approaches. However the required cpu times for discrete models are in strong conflict with the first aspect.

These considerations suggest that a new model is demanded that sufficiently balances both requirements.

For the formal optimization of the spring design a further aspect has to be looked at. It has been suggested that the excitation can not be sufficiently altered to improve substantially the spring vibrations in contrast to the possible improvement for the remaining valvetrain components. But this does not automatically imply that the vibrations of the rest of the valvetrain are unimportant for the spring response. At first sight the valvetrain clearly forms an elastic system as a whole, including the valve spring. An efficient valve spring model is then not very helpful, since the rest of the valvetrain requires detailed non-linear models, again leading to substantial total cpu effort. Fortunately it turns out that for stiff

modern valvetrains, the dominant lower frequency modes of spring vibration are sufficiently decoupled from the much higher frequency vibrations of the remaining valvetrain components to allow independent analysis. For linear systems this follows directly from standard linear vibration theory but for the present case with a progressive valve spring and a non-linear valvetrain model, this is not so obvious. Here the justification for this simplification will be made via the comparison with measured results in Section 7.

The assumption of largely decoupled vibrations immediately suggests that an isolated optimization of the valve spring is feasible. However, to perform this optimization the following objectives have to be addressed:

1) A suitable model has to be devised and experimentally validated; this must take efficiency and accuracy aspects into account.

2) Physical spring design parameters have to be transformed into a suitable idealised parameter space, and therefore to link the spring design to its dynamic response by a limited number of free parameters.

3) Suitable objective functions have to be devised to allow one to quantify the quality of the spring response and to formulate target functions for the optimization.

4) Numerical optimization procedures have to be established.

5) In view of the necessary assumptions and idealisations, the results from the optimization should ideally be validated in an experimental study.

In regard to objective 1, one important property of the valve spring has to be considered. In contrast to the other components of the valvetrain, the valve spring is able to vibrate throughout the base circle period of the camshaft rotation. As a consequence of this, the valve spring represents a steady state response problem, rather than an initial value problem. To solve such a problem, one may chose to integrate the valve spring model in the time domain starting with zero initial conditions and monitor the results from one cycle compared to the previous one, until a sufficiently small difference indicates that steady state response has been reached. For a heavily damped system, this approach would not be unreasonable since the influence of the initial conditions would rapidly decay. Unfortunately a valve spring is very lightly damped, in the order of 1.5 to 3% modal damping. Hence numerical integration would be required over a significant number of camshaft cycles before steady state response is achieved.

For a linear modal model with constant coefficients the solution can be obtained more efficiently in the frequency domain. Since the principle of superposition can be applied for such systems, the desired result can be gained by breaking the solution down to the response of each mode to each harmonic of the excitation separately and summing up the solution afterwards. For a progressive spring there is a natural generalization of this model, where the frequency of each mode is allowed to depend on the valve lift, leading to a non-linear modal description. The drawback is that for a truly non-linear system there is no efficient way to solve it in the frequency domain. The solution to this issue comes from the previously discussed assumption of the decoupled vibrations of valvetrain and valve spring. This decoupling may be used to transform the non-linear modal model into a linear modal model with periodically time variant coefficients. One major task of this thesis is to devise a frequency domain solution method for such systems based on a Fourier representation of the time variant properties. This method is not only essential to the main aim of the work, the spring optimization, it also allows one to estimate initial conditions for the time domain integration of a full valvetrain model and thus provides a means to substantially reduce the cpu costs for formal excitation optimization approaches.

In line with objective 2 it has to be considered how the change of the spring frequency is achieved in hardware. It has been mentioned already, that this can be done by a varying pitch spacing causing coils to close up during the spring compression. However there is no unique spring design that results in one frequency versus lift characteristic. In general the same frequency characteristic can be achieved by an infinite number of different designs. This one-to-many relationship suggests that the number of free parameters will be very large if physical spring parameters are used directly in design optimization parameter space. Furthermore such a design parameter space would need to be heavily constrained to allow for a realistic installation envelope. On the other hand the mathematical definition of the employed model shows, that the dynamic response of the spring is determined by its frequency characteristic. It is thus natural to parameterize the frequency versus displacement characteristic of the spring directly instead of the real spring design parameters. In this way one is able to avoid the problem of the one-to-many relationship and hence to substantially reduce the complexity of the optimization problem.

Having characterized the spring design by means of its frequency characteristic, this representation may be used to address objective 3. On the basis of the function parameters a large number of possible objective functions can be considered in a statistical experiment, which covers a wide range of possible spring characteristics. The experiment allows one to assess the usefulness of the different candidate objective functions. Furthermore, a formal analysis can be used to determine which parameters of the spring frequency characteristic are most important for the dynamic response.

In line with objective 4 the parameterized frequency characteristic may be used to formally optimize this characteristic. For this purpose a standard iterative parameter optimization algorithm is employed with some modifications to allow for the efficient treatment of constraints. The need to consider constraints is essential, partly due to real engineering constraints from material stress limits and manufacturing aspects, and partly because of the mathematical nature of the employed functions (parametric splines). Both types of constraints will be addresses before the actual optimization is carried out. The results from the optimization suggests the importance and usefulness of a novel progressive spring design in contrast to linear or more conventional progressive ones.

Finally, to validate the analytical work, objective 5 is addressed by defining a physical spring design with an optimized frequency characteristic. The general one-to-many relationship is for this purpose narrowed down by the conditions and the installation envelope of the available engine test specimen. The work has then been finalised by a brief engine test study carried out for both the base line spring of the test engine and the optimized one. These tests clearly validate the findings from the analytical work, and also reveal further open issues from both the modelling and manufacturing points of view.

The contents of the work outlined above has been structured in 15 sections. Section 3 establishes a basic understanding of valvetrain design and functionality. In Section 4 simulation tools are presented, and the scope of such models is discussed. In Section 5 two different spring models are outlined to emphasise important model features. At this stage the background to the study is completed, and the above objectives are addressed in sequence. Section 6 concentrates on developing frequency domain solution methods for valve spring models. Section 7 deals with the model correlation to establish its usefulness for optimization purposes. Section 8 provides a brief review of spring manufacturing and the important spring design parameters to establish the requirements for spring optimization and to motivate the chosen parameterization. Section 9 investigates the usefulness of potential objective functions and analyses important factors of the frequency characteristic function. The numerical optimization is carried out in Section 10, and the description of how a real spring design can be derived from an optimized spring characteristic is considered in Section 11. This spring design is then tested and the results compared with predictions in Section 12. Finally Section 13 gives a brief discussion of the achievements and conclusions of the work. References and additional background information is given in Sections 14 and 15 respectively.

3

Valvetrain Design Basics

The objective of this section is to summarize standard practice in valvetrain design together with implications for valvetrain performance. The function of the valvetrain is, to control gas exchange, and this has not changed since the first 4-stroke engines were developed. During the history of engine design a number of techniques to control the valve actuation have been tried, among them the so called desmodromic actuation which does not need any valve spring at all. But for modern high speed, large volume production engines, popped valves controlled by springs are being used exclusively. The remaining parts of the actuation differ widely depending on the engine design.

In the past the most frequently used valvetrain design for overhead valves was the pushrod type valvetrain as shown in Figure 1. For more modern engines, with overhead camshafts, there are three more widely used concepts. Rocker actuation, with and without roller (Figure 2), finger follower actuation (Figure 3) and direct acting bucket tappets (Figure 4). All these designs have their specific advantages and drawbacks.

The pushrod engine is a very cheap design, since it avoids an overhead camshaft. This is the main reason, why this design is still widely used for engines with moderate operating speeds. At higher speeds the flexibility of the many moving parts involved cause vibration problems. The desire for high low speed torque , high power engines leads to increasing demands for rapid valve opening in a very short time period. This is equivalent to high accelerations, what implies high inertial loading at high speeds. To cope with these increased requirements, it is natural to choose a valvetrain design which is stiffer and, as such, is less prone to vibration problems. This is achieved by overhead camshaft arrangements, although not all of the overhead camshaft designs are equal in terms of their high speed potential and in terms of their geometric properties.

The rocker design (Figure 2) permits a very compact cylinder head design because the camshaft location is relatively low compared to other overhead cam alternatives. On the other hand the cam aggressiveness is limited by the radius of curvature of the cam itself, because for a curved follower, the cam lobe becomes concave if the valve accelerations are too high, and this leads to manufacturing problems for large volume production. Furthermore while the rocker follower is stiff compared to a pushrod design it is still flexible to some degree. This is mainly because of the following reasons. The mechanics of the layout show that a given force needed to open the valve is multiplied by the rocker ratio when it acts on the cam, and roughly the sum of the valve side force and the cam force act on the rocker pivot. Then this magnified force acts on a rocker and rocker bearing which is commonly of very limited stiffness. These aspects together lead to quite poor

figures for the valvetrain stiffness and correspondingly to low natural frequencies. Typical figures for the fundamental natural frequency of a rocker follower valvetrain lei in the range of 800 to 1100 Hz compared to 600 to 900 Hz for a pushrod design.

The finger follower design represents a significant improvement in the direction of high performance valvetrains. It still has the same geometric constraints and the same drawback of force magnification. But the stiffness of the camshaft bearing is generally greater than for most rocker pivots. Furthermore if a hydraulic lash adjuster is used, it can be placed at the rocker arm pivot, which means that the adjuster does not contribute to the oscillating masses. This allows a large dimension, high stiffness element. A major disadvantage of the finger follower design is the large package envelope required, due to the high position of the camshaft. The frequency range achievable in practice is roughly 1000-1300 Hz.

In respect to packaging conditions, the bucket tappet design is intermediate between the other two overhead concepts. In terms of stiffness, the bucket tappet represents the ultimate of these designs. Typical frequencies are from 1200Hz for heavy hydraulic lash adjuster (HLA) valvetrains up to 2800 Hz for small light weight mechanical versions. From the geometric aspect, the flat faced follower allows an infinite acceleration, at least in theory; on the other hand the diameter of the tappet limits the opening velocity of the valve. The most important drawback of the bucket tappet design is that it is not practical to use a roller, which results in a serious friction disadvantage against the roller rocker and roller finger follower designs.

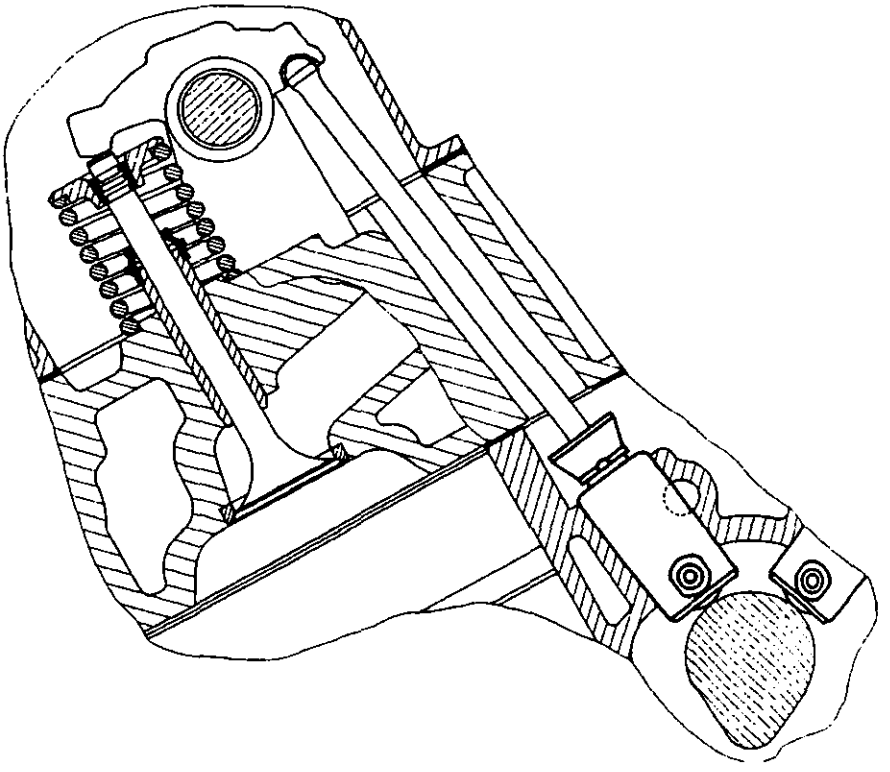

Figure 1: Sketch of a pushrod valvetrain

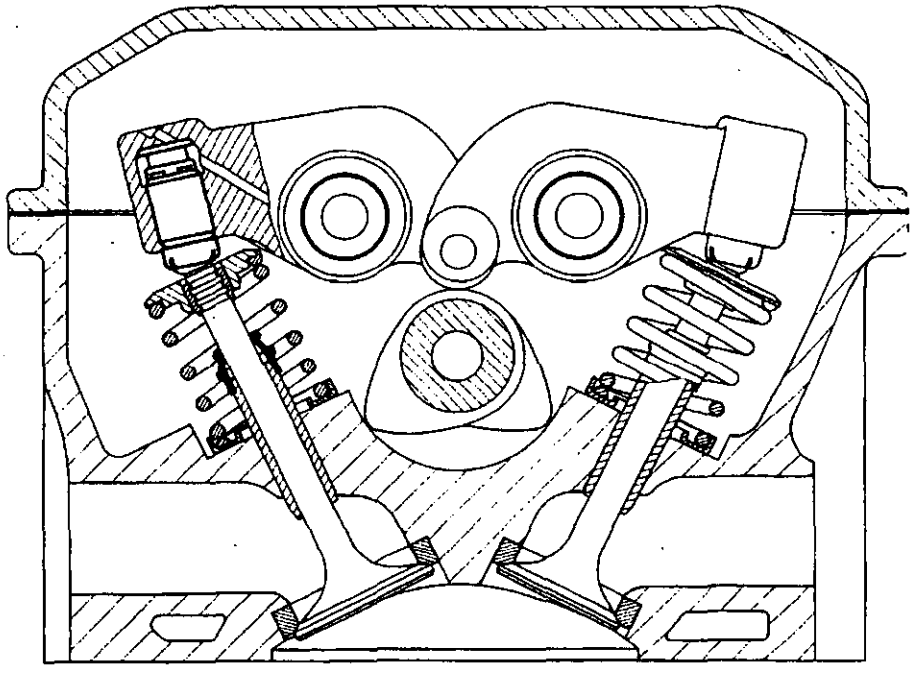

Figure 2: Sketch of a roller rocker valvetrain

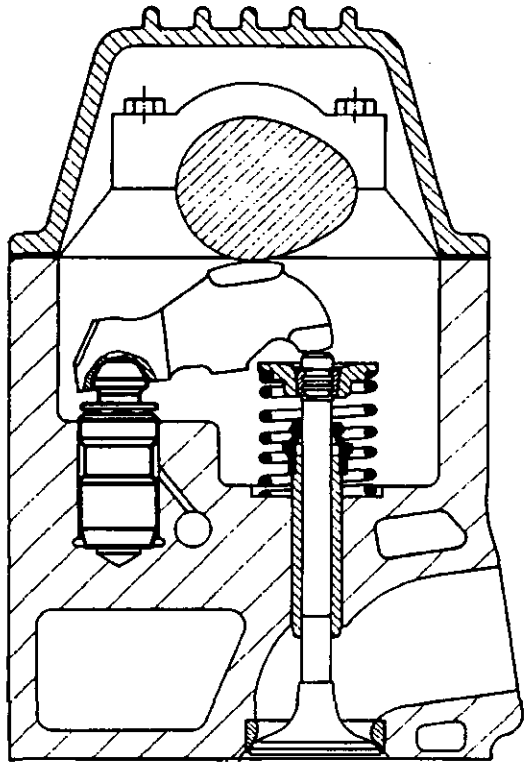

Figure 3: Sketch of a finger follower valvetrain

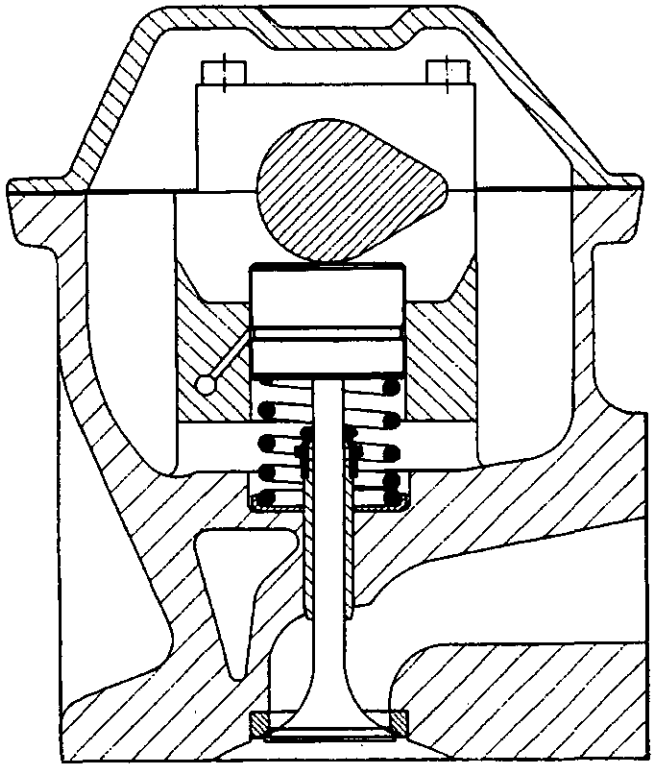

Figure 4: Sketch of a direct acting bucket tappet valvetrain

4

Simulation Tools

Having considered different valvetrain layouts, this section considers the scope and potential of simulation tools for valvetrain dynamics. As discussed in the last section, there are different standard ways to increase the natural frequency of a valvetrain design, leading to reduced vibration problems. But this is only true, if the valve lift characteristic and speed range stay constant, and the main reason to employ more expensive valvetrain designs is to permit higher engine speeds and to enable the use of more aggressive cam profiles to achieve a more efficient gas exchange. So whatever improvements are achieved by design changes, increased demands will always make up for it.

In the past, the development of a valvetrain and cam lobe design for efficient gas exchange control was a matter of laborious and time consuming test iterations. Often, durability was achieved at the expense of a painful compromise of engine torque and performance. To overcome this situation, simulation tools have been developed using models of the valvetrain which represent the flexibilities and the mass distribution of the real valvetrain. Two examples of such models for a bucket tappet and a finger follower valvetrain are shown in Figure 5. These sketches show that the valvetrain is represented by a number of masses, springs and dampers, many of them non-linear in nature.

The hydraulic element for example can be treated as a spring and a damper connected in series, where the spring stands for a non-linear representation of the aerated oil column in the high pressure chamber of the hydraulic element (Figure 6) and the damper reflects the leakage of oil (Phlips *et al* 1991).

Another important element is the structural stiffness of the bucket tappet in a direct acting valvetrain. Here a significant change in the apparent axial stiffness and correspondingly in the natural frequency of the valvetrain can be observed, depending on the position of the contact point between cam and tappet (Phlips *et al* 1989). This results from the solid transmission of the force in middle contact (Figure 7) while during edge contact the bucket structure acts like a bending plate.

Another non-linear element in the valvetrain is the valve spring itself. Even a so called linear spring (a valve spring with constant radius and constant pitch) shows non-linear behaviour if the characteristics are examined in detail. One important non-linearity is the interference of coils, whenever the amplitude of vibration is large. Furthermore no springs have truly constant pitch, since every valve spring has to have ground ends to seat on the cylinder head and the retainer.

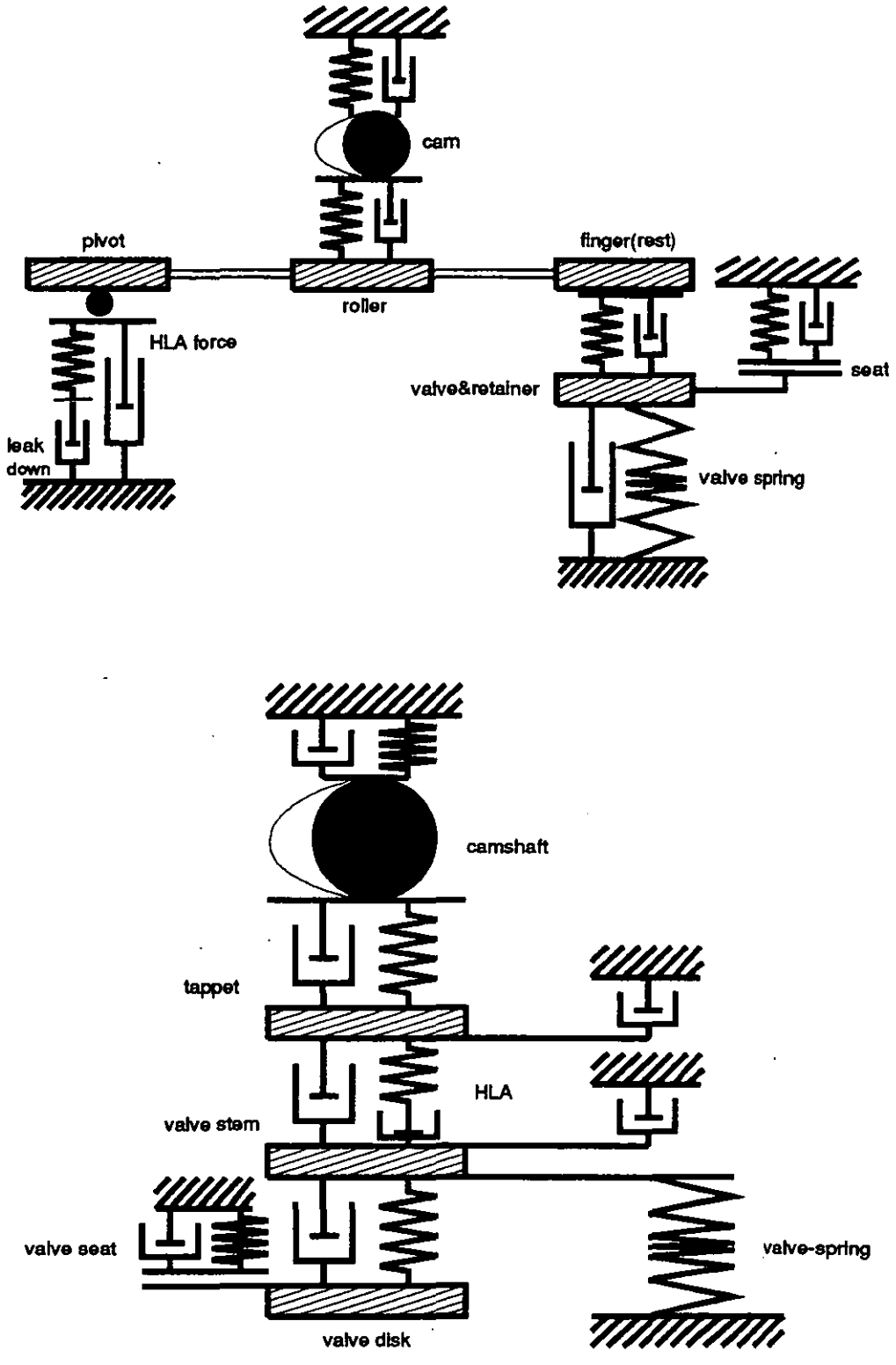

Figure 5: Lumped mass dynamic models for a) a roller finger follower valvetrain (top) and b) a direct acting hydraulic bucket tappet valvetrain (bottom)

A further non-linearity in a valvetrain is the valve seat, and this has very direct implications on the valve spring dynamics, in contrast to much of the rest of the valvetrain. The valvetrain forms an elastic system, able to undergo mechanical vibrations, but this is only true for the valve open position of the system. During the closed position, the boundary condition at the valve head changes from free to fixed. This causes the remainder valvetrain components to be decoupled, therefore any remaining vibrations rapidly decay before the start of the next event. Hence, for each new camshaft cycle the valvetrain starts from zero initial conditions, representing an initial value problem for the dynamic simulation.

For the valve spring, the situation is different. The valve spring is fixed between its seat in the cylinder head and the retainer at the valve end. When the valve has closed the excitation of the spring is over, but there is no sudden change in the boundary conditions. Any vibration left in the spring at this point in time continues as a free oscillation and is only damped by a small amount of material damping and oil film squeeze damping. This means that at high speeds, when only a small number of vibration cycles may take place during the base circle phase of the cam revolution, the remaining oscillations in the valve spring can be quite substantial. Treating the valve spring as an initial value problem with zero initial conditions can thus introduce a substantial error.

This fact is an important side aspect for the motivation to develop an efficient frequency domain method for the simulation of valve spring surge as a means of estimating the initial conditions for the time domain integration of a full valvetrain model. Later, when the valve spring is discussed in detail, this aspect will be investigated.

To show the potential and usefulness of simulation models we now consider as a specific example a full valvetrain model for a roller finger follower design. The valvetrain in question belongs to a 4.0L engine with 2 valves per cylinder and a single overhead camshaft. The maximum intermittent running speed of the engine is 6100 rpm. A specific problem of this engine is, that the installation envelope for the spring is so restricted, that only a limited amount of spring force can be obtained with current spring technology. This requires the valvetrain to run very close to the nominal valve spring deceleration capacity. Thus any significant vibrations of the valvetrain close to maximum speed will result in valvetrain failure. Hence, it is essential to use a cam profile which minimises valvetrain vibrations without detrimental effects on engine performance.

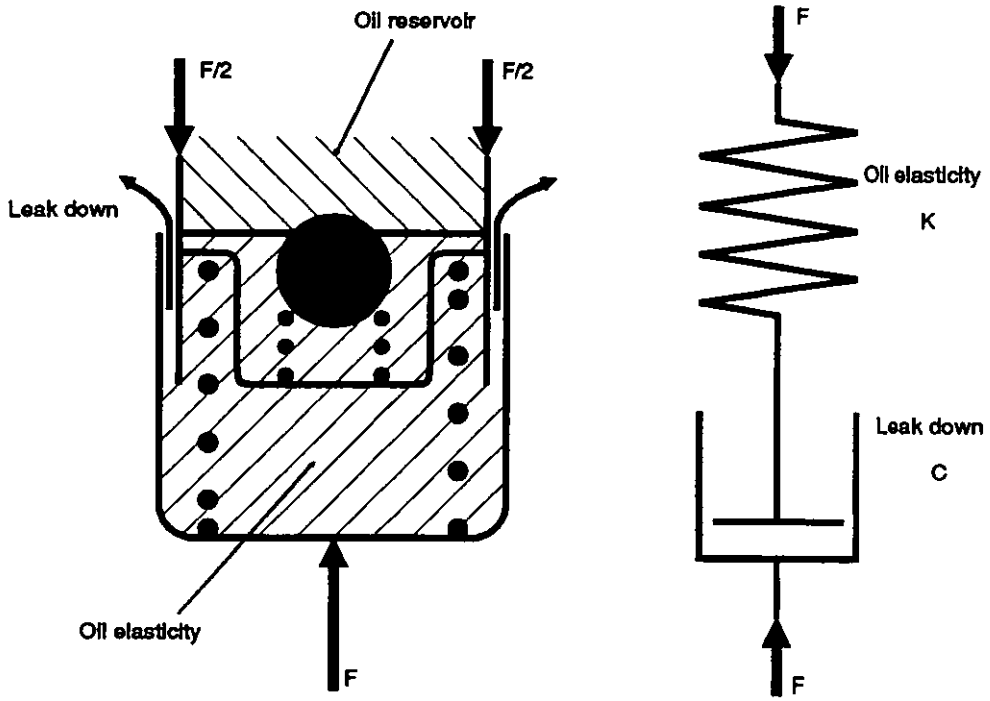

Figure 6: Sketch of a hydraulic lash adjuster element (left) and corresponding spring damper model (right)

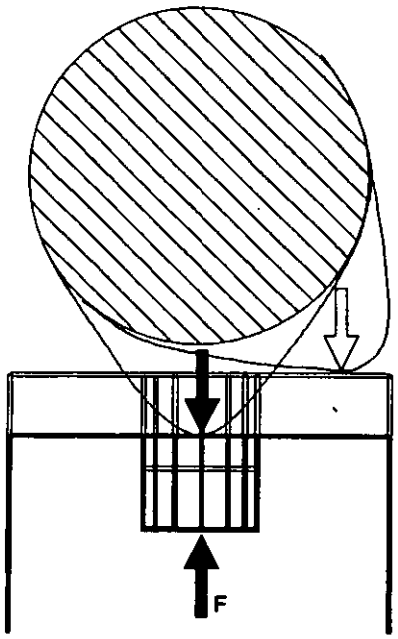

Figure 7: Sketch illustrating the different force paths through the bucket tappet structure with different contact point locations

Figures 8 show the comparison of the results of a simulation run (using an original profile designed by conventional considerations) with actual strain gauge readings taken at the finger close to the valve tip. First of all it can be noted that the correlation of the model is reasonable acceptable. One further sees that the valvetrain vibrations seem to be of higher frequency at 6100 rpm (Figure 8b) than at 5700 rpm (Figure 8a). At 6100 rpm the vibration frequency is approximately 1050 Hz, while at 5700 rpm the dominant frequency is about 700 Hz. The explanation is, that the 5700 rpm case is totally dominated by the spring vibrations. The spring model used for this simulation is a modal description of the spring surge derived from the wave equation - see Section 5.

While the results from the measured location do not seem to be critical, a look at the result of the model between roller and cam (Figure 9, together with the spring forces) shows that the system is very close to loss of contact, especially at 6100 rpm, and a very small variation in the tolerance conditions for the parts might cause this to happen. This is particularly problematic for a HLA finger follower valvetrain, since the HLA element stays under constant oil pressure supply and even a short period of contact loss will cause the HLA to pump up. This prevents the valve from closure and will subsequent cause an engine failure.

Figure 10 shows the same results as Figure 9 for a so called optimized cam profile, which is compared to the original one in Figure 11. As can be seen, the vibrations in the valvetrain fundamental mode are nearly gone and the comparison with the spring forces at both speeds clearly shows that only the spring vibrations are left. This was possible even though the event has been shortened, even though this requires a larger deceleration (using quasi static considerations an earlier loss of contact would be predicted).

How this can be achieved has been shown in principle by the author in his MSc thesis (Schamel 1991). In general it is a matter of providing the right shape and duration of the forcing acceleration of the cam profile, according to a given valvetrain frequency and a given speed. In the simplest case one can view the forcing acceleration peak as a combination of two ramp inputs. For a simple one degree of freedom linear oscillator it is well known, that if the ramp duration is exactly an integer multiple of the system period there will be no oscillation left after the ramp input. This is clearly also the case for two ramp inputs. Generally such a condition exists also for other input characteristics than a ramp input. However the ratio of input duration and system period where the response is optimal is not always an integer number.

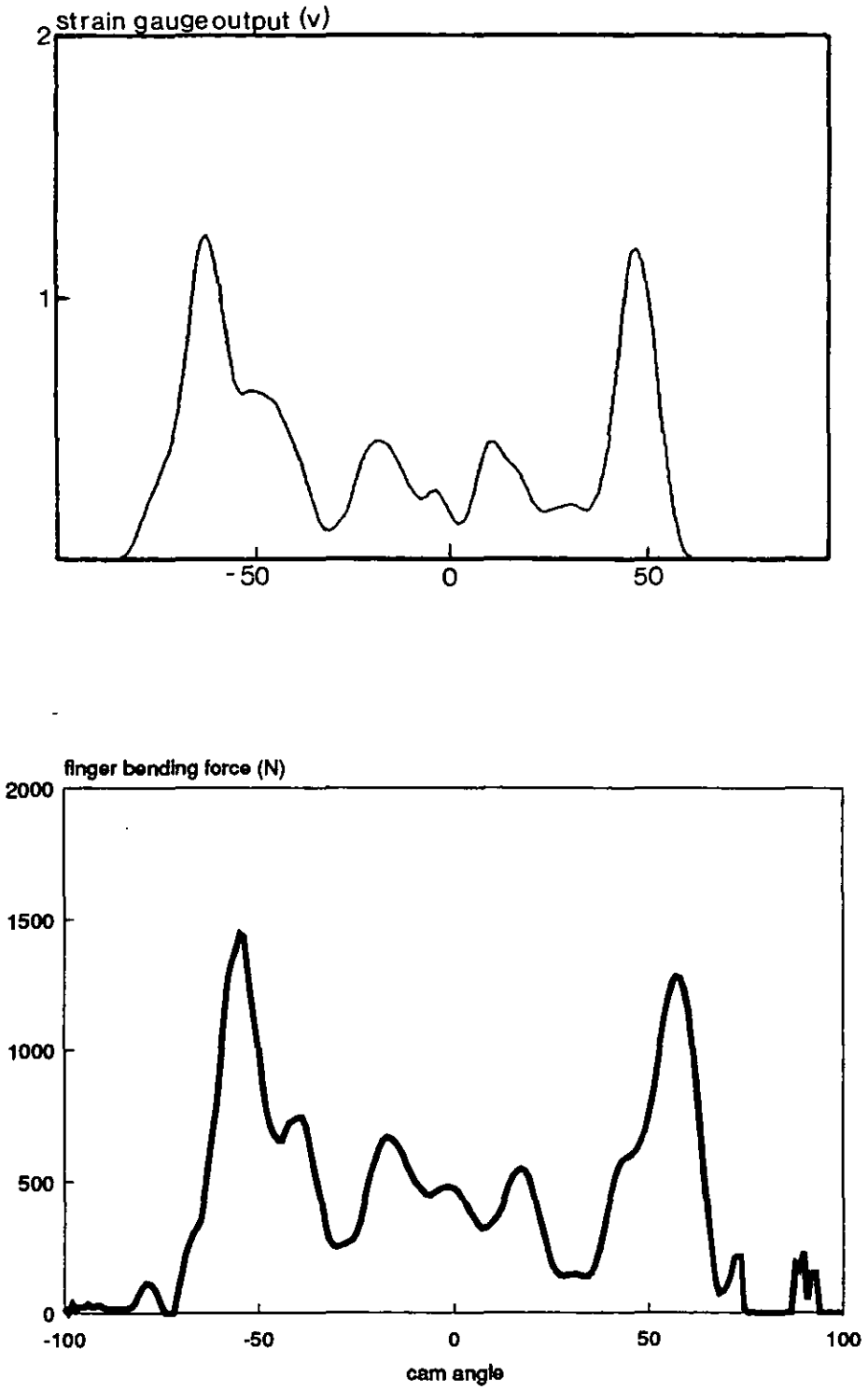

Figure 8a: Comparison of measured (top) and calculated (bottom) finger bending force for a roller finger follower valvetrain at 5700rpm engine speed

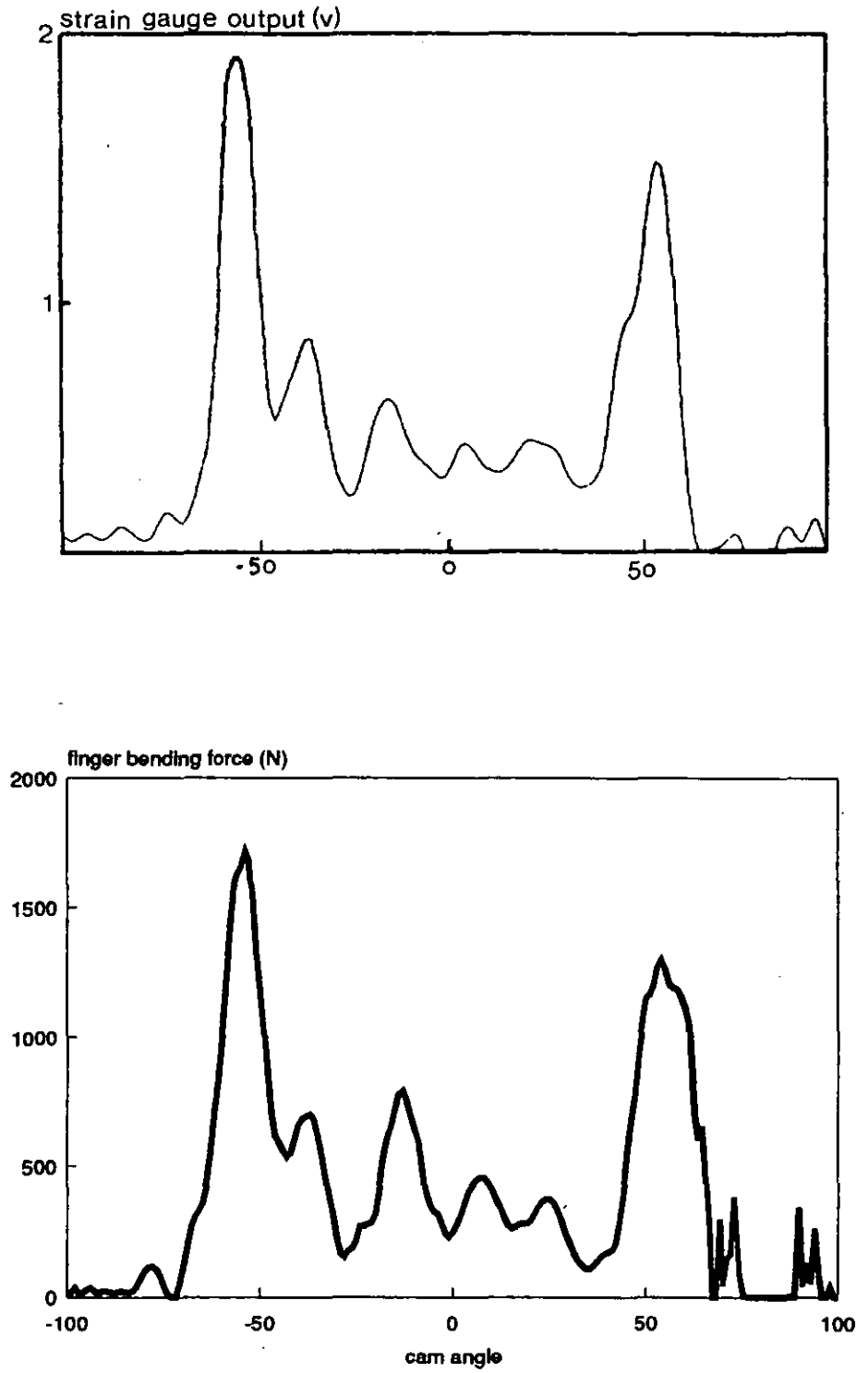

Figure 8b: Comparison of measured (top) and calculated (bottom) finger bending force for a roller finger follower valvetrain at 6100rpm engine speed

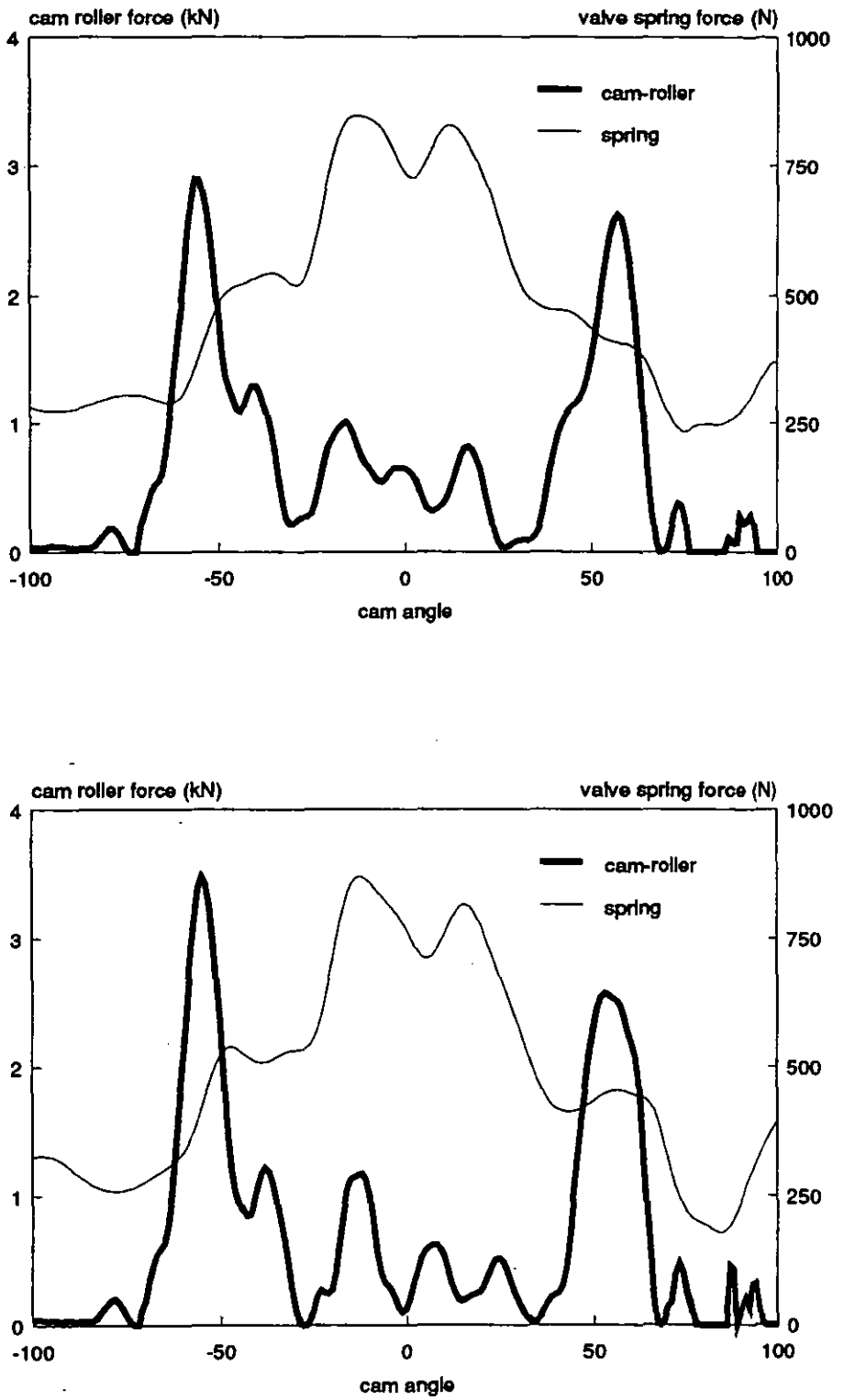

Figure 9: Calculated roller/camshaft and valve spring force corresponding to the finger bending force from Figures 8a+b using the original cam from Figure 11. Top: 5700 rpm engine speed, bottom: 6100 rpm engine speed

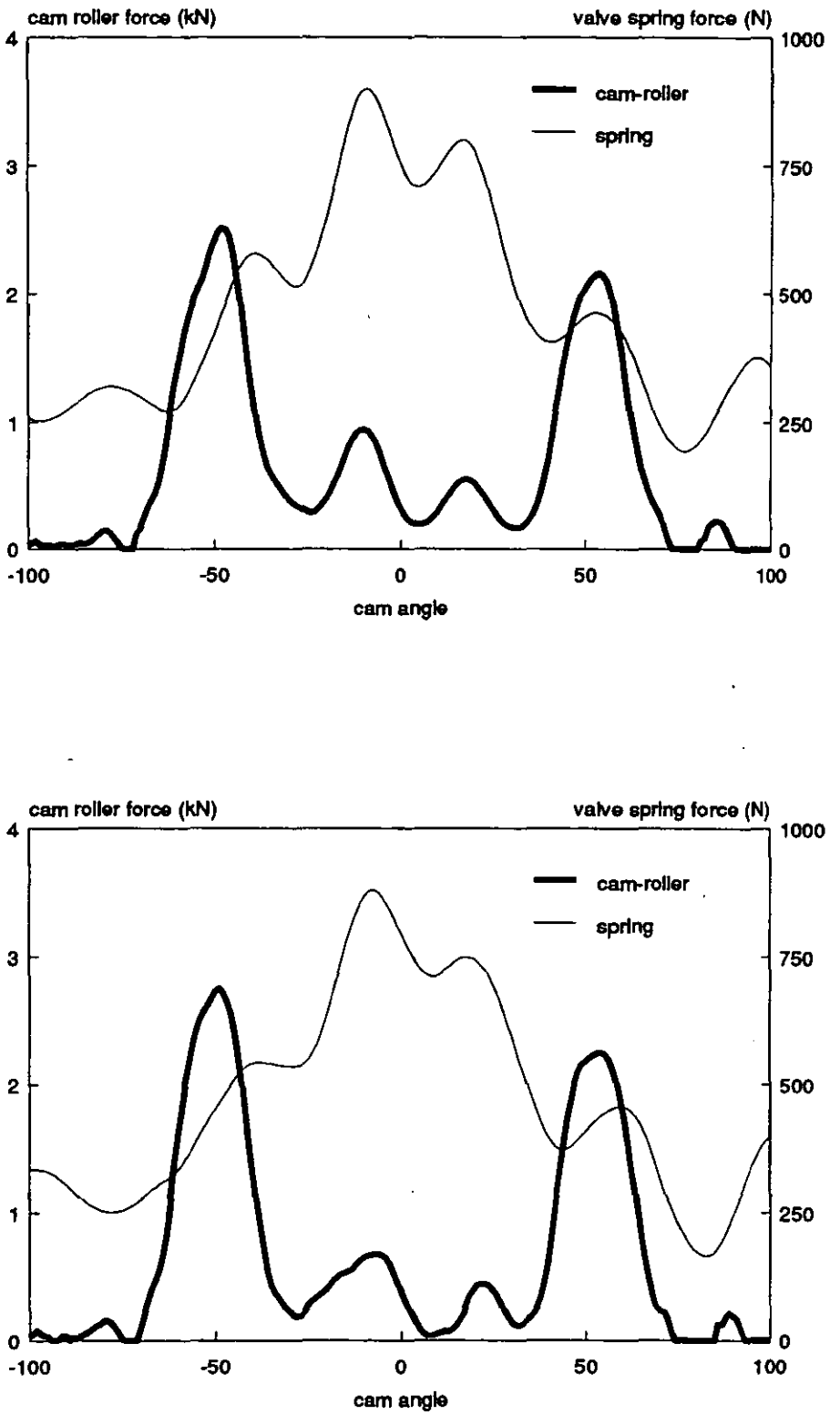

Figure 10: Calculated roller/camshaft and valve spring force using the optimized cam from Figure 11. Top: 5700 rpm engine speed, bottom: 6100 rpm engine speed

Beside the positive effects on the fundamental valvetrain mode, the comparison of the spring force for both calculations show that there is very little effect on this arising from the cam modification. It has been mentioned in the introduction that this is the case and the reasons will be shown more formally in Section 8, but this example illustrates the importance of valve spring design optimization.

Looking at the results from Figure 10 shows that an elimination of the spring vibrations would allow one to reduce the static spring force by more than 10% with a corresponding friction advantage. The spring vibrations lead also to significant dynamic stress magnification of the spring wire, which indicates a potential failure due to wire breakage. There have been desperate attempts in the past in such cases to control the vibrations of the valve spring by other means. Figure 12 shows an example of a friction damper applied to the spring to control the spring surge. However in many engines the installation envelope for the spring gives sufficient freedom to control the spring surge in a more reasonable way, via a dedicated spring optimization.

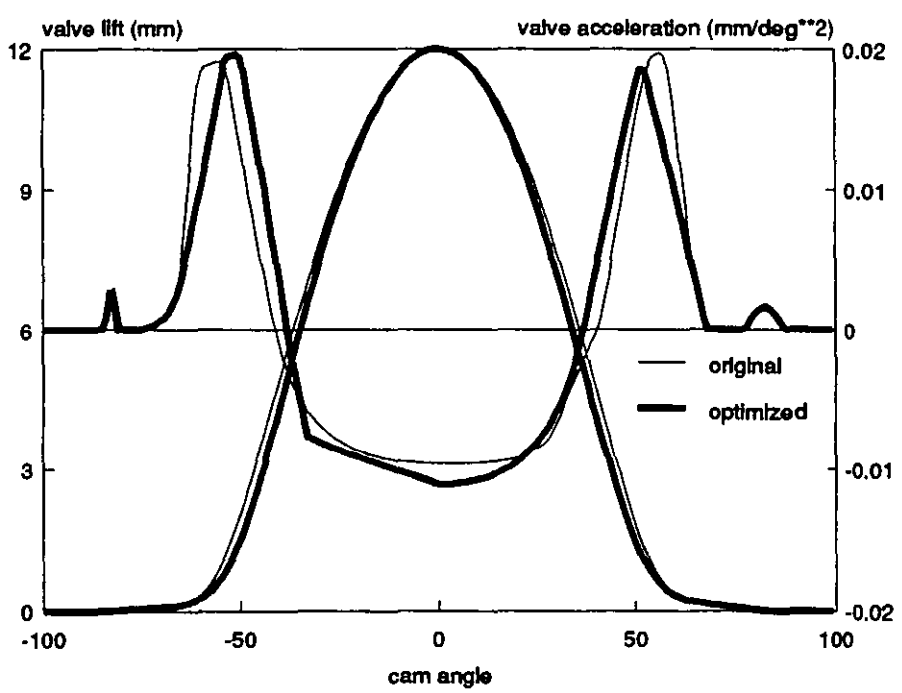

Figure 11: Comparison of lift and acceleration for the original cam profile used for Figures 8 and 9 (thin line) and the optimized profile used for Figure 10 (thick line)

Figure 12: Conventional linear valve spring fitted with a friction damper

5

Fundamentals of Valve Spring Dynamics

Simulation

The aim for this section is to review the fundamentals of valve spring dynamics. For this purpose, two different models are considered. In respect to the classes of models discussed in the introduction, the first one is of the very simple and efficient type, while the second one is more detailed and far more cpu expensive. In the context of these two models, the advantages and drawbacks of the two approaches will be discussed.

5.1 Linear Modal Valve Spring Model

The approach reviewed in this section was developed by Phlips *et al* (1989). Figure 13 depicts two examples of typical "linear" engine valve springs where this approach gives reasonable accuracy.

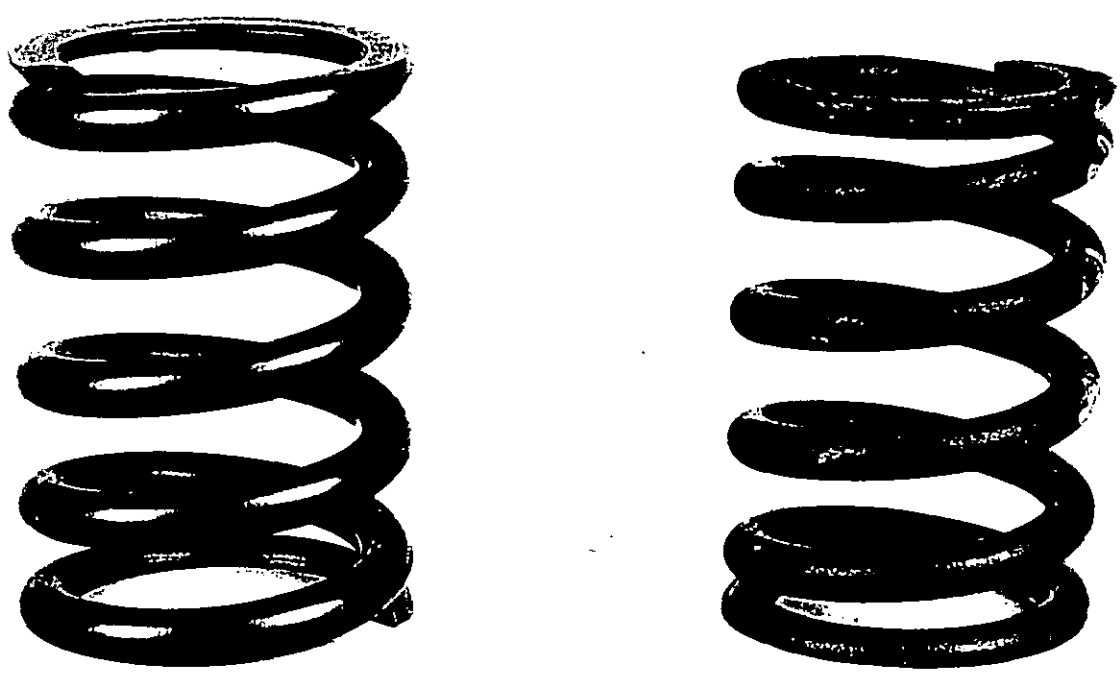

Figure 13: Two examples of conventional linear valve springs from 2 valve engines

The spring forms an elastic body which is able to vibrate internally if it is excited by the valve movement at the retainer end of the spring. To a good approximation, the spring shows wave propagation of disturbances. This leads to the approach that the valve spring vibrations are governed by the wave equation:

$$\frac{\partial^2\psi(x,t)}{\partial t^2} = c^2\frac{\partial^2\psi(x,t)}{\partial x^2} \qquad /5.1.1/$$

where ψ is the particle displacement and $c = \sqrt{L^2k/m}$ is the speed of wave propagation in the spring, L as the spring length, k as the spring stiffness and m as the active spring mass.

The eigenmodes of the spring are the characteristic forms of motion, forming an infinite series with increasing frequency. The first mode with the lowest frequency (in the range of 500Hz) is an in phase motion of all the spring particles with the maximum amplitude in the middle of the spring. Due to the mounting of the valve spring in the retainer and in the cylinder head the ends are fixed and the vibration amplitude is zero at both ends of the spring. The assumption of fixed ends is valid, since valve springs are assembled with sufficient high preload forces to stay attached to the retainer and cylinder head even under large surge amplitudes.
In the second mode, with twice the frequency, the two halves of the spring move in antiphase as shown in Figure 14. And so on for the higher modes.

With the two boundary conditions, that the spring displacement is equal to the valve displacement at the retainer end, and zero at the other end,

$$\psi(0,t) = h(t) \quad , \quad \psi(L,t) = 0 \qquad /5.1.2/$$

The total force exerted by the spring on the valve, including the preload due to the pre-compression in the installed position $F_0 = kS$, is then given by

$$F = F_0 + Lk\frac{\partial\psi}{\partial x} \qquad /5.1.3/$$

In the static case the particle displacement follows the relation

$$\psi(x) = \frac{(L-x)}{L}h \qquad /5.1.4/$$

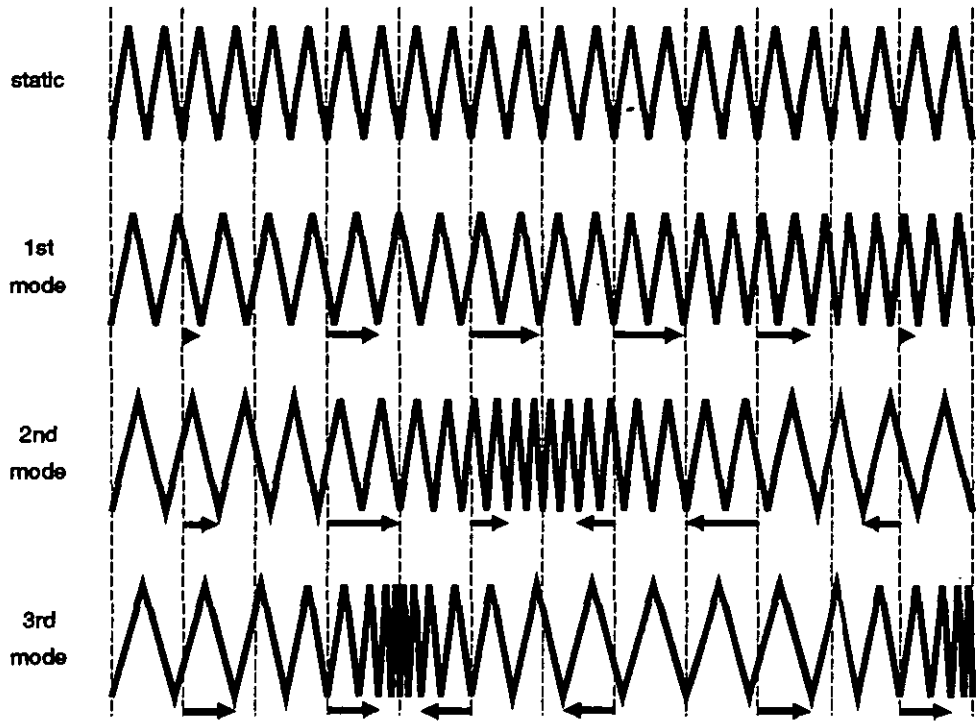

Figure 14: Sketch of the first three mode shapes in a valve spring

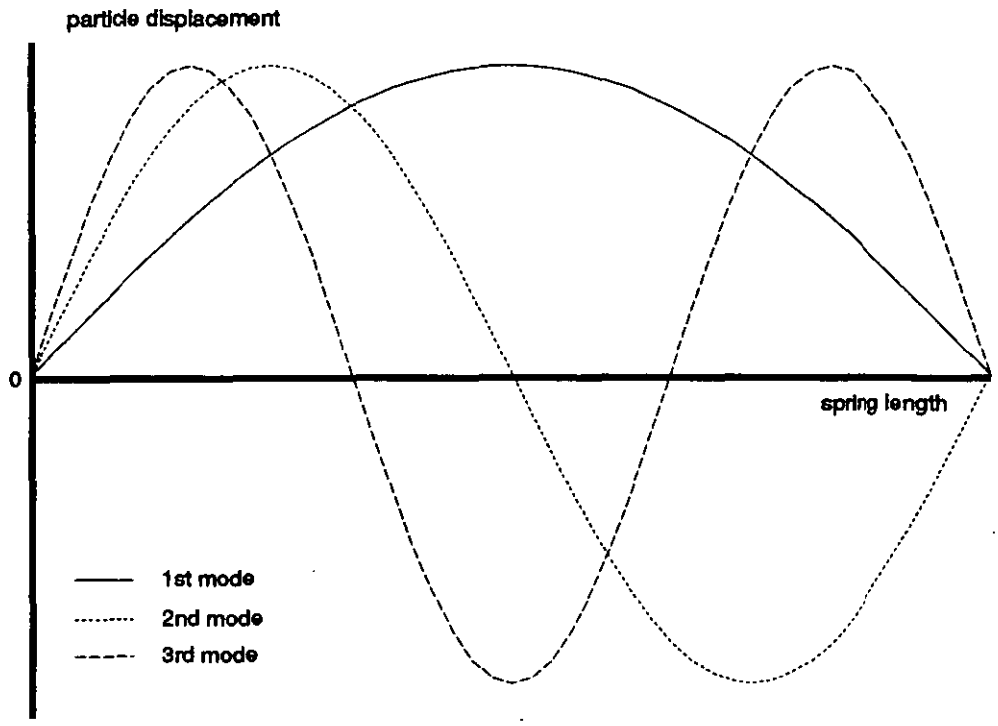

Figure 15: Particle displacement against spring length for the first three spring modes

For a time dependent excitation one can take the approach described by Phlips *et al* (1989) to write the total solution as the sum of the static contribution plus a dynamic deviation $\mu(x,t)$,

$$\psi(x,t) = \frac{(L-x)}{L}h + \mu(x,t) \qquad /5.1.5/$$

Combining equation 5.1.1 and 5.1.5 the equation governing the dynamic deviation from the static solution becomes

$$\frac{\partial^2\mu}{\partial t^2} = c^2\frac{\partial^2\mu}{\partial x^2} - \frac{L-x}{L}\frac{d^2h}{dt^2} \qquad /5.1.6/$$

with the changed boundary conditions $\mu(0,t) = \mu(L,t) = 0$.

Examining the free solutions for the dynamic component of the spring motion, one is looking for oscillatory solutions of the separable form

$$\mu(x,t) = M(x)e^{j\omega t} \qquad /5.1.7/$$

Substituting equation 5.1.7 in 5.1.6 and neglecting the forcing to get the free solution leads to

$$\frac{d^2M}{dx^2} + \frac{\omega^2}{c^2}M = 0 \quad with \quad M(0) = M(L) = 0 \qquad /5.1.8/$$

This ordinary differential equation has the solution

$$M(x) = \sin\left(\frac{n\pi x}{L}\right) \quad n = 1,2,3,\ldots \qquad /5.1.9/$$

where $\omega/c = n\pi/L$

Using $c^2 = L^2k/m$ the frequency in the n'th mode is given by

$$\omega_n = n\pi\sqrt{\frac{k}{m}} \quad n = 1,2,3,\ldots \qquad /5.1.10/$$

In the above derivation, the spring dynamic response problem has been reduced to a set of ordinary differential equations. A graphical representation of the approach used to solve these is depicted in Figures 14 and 15. In general, the solution can be expressed as the superposition of modes in the form,

$$\mu(x,t) = \sum_n G_n(t) \sin\left(\frac{n\pi x}{L}\right) \qquad /5.1.11/$$

In order to find the solution one must be able to express the spatial component of the excitation by the mode shapes leading to

$$\frac{(L-x)}{L} = \sum_n a_n \sin\left(\frac{n\pi x}{L}\right) \quad 0<x<L \qquad /5.1.12/$$

(see equ. 5.1.5)

Since the spatial component of the excitation is a segment out of a saw-tooth characteristic and the modeshapes form a sine series, the solution is simply the Fourier coefficients of a falling saw-tooth characteristic, namely

$$a_n = 2/n\pi \qquad /5.1.13/$$

Substituting equation 5.1.12 and 5.1.13 in 5.1.6 now gives

$$\frac{\partial^2\mu}{\partial t^2} = c^2\frac{\partial^2\mu}{\partial x^2} - \frac{2}{n\pi}\sin\left(\frac{n\pi x}{L}\right)\frac{d^2h}{dt^2} \qquad /5.1.14/$$

further substituting equation 5.1.11 into equation 5.1.14 transforms the partial differential equation from equation 5.1.6 into a series of ordinary differential equations

$$\frac{d^2G_n}{dt^2} + \frac{kn^2\pi^2}{m}G_n = -\frac{2}{n\pi}\frac{d^2h}{dt^2} \qquad /5.1.15/$$

Using equation 5.1.10, equation 5.1.15 becomes the standard form for a simple undamped harmonic oscillator with explicit time dependent forcing,

$$\frac{d^2G_n}{dt^2} + \omega_n^2 G_n = -\frac{2}{n\pi}\frac{d^2h}{dt^2} \qquad /5.1.16/$$

In the practical application for the valve spring, spring internal damping has to be taken into account. The magnitude of damping can only be determined by tests, and experience shows that there is an influence on damping by the surge amplitude and the spring nonlinearity (progressivity). Purely because of its mathematical simplicity and because the damping levels are low, a viscous damping model may be used. So equation 5.1.16 is generalised as follows

$$\frac{d^2G_n}{dt^2} + 2\zeta\omega_n\frac{dG_n}{dt} + \omega_n^2 G_n = -\frac{2}{n\pi}\frac{d^2h}{dt^2} \qquad /5.1.17/$$

In practice it proved useful to scale equation 5.1.17 to refer to cam angle rather than time. Hence by substitution of $dt = d\phi/\omega_{cs}$, one arrives at an equation governing the modal amplitudes of the spring displacement,

$$\frac{d^2G_n}{d\phi^2}\omega_{cs}^2 + 2\zeta\omega_n\omega_{cs}\frac{dG_n}{d\phi} + \omega_n^2 G_n = -\omega_{cs}^2\frac{2}{n\pi}\frac{d^2h}{d\phi^2} \qquad /5.1.18/$$

For the dynamic part of the force exerted on the valve, for each normal mode, one has

$$\begin{aligned} F_d &= kL\ G_n(t)\frac{n\pi}{L}\cos\left(\frac{n\pi x}{L}\right) \\ at\ \ x = 0 &\Rightarrow F_d = \pi k\, nG_n \end{aligned} \qquad /5.1.19/$$

Thus the total force on the valve is given by the following equation

$$F = -k(S + h(t)) + \pi k \sum_n nG_n(t) \qquad /5.1.20/$$

5.2 A Discrete Model for Valve Spring Dynamics

The model reviewed in this section has been developed by the author for his MSc thesis (Schamel 1991). It is a typical model for discrete approaches and is in the same range of complexity as the one presented by Priebsch *et al* (1992) but incorporates some enhancements for non cylindrical springs. It has a significantly larger degree of detail than the modal one from Section 5.1 and is based on the discretisation shown in Figure 16.

The model shown in Figure 16a is governed by the following set of equations

$$m_i\ddot{h}_i = +c_i(\dot{h}_{i-1}-\dot{h}_i)+c_{i+1}(\dot{h}_{i+1}-\dot{h}_i)+k_i(h_{i-1}-h_i)+k_{i+1}(h_{i+1}-h_i) \qquad /5.2.1/$$

Here $h_i(t)$ represents the deflection oh the i'th coil and where $h_0=h_v$ is the forcing valve lift. Let $h(t)=s(t)+d(t)$, where $s(t)$ is the kinematic lift and $d(t)$ is the dynamic deviation. Then

$$\begin{gathered} m_i\ddot{d}_i - c_i(\dot{d}_{i-1}-\dot{d}_i)-c_{i+1}(\dot{d}_{i+1}-\dot{d}_i)-k_i(d_{i-1}-d_i)-k_{i+1}(d_{i+1}-d_i) \\ = \\ -m_i\ddot{s}_i + c_i(\dot{s}_{i-1}-\dot{s}_i)+c_{i+1}(\dot{s}_{i+1}-\dot{s}_i)+k_i(s_{i-1}-s_i)+k_{i+1}(s_{i+1}-s_i) \end{gathered} \qquad /5.2.2/$$

Defining the total spring stiffness $k = 1/\sum(1/k_i)$, and using s_v for the kinematic valve lift,

$$s_i = s_v\left(1-\sum_{n=1}^{i}\frac{k}{k_n}\right) \qquad /5.2.3/$$

$$s_{i-1}-s_i = s_v\frac{k}{k_i} \qquad /5.2.4/$$

Assuming stiffness proportional damping ($c_i/k_i = const$) equation 5.5.2 simplifies to give

$$\begin{gathered} m_i\ddot{d}_i + c_i(\dot{d}_{i-1}-\dot{d}_i)+c_{i+1}(\dot{d}_{i+1}-\dot{d}_i)+k_i(d_{i-1}-d_i)+k_{i+1}(d_{i+1}-d_i) \\ = \\ -m_i\ddot{s}_v\left(1-\sum_{n=1}^{i}\frac{k}{k_n}\right) \end{gathered} \qquad /5.2.5/$$

Here $d_0=d_v$ is the deflection of the valve mass in the model.

This set of differential equations represents the discrete model in Figure 16a. In the limit as the number of masses approaches infinity, this model is nothing other than the discrete equivalent to the modal formulation. Clearly, as with the modal model, spring deflection can perform vibrations of unlimited amplitude. However in this case one can prevent this occuring by introducing additional force laws, which act if the total deformation between two neighbouring mass elements exceeds the available free space X_i between the two elements. This force, called clash force, results from two coils impacting together, namely

$$F_{cl_i} = f\left(d_{i-1}, d_i, \dot{d}_{i-1}, \dot{d}_i, s_v \frac{k}{k_i}\right) \quad if \quad d_{i-1} - d_i + s_v \frac{k}{k_i} > X_i$$

$$and \qquad /5.2.6/$$

$$F_{cl_i} = 0 \quad if \quad d_{i-1} - d_i + s_v \frac{k}{k_i} \le X_i$$

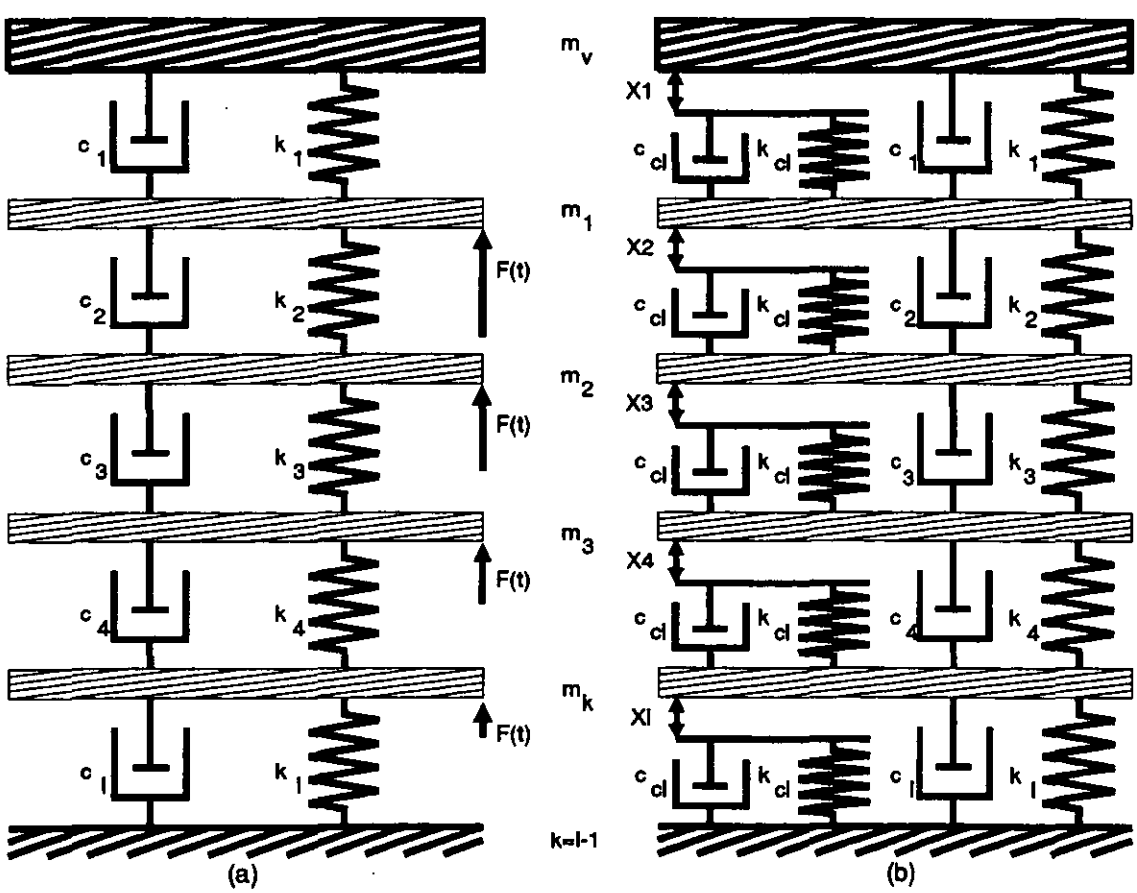

Figure 16: Sketch of discrete spring models (a) without force laws to prevent coil interference, (b) with additional impact conditions to simulate coil clash

While defining the force laws for this normal stiffness terms for the model in Figure 16a is straight forward, defining the law for this clash force in the model from Figure 16b is not. First consider the elastic component. Figure 17 shows the clash force characteristic if the stiffness is taken to be linear. Due to the two ranges of definition, the resulting characteristic has a sharp edge where the deformation reaches X_i. This means, that the first derivative of the force against time will be discontinuous. This has implications on most standard numerical algorithms for differential equations. The Gear algorithm used for the work presented here, is a predictor-corrector integrator which fits a polynomial through the last few time steps to estimate the solution at the next time step. This requires the derivative of the force to be continuous to ensure an efficient large time step. Otherwise the algorithm is forced to consider excessively small time steps, thus increasing the computer costs. Since with decreasing time steps the round off errors from the matrix manipulations become more and more important, the solver might even be unable to solve the problem at all, if the stiffness of the clash condition is very high.

The problem may be handled by making the force law non-linear, namely

$$F_{cle_i} = k_{cl_i}\left(d_{i-1} - d_i + s_v \frac{k}{k_i} - X \right)^y \qquad /5.2.7/$$

where the exponent y is chosen large enough to ensure sufficient rounding of the corner at deformation X, but small enough not to cause an unrealistic force law. An exponent of y=1.15 for example has been shown to give acceptable results (Schamel 1991).

If one now examines the damping term of the clash force, the situation is more problematic. The damping mechanism at this stage is most probably best approximated by standard viscous damping, since the damping results mainly from oil film squeeze effects. But if standard viscous damping is used, the result would be a discontinuity at a deformation equal to X_i (Figure 17). As the discontinuity in the first derivative for the elastic part of the force law already caused a problem, the discontinuity in the force function itself would make it very difficult to integrate the problem numerically.

This problem may be avoided by making the damping not only dependent on velocity but also dependent on the elastic part of the clash force:

$$F_{cld_i} = 0 \qquad F_{cle_i} = 0$$

$$F_{cld_i} = (\dot{d}_{i-1} - \dot{d}_i) c_{cl_i} \left(\frac{F_{cle_i}}{F0_{cle}} \right)^2 \left(3 - 2\frac{F_{cle_i}}{F0_{cle}} \right) \qquad 0 < F_{cle_i} < F0_{cle}$$

$$F_{cld_i} = (\dot{d}_{i-1} - \dot{d}_i) c_{cl_i} \qquad F_{cle_i} > F0_{cle}$$

/5.2.8/

where $F0_{cle}$ is the value for the elastic component of the force from where on the full damping coefficient is applied. The resulting force characteristic for constant difference velocity is shown in Figure 17 (thick line). Obtaining the parameters needed for this damping term is a matter of doing exemplary test work to correlate the model and represents an area where further test oriented research is required.

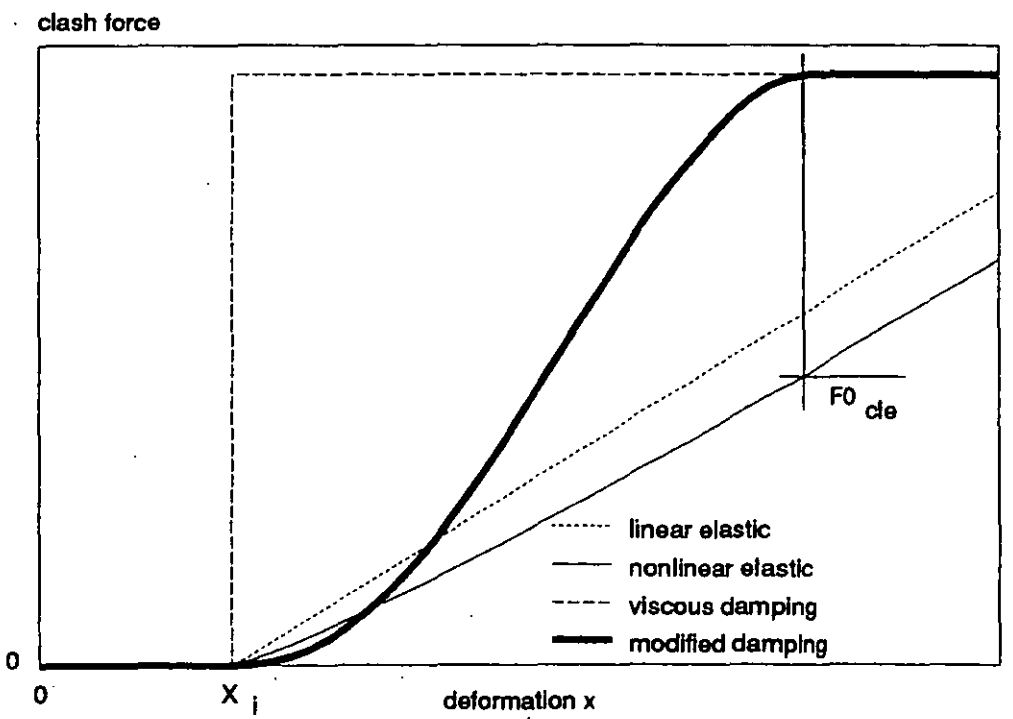

Figure 17: Different force laws for the coil clash conditions in the discrete spring model

5.2.1 Calculation of Spring Properties

Having defined the basic structure of the model, one has to define the free parameters. To describe the valve spring several design guide-lines are available from the spring manufacturers (Scherdel 1987, Associated Springs 1987) where the well known equations for calculating the spring properties can be found; these are based on not much more than wire diameter, number of active coils and mean spring diameter. These equations may be used to calculate the free parameters of the discrete spring model.

Since the pitch angle in a valve spring is very small, one can approximate the total length of the spring wire as the length resulting from the plane arc length corresponding to the number of coils. This implies the assumption that the free length L_0 satisfies $L_0 \ll N2\pi\bar{r}$, leading to the following equation for the total mass of the spring

$$m = \rho V = \rho A l = \rho A N 2\pi\bar{r} \qquad /5.2.1.1/$$

Here the following notation has been used

- N: number of coils
- $\bar{r}$: mean radius of spring
- A: sectional area of spring wire
- ρ: density of spring material

This equation for the complete spring gives good results for the total mass, but it does not describe the varying mass distribution along the spring. Simply dividing equation 5.2.1.1 by the number of coils and the radius r now yields an equation for the mass per coil and radius.

$$\frac{m}{Nr} = \rho A 2\pi \qquad /5.2.1.2/$$

Multiplying this by the fraction of a coil used for each discrete element and the local radius derived from linear interpolation of the diameter data in the spring drawing, one is able to reflect the varying mass distribution by very simple calculations.

$$m_i = \rho A 2\pi \Delta N_i r_i \qquad /5.2.1.3/$$

The procedure to calculate the stiffness is very similar. The definition for the stiffness of a small pitch angle helical compression spring is defined according to the design guides (e.g. Scherdel 1987) as

$$K = \frac{I_t G}{2\pi r^3 N}\cos\alpha \qquad /5.2.1.4/$$

With I_t: torsional moment of inertia
G: shear modulus of spring material
α: pitch angle

By dividing through by the number of coils, and using the local radius and local pitch angle, the stiffness can be described as a function of position along the spring length.

$$k_i = \frac{I_t G}{2\pi r_i^3 \Delta N_i}\cos\alpha_i \qquad /5.2.1.5/$$

where α_i is defined by

$$\alpha_i = \tan^{-1}\left(\frac{T + X_i}{2\pi r_i}\right) = \tan^{-1}\left(\frac{L_s/N + X_i}{2\pi r_i}\right) \qquad /5.2.1.6/$$

With T: thickness of spring wire
L_s: solid length of the spring

The above given equation for the stiffnesses k_i, together with the free space between coils, X_i, from the drawing, describes the spring under free length condition, as shown in the left part of Figure 18. If the very small effect of the change in the cosα term is neglected, each local stiffness term k_i will be linear. The non-linearity effect in the model thus comes from the contact conditions which deactivate coils at the ends as the spring is compressed, as it can be seen in the middle and right part of Figure 18. Since a spring model under installed length conditions is needed, one now has to "compress" the model until it reaches installed length. Because the input data is often not precise this "compression" may be carried out in an iterative procedure which adjusts the model to give the specified force at installed length and the correct residual compression between installed and solid height of the spring.

This completes the discrete model description, based on the data for varying pitch and spring diameter.

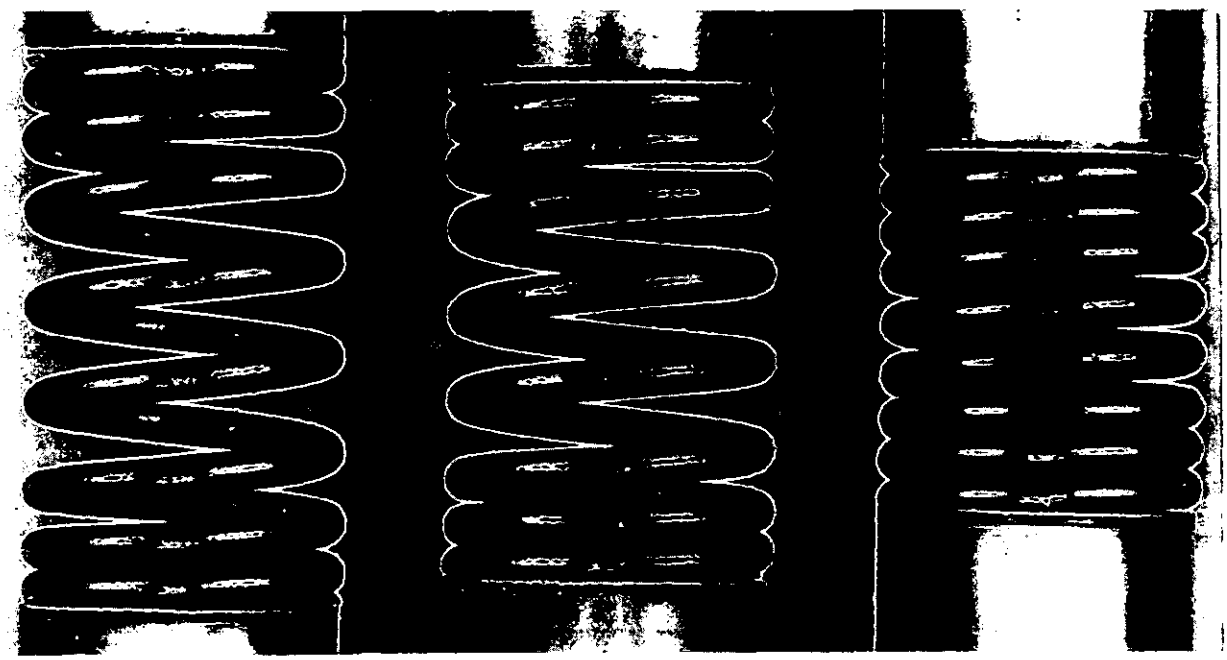

Figure 18: Different stages of spring compression, left: free length, middle: installed length, right: at maximum valve lift

5.3 Discussion

In Section 5.1 the modal model of Phlips *et al* (1989) was reviewed. While this model is very efficient and accurate for linear valve springs, it has certain shortfalls. Because of this, the discrete model shown in Section 5.2 has been developed for special applications.

The necessity to develop this model resulted partly from developments in spring technology. The increased speed requirements for modern engines cause lower and lower cam harmonics to be important for the spring oscillations, since the basic spring frequency can not be increased significantly. Taking a modern engine with a maximum speed of 7000rpm, a typical guide-line given by spring suppliers, to have a spring with a base natural frequency above the 11th harmonic, would require a frequency of roughly 650 Hz. This represents in most cases the absolute borderline in spring technology, since in general the spring frequency is related to the stress level of the spring wire. Instead, non-linear (so called progressive springs) springs which change their natural frequency with lift are being used to avoid excessive resonance. In a strict sense the term natural frequency is no longer correct for a non-linear spring, since the active part of the spring depends on deformation and spring surge amplitude. In spite of this, it is convenient to retain the term natural frequency since it describes the frequency of low amplitude free vibrations of the spring at any given length of the spring.

The increase in frequency is caused by coils becoming inactive as they close up to the adjacent coil and not by an actual non-linearity of the spring wire stiffness, as it can be seen in Figure 18 and is not reflected by the linear modal model in its present form.

An alternative way to limit spring oscillations is to purposely drive the spring near to solid length during the valve lift, causing additional damping by coil clash effects. This method for example is used in racing engines where long term durability is not an issue and extremely close control on all tolerances is possible. Representing such a spring is a point where the modal description totally fails, since the amplitude in each mode in equation 5.1.17 is not restricted by any means.

In reality, if the free space left between two neighbouring coils is small, the amplitude for the surge is restricted by the two coils coming into solid contact. This can be modelled by the discrete description of the valve spring, since it allowed the definition of a force between two elements, which only acts if the two elements get too close. The disadvantage of this approach is, that one ends up with one second order differential equation for each

element. If one wants to represent the springs natural frequencies, lets say up to the 3rd mode, accurately by a discrete representation, considerably more than 3 second order differential equations are needed.

Representing modes accurately is not the only reason for requiring a fine resolution of the discretisation. Since the nonlinearity of the spring is represented by discrete elements becoming inactive when they close up, this results in discrete steps occuring in the natural frequency of the remaining active part of the spring. If these steps are too coarse, the response of the model will be unrealistic.

As a result, the number of discrete elements has to be relatively large. Consequently the mass of each element will be small, resulting in high frequency local modes as the coil closures occur. Hence the model is extremely cpu intensive compared to the modal one. In summary it can be noted that the first model is simple and efficient but not adequate to model the effects in a progressive spring, while the discrete model is able to reflect these effects, but is not adequate for optimization purposes too, because of its cpu requirements.

Thus some intermediate model is clearly required. This model has to accommodate both requirements: to realistically represent a progressive spring and to be computationally efficient. For the modal model (Phlips *et al* 1989) there is an efficient way to solve it in the frequency domain by a Fourier series approach. This suggests that the solution might be found by an extended modal model to reflect what was considered to be the main impact of the spring progressivity, the change in frequency due to the spring compression. This may be realised by a lift dependant ratio of k/m in equation 5.1.15 or correspondingly a variation with lift of ω_n, the frequency of each spring mode, in equation 5.1.16. The method is developed in Section 6.2, but since this method is based on the same fundamentals as for the constant frequency modal model, this method will be reviewed first in Section 6.1.

6

Frequency Domain Solutions for Spring Dynamics

As discussed in Section 4, valve spring vibrations represent a steady state forced response problem, in contrast to the initial value problem nature of the other valvetrain components. The aim of this section is to develop a method to solve this problem efficiently for the case of a progressive spring. In the time domain one would need to integrate over multiple revolutions and monitor the results (change from revolution to revolution) until a tolerable error limit is reached. More promising is a frequency domain method which directly delivers the steady state response. For the constant frequency modal model there is already a solution approach available (Phlips *et al* 1989), and the derivation will be briefly repeated here. Based on that, a new method is developed which applies to a nonlinear spring, and generally allows one to solve linear systems with periodically time variant coefficients in the frequency domain.

Before this is done one aspect has to be considered which is instrumental to both methods. This aspect is the coupling of the valvetrain and valve spring vibrations. As mentioned earlier several of the elements of the valvetrain are non-linear in nature. The consequence of this is that their response can only be calculated by time stepping integration. If the dynamics of the valve spring strongly interacted with the other components, even a linear spring model would require time stepping integration, since otherwise the coupling effect could not be calculated. So to justify a frequency domain approach for the solution of the valve spring surge it is required that at least the dominant lower frequency modes of the spring surge are decoupled from the rest of the valvetrain.

In the case of a simplified linear valvetrain model, the validity of this assumption of decoupled vibrations of the valvetrain and the valve spring can be formally derived, as has been done by Phlips *et al* (1989). The principle justification is that the fundamental frequency of a stiff valvetrain is at least three times as high as the first spring mode frequency. From linear vibration theory it is known that if two systems with such separated frequencies are coupled, the combined modes will lie close to the isolated modes. Or in other words, the eigenvector for the lower mode will only have a significant component for the spring degree of freedom, while for the valvetrain mode eigenvector the spring degree of freedom has a negligible contribution. This allows one to solve the spring response as being decoupled, dynamically separated from the rest of the valvetrain.

However in a strict sense this simple linear analysis is no longer valid for the nonlinear spring, and therefore details are not repeated here. Here we have a combination of a non-linear valvetrain model with a non-linear spring model; one can only say that it is likely that the same separation of valvetrain mode vibration and spring vibration is possible at least for the first spring mode. However, the best (and in the end the only) justification will be in the simulation results, as compared to actual measurements. This is carried out in Section 7.

6.1 The Fourier Solution for Linear Valve Springs

6.1.1 Solution Method

The assumption of a decoupled system now allows one to approximate the dynamic valve acceleration, $\ddot{h}(t)$, by the kinematic valve acceleration, $\ddot{s}(t)$, which results in equation 5.1.17 to be rewritten as

$$\frac{d^2G_n}{d\phi^2}\omega_{cs}^2 + 2\zeta\omega_n\omega_{cs}\frac{dG_n}{d\phi} + \omega_n^2 G_n = -\omega_{cs}^2\frac{2}{n\pi}\frac{d^2s}{d\phi^2} \qquad /6.1.1/$$

This equation can now be solved very elegantly by expressing the excitation as a Fourier series, rewriting equation 6.1.1,

$$G''_n + 2\zeta\frac{\omega_n}{\omega_{cs}}G'_n + \frac{\omega_n^2}{\omega_{cs}^2}G_n = -\frac{2}{n\pi}\sum_{l=0}^{\infty}(a_l\cos l\phi + b_l\sin l\phi) \qquad /6.1.2/$$

The solution will then also be a Fourier series for each spring mode given by

$$G_n = \sum_{l=0}^{\infty}(p_l\cos l\phi + q_l\sin l\phi) \qquad /6.1.3/$$

By substituting equation 6.1.3 in 6.1.2

$$\sum_{l=0}^{\infty}\begin{pmatrix} -l^2(p_l\cos l\phi + q_l\sin l\phi) \\ +\frac{2\zeta\omega_n}{\omega_{cs}}(lq_l\cos l\phi - lp_l\sin l\phi) \\ +\frac{\omega_n^2}{\omega_{cs}^2}(p_l\cos l\phi + q_l\sin l\phi) \end{pmatrix} = -\frac{2}{n\pi}\sum_{l=0}^{\infty}(a_l\cos l\phi + b_l\sin l\phi) \qquad /6.1.4/$$

Comparison of coefficients results in a set of algebraic equations, which can be solved for the coefficients p and q.

Defining

$$U = \frac{\omega_n^2}{\omega_{cs}^2} - l^2 \quad , \quad V = \frac{2\zeta\omega_n l}{\omega_{cs}} \quad \text{and} \quad W = -\frac{2}{n\pi}$$

one obtains

$$p_l = \frac{Wa_l - Vq_l}{U} \quad \text{and} \quad q_l = \frac{VWa_l + UWb_l}{U^2 + V^2} \qquad /6.1.5/$$

With the above method, one is able to calculate the spring dynamics, simply from knowing the excitation and a few spring properties (natural frequency, preload, stiffness and damping).

6.1.2 Application and Discussion

As mentioned in Section 4, one problem for the simulation of a full valvetrain is the initial conditions for the spring surge. To estimate these at the point in time where the numerical integration starts, is an application where this Fourier approach for a linear modal model may be used.

The quality of calculating the initial conditions this way depends on the degree of coupling as discussed before and also on the progressivity of the spring. Figure 19 compares the results obtained from the Fourier solution with the results from the first and second integrated cycle gained from a full model of a bucket tappet valvetrain, like the one shown in Figure 5. In Figure 19a this comparison is made for a linear spring and in Figure 19b for a moderately progressive spring. As can be seen, the quality of the Fourier solution for the initial conditions is excellent in the case of the linear spring, although the Fourier results do not show the 3rd order vibrations caused by the coupling of the springs 3rd mode with the valvetrain vibrations, which in this case are in the range of 1600 to 1800Hz. For the progressive spring the result is a lot worse. Taking the Fourier solution as initial conditions is still better than starting with zero initial conditions, but comparing the Fourier solution with the time integrated results shows a significant error in both amplitude and phase. This error is likely to be even larger for springs with a stronger progressivity. This shortfall can be resolved by a new approach to calculate the response of a progressive spring in the frequency domain, and this will be described in the following section.

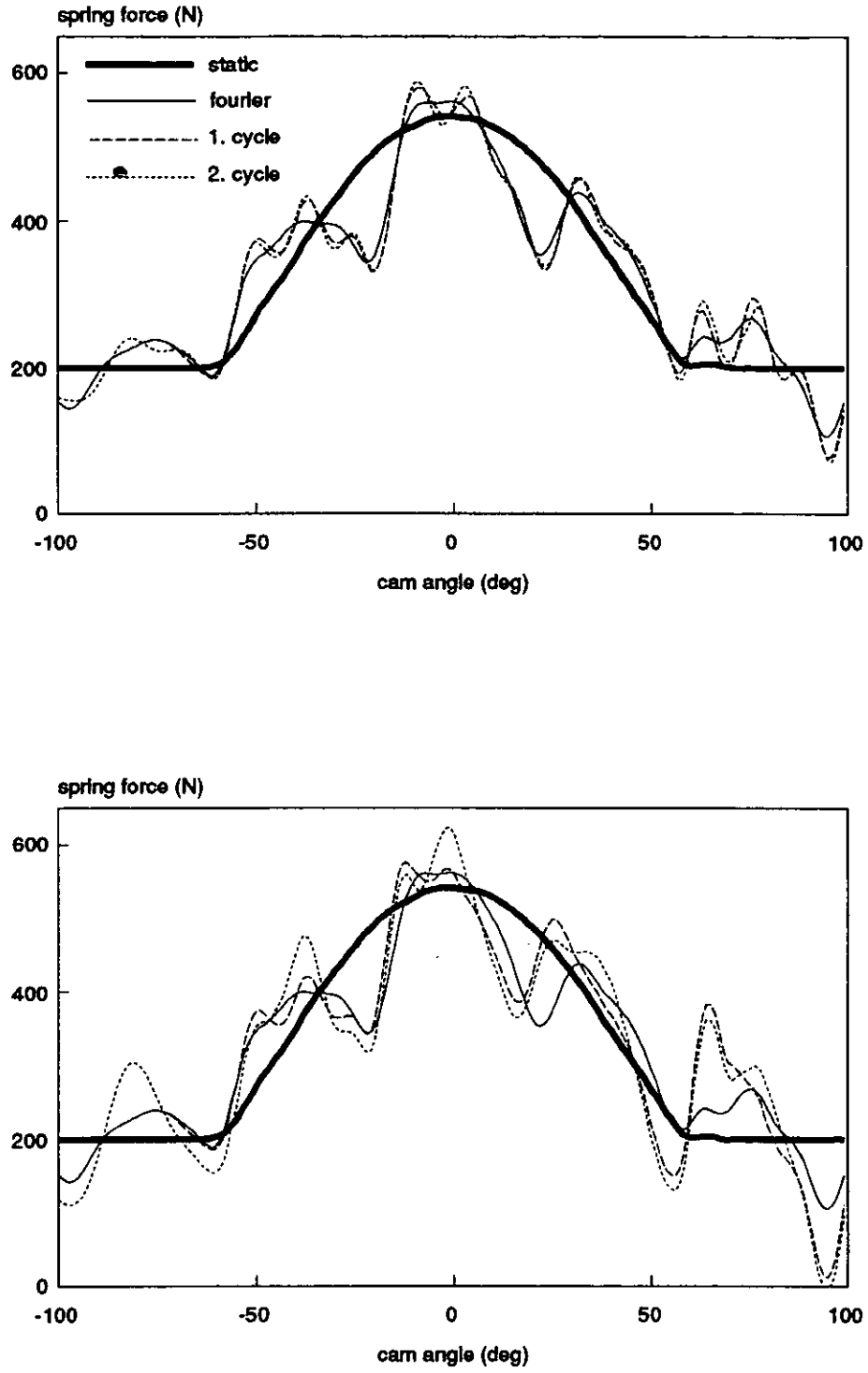

Figure 19: Simulated valve spring force, decoupled Fourier solution, first integrated cycle for coupled system, and second time integrated cycle for coupled valvetrain model. Top: results for a constant frequency linear valve spring, bottom: results for a moderately progressive valve spring.

6.2 A Frequency Domain Solution Method for Progressive Springs

6.2.1 Modelling Approach and required Approximations

The above modal model is now generalized for the case of a progressive valve spring in the frequency domain. One can rewrite equation 5.1.18 as

$$\frac{d^2G_n}{d\phi^2}\omega_{cs}^2 + 2\zeta\omega(h)_n\omega_{cs}\frac{dG_n}{d\phi} + \omega(h)_n^2 G_n = -\omega_{cs}^2\frac{2}{n\pi}\frac{d^2h}{d\phi^2} \qquad /6.2.1/$$

This is only approximate, since the change in frequency with lift is due to the change of the springs active boundary. Consequently, the underlying assumption for the modal model of fixed boundary conditions is no longer valid. The question whether equation 6.2.1 is still a satisfactory approximation will depend critically on the speed of the boundary movement. Here two effects have to be separated. The movement of the active boundary due to the valve lift and the motion of the boundary due to the spring vibrations.

For the first, it is likely that the approach is valid; in the limit of very slow boundary movement the approach would represent an exact solution. In the valve spring application, the speed of travel of the boundary is slow compared to the speed of the wave propagation in the spring. This can be checked with the following coarse estimation. Evaluation of the speed of wave propagation in equation 5.1.1 with typical figures for a valve spring (L=30mm, k=40N/mm and m=0,04kg) delivers a value of approximately 175m/s. The boundary movement on the other hand takes place over approximately 60° camshaft angle. In this time the boundary travels by about 10mm in a highly progressive spring. At 6000rpm this equates to a speed of approximately 3m/s. However this assumes that the speed of boundary movement is constant, what is clearly not the case. In reality the speed depends on the progressivity characteristic of the spring and the interaction with the valve lift profile. But even if the peak value is ten times higher than this estimated mean, it is still substantially smaller than the speed of the wave propagation. In extreme applications however this may be different.

The importance of the second effect clearly depends on the vibration amplitude. For small amplitudes one should be able to neglect the effect. For larger amplitudes an increasing amount of error will be the result. A comparison with measured results will reveal the magnitude of this error.

Now assuming fixed boundary conditions, we turn to the solution of equation 6.2.1. This in itself does not help compute valve spring vibrations efficiently. A series of non-linear second order differential equations still has to be solved, and this can only be performed by time stepping numerical integration.

Let the dynamic valve lift again be approximated by the kinematic valve lift. Applying this to equation 6.2.1 and rearranging gives

$$\frac{d^2G_n}{d\phi^2}+\frac{2\zeta\omega(s)_n}{\omega_{cs}}\frac{dG_n}{d\phi}+\frac{\omega(s)_n^2}{\omega_{cs}^2}G_n=-\frac{2}{n\pi}\frac{d^2s}{d\phi^2} \qquad /6.2.2/$$

While the main advantage of this step for the constant frequency modal model was to decouple the spring from the dynamics of the rest of the valvetrain, now an additional significant benefit is observed. Since the kinematic valve lift is strictly a function of cam angle (or time), the series of non-linear second order differential equations can now be transformed into a set of linear differential equations with periodically time variant coefficients. This allows the system to be solved in a similar way as for the constant frequency modal model. For the constant frequency model, the Fourier technique was directly applicable, since it is known that for a linear system with constant coefficients the frequency of the response is equal to the frequency of the excitation. This in turn allows the separate solution for each Fourier component. In case of the time variant system this is no longer true. Each excitation frequency can result in a wide range of response frequencies. Nevertheless the solution by a Fourier series approach is still possible.

6.2.2 Solution Method

As before, the Fourier series from equation 6.1.2 is used

$$\frac{d^2s}{d\phi^2} = \sum_{l=0}^{\infty}(a_l\cos l\phi + b_l\sin l\phi) \qquad /6.2.3/$$

For the spring modes one has, as before, from equation 6.1.3

$$\begin{aligned} G_n &= \sum_{l=0}^{\infty}(p_l\cos l\phi + q_l\sin l\phi) \\ G'_n &= \sum_{l=0}^{\infty} l(-p_l\sin l\phi + q_l\cos l\phi) \\ G''_n &= \sum_{l=0}^{\infty} l^2(-p_l\cos l\phi - q_l\sin l\phi) \end{aligned} \qquad /6.2.4/$$

But now the spring frequency is a function of cam angle, giving two additional Fourier series namely

$$\begin{aligned} \omega_n &= \sum_{k=0}^{\infty}(r_k\cos k\phi + s_k\sin k\phi) \\ &\quad and \\ \omega_n^2 &= \sum_{k=0}^{\infty}(u_k\cos k\phi + v_k\sin k\phi) \end{aligned} \qquad /6.2.5/$$

Substituting the above Fourier series into equation 6.2.2 gives for the following inertia, damping, and stiffness terms:

$$\sum_{l=0}^{\infty} l^2(-p_l\cos l\phi - q_l\sin l\phi) \qquad /6.2.6/$$

$$\frac{2\zeta}{\omega_{cs}} \sum_{k=0}^{\infty}(r_k\cos k\phi + s_k\sin k\phi)\sum_{l=0}^{\infty} l(-p_l\sin l\phi + q_l\cos l\phi) \qquad /6.2.7/$$

$$\frac{1}{\omega_{cs}^2} \sum_{k=0}^{\infty}(u_k\cos k\phi + v_k\sin k\phi)\sum_{l=0}^{\infty}(p_l\cos l\phi + q_l\sin l\phi) \qquad /6.2.8/$$

The latter two terms include a product of two Fourier series, and in standard fashion this is again a Fourier series.

In general, let

$$f(x)=\frac{a_0}{2}+\sum_{n=1}^{\infty}(a_n\cos nx+b_n\sin nx) \qquad /6.2.9/$$

and

$$F(x)=\frac{A_0}{2}+\sum_{n=1}^{\infty}(A_n\cos nx+B_n\sin nx) \qquad /6.2.10/$$

the product is given by

$$f(x)F(x)=\frac{\alpha_0}{2}+\sum_{n=1}^{\infty}(\alpha_n\cos nx+\beta_n\sin nx) \qquad /6.2.11/$$

where

$$\alpha_n=\frac{a_0A_n}{2}+\frac{1}{2}\sum_{m=1}^{\infty}[a_m(A_{m+n}+A_{m-n})+b_m(B_{m+n}-B_{m-n})] \qquad /6.2.12/$$

and

$$\beta_n=\frac{a_0B_n}{2}+\frac{1}{2}\sum_{m=1}^{\infty}[a_m(B_{m+n}+B_{m-n})-b_m(A_{m+n}-A_{m-n})] \qquad /6.2.13/$$

and for the mean

$$\alpha_0=\frac{a_0A_0}{2}+\sum_{n=1}^{\infty}(a_nA_n+b_nB_n) \qquad /6.2.14/$$

where the following relation has been used

$$A_{-k}=A_k \qquad and \qquad B_{-k}=-B_k \qquad /6.2.15/$$

Since in the present case there is zero mean for the forcing acceleration term, one also expects a zero mean in the response. This allows one to neglect the terms involving p_0. Applying equations 6.2.9 to 6.2.15 thus yields for the stiffness term

$$P_l = \frac{1}{\omega_{cs}^2} \frac{1}{2} \sum_{k=1}^{\infty} [p_k(u_{k+l} + u_{k-l}) + q_k(v_{k+l} - v_{k-l})]$$
$$Q_l = \frac{1}{\omega_{cs}^2} \frac{1}{2} \sum_{k=1}^{\infty} [p_k(v_{k+l} - v_{k-l}) - q_k(u_{k+l} - u_{k-l})] \qquad /6.2.16/$$

It is convenient to define the following abbreviations:

$$A_{kl}^s = \frac{1}{2\omega_{cs}^2}(u_{k+l} + u_{k-l}) \qquad B_{kl}^s = \frac{1}{2\omega_{cs}^2}(v_{k+l} - v_{k-l})$$
$$C_{kl}^s = \frac{1}{2\omega_{cs}^2}(v_{k+l} - v_{k-l}) \qquad D_{kl}^s = \frac{1}{2\omega_{cs}^2}(u_{k+l} - u_{k-l}) \qquad /6.2.17/$$

A represents the cosine coefficients in cosine excitation rows, B represents the sine coefficients in the cosine rows, C is for the cosine coefficients in the sine rows and finally D represents the sine coefficients in sine rows.

Notation for the damping term can be defined in a similar way. Here one has for the combined series

$$R_l = \frac{2\zeta l}{\omega_{cs}} \frac{1}{2} \sum_{k=1}^{\infty} [-p_k(s_{k+l} - s_{k-l}) + q_k(r_{k+l} + r_{k-l})]$$
$$S_l = \frac{2\zeta l}{\omega_{cs}} \frac{1}{2} \sum_{k=1}^{\infty} [p_k(r_{k+l} - r_{k-l}) + q_k(s_{k+l} + s_{k-l})] \qquad /6.2.18/$$

Again collecting similar terms in abbreviations A,B,C and D as before

$$A_{kl}^d = -\frac{\zeta l}{\omega_{cs}}(s_{k+l} - s_{k-l}) \qquad B_{kl}^d = \frac{\zeta l}{\omega_{cs}}(r_{k+l} + r_{k-l})$$
$$C_{kl}^d = \frac{\zeta l}{\omega_{cs}}(r_{k+l} - r_{k-l}) \qquad D_{kl}^d = \frac{\zeta l}{\omega_{cs}}(s_{k+l} + s_{k-l}) \qquad /6.2.19/$$

For the inertia terms one simply has the cosine terms in the cosine rows

$$A_{ll}^{i} = -l^2 \qquad /6.2.20/$$

and the sine coefficients in the sine rows of excitation

$$B_{ll}^{i} = -l^2 \qquad /6.2.21/$$

Collecting these terms together, let

$$A_{kl} = A_{kl}^{s} + A_{kl}^{d} + A_{kl}^{i} \qquad /6.2.22/$$

$$B_{kl} = B_{kl}^{s} + B_{kl}^{d} + B_{kl}^{i} \qquad /6.2.23/$$

$$C_{kl} = C_{kl}^{s} + C_{kl}^{d} + C_{kl}^{i} \qquad /6.2.24/$$

$$D_{kl} = D_{kl}^{s} + D_{kl}^{d} + D_{kl}^{i} \qquad /6.2.25/$$

Now one can assemble a matrix for a set of algebraic equations for each spring mode, which enables one to calculate the unknown p_l and q_l for the spring surge response.

$$\begin{pmatrix} A_{11} & B_{11} & A_{21} & B_{21} & \dots & \dots & A_{kl} & B_{kl} \\ C_{11} & D_{11} & C_{21} & D_{21} & \dots & \dots & C_{kl} & D_{kl} \\ A_{12} & B_{12} & A_{22} & B_{22} & \dots & \dots & A_{k2} & B_{k2} \\ C_{12} & D_{12} & C_{22} & D_{22} & \dots & \dots & C_{k2} & D_{k2} \\ \dots & \dots & \dots & \dots & \dots & \dots & \dots & \dots \\ \dots & \dots & \dots & \dots & \dots & \dots & \dots & \dots \\ A_{1l} & B_{1l} & A_{2l} & B_{2l} & \dots & \dots & A_{kl} & B_{kl} \\ C_{1l} & D_{1l} & C_{2l} & D_{2l} & \dots & \dots & C_{kl} & D_{kl} \end{pmatrix} \begin{pmatrix} p_1 \\ q_1 \\ p_2 \\ q_2 \\ \dots \\ \dots \\ p_l \\ q_l \end{pmatrix} = -\frac{2}{n\pi} \begin{pmatrix} a_1 \\ b_1 \\ a_2 \\ b_2 \\ \dots \\ \dots \\ a_l \\ b_l \end{pmatrix}$$

/6.2.26/

6.2.2.1 Numerical Efficiency

If the above set of equations is examined, one can note the special case for constant spring frequency. In that case, all Fourier coefficients for the ω_n and the ω_n^2 apart from the mean are zero, thus only leaving the $k-l$ coefficients for $k=l$. This leads back to the case where one has only two coupled equations for each order.

In the general case it is important to decide up to which order the Fourier coefficients have to be calculated. For the excitation and response coefficients this depends on the number of spring surge modes to be calculated, the speed range, and the spring frequency. Considering a typical example one gets for 6000rpm engine speed a camshaft frequency of 50Hz. Thus 50 cam harmonics are sufficient to represent excitations up to 2500Hz. For most springs this is enough to reflect the excitation up to the third mode with sufficient accuracy.

For the spring frequency characteristic the situation is better. An example of a spring frequency characteristic is shown in Figure 20, the actual function being compared with approximations using 5,10 and 15 harmonic orders. This frequency characteristic is taken from a spring with a very high degree of progressivity. As it can be seen 10 orders already give an acceptable representation, while above 15 there is no useful improvement. In general 12 to 15 orders prove to be adequate to represent the frequency against cam angle characteristic within 2% accuracy for highly progressive springs. For the matrix shown in equation 6.2.26 this means, that is has a band-diagonal structure.

We now turn to the solution of this equation, and here several algorithms have been tried. These algorithms have been taken from standard texts: "Formelsammlung zur Numerischen Mathematik" (Engeln-Müllges *et al* 1986) and "Numerical Recipes" (Press *et al* 1990). Among the algorithms tried are "BAND" from "Formelsammlung zur Num. Mathematik", an iterative algorithm from the same source, and Crout's algorithm for LU decomposition from "Numerical Recipes". All three seem to have specific advantages and drawbacks; for example BAND proved to be the fastest for a small matrix bandwidth, equivalent to a moderate and smooth change in frequency of the spring model.

The iterative algorithm showed the most interesting behaviour. Since the iterative procedure is based on an initial estimate, it is very economical for a full speed sweep of fine resolution. The first speed point needs considerably more time than for the direct methods, but provides the initial guess for the next engine speed and this results in an extremely fast solution. However, this result was found to be true only if the changes

between speed points are small, or in other words if the solution at the new speed point is of no interest ! Crout's algorithm proved to be the fastest for a fully occupied matrix, and the overall most efficient method is to use Crout's algorithm, suitably modified to incorporate the band features of the routine "BAND".

A further aspect for the efficiency of this method is the calculation of the Fourier coefficients and the back transformation of the results into the time domain. If the Fourier series is evaluated in the standard way, it requires a large number of sine and cosine evaluations, requiring a significant amount of cpu time. This can be avoided by the restriction that the solution is only required at integer camshaft angles. This allows to evaluate the trigonometric functions only once and afterwards use an efficient index calculation instead. This helped to speed up this part of the solution by a factor of 8 to 10 compared to the more obvious procedure.

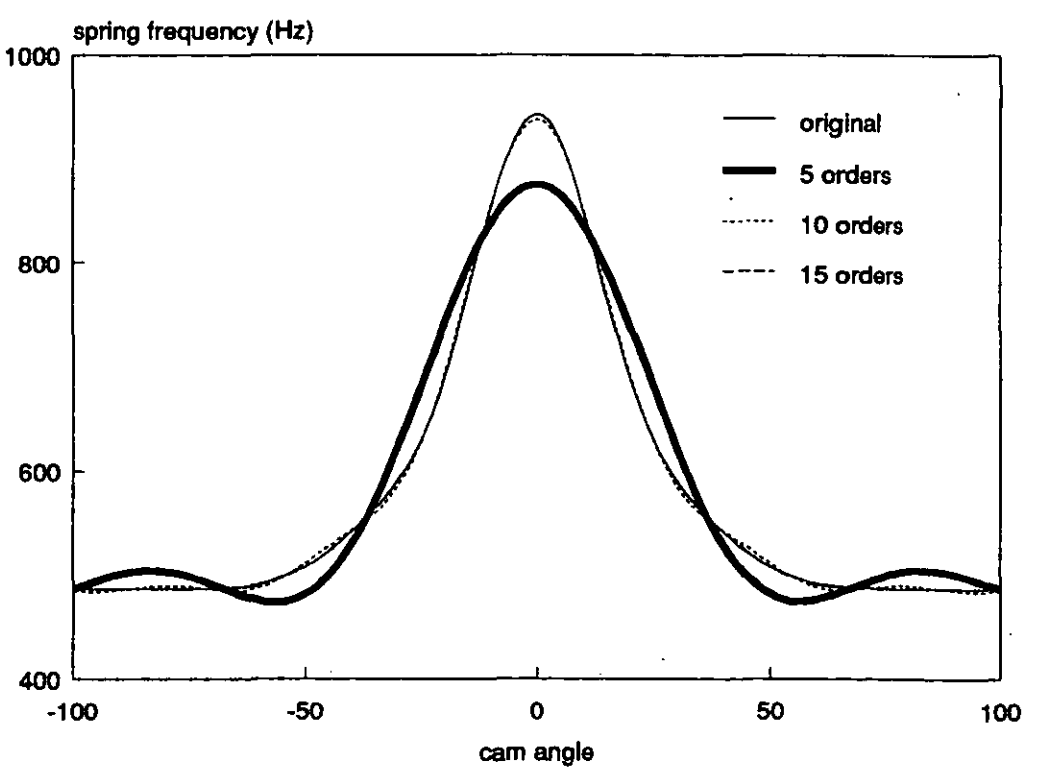

Figure 20: Comparison of original frequency characteristic against cam angle with the result from an approximation by the first 5, 10, and 15 harmonics of the Fourier series

6.2.3 Simulation Studies

Before the work carries on to valve spring optimization two applications for the new method will be discussed in this section.

The first one being looked at deals with the previously raised concern of the initial conditions for a full valvetrain model. The discussion of this aspect serves the following purposes: it will show whether the new approach is able to overcome the shortfalls of the linear modal model, but far more important it will also give an indication of the quality of the results from the decoupled time variant model and about the advantage of this direct steady state response solution in comparison to a numerical integration from rest.

The quality and efficiency shown in the first application is important for the second area of application: the stand alone analysis of a valve spring. This application is vital to the success of the subsequent work presented in this thesis. Efficient and accurate results for the dynamics of valve springs are the central point for the evaluation of the target function in the formal optimization.

To address the first aspect Figure 21 depicts the first 4 cam revolutions for a highly progressive spring (with the frequency characteristic from Figure 27), which starts with zero initial conditions. The results show that the first cycle has a substantial error compared to the 4th revolution, and even between the 3rd and the 4th cycle the differences are noticeable.

In Figure 22 the derived method for time variant systems has now been used to calculate the response of the decoupled spring and the values of the state variables at the start angle of the numerical time stepping integration has been used as initial conditions. Here the differences between the 1st and the 4th cycle are in the same order of magnitude than the differences between 3rd and 4th cycle for the zero initial condition case. The 3rd and the 4th cycle in Figure 22 are absolutely identical, which proowes that the spring had reached steady state response at the end of the second cycle.

If both results from the 4th cycle are compared one can see that there are clear differences (most obvious around -80°) which indicates that the 4th cycle from the zero initial condition run still does not adequately represent the steady state response. All results have been obtained at 6000rpm, and one can suspect the differences to be even larger at higher speeds, where less vibration cycles take place during a cam cycle.

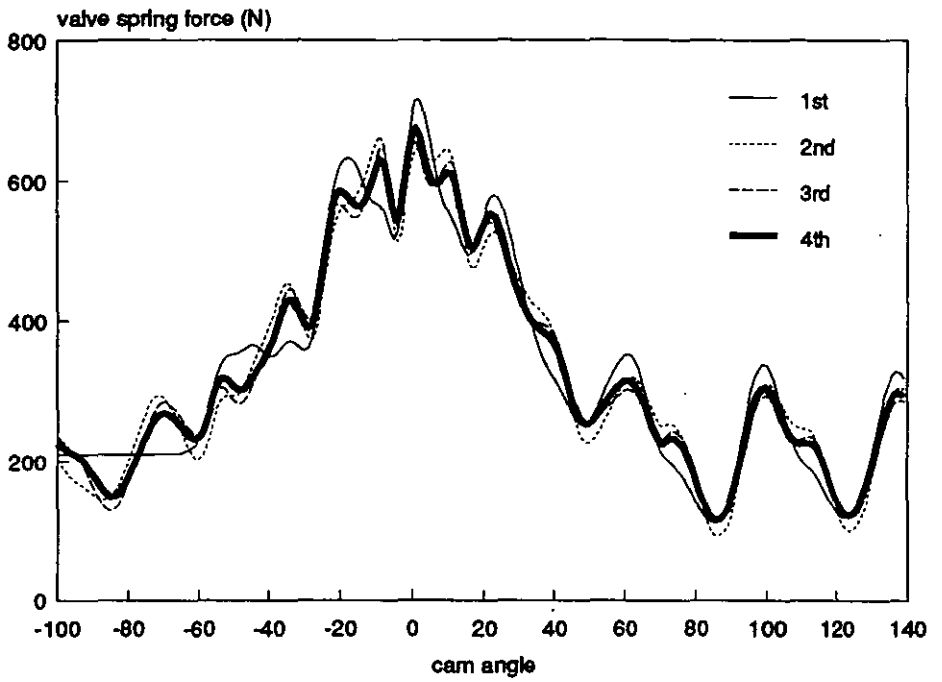

Figure 21: Simulated valve spring force for the first 4 camshaft revolutions starting with zero initial conditions

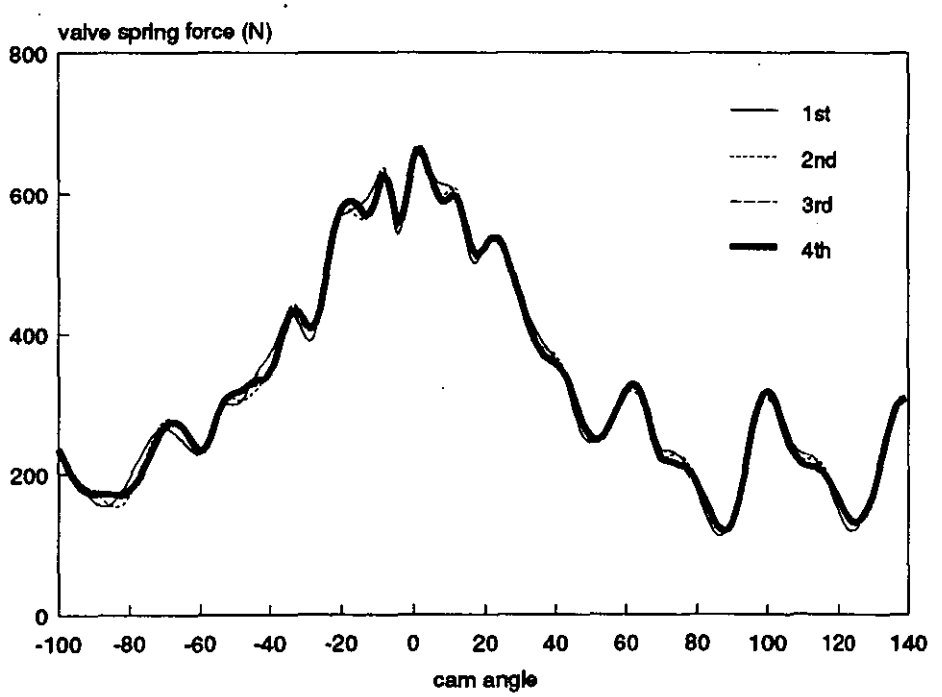

Figure 22: Simulated valve spring force for the first 4 camshaft revolutions starting with initial conditions calculated by the Fourier approach for time variant systems

These excellent results for the initial conditions derived from the decoupled solution build confidence that the method may be satisfactory for investigating the complete spring response, thus making full use of the methods efficiency. Doing this enables one to detect critical speeds which may need further investigation by the full valvetrain model and also allows one to compare different spring designs efficiently at a pre-hardware stage. As an example of this, the frequency domain method has been used to map the responses for the dynamic spring force (Figure 24); this clearly shows the speed ranges where resonances occur. Arriving at the same degree of resolution for the speed response of a valve spring by numerical integration would require between one and two orders of magnitude more cpu time.

In Figure 25 one can see the corresponding surface plot of the spring surge modal amplitude. This plot depicts two effects. At about -50 and +50 degrees, a sudden increase in the vibration amplitude can be noticed. From equation 5.1.18 it is known that the valve acceleration is the forcing function for the spring response. If one looks at the corresponding valve lift and acceleration in Figure 23 it can be seen that -50 and +50 degree cam are just the areas of the opening and closing acceleration pulse, while the deceleration is a relatively smooth period where no excitation takes place.

Beside this, the surface plot of the spring surge explains why the constant frequency Fourier approach still gives some benefits for estimating the initial conditions, compared to a calculation from rest. As the plot shows, the location against cam angle for the vibration shifts with engine speed, since the spring vibration cycle time is speed invariant, but the corresponding number of cam degrees vary with speed. But a look at +50 degree shows, that the closing acceleration pulse triggers the spring surge in phase, independent on the engine speed. Since the closing acceleration pulse takes place close to zero lift, the spring frequency is already close to the base circle frequency. Hence the phase relation from a constant frequency Fourier solution is not too far away from the phase relation of a progressive spring, as far as the base circle period (and hence the initial conditions for the next event) is concerned.

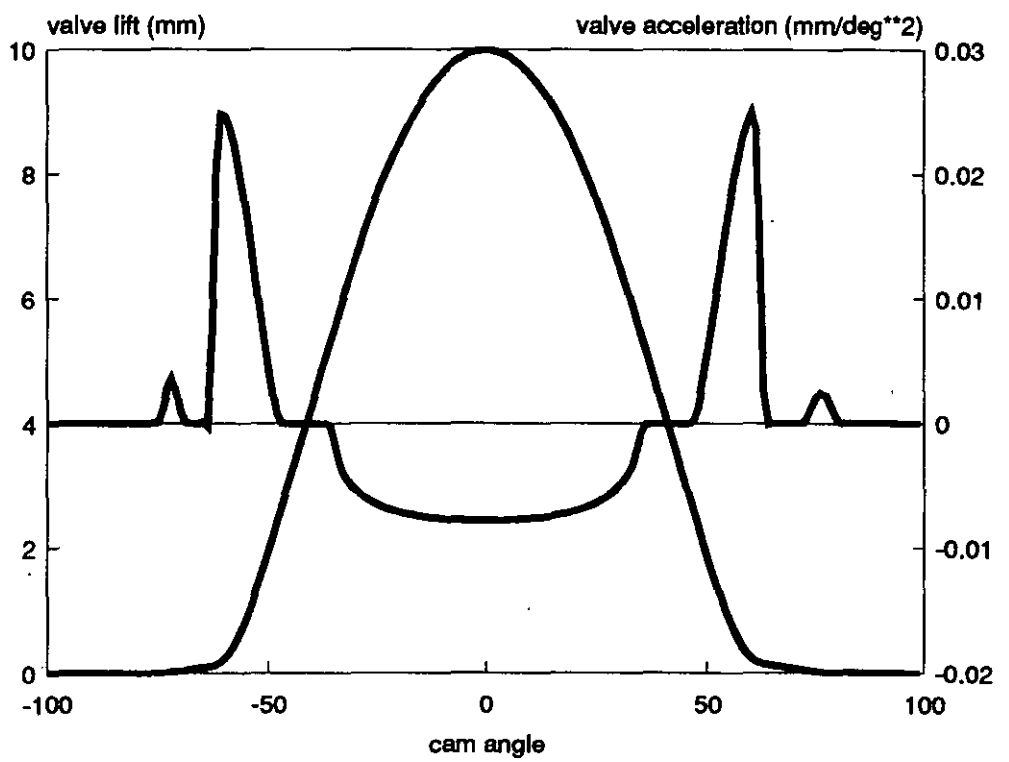

Figure 23: Lift and acceleration for the cam profile used to calculate the responses in Figure 21,22 and 24,25

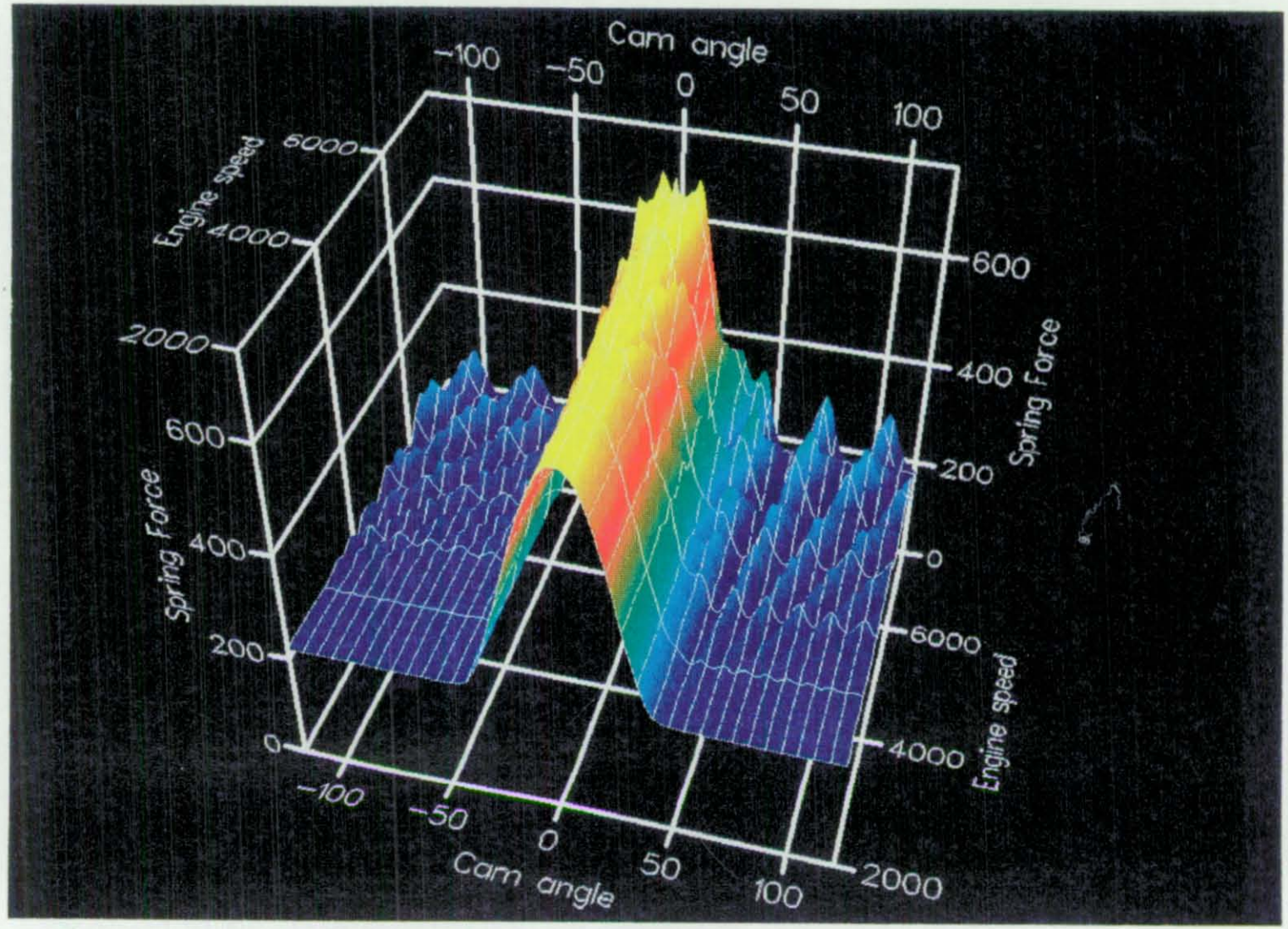

Figure 24: Surface plot of simulated dynamic spring force calculated with the decoupled Fourier solution for time variant systems from 2000 to 7000 rpm engine speed

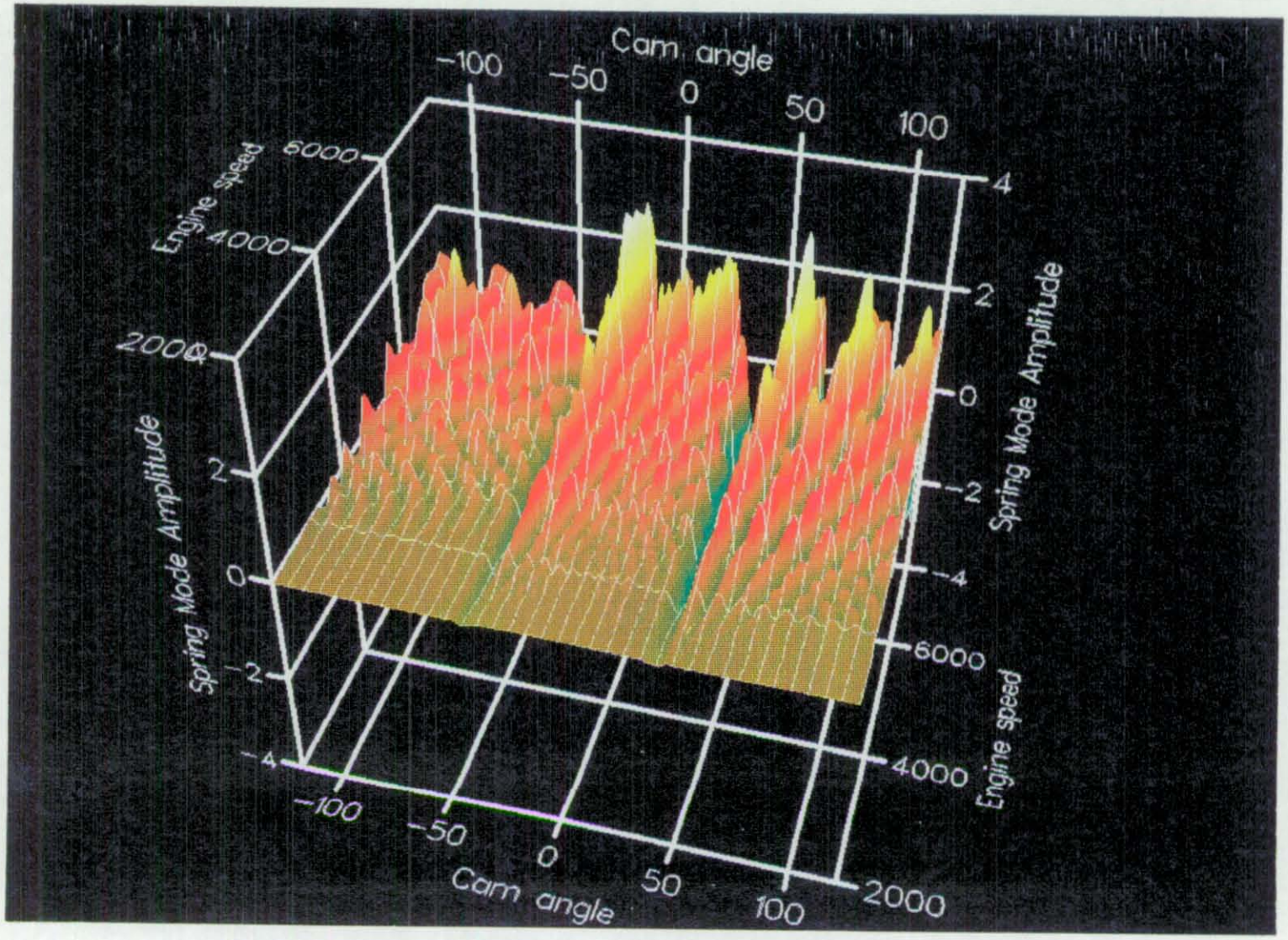

Figure 25: Surface plot of simulated sum of the modal amplitude corresponding to Figure 24

6.2.4 Further Aspects

The above solution technique for periodically time variant systems is by no means restricted to the application for the valve spring. Any periodic dynamics problem in engineering which shows periodically time variant properties, or can be approximated this way, can be solved by the above derived technique. Whether this is the most economical way compared to time integration depends very much on the system. Among others the following considerations influence the choice:

Frequency range of interest In general it is more expensive to solve a system with higher frequencies. If the time domain integration is compared with the Fourier solution, the computational effort for time stepping integration increases roughly linearly with the frequencies to be solved. This is because to resolve one vibration cycle approximately 10 output steps are required. Thus the higher the maximum frequency, the smaller the time step that needs to be used. For the Fourier solution the increase is between linear for systems with constant coefficients and cubic for fully occupied matrices. The case of linear increase will be approached for a system with a matrix that has an extremely small band-width (like it has been shown for a linear spring). In the limit, only two coupled equations have to be solved for each order. Hence computational costs increase proportional to the number of orders required for the intended frequency to be resolved. The other extreme of a cubic dependence results from a system with a fully occupied matrix. It is known (e.g. Press *et al* 1990) that the effort to solve such a set of linear algebraic equations by direct methods (like the Gauss elimination) requires order N^3 operations for a NxN matrix.

Number of degrees of freedom Depending on the bandwidth of the system, the solution effort for the Fourier method increases between linear and cubic with the number of degrees of freedom. The reasoning is in analogy to the explanation for the last argument, since an increase in the degrees of freedom, as well as an increase in the harmonics to be solved, causes a proportional increase in the size of the resulting matrix.

Degree of variation in the coefficients If the change of the time variant characteristics is very smooth, or in other words can be approximated by a low number of Fourier coefficients, the bandwidth of the system will be small, thus allowing a fast solution.

Time range of results needed A significant percentage of the solution time of the Fourier technique is needed to calculate the time domain results from the response Fourier coefficients. If the results are only needed in the frequency domain, or only a small fraction of the cycle is of interest in the results, the speed of the Fourier technique increases significantly.

Damping levels of the system If the damping of the total system or the damping of some of the degrees of freedom in the system is light, the Fourier technique has a clear advantage against the time domain integration. Light damping requires a large number of integration cycles to be carried out, in order to obtain a steady state response.

Number of solutions for a given configuration About 90% of the effort for the Fourier solution of larger systems is dedicated to the LU decomposition of the matrix in equation 6.2.26. Once this step has been performed, the backward substitution for a given excitation vector is extremely fast. Hence if multiple excitations of the same system at the same speed are required, even a large number of degrees of freedom can be solved efficiently.

Memory available in the employed computer hardware From a practical point of view, the previous argument only holds true if the available computer main memory is sufficient to store the system matrices. Otherwise the system must swap the data to hard disk, and the time domain solution may run more quickly.

6.2.5 Other Applications

Two other possible areas of application will now be briefly discussed. Firstly consider vibrations in the valvetrain drive; the crankshaft - belt/chain - camshaft system can interact in a way that causes problems for the ignition system sensors, or belt/chain failures can occur. The similarity to the valve spring application is, that this system also represents a steady-state forced response problem, rather than an initial value problem. Whether a fully linear model with constant coefficients is sufficient, or some of the properties can be usefully modelled as time variant, would need to be investigated. But if a very low number of degrees of freedom are used in an initial model of the full valvetrain drive, the varying inertia of the crankshaft (dependent on the position of the conrod and pistons for example), could be modelled as a time variant property.

Secondly there is the application to a full valvetrain model. Figure 26 shows a simplified representation of a valvetrain model. In terms of the degrees of freedom, this model is sufficient for the initial analysis of design trends. On the other hand three degrees of freedom allow a very efficient application of the frequency domain solution method. A problem arises however, due to the fact that only the spring surge represents a steady state response problem. The tappet and valve degrees of freedom start with zero initial conditions for each new cycle. Furthermore the stiffness of the tappet depends on the position of the contact point between cam and tappet. Also the impact from the valve seat at the end of the event represents an important non-linearity.

Nevertheless an approximate frequency domain solution is still possible. The contact point for example is a function of the cam velocity, which in turn may be written as a function of time.

The valve seat impact is not really of interest, To investigate the system it is sufficient to observe the state variables (e.g. valve velocity) shortly before the valve would hit the seat, which can be done without actually modelling the seat. The important aspect of the seat is the decoupling of the system during the base circle, with the resulting damping, which causes the system to start from rest at the next cam event. This effect can be achieved in the frequency domain model by applying an artificial rise of system damping during the base circle phase, for the tappet and valve degree of freedom.

Another aspect is the fact that some of the other valvetrain contacts occur only with compression forces. These can be modelled as linear contacts, and results examined for tension forces. This is sufficient to judge a design, since a well designed valvetrain configuration should always stay in contact up to the maximum engine speed.

The above two examples show, that there are additional potential applications in the field for the derived frequency domain solution method for time variant systems and investigations on the application of the method to these areas have already been initiated.

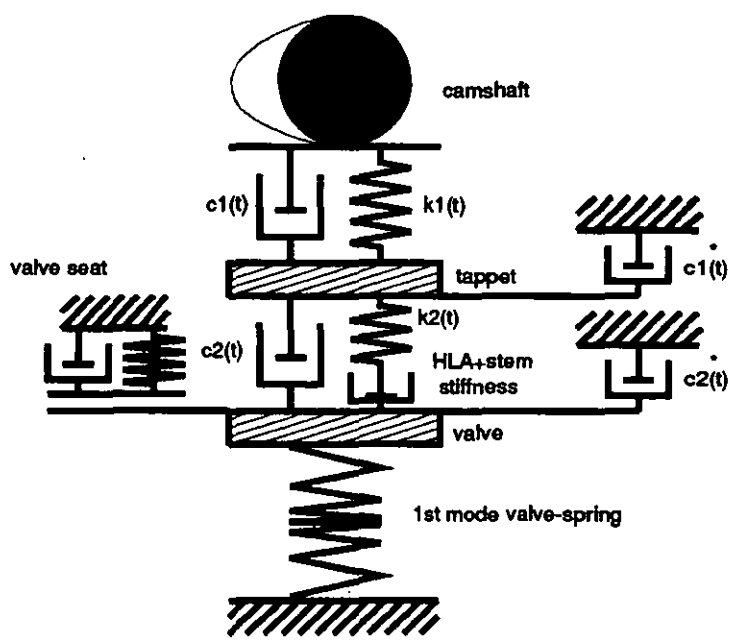

Figure 26: Simplified bucket tappet model to illustrate the feasibility of a time variant approximation for a full valvetrain model

7

Correlation of Valve Spring Dynamics Simulation

In the last section a new valve spring modelling approach and corresponding solution method have been considered . The efficiency of this model and the likely range of application has also been discussed. The efficiency aspect is one of the main requirements for the planned formal optimization. As mentioned in the introduction however, the second requirement is that the model be sufficiently accurate. To assess this point is the objective for this section; results from the time variant linear modal model will be compared with measured results and also with results from the discrete model of Section 5.2. The first part of the section will discuss how appropriate parameters for the model can be calculated, and what the different options are for spring response measurements. The actual results are considered in Section 7.2.

7.1 Model Parameters and Test Methods

Before the above method for time variant systems can be applied to solve the dynamic response of a real spring one needs to determine parameter values. The most important parameter, as can easily be seen from equation 6.2.1, is the spring frequency characteristic. One possible source of information is the spring manufacturer; unfortunately in the experience of the author this information is not readily available, nor very reliable.

To overcome this shortfall, the discrete model presented above can be used to derive the frequency characteristic. For this purpose an extremely fine resolution was used (150 masses) and at each simulated length an eigenvalue analysis of the active portion performed. To validate the accuracy of this approach to compute the frequency characteristic, the characteristic has also been measured. For this purpose the spring shown in Figure 28 was fitted with a force transducer described below. The spring was then compressed in steps of 0.5mm and excited by an impulse hammer at each length. The measured free vibration was processed by an FFT analyser to compute the fundamental frequency. A comparison of the measured frequency characteristic and the calculated one is shown in Figure 27. Although the calculation misses some minor dwells in the true characteristic, the correlation appears fully satisfactory.

For the correlation of the spring models, two measurement locations developed by Hammacher and Utsch (1991) proved to be useful.

The first one is underneath the spring. For this location a specially designed force transducer has been developed which is shown in the top of Figure 29. It consist of a washer with four ribs on either side, each separated by 90 degrees, where the set on one side is rotated 45 degree against the one on the other side. If this device is loaded, each quarter

section of the washer acts as a bending beam. This bending is then measured by strain gauges and calibrated to the static spring force characteristics. The reason for this development was that commercially available force transducers where too thick to fit underneath the spring (only a very limited amount of material can be removed in the spring seat area without cutting into the water jacket of the engine).

The more common application of strain gauges on the spring wire directly has two disadvantages. The first disadvantage for correlation purpose is the relative position of the strain gauge relative to the mode shapes. If the place is chosen for example right in the middle of the spring, there is no contribution to the strain from the first mode, hence the most important vibrations will be missed in the measurements. So each location along the spring will result in a specific combination of the different modes. For a linear spring, this is not too much of a problem, if the position is chosen close to the ends, but for a progressive spring, the situation is different. Since in this case, the border of the active portion of the spring moves with valve lift, the relative location of a strain gauge to the mode shapes moves too. Figure 30 illustrates this effect (To enable the usage of strain gauge readings to some degree, a simulation of this effect has been incorporated in the spring analysis program, but using the force transducer data avoids the issue in the first place).

The second disadvantage is that such strain gauges actually measure torsion. Because of this they cannot show whether coil clash occurs. Since the mechanism for this is impact forces from interfering coils, not torsion, strain gauge readings from valve spring measurements tend to appear smooth with frequencies up to the third spring mode.

The second important location for measurements is a set of strain gauges placed on the valve stem as shown in the bottom part of Figure 29. The valve stem represents a comprehensive mix of information about the full valvetrain. During the base circle phase (before -65deg and after +65 deg, Figure 33) it directly reflects the residual vibrations of the valve spring, since the force path is through the retainer, the valve stem, into the valve seat. During the valve open period the valve disk acts as a mass probe and forms together with the strain gauge an accelerometer which reflects the dynamics of the complete valvetrain. Furthermore the complete duration between valve opening and valve closing together with the theoretical valve event length information allows one to determine accurately the effective aeration of the hydraulic element. In addition, if coil clash occurs this strain gauge will reflect it in the measurements too. Since the results from the strain gauges at the valve stem indicate what is happening at the retainer end of the spring, it allows one to correlate the phase relationship of results seen by the spring force washer and the opposite spring end.

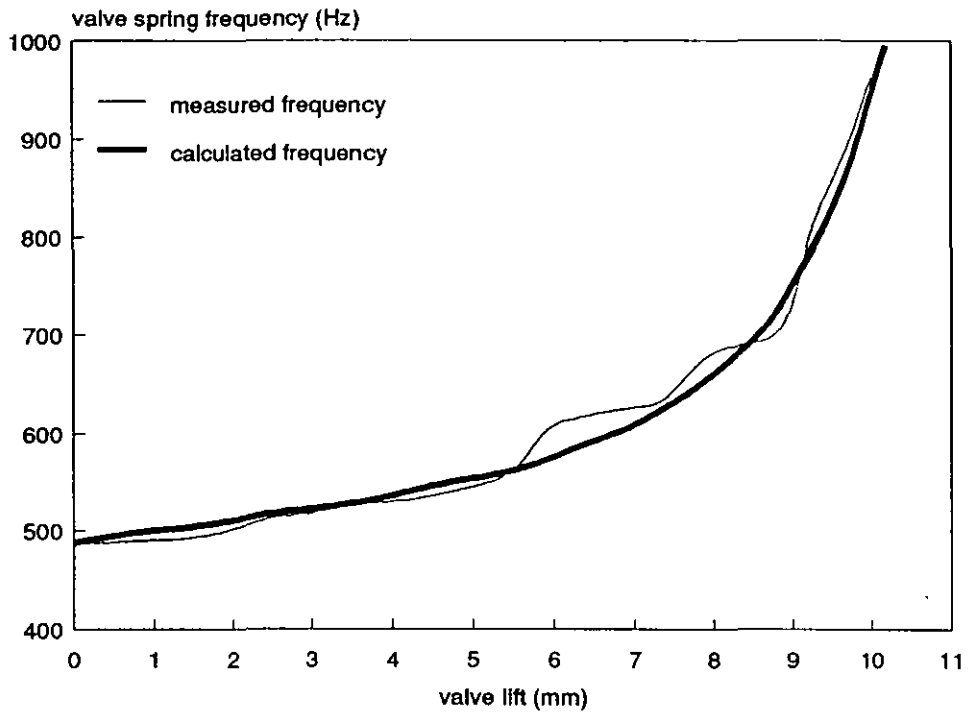

Figure 27: Comparison of measured and calculated frequency against valve lift for the original spring shown in Figure 28 which has been used for the calculations shown in Figure 21,22 and 24,25

Figure 28: Photograph of the spring used for the calculations shown in Figures 21,22 and 24,25 as well as for the correlation and as the start point for the optimization

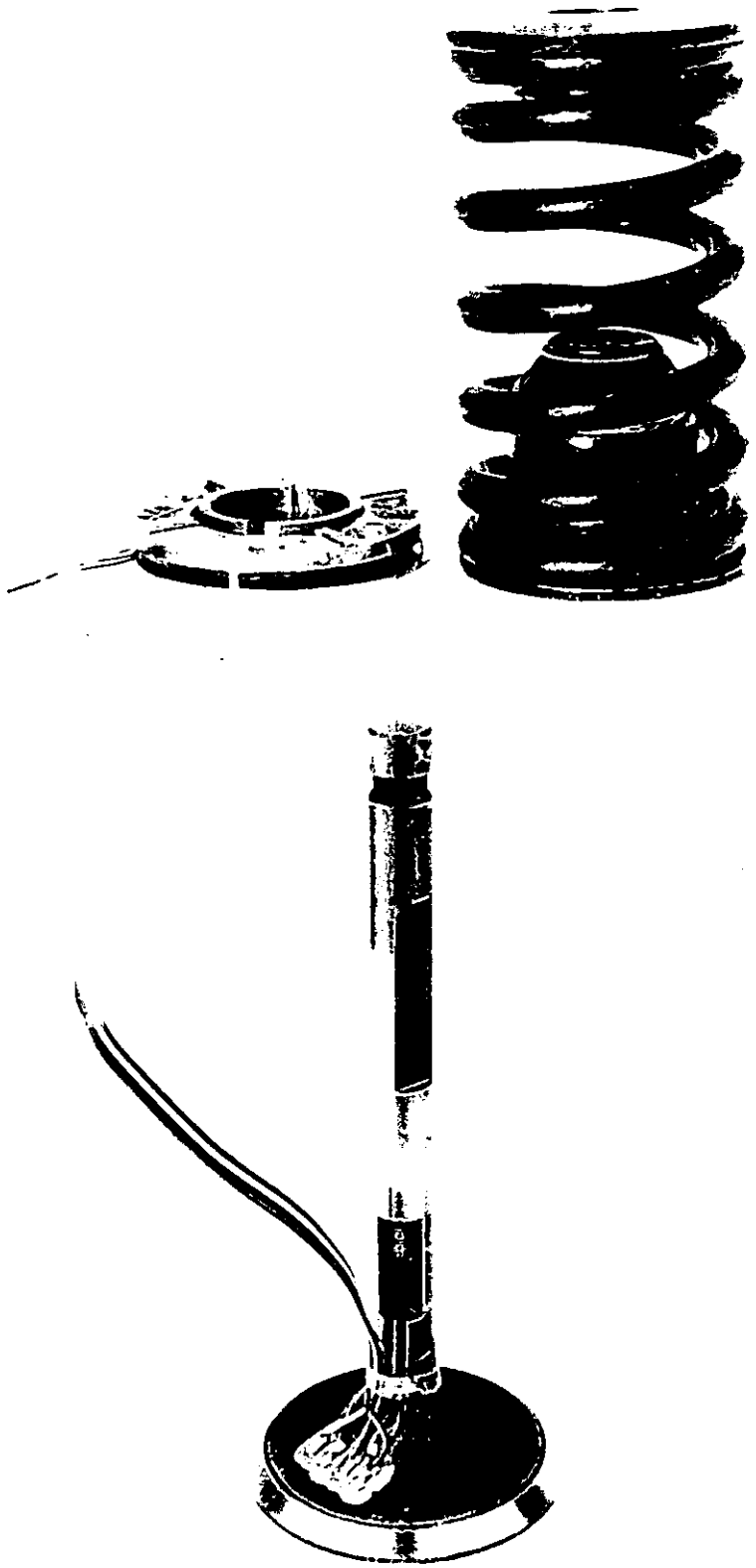

Figure 29: Measurement devices for valvetrain dynamics. Top: valve spring force transducer to measure spring force at the bottom end of the spring. Bottom: strain gauges on valve stem to measure valve stem force and thus retainer end spring force during the base circle

For the discrete model the results from the force transducer underneath the spring can be directly compared to the corresponding signal of the discrete model. For the modal model one has to take into account that the summation of modes at the bottom of the spring will be different from the top. For the force at the bottom of the spring equation 5.1.20 becomes

$$F = -k(S + h(t)) + \pi k \sum_{n} (-1^{n}) n G_{n}(t) \qquad /7.1/$$

For the results from the modal model to be compared with the measured forces, it must be remembered that the modal model is unable to predict frequencies higher than the highest mode being considered. To ease the comparison to the modal results, the measured signal has been processed by a digital low pass filter (3000Hz cut off frequency) to remove any high frequency noise in the signal. The test results where obtained from the spring (Figure 28) with the frequency characteristic shown in Figure 27 running in a DOHC 16 valve engine with hydraulic bucket tappets. For the full valvetrain simulations a model according to Figure 5 has been used including valve shaft flexibility to reflect the strain gauge position. Figure 24 shows the profile used for the test and calculations shown in Figure 31, 32, 33 and 34.

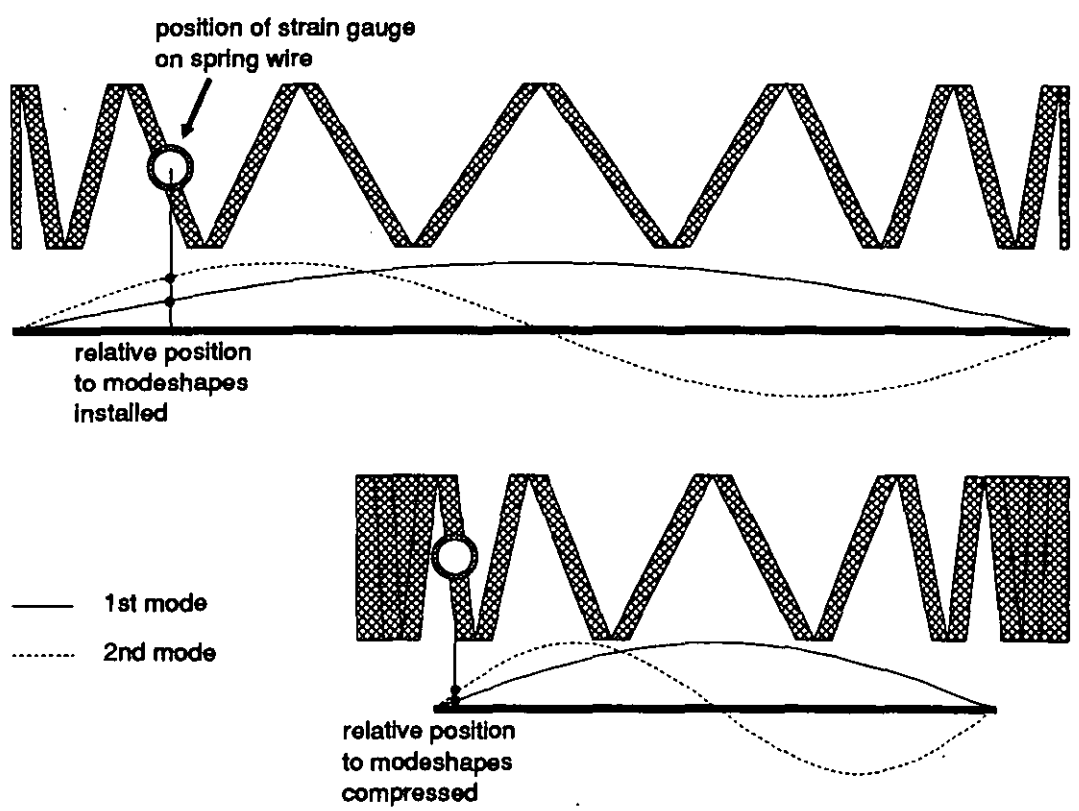

Figure 30: Sketch to illustrate the effect of spring compression on the relative position of a strain gauge in respect to the spring modes

7.2 Correlation and Discussion

The comparison of the filtered measured signal and the simulated modal results, obtained from the Fourier technique solution, are shown for 3 engine speeds in Figure 31. As can be seen the correlation is quite good. The amplitude and phase for the fundamental mode agree very well. At 6000 rpm one can see a more dominating influence from the second spring mode, which is not fully predicted by the modal model, but for spring evaluation purposes the correlation appears adequate.

Closer inspection reveals the influence of the missing coil clash effects in the modal model. As the coils close up approaching maximum valve lift (maximum lift is at 0 °), the coil clash effects appear to cause additional damping, and this effect is not present in the modal model. This would cause the higher amplitudes on the closing flank in the modal solution, as compared to the measured signal.

That coil clash is responsible for this effect is further suggested by the comparison of the unfiltered measurement and the results from the discrete model in Figure 32. Here it can be seen that the correlation, even of the high frequency clash events, is very good, and the reduced vibration amplitude on the closing flank of the valve event is also predicted. However on the base circle, the results from the modal model are clearly better than from the discrete one. This is possibly due to the fact, that the modal model more accurately represents the mix of higher order modes.

Figure 33 shows the valve stem force corresponding to the spring force from Figure 32. Here there is a large amplitude vibration, with high frequency content between -30 and 0 degrees. Two possible causes suggest themselves. The more dramatic one would be the sharp impact following a loss of contact between cam and tappet. The other possible reason would be coil clash at the retainer end, corresponding to the observed coil clash at the bottom of the spring. Performing the analysis with both the modal and discrete models allows one to attempt to determine the actual source. The modal spring model shows no such loss of contact and no high frequency excitation. The discrete model also does not show any loss of contact, but still displays the measured high frequency effects in the valve stem; this arises from coil clash events in the model, suggesting that this must also be the mechanism responsible for the measured results.

The results shown in Figure 32 and Figure 33 were derived from a discretisation into 19 masses. However, the number of active masses can be considerably lower depending on the stage of compression. Accordingly the accuracy of the representation of the higher modes deteriorates. This can be proved by comparing the results from a run of the discrete

model with 35 masses instead of 19. The results for this are shown in Figure 34. As can be seen the correlation on the base circle is a bit closer to the one from the modal model, but still does not reach the same degree of correlation. In addition the high clash frequencies start to cause numerical problems for the numerical integration, which makes this run very slow (the solution for this case required 4000cpu seconds for 1 cam cycle on a DEC5000/200 workstation). Hence in practice the most accurate result with reasonable amount of cpu effort is achieved using a reasonable detailed discrete model with the initial conditions derived from the modal model, rather than calculating several camshaft revolutions with the discrete model.

The most significant feature of the above results, is to confirm the time variant modal model for progressive springs is reasonably accurate and is also appropriate for optimization purposes. It clearly reflects the amplitude and phase changes due to the frequency variation caused by the springs progressivity. The main source of error in the modal model is that it misses the high frequency clash events and as a result of this lacks some of the damping of a real spring. For satisfactory prediction of performance trends though, these effects may be expected to be of secondary importance.

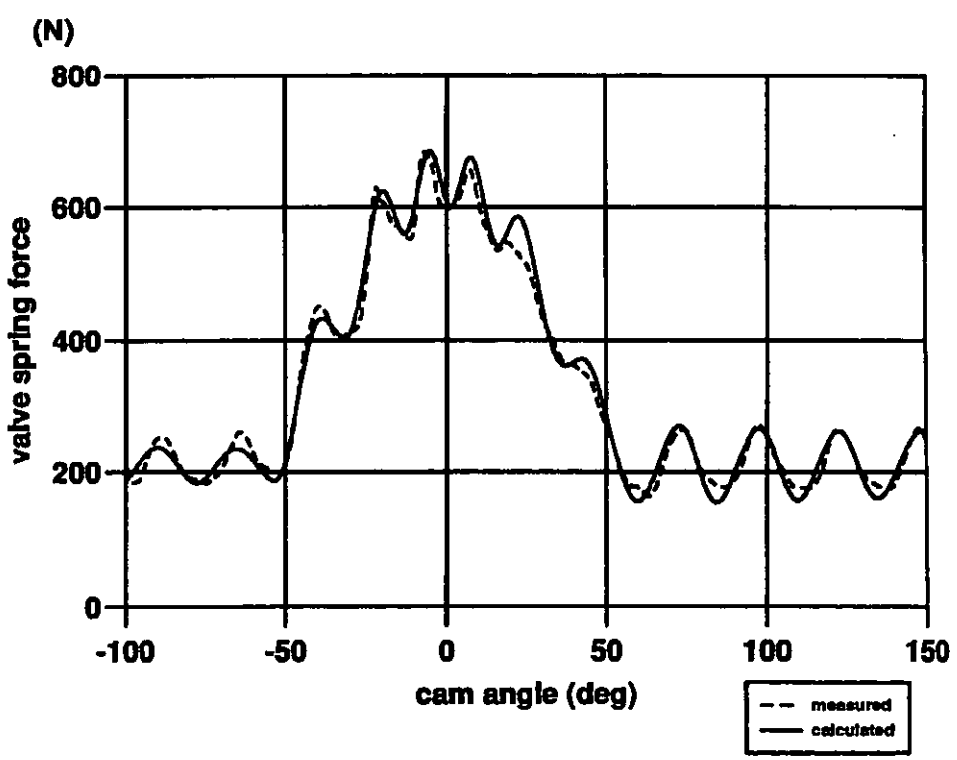

(a)

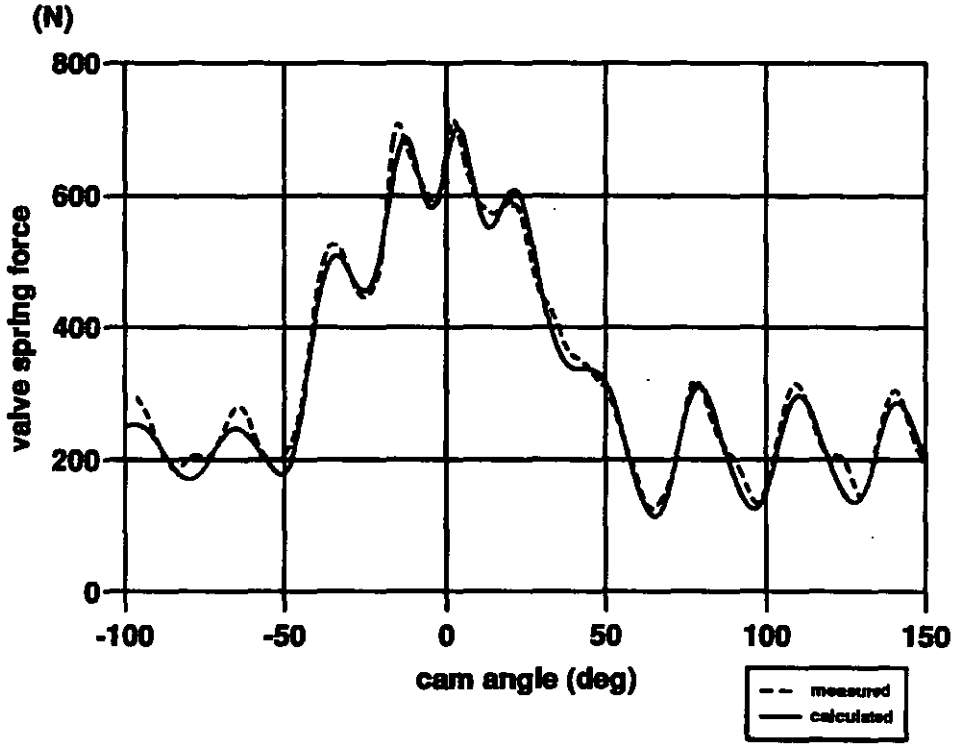

(b)

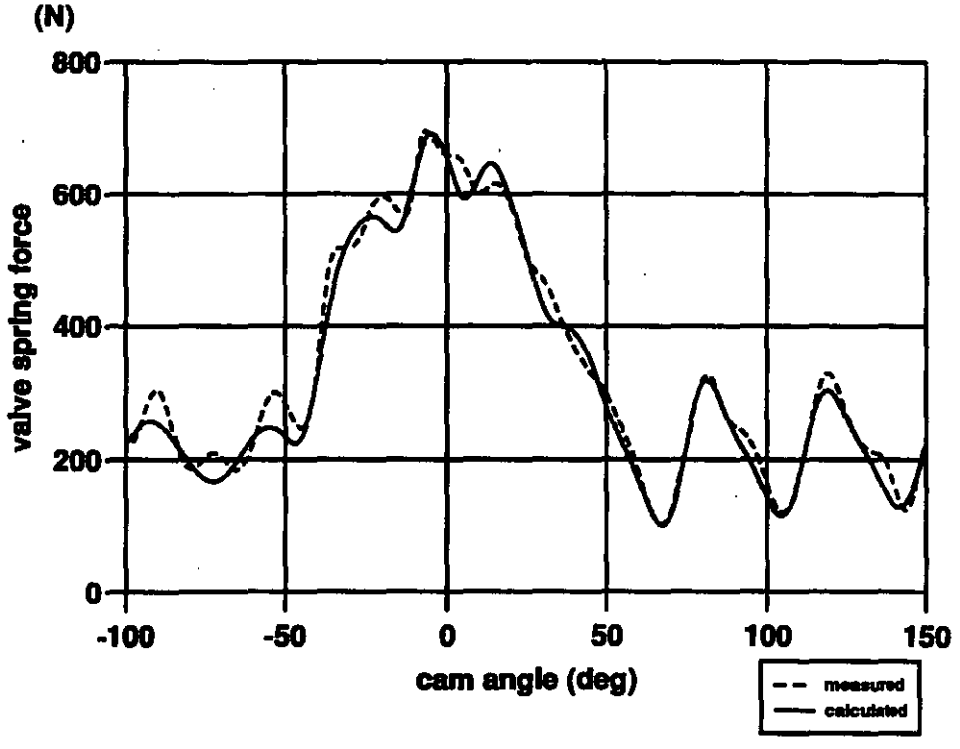

(c)

Figure 31: Comparison of filtered measured spring force and simulated spring force using the Fourier solution for time variant frequency modal spring model. (a) 4000 rpm engine speed, (b) 5000 rpm engine speed, (c) 6000 rpm engine speed

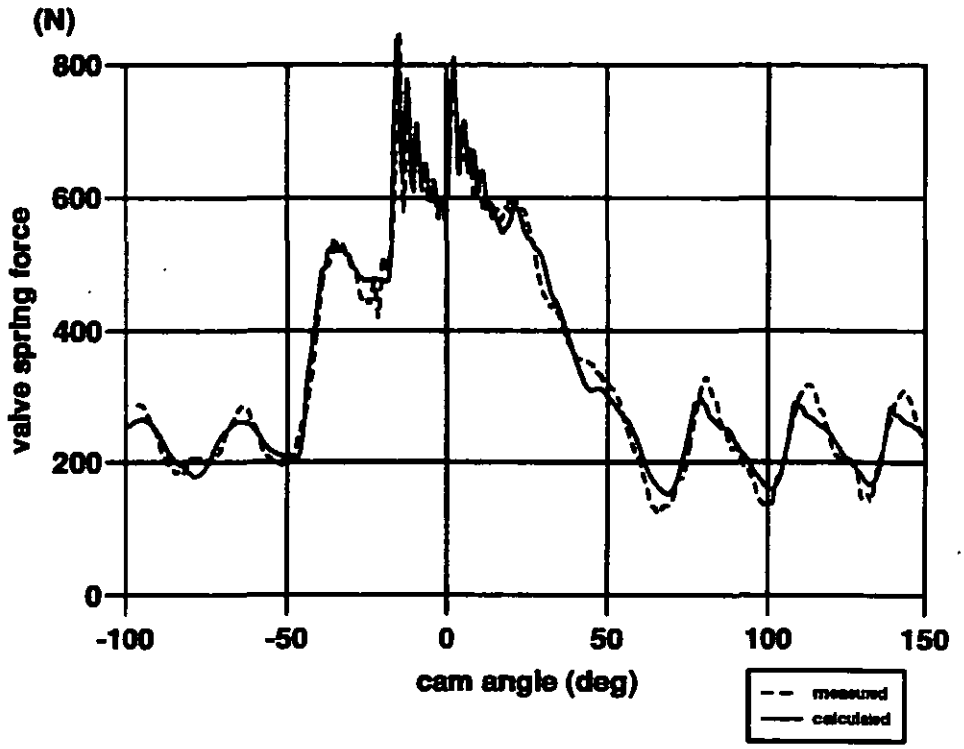

Figure 32: Comparison of measured spring force and simulated spring force using the discrete spring model with 19 masses at 5000 rpm engine speed

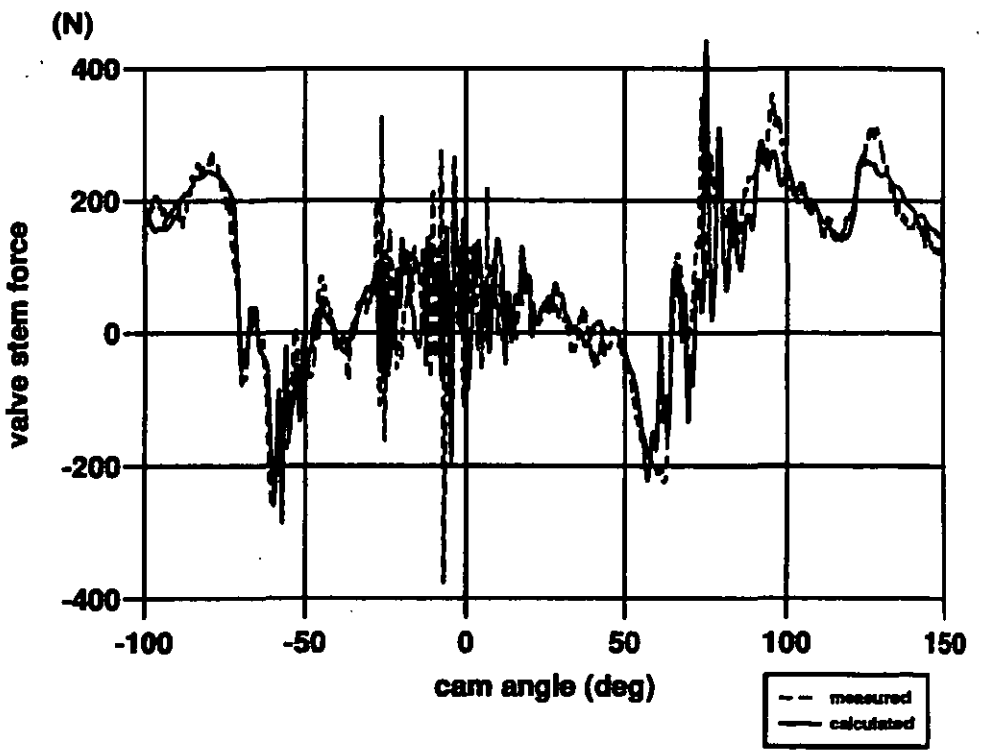

Figure 33: Comparison of valve stem forces corresponding to Figure 32

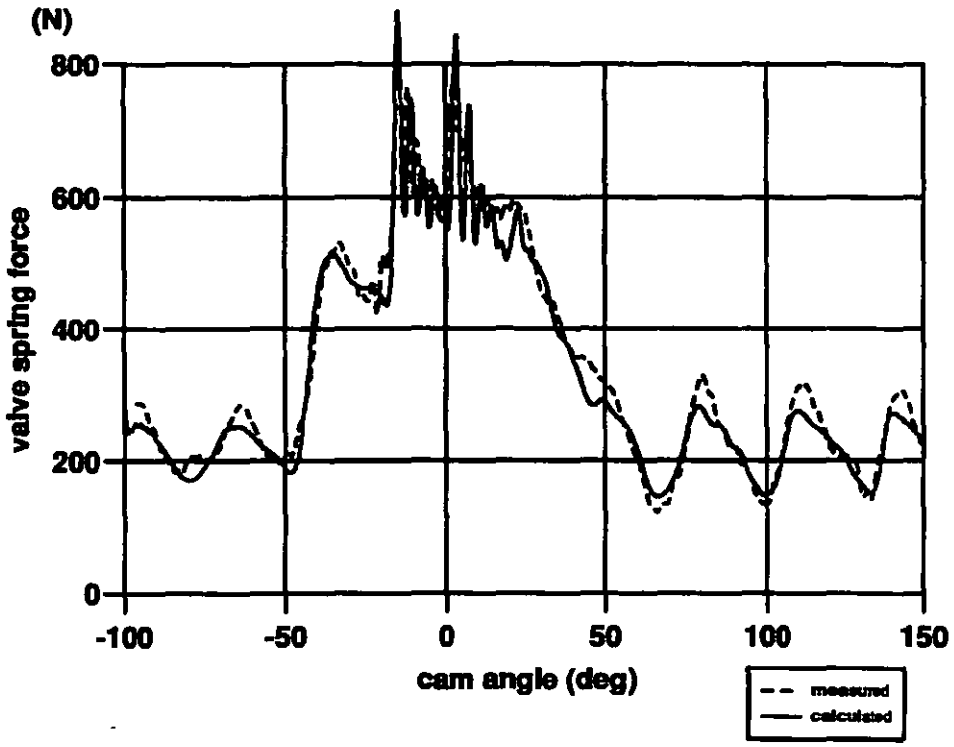

Figure 34: Comparison of measured spring force and simulated spring force using the discrete spring model with 35 masses at 5000 rpm engine speed

8

Requirements for Valve Spring Optimization

The aim of this section is to consider why it is the spring design that should be optimized to reduce spring vibrations, rather than the excitation. For this purpose a brief introduction into the manufacturing and design of springs will be given, and this lays the ground for a discussion on the most appropriate choice for the parameter space for the subsequent formal optimization.

So far, in the analytical work presented in the previous sections, the discussion was concentrated on the simulation of existing valvetrains to establish the dynamic properties and the response from a given configuration. This alone is a valuable tool in the development process for a new engine, since it may lead to shorter development cycles through reduced hardware testing. Modelling studies carried out at a pre-hardware point allow one to optimize the system before prototypes are actually manufactured. An example of the potential of such an optimization has already been seen in Section 4. In this example the cam profile had been modified to reduce the valvetrain vibrations. While this was done manually there are also approaches to automate this process by formal optimization algorithms (Ernst *et al* 1992).

For the valve spring itself such a formal design optimization has not previously been carried out. This is somewhat surprising since it has been seen how important the spring vibrations are for the valvetrain performance. Optimization of the excitation does not help too much for the valve spring response. The limited influence of the cam profile can be demonstrated by considering the Fourier spectra of the excitation. Considering a typical spring frequency of 500 Hz and a typical maximum engine speed of 6000 rpm, one finds from the Fourier approach that the dominant excitation for a linear spring will be the 10th cam harmonic. Figure 35 now shows the original lift and acceleration curves for the profile from Figure 23 and compares them with the curves gained from a Fourier series up to the 10th harmonic. As can be seen, the lift curve is represented very accurately, while the acceleration is very different than the original curve. Formally this is simply due to the second derivative (the acceleration) being represented by $(l\omega)^2$ multiplication in the Fourier representation, this emphasising the higher harmonics in the error. Conversely, if a modification of the low frequency response of the valve spring is required, by cam profile modifications, there would have to be a significant change of the lift characteristics. In most practical cases this is not possible, since the base lift characteristics are determined by gas exchange requirements. At higher frequencies the situation is different, and a significant improvement can be achieved through cam modifications.

The clear conclusion is that, if one wants to optimize the spring performance at a given engine speed or speed range, one has to optimize the spring design rather than the cam profile. Although this can be done simply by manufacturing a large number of alternatives and choosing the best one in engine tests, a more systematic approach, based on computer simulation, is desirable. For this purpose the above derived frequency domain method represents a useful tool. At the final stage it is desirable to directly optimize a spring for a given valvetrain configuration, cam profile, and speed range by means of an automated computer algorithm. To determine what may be the best set of parameters for this spring design optimization, a short review of spring manufacturing and the spring design variables will first be considered.

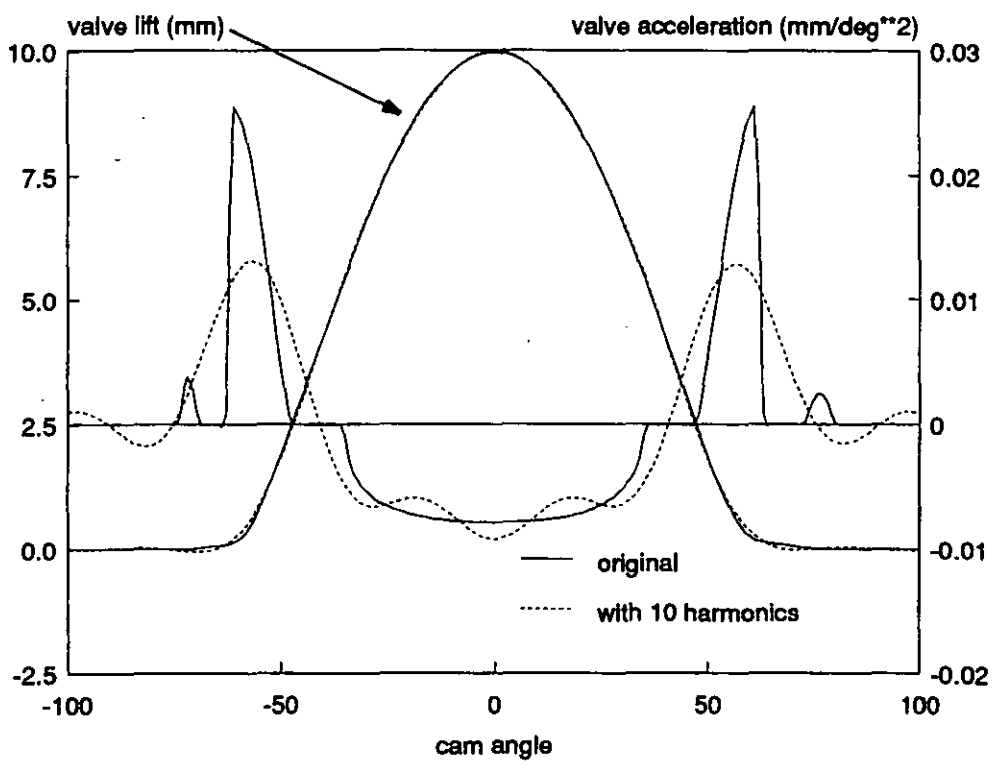

Figure 35: Comparison of original lift and acceleration with the lift and acceleration calculated using the first ten cam harmonics from the Fourier series

Modern valve springs are more or less exclusively made from raw material from Japan. The most commonly used materials for high performance valve springs is oil tempered wire made from either chrome silicon or chrome vanadium alloyed steel, with a trend towards CrSi material. A discussion on the benefits and drawbacks of the different materials and the different properties as well as the influence of the manufacturing process is given by Muhr (1993) and most of the following discussion of the manufacturing process is taken from there. However, since some aspects are discussed quite controversially between different manufacturers and the above mentioned author has a close relation to one of them, the following arguments include broader views from different spring manufacturers, expressed in informal discussions with the author. Since some of these aspects depend more on the specific manufacturing methods and expertise of different manufacturers than on engineering science, they should not be taken as hard facts.

The wire material and quality mainly determines the stress limits which can be utilised for the spring. Important points which have a detrimental effect on valve spring durability are surface defects and non-metallic inclusions. Influencing non-metallic inclusions is a task of the steel-works and the rolling mill and can thus not be influenced by the spring manufacturer. However, one measure to improve the wire performance is a shaving operation to remove surface defects.

The actual manufacturing process at the spring manufacturer starts with large coils of raw wire material. Depending on company standards this wire material is checked for the required specifications: chemical properties, mechanical properties, inclusions and surface defects. For non round wires some manufacturers claim to be able to inspect the surface as reliably as for round wire, while others state that the current technology does not allow it.

The first manufacturing process is the actual coiling of the springs. The raw wire is fed to a spring coiler. The displacement of the coiling tool which controls the pitch of the raw spring is either performed by a cam mechanism or by a numerically controlled system.

The accuracy at this stage can be very high for numerically controlled machines. Problems arise for non round section wires because of the importance of the wire feeding orientation during the coiling operation.

After the coiling, the material on the inside of the spring is upset and shortened by plastic deformation where the outside is extended and subjected to tensile stress. When the spring bounces back after coiling, the inhomogeneous changes to the wire shape causes residual tensile stresses at the inside of the spring. This residual stresses significantly lowers the

fatigue strength of the spring. To remove them, the raw spring is exposed to a stress relief heat treatment. To avoid any negative effect on the desired tensile strength, the annealing temperature must not exceed 430°C. The next step is the grinding of the ends to give a plane surface to seat on the retainer and in the cylinder head.

In a further operation the spring is shot peened. This operation increases the springs tolerance against surface defects and non-metallic inclusions close to the surface. As it is known the maximum tensile stress of a helical compression spring appears at the inner edge of the spring at the wire surface. The shot peening operation introduces compression stresses into the surface which prevents crack creation and propagation due to surface defects and non metallic inclusions. Here again non round wire material imposes an additional problem.

For round wire helical springs the location of maximum stress concentration is at the inner edge of the wire where the shot peening process can reach in a reliable and consistent manner. Non-round cross sections are used to increase the utilisation of the wire material. For an egg shape wire for example, this results in two areas of stress concentration at about 45° above and below the inner edge of the wire. Here the shot peening operation is partly shielded by the neighbouring coils, and is thus less efficient and reliable. The result of this, and the inability to have the same surface inspection, is that some manufacturers are hesitating to stress egg shape wire to the same limits as the same material for round wires.

A further step is a heat setting to ensure that the spring will not further weaken during normal operation.

For extremely highly stressed springs, some manufacturers have included a further special heat treatment by piece hardening and tempering which increases the allowable stress range. Since this piece hardening and non round wires cause a significant additional cost on valve springs, both options can be in competition for a high performance spring. If round wire can be stressed higher, a smaller wire diameter can be utilised, allowing for smaller installation envelope, more progressivity or higher frequency, depending on the way the additional design freedom is used. Egg-shape wire springs can be designed in a similar way. The lower height of an egg-shape wire compared to a round wire with the same torsional moment of inertia also allows for more progressivity or smaller installation envelope, and the better utilisation of the material results in less mass for the same stiffness allowing for a design with increased natural frequency. Although, from a purely technical point of view, both options could be combined for an even higher performance spring, this option is in most cases cost prohibitive. In cases where both options are in competition,

the arguments from different manufacturers are emphasised differently according to the specific manufacturing and process capabilities, rather than towards specific technical facts.

When the spring is ready, the heat treatment and heat setting has caused quite a substantial difference between the pitch characteristics of the raw coiled spring and the final product. For a linear spring however, this change takes place more or less uniformly along the spring. For extremely progressive springs it requires substantial experience to establish the right raw coiling to achieve the intended final product.

This short description is not meant to be a detailed description of spring manufacturing, but it is meant to aid the understanding of some of the manufacturing implications on spring design.

As a result of the above discussion, it is clear that the spring design process requires a lot of practical knowledge, which can not be achieved by analytical means. The list below summarises some of the arguments above, and states additional aspects which need to be taken into account in spring design.

Stress limits allowed for a durable spring The important factors here are material properties, manufacturing process, heat treatment and surface treatment. This is an area where a large amount of experience has been achieved by the spring manufacturer, where an easy knowledge transfer is not possible, and no simple analytical formulation is readily available.

Manufacturing capabilities for different spring suppliers This is quite variable. For example, one manufacturer claims to have a specific strength in the manufacturing and surface control for non round cross-section wire springs, while another has a specific knowledge and strength in heat and surface treatment.

Available wire types and dimensions In the past only round wire material has been used for valve spring coiling. This means a stress concentration in the inner edge of the spring and correspondingly an under utilisation of the rest of the material. To overcome this problem a number of different cross-sections for spring wire have been introduced, which essentially remove material from areas of the cross-section where lower stress levels exist. The most frequently used cross-section among these non round wires in Europe is an egg

shape wire, where one side is a half circle and the other half is elliptic. In general the available material alternatives are too many to keep track of all implications for the spring design.

Different design possibilities for pitch and diameter variations While the arguments above already create a complex task in the spring design for a standard cylindrical spring, the variation can be further increased by the utilisation of conical springs, bee-hive spring designs and various others coiling diameter and pitch variations. A set of examples of todays variation in spring design is shown in Figure 36. While the method used in Section 7.1 to calculate the frequency characteristic can be applied to all such variations, the number of parameters for a physical spring design, is too large to be chosen without a large amount of manufacturing and spring design experience.

So in general the number of possible design variables is extremely large. On the other hand it is required to formulate objective measures to link the spring response to a limited number of parameters to permit an efficient optimization. It has been mentioned that an infinite number of different springs can all have the same frequency characteristic. This can be understood from equations 5.1.10, 5.2.11 and 5.2.1.4. The same ratio of k/m can be achieved by an infinite number of combinations of coiling radius, torsional moment of inertia and number of active coils.

Furtunately, from the point of view of dynamic response, all one really needs to optimize is the springs frequency characteristic (see equation 6.2.1). Once the optimum for this has been determined, it is a second step to find a spring which has this characteristic. It is clear that the two tasks are not completely independent since not every frequency characteristic can be achieved in the limits of current spring technology. Working with the frequency characteristic directly though, permits one to significantly limit the number of optimization parameters. Hence the choice has been made to use the frequency characteristic to determine the optimization parameter space rather than the actual spring design.

Before an automated optimization algorithm is employed for this optimization task, it is important to first establish a basic understanding on the frequency characteristics which determine the response of a spring. For this purpose a statistical experiment on the springs dynamic response will be carried out.

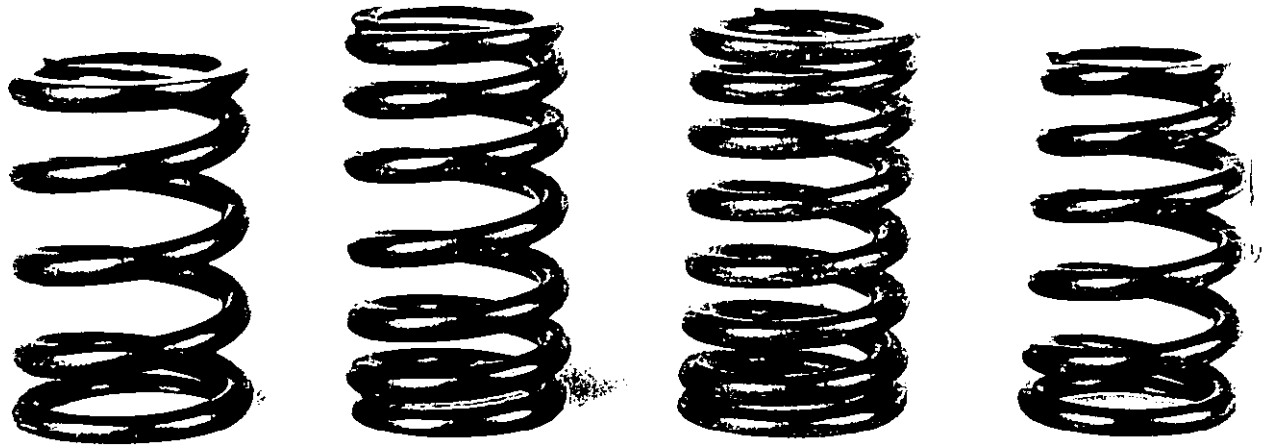

Figure 36: Four examples of different valve springs, from left to right, conventional linear spring, highly progressive round wire spring, egg-shape wire spring, and bee-hive spring

9

Effects of Spring Frequency Characteristics

In the last section it has been concluded that the key characteristic which determines the spring response is its frequency versus lift characteristic. The aim of this section is to investigate the influence of the spring frequency characteristic on the springs performance. This will be attempted by a statistical experiment. To do so, one first has to find a suitable parameterization of the spring frequency characteristic; this allows one to explore a wide envelope of possible designs by a limited number of influencing parameters with reasonable time and effort. Secondly an excitation has to be defined which is close to a realistic cam profile, but has well controlled properties. Thirdly the performance of the spring has to be assessed in an objective manner. For this purpose, a number of candidate performance measures will be defined, which quantify the springs ability to serve the design functions discussed in the introduction.

9.1 Parameterization

A simple and well-established numerical technique is offered by cubic parametric splines to represent the frequency characteristic of a hypothetical spring. These splines also offer the advantage that there is significant knowledge about their behaviour available (indeed the same splines have been used for a cam lift design program developed by the author (Schamel 1987)).

These splines link the valve lift s to the valve spring frequency f as follows:

$$\begin{aligned} s &= s(T) = K_1 + K_2 T + K_3 T^2 + K_4 T^3 \\ f &= f(T) = K_5 + K_6 T + K_7 T^2 + K_8 T^3 \end{aligned} \qquad T \in [0,1] \quad /9.1.1/$$

The necessary 8 equations for the 8 unknown K_i in the equations above can be calculated from the location of the spline end points (in this case lift and corresponding frequency) and from the tangent vector of the frequency characteristic at these points (in this case the rate of change in spring frequency at zero and maximum valve lift). From previous experience it is known that it is useful to use the angle of the tangent and the tangent length rather than the tangent vector directly. An example of a resulting frequency characteristic is given in Figure 37.

The behaviour of the spline can then be easily explained. The spline naturally passes the end definition points with the angle of the specified tangent vector. The longer the tangent vector the longer the spline follows this angle.

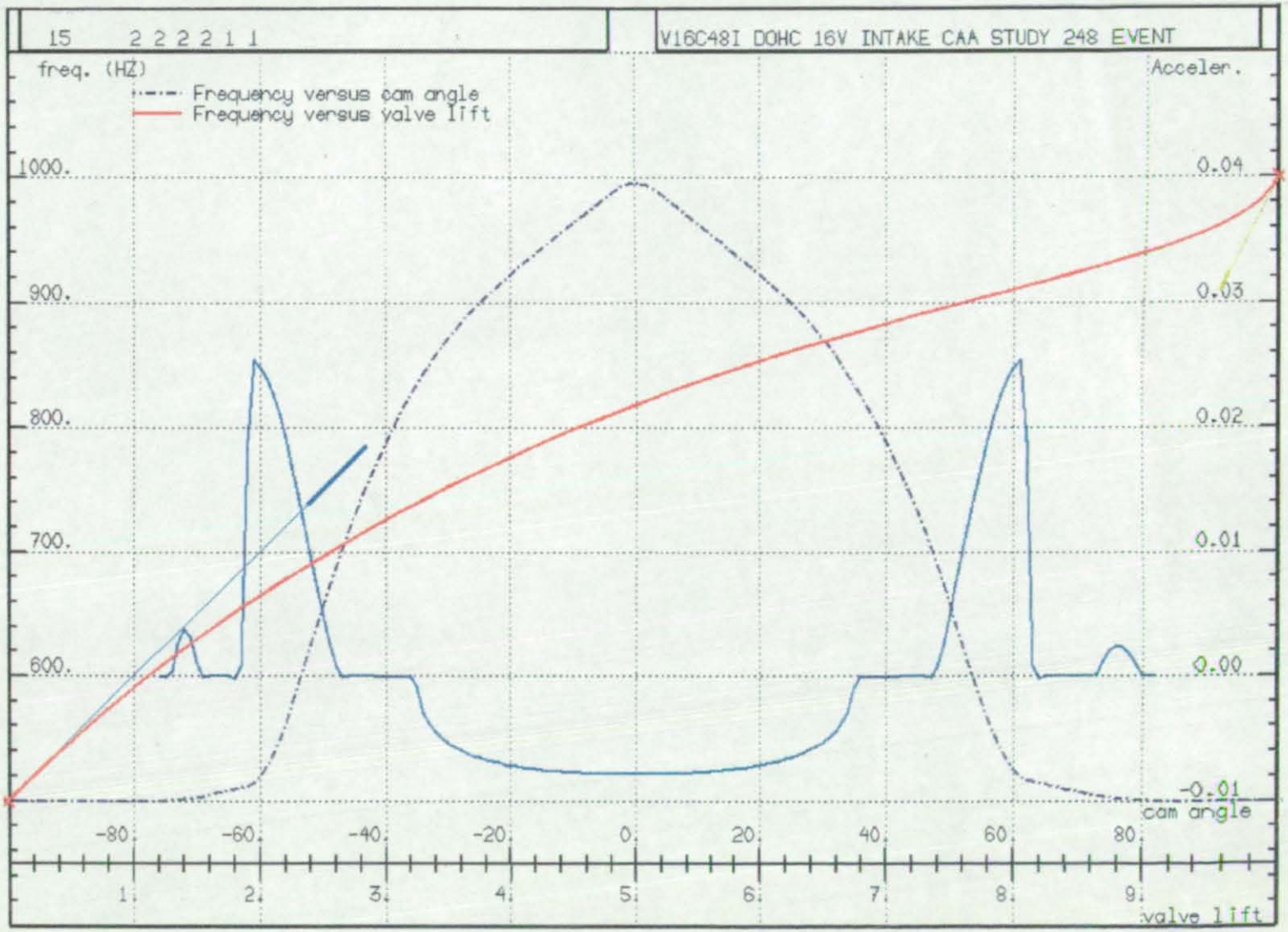

Figure 37: Example of a frequency characteristic resulting from the representation by parametric cubic splines (light blue curve: valve acceleration)

Limiting the spring frequency characteristic to one spline section, leads to the 8 parameters discussed above which define the characteristic of the spring frequency - see Table 1.

Parameter	Unit	Physical Meaning
s_1	mm	displacement for base circle frequency (lift for installed height)
s_2	mm	displacement for valve open (maximum valve lift)
f_1	Hz	installed height frequency (at s_1)
f_2	Hz	valve open frequency (at s_2)
df/ds_1	Hz/mm	slope for tangent vector in s_1 (rate of frequency change in point s_1)
df/ds_2	Hz/mm	slope for tangent vector in s_2 (rate of frequency change in point s_2)
Rf_1	-	relative length of tangent vector in point s_1
Rf_2	-	relative length of tangent vector in point s_2

Table 1

The number of free parameters can be further reduced by keeping some of them fixed at suitable levels. s_1 can be fixed to zero lift, s_2 can be set to maximum valve lift for a given profile, in this case 10mm. Since it is also known *a priori* that a complete shift of the frequency characteristic only shifts the corresponding response in the speed range, the base spring frequency at valve closed position, f_1, was held constant at 500Hz. However keeping this value fixed is only useful for the purpose of this pre-study, since shifting the response in speed can be a major tool for optimizing a spring for a given valvetrain configuration.

The remaining parameters have been varied, to assess their effects, in a two level experiment. The formal statistical analysis of this experiment allows one to identify the influence and importance of any of the varied parameters as well as the influence of parameter interactions. The basics of the two level full-factorial experiment used here, together with an example how the effects of a single parameter are calculated, are outlined in the Appendix (Section 15.2).

The parameters for the study are as follows:

Parameter	Physical Meaning	Label	Level 1	Level 2
f_2	Frequency at valve open position	A	750	1000
df/ds_1	Slope of frequency characteristic at 0mm valve lift	B	0	100
df/ds_2	Slope of frequency characteristic at max (10 mm) valve lift	C	25	200
Rf_1	Relative length of tangent vector at 0mm valve lift	D	0.5	2.0
Rf_2	Relative length of tangent vector at max valve lift	E	0.5	2.0
cam 1/ cam 2	Cam profile used as excitation	F	cam 1	cam 2

Table 2

For the identification of the chosen levels in this factorial experiment the run number and the corresponding levels can be found in table 3 (cam 1) and 4 (cam 2). The properties of the two used excitations cam 1 and 2, parameter F, are explained in the next section.

Using the parameters A to E above at the two specified levels, a full factorial experiment has been carried out, i.e. the above set of parameters has been used in all combinations giving $2^5 = 32$ different characteristics for each cam profile. The two values used for each parameter have been chosen under two considerations:

a) Not to limit the design envelope too much into the direction for a fully realistic spring design. This has been done to avoid missing any insight of effects at the border of a "traditional" spring design.

b) On the other hand the parameters have been limited to a range which avoids frequency characteristics which are totally impossible. For example the frequency has to increase with lift, and the slope at 0 lift may not approach extremely large values.

The parametric splines are used for all parameter combinations, in a way that local scaling is applied to the frequency (f) and the lift (s). So whatever the real distance between point 1 and 2 of the spline definition is, they are modified to give $\Delta f/\Delta s = 1$ and a distance of 1. This decouples the effects of tangent vector direction and length from the lift and frequency position, and thus avoids interactions in the design parameters not coming from the spring response but from the splines definition.

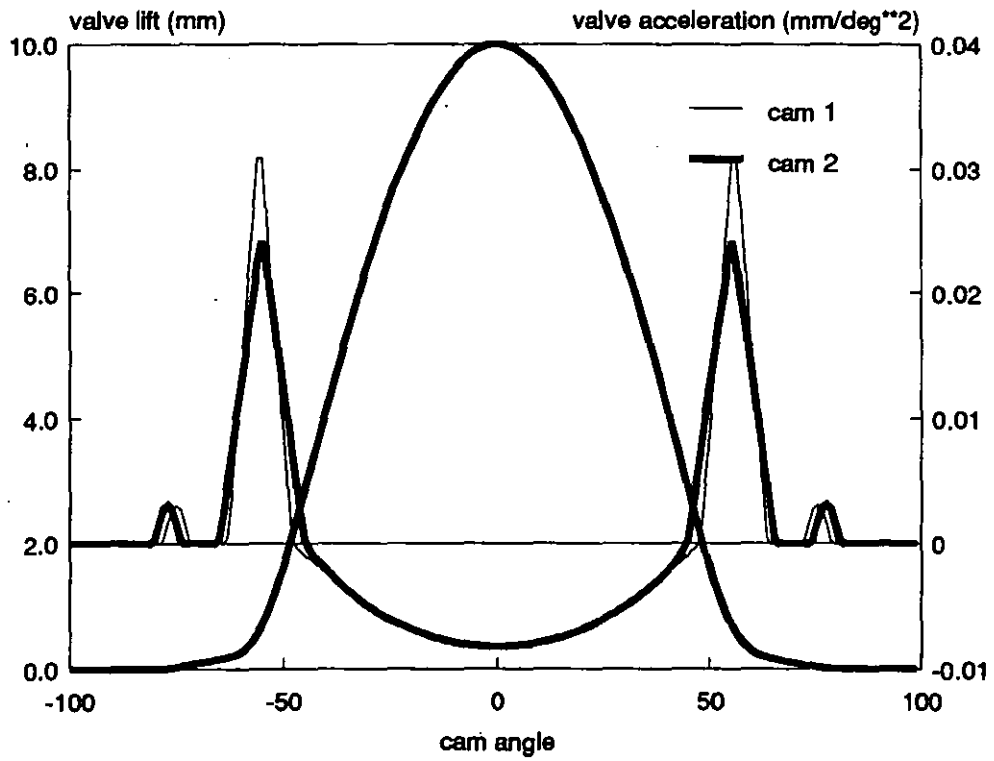

Figure 38: Graph of the two cam profiles used for the statistical study to investigate the basic influences on the springs dynamic response

9.2 Excitations

For the excitation, two special cam/valve lift profiles have been generated (Figure 38). They are more or less realistic profiles for a bucket tappet 16valve cylinderhead like the one shown in the results of the correlation in Section 7, but feature specific characteristics. The acceleration phases of the two profiles consist of two ramp inputs and are both fully symmetric. The first profile (cam 1) has an acceleration peak duration of 15 degree camshaft, the second one (cam 2) of 20 degree camshaft. This would result in a full cancellation of any vibrations for a simple one mass model of a valvetrain with 1800Hz/2400Hz frequency at 6000 rpm (this is a typical range for a 16 valve bucket tappet valvetrain). The profiles are designed to have almost the same deceleration period to give comparable results on the spring force reserve, and as close as possible the same lift curve to give the same force levels. In the factorial experiment the variation of the two profiles is labelled as parameter F; however, the formal analysis has been restricted to parameters A-E.

Figure 39 shows the resulting frequency characteristics for the above described parameter combinations for both profiles. As can be seen, they cover a wide range of significantly different shapes. All these combinations have been used to calculate the dynamic response of the "artificial" springs.

While for the surge mode amplitude only the frequency is important, the force results for the real spring depend also on the springs preload and rate. A complication arises from the fact that the local spring rate is directly proportional to spring frequency. This would mean that a spring with higher progressivity would result in larger forces leading automatically to a better spring force reserve and a deterioration of the friction level. On this basis the different "artificial" springs are not comparable. To resolve this, all spring characteristics have been normalized to give the same stored energy under the valve lift of the profile, keeping the proportional relation between rate and frequency.

$$W = \int_s F(s)ds = constant \qquad /9.2.1/$$

and

$$f(s)_{spr} \propto k(s)_{spr} \qquad /9.2.2/$$

This makes it possible to track changes in the frequency response also back to performance measures like spring force reserve.

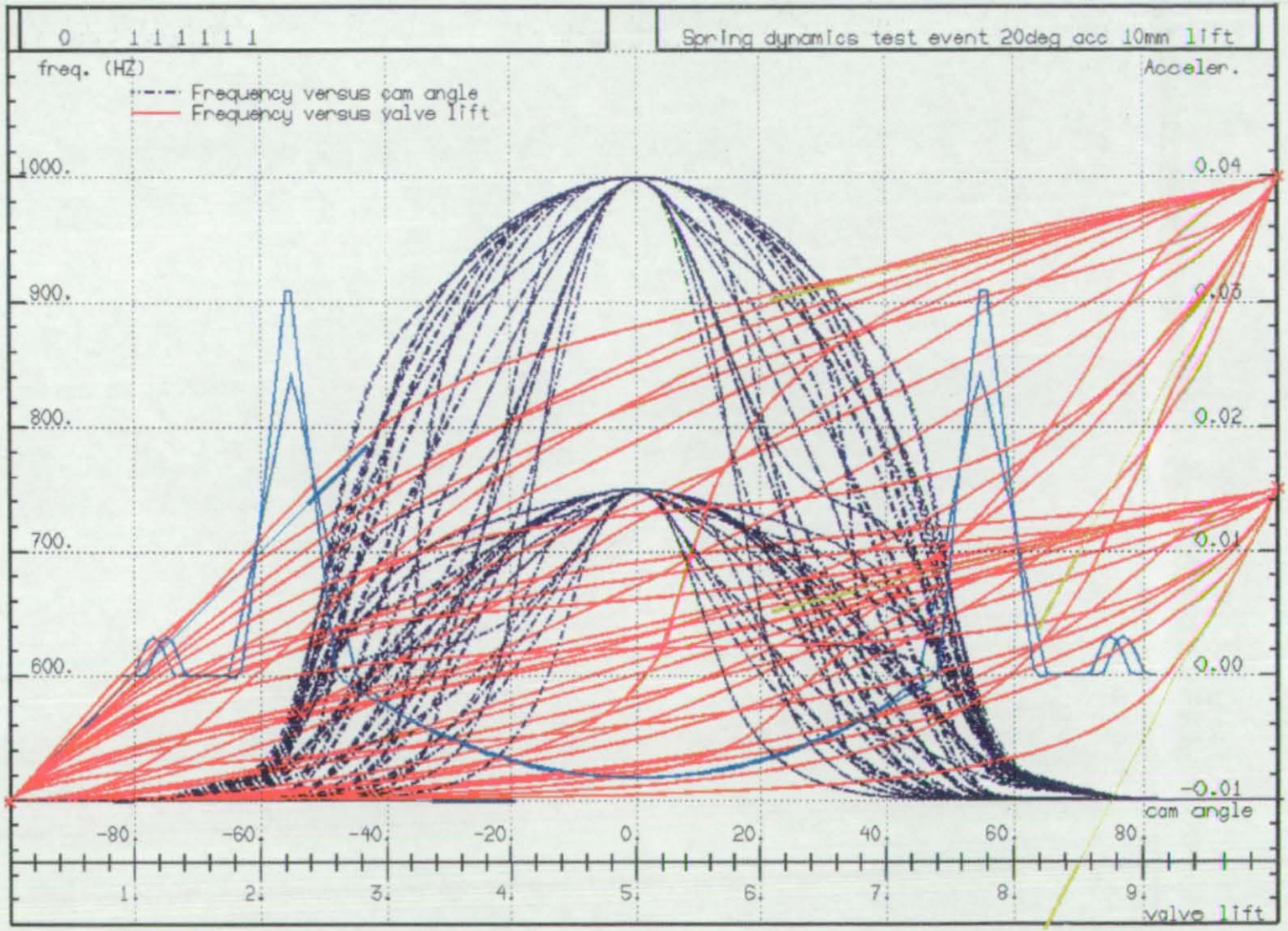

Figure 39: Envelope of frequency characteristics used for the statistical experiment. Red curves: frequency against valve lift, dark blue curves: frequency against cam angle, light blue: corresponding valve acceleration against cam angle

9.3 Preliminary Discussion of Results

The next step is to judge informally the different responses for the various spring frequency characteristics. A useful characteristic of the response is the maximum surge amplitude at each speed point. It is a direct measure of the dynamic deviation from the kinematically expected spring response. A surface plot of this characteristic over speed for all parameter combinations is shown in Figure 40a. While this gives a "nice" impression of the different dynamic responses, this plot is not too useful to locate and trace back any specifically good or bad combination. In this respect Figure 40b is one step better. This Figure depicts the projection of Figure 40a on the plane given by run number and speed. Blue colour represents low surge amplitude, and red to yellow colour indicates large amplitudes.

A number of effects can be seen from this plot. It can be noted that the average amplitude for cam 2 is smaller than for cam 1. This suggests that there is a significant influence on the spring response by the cam design. This is only partly true though. In spite of the effort to keep the two used profiles as close a possible, they already represent a difference that would not be achievable under practical constraints. As previously noted, they have the same lift, but they do not have the same event. This significantly effects idle quality of the engine and torque/power trade-off over speed. Hence, in practice achievable differences in the exciting cam acceleration would be much smaller. Furthermore looking at an example of the isolated surge characteristics for the same spring parameters for both profiles in Figure 41 reveals that the response is not really that much different. The overall amplitude for cam 2 is lower but the location and character of resonances is the same. This low influence of cam profile modification on the spring response was already apparent in the results from Section 4 and here is another case where the relatively low harmonics of the cam profile responsible for the spring response are more or less dependent on broad characteristics of the profile, such as total event, lift, and the distance between the acceleration peaks.

More interesting than the influence of the cam profile on the response, is the observation that there is some regular pattern in the response plot. This indicates that some of the chosen parameters seem to have always a similar influence, independent of other parameters. If this can be verified, quite simple guide-lines for the spring design might be derived.

Furthermore, one can note that the various parameter combinations not only influence the amplitude of the response, but also shift the speed positions for the local resonances. This is an indication that there is a possibility to avoid coincidence of spring resonance and resonance of the rest of the valvetrain. If this is possible without modifying the springs fundamental natural frequency, this gives additional design freedom to match a spring to a given valvetrain configuration.

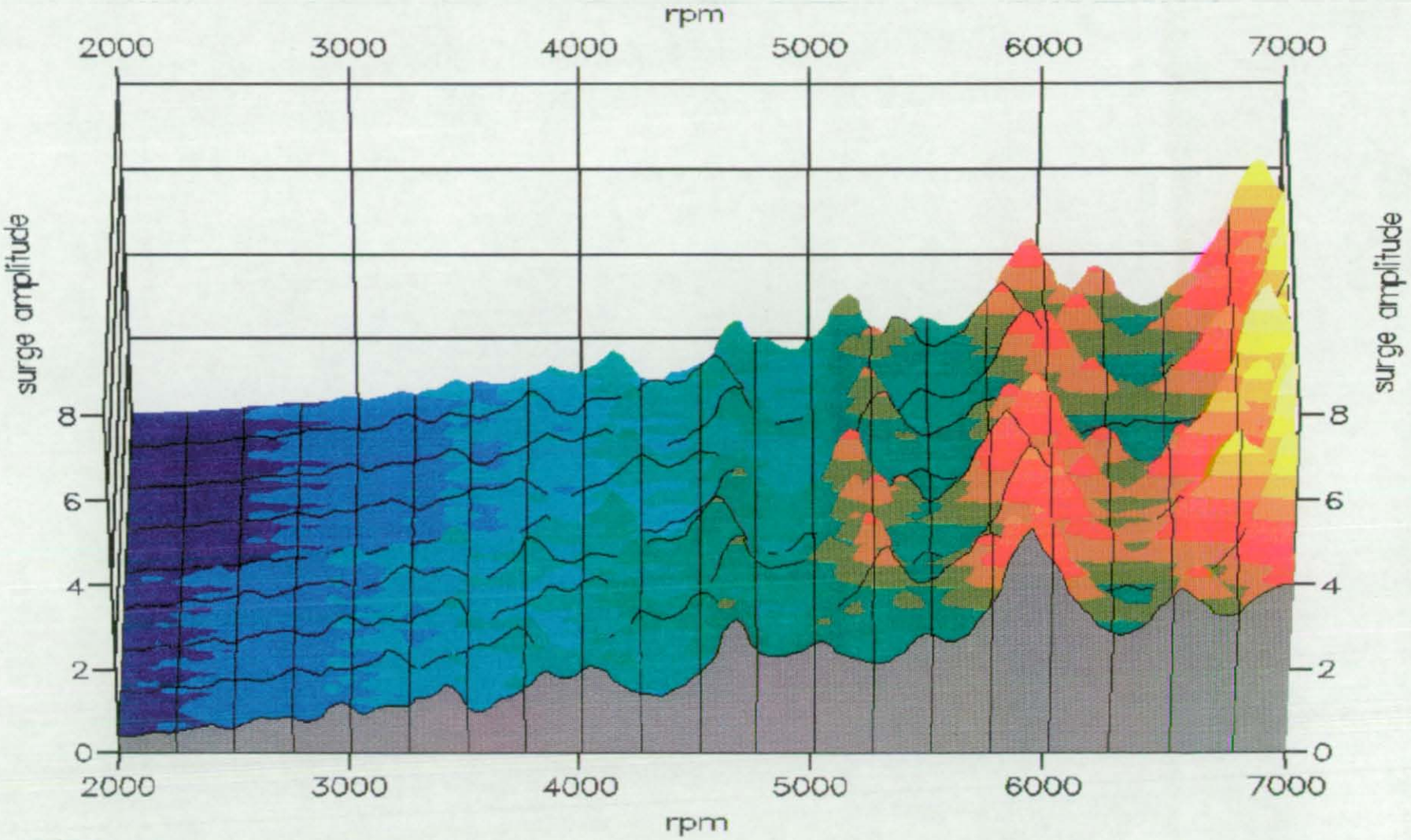

Figure 40a: Surface plot of spring surge extremes against engine speed for all parameter combinations from the statistical experiment

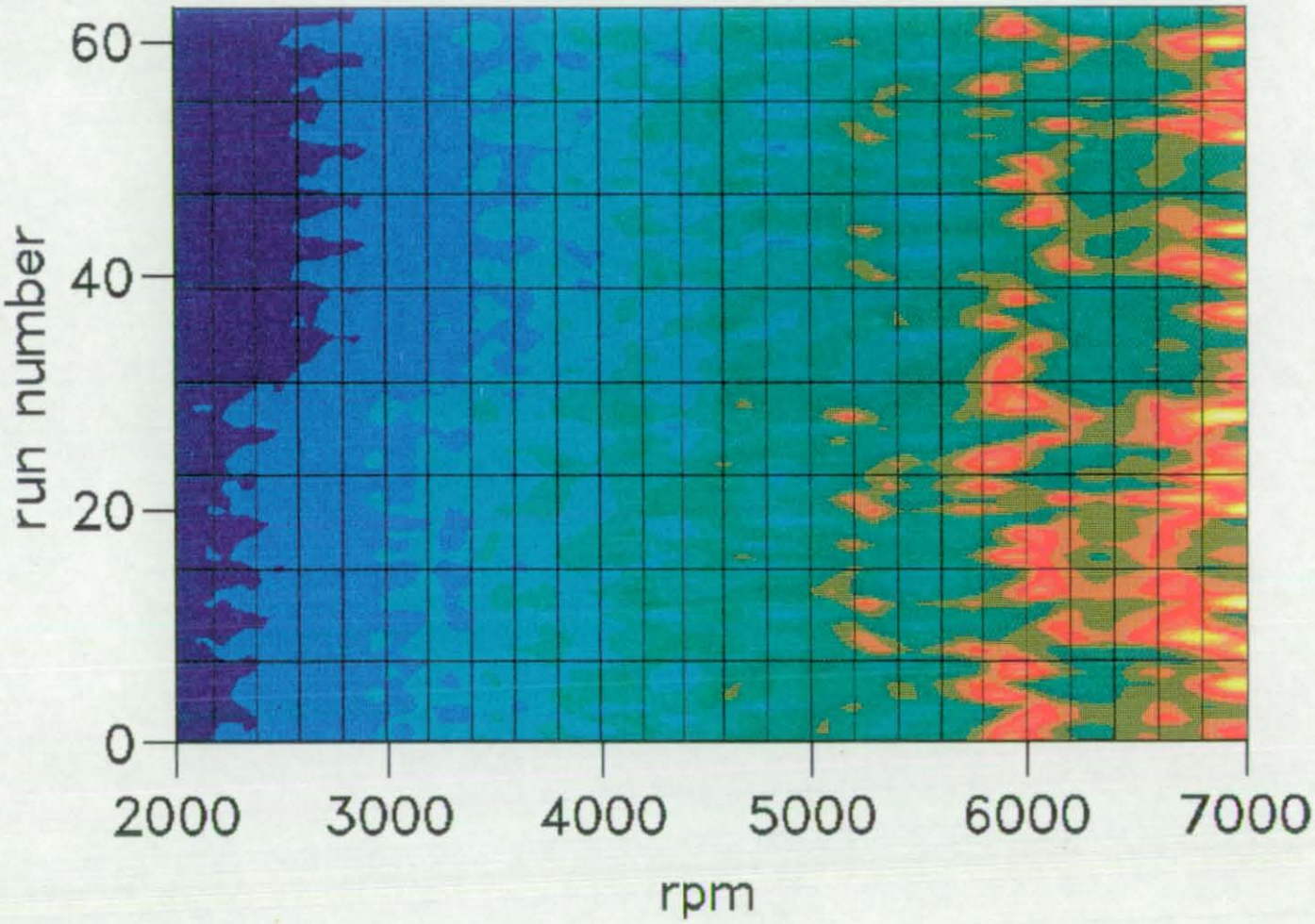

Figure 40b: Projection of Figure 40a on the speed / parameter combination plane. Amplitude represented by colour. Dark colour: low amplitude , bright colour: high amplitude

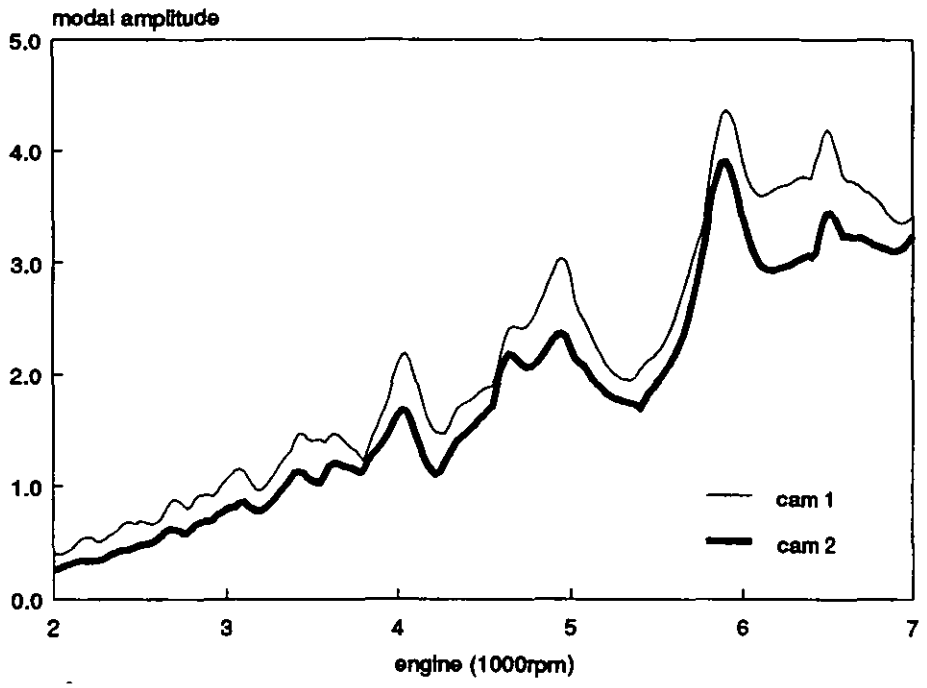

Figure 41: Comparison of modal amplitude against speed for the same frequency characteristic using cam 1 and cam 2 from Figure 37

9.4 Definition of Performance Measures

Although Figures 40a and 40b clearly showed that there are differences in the response due to the different frequency characteristics, a more formalised method is required, to make the problem accessible for both a statistical evaluation and later on for an automatic optimization; it is therefore necessary to introduce a number of measures which quantify the relative merits of any parameter combination. As has been shown, the location of the spring surge resonance moves due to changes in the spring characteristic. (There is also a clear tendency for a resonance at 6000 rpm, which is no surprise since a linear spring with the chosen 500Hz installed frequency would perfectly resonate with the 10th order of the cam profile at 6000 rpm). Because of this, using a fixed position in speed to quantify the spring performance would lead to misleading conclusions. On the other hand, as mentioned previously, the position in speed for some of the results may be important to the overall performance of the valvetrain.

A number of candidate measures are now introduced, to enable both the assessment of the overall response of the spring and the influence of the relative speed and cam angle location of the values. These measures are:

1 Area under the spring surge mode maximum amplitudes

$$P_1 = \sum_{speed} \max_{\phi}\left(\sum_n G_n(\phi)\right) \qquad /9.4.1/$$

This gives an overall figure for the amount of vibration in the spring. Here $G_n(\phi)$ represents the spring vibration amplitude for the n'th harmonic, and is implicitly dependent on engine speed

2 Area under the squared spring surge mode maximum amplitudes

$$P_2 = \sum_{speed}\left(\max_{\phi}\left(\sum_n G_n(\phi)\right)\right)^2 \qquad /9.4.2/$$

This is similar to P_1 but giving more emphasis to extreme values

3 The absolute maximum spring surge amplitudes occurring in the investigated speed range

$$P_3 = \max_{speed}\left(\max_{\phi} \sum_{n} G_n(\phi)\right) \qquad /9.4.3/$$

This measures the worst spring response observed

4 Position in the speed range (in engine rpm) for performance figure 3

$$P_4 = speed\left(\max_{speed}\left(\max_{\phi} \sum_{n} G_n(\phi)\right)\right) \qquad /9.4.4/$$

This, together with P_3, gives an indication where problems are to be expected.

5 Area under maximum dynamic force for each speed (expressed by overshoot above static maximum force)

$$P_5 = \sum_{speed} \max_{\phi}(F(\phi)_{dyn} - F_{\max_{static}}) \qquad /9.4.5/$$

This is mainly linked to the surge mode extremes but also takes into account the cam angle at which the surge extremes take place.

6 Area under minimum dynamic force for each speed (expressed by undershoot below installed height static force)

$$P_6 = \sum_{speed} \min_{\phi}(F(\phi)_{dyn} - F_{preload}) \qquad /9.4.6/$$

This is similar to P_5 and gives a clear indication of any tendency of the valve to reopen on the base circle because of insufficient residual force.

7 Absolute maximum dynamic force in the investigated speed range (expressed by overshoot above static maximum force)

$$P_7 = \max_{speed}(\max_{\phi}(F(\phi)_{dyn} - F_{\max_{static}})) \qquad /9.4.7/$$

This is an indication of the worst case peak force in the speed range.

8 Speed location for P_7

$$P_8 = speed(\max_{speed}(\max_{\phi}(F(\phi)_{dyn} - F_{\max_{static}}))) \qquad /9.4.8/$$

This figure allows one to investigate any coincidence of spring problems and valvetrain vibrations

9 Absolute minimum dynamic force (expressed by undershoot below installed height static force)

$$P_9 = \min_{speed}(\min_{\phi}(F(\phi)_{dyn} - F_{preload})) \qquad /9.4.9/$$

This indicates the worst case situation for valve re-opening in the speed range

10 Speed location for P_9

$$P_{10} = speed(\min_{speed}(\min_{\phi}(F(\phi)_{dyn} - F_{preload})_{speed})) \qquad /9.4.10/$$

This figure again allows one to investigate a coincidence of spring problems and valvetrain vibrations

11 Location of median speed, with respect to the area under spring surge extremes

$$\sum_{speed=\min}^{P_{11}} \max_{\phi}\left(\sum_{n} G_n(\phi)\right) = \sum_{P_{11}}^{\max} \max_{\phi}\left(\sum_{n} G_n(\phi)\right) \qquad /9.4.11/$$

This gives an indication whether the complete response is shifted in the speed range by any parameter combination.

12 Maximum local difference between a resonance peak and an out of resonance valley for the spring surge mode extremes.

$$P_{12} = \max\left(\left(\max_{i_{speed}}\left(\max_{\phi}\sum_{n} G_n(\phi)\right)\right) - \left(\min_{i\pm1_{speed}}\left(\max_{\phi}\sum_{n} G_n(\phi)\right)\right)\right) \quad /9.4.12/$$

i denoting the i'th local surge maximum in speed.

This gives an indication how critical a small change in speed might be for the response of the complete valvetrain. This results from the observation that in practice sometimes small design changes result in catastrophic results, because most of the durability tests are done at a set of fixed speeds. So a small change in the design might bring the valvetrain out of or into serious trouble. This figure gives some indication about the robustness against this kind of effect.

13 Total residual area between valve deceleration and spring deceleration capacity.

$$P_{13} = \sum_{\phi}\left(\min_{speed}\left(\min_{\phi}\left(\frac{F(\phi)}{m_{red}\omega^2} + \frac{d^2h(\phi)}{d\phi^2}\right)\right)\right) \quad /9.4.13/$$

This measure can be understood from Figure 42. The dotted line is the valve acceleration and the area of solid lines is the spring deceleration capacity, with one line for each speed. Since the spring deceleration capacity (in mm/deg^2) depends on engine speed, one has an automatic weighting function for the position in speed, where resonances occur. In other words large amplitudes at low speeds do not cause any harm, since the valvetrain needs only small forces at low speeds for deceleration. The total remaining area between the set of deceleration capacity lines and the valve deceleration (shaded area) is now a measure for the quality of the match between spring and camshaft/valvetrain configuration. A cross-over of a spring deceleration capacity line with the valve deceleration means a loss of contact in the valvetrain with all its associated negative effects.

This figure furthermore lends itself to the next step of automatic optimization. So far the spring response has been calculated decoupled from the rest of the valvetrain by excitation through the kinematic valve acceleration. If the coupled system is used instead, one gets an automatic interaction between speeds where valvetrain vibrations represent a problem and the spring response at these speeds. Since this would be prohibitive in terms of cpu time in the moment, an intermediate step can be done by the assumption that the two systems are still decoupled, but using the dynamic valve acceleration for an initial spring configuration varied with speed, rather than using the kinematic valve acceleration.

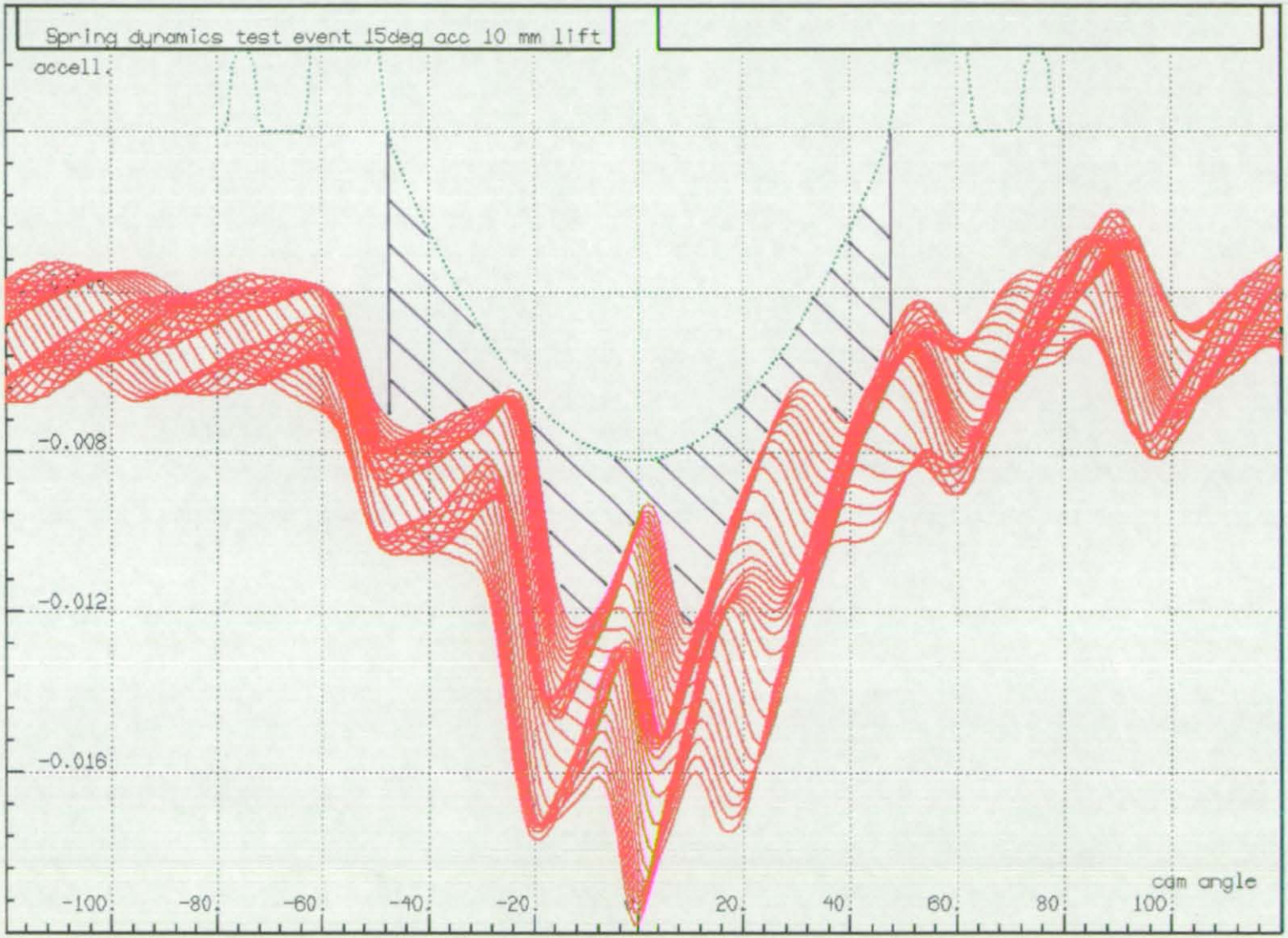

Figure 42: Sketch illustrating the spring force reserve area (performance Figure 13)

9.5 Preliminary Analysis of the Performance Measures

The above quantities P_1 - P_{13} have been calculated for all parameter combinations representing the design envelope shown in Figure 38. The results are given in Table 3 for cam 1 (runs 0 to 31) and in Table 4 for cam 2 (run 32 to 63). For the subsequent plots of this section the force minimum results have been taken as absolute values to give the same direction for advantageous and disadvantageous combinations in the plots.

Figure 43 shows the first three performance figures against the run number. It can be noted that there are significant differences in these figures for the different parameter combinations. This means that response can be influenced by a change in the frequency characteristic, which is the most basic requirement to have any hope of optimizing a spring design to a given valvetrain configuration. It can also be seen that combinations performing well show less spread in all three performance figures, compared with less advantageous combinations (one has to be careful with this conclusion because of the different scaling, and zero suppression in the plot).

Figure 44 shows a plot of the force performance measures (5,6,7,9) again showing a significant difference among the different spring designs.

Figure 45 shows the location in the speed range for the performance measures 4,8,10, and 11. It seems that one has broadly two ranges for the combinations. One range showing its worst response around the resonance speed for a linear spring, and the second showing worst behaviour towards the end of the speed range. Also among these two groups a speed shift of 200-300rpm can be observed, going from one parameter combination to the next.

As expected the median speed of the surge area does not move too much, but the observable variation verifies that there is some influence on how early a spring starts to resonate.

Figure 46 shows the maximum local change in surge amplitude. A low value in this figure does not necessarily mean a good spring design, because it could mean a merely constant high surge amplitude, but a low figure means to have only moderate surge changes due to small speed variations, thus quantifying the robustness (even if this means a "robust" catastrophe !).

Figure 47 shows the results for the spring force reserve area. In this plot large values represent an advantageous design, while small numbers indicate a tendency to loose contact between the valvetrain components. As it can be seen there is a variation of almost 100%, encouraging the hope for effective optimization by modification of the spring frequency characteristic.

NR	PARCOMB ABCDEF	SUM MOD	SUM**2 MOD	GNMA	RPM	SUM MAX F	SUM MIN F	FMAX	RPM	FMIN	RPM	MEDSP	MAXDR	MINSPRES
0	111111	433.10	1219.0	5.347	5925	7206	-11157	124.77	5925	-168.57	5975	5500	2.67	0.20417
1	211111	408.20	1084.2	4.933	5925	7929	-9225	144.50	7000	-132.02	5975	5500	2.54	0.21313
2	121111	407.20	1101.2	4.989	6025	6368	-10384	108.34	6000	-146.06	6075	5550	3.08	0.19693
3	221111	369.90	900.0	4.292	6075	6255	-8073	100.91	6675	-106.87	6125	5500	2.54	0.22180
4	112111	430.80	1197.7	5.177	5875	7223	-11173	123.90	5875	-168.28	5925	5475	2.62	0.19879
5	212111	421.20	1218.5	6.948	6975	8840	-9920	187.49	6950	-191.16	7000	5525	4.07	0.17279
6	122111	407.80	1092.7	5.109	5975	6396	-10328	112.79	5975	-154.95	6025	5525	2.64	0.20626
7	222111	369.80	893.0	4.468	5950	6805	-8126	126.38	7000	-121.39	6000	5500	2.18	0.22176
8	111211	442.70	1282.5	6.572	7000	7941	-11742	181.40	7000	-177.60	7000	5475	2.20	0.16356
9	211211	472.40	1546.9	6.530	6775	10470	-12405	212.51	6800	-214.62	6825	5600	2.87	0.13975
10	121211	394.80	1075.8	4.878	6750	5660	-9541	109.38	6750	-150.08	6750	5600	2.25	0.18614
11	221211	366.00	905.0	4.509	6725	5559	-7664	110.78	6750	-117.60	6725	5550	1.87	0.20900
12	112211	456.50	1417.0	7.688	7000	7801	-11900	188.15	7000	-243.56	7000	5500	2.27	0.14591
13	212211	448.10	1333.3	5.217	6050	10211	-12416	158.44	6675	-173.48	6650	5525	3.16	0.17035
14	122211	392.20	1050.3	4.607	6700	5692	-9642	103.58	6725	-143.76	6700	5600	2.98	0.19105
15	222211	359.80	857.6	4.187	6100	5765	-7696	96.98	6675	-101.91	6625	5500	2.18	0.22257
16	111121	435.40	1234.9	5.382	5950	7254	-11254	124.01	5950	-167.32	6000	5525	2.74	0.20369
17	211121	410.90	1101.9	4.499	6075	7018	-8979	119.08	6650	-116.37	6625	5500	2.28	0.21212
18	121121	403.90	1081.8	4.989	6025	6318	-10288	108.35	5975	-147.39	6050	5550	2.74	0.19925
19	221121	355.30	858.1	4.403	6725	5317	-7399	105.56	6750	-114.48	6725	5575	1.86	0.21102
20	112121	446.50	1327.2	7.336	7000	7751	-11731	184.16	7000	-210.63	7000	5475	2.35	0.15641
21	212121	461.50	1459.4	5.926	6725	10119	-12281	190.29	6775	-203.95	6775	5575	2.28	0.15166
22	122121	410.30	1090.3	5.007	7000	6763	-10656	125.04	7000	-152.75	5850	5450	2.14	0.18819
23	222121	416.70	1237.5	6.444	6875	8550	-10122	181.21	6900	-194.32	6925	5600	3.40	0.15860
24	111221	432.60	1213.9	5.148	5850	7741	-11621	128.69	5875	-175.40	5875	5475	2.69	0.18988
25	211221	417.40	1136.6	5.852	7000	8644	-9968	174.35	7000	-146.55	5900	5475	2.19	0.19033
26	121221	383.00	1002.9	4.481	6100	5521	-9377	98.96	6725	-139.04	6700	5600	2.89	0.19267
27	221221	366.30	927.4	4.837	6775	5204	-7391	111.98	6800	-122.72	6775	5600	1.68	0.20582
28	112221	479.60	1625.7	7.597	6900	8356	-13270	195.80	6925	-271.93	6950	5575	4.25	0.12183
29	212221	450.90	1320.5	5.426	5950	10461	-12173	167.04	5950	-184.42	6000	5500	2.74	0.18281
30	122221	383.40	963.6	4.810	5950	5680	-9428	105.38	5925	-146.82	5975	5525	2.33	0.21148
31	222221	353.40	830.9	5.452	7000	6643	-7786	142.68	7000	-119.77	7000	5475	2.10	0.21139

Table 3

NR	PARCOMB ABCDEF	SUM MOD	SUM**2 MOD	GAMA	RPM	SUM MAX F	SUM MIN F	FMAX	RPM	FMIN	RPM	MEDSP	MAXDR	MINSPRES
32	111112	356.20	846.3	4.522	5925	4874	-8583	99.82	5950	-140.77	5975	5525	2.36	0.20186
33	211112	333.10	744.5	4.274	7000	5821	-7118	125.85	7000	-110.09	5950	5525	2.11	0.20877
34	121112	331.90	753.1	4.341	6025	4118	-7807	88.50	6000	-124.93	6050	5600	2.26	0.20545
35	221112	291.80	581.2	3.752	6075	4233	-5923	77.45	6075	-90.52	6100	5575	2.58	0.22568
36	112112	352.40	826.7	4.270	5875	4817	-8562	95.83	5900	-138.24	5900	5500	2.30	0.19335
37	212112	356.70	917.8	6.157	6975	6557	-7901	162.78	6975	-176.17	7000	5600	3.50	0.17129
38	122112	331.30	740.4	4.307	5975	4107	-7769	90.63	5975	-129.30	6000	5550	2.16	0.20728
39	222112	294.30	583.5	3.728	7000	4728	-6078	104.98	7000	-96.79	5975	5525	1.99	0.21688
40	111212	378.40	986.0	6.361	7000	5431	-9154	166.44	7000	-176.17	7000	5550	2.16	0.15856
41	211212	395.30	1125.5	5.500	6775	8049	-10180	177.72	6825	-184.26	6825	5675	2.17	0.14812
42	121212	313.90	705.5	3.895	6150	3591	-7130	77.62	6750	-115.48	6750	5675	2.65	0.19397
43	221212	289.10	585.3	3.415	6675	3699	-5679	81.41	6775	-88.86	6725	5625	1.65	0.21572
44	112212	392.90	1109.7	6.980	7000	5431	-9694	175.25	7000	-230.29	7000	5575	1.73	0.14359
45	212212	372.00	949.4	4.692	6050	7500	-9651	132.01	6025	-145.57	6075	5600	2.86	0.18180
46	122212	313.50	693.5	4.022	6100	3579	-7158	75.31	6075	-108.37	6700	5675	2.67	0.19886
47	222212	282.00	545.7	3.615	6100	3795	-5582	69.01	6075	-84.12	6125	5575	2.48	0.22724
48	111122	359.80	865.1	4.593	5950	4951	-8687	101.88	5950	-142.23	5975	5550	2.34	0.20352
49	211122	333.30	750.4	4.082	6075	5043	-6848	88.58	6675	-95.86	6125	5575	2.67	0.21998
50	121122	328.60	736.4	4.292	6025	4053	-7719	88.79	6000	-125.62	6050	5600	2.16	0.20709
51	221122	278.70	545.8	3.298	6200	3448	-5411	76.55	6775	-85.01	6725	5625	1.59	0.21750
52	112122	384.30	1039.4	6.819	7000	5305	-9319	169.79	7000	-205.42	7000	5550	2.05	0.15272
53	212122	381.90	1037.9	4.956	6725	7617	-9883	154.17	6775	-170.11	6775	5675	2.15	0.16073
54	122122	340.10	778.8	4.784	7000	4246	-8023	106.47	7000	-121.59	7000	5500	2.05	0.18294
55	222122	344.40	878.8	5.400	6875	6128	-8016	145.83	6900	-164.59	6925	5675	2.56	0.16404
56	111222	356.10	851.9	4.347	7000	5262	-8936	109.07	7000	-142.74	5875	5500	2.15	0.18526
57	211222	340.90	794.1	5.527	7000	6596	-7893	158.95	7000	-146.95	7000	5500	2.03	0.18591
58	121222	305.00	655.8	3.927	6100	3374	-6872	72.96	6075	-104.71	6125	5675	2.57	0.20043
59	221222	288.70	592.8	3.816	6725	3409	-5485	82.11	6800	-93.81	6775	5650	1.48	0.21199
60	112222	405.40	1227.1	6.618	6900	5920	-10834	176.13	6925	-238.27	6950	5700	3.49	0.12477
61	212222	373.20	935.1	4.665	5950	7750	-9497	140.74	5975	-159.58	6000	5550	2.48	0.18517
62	122222	303.90	621.4	3.938	5950	3344	-6872	79.81	5950	-116.70	5975	5525	2.17	0.20608
63	222222	285.50	566.1	4.793	7000	4468	-5767	115.55	7000	-110.12	7000	5550	1.49	0.20836

Table 4

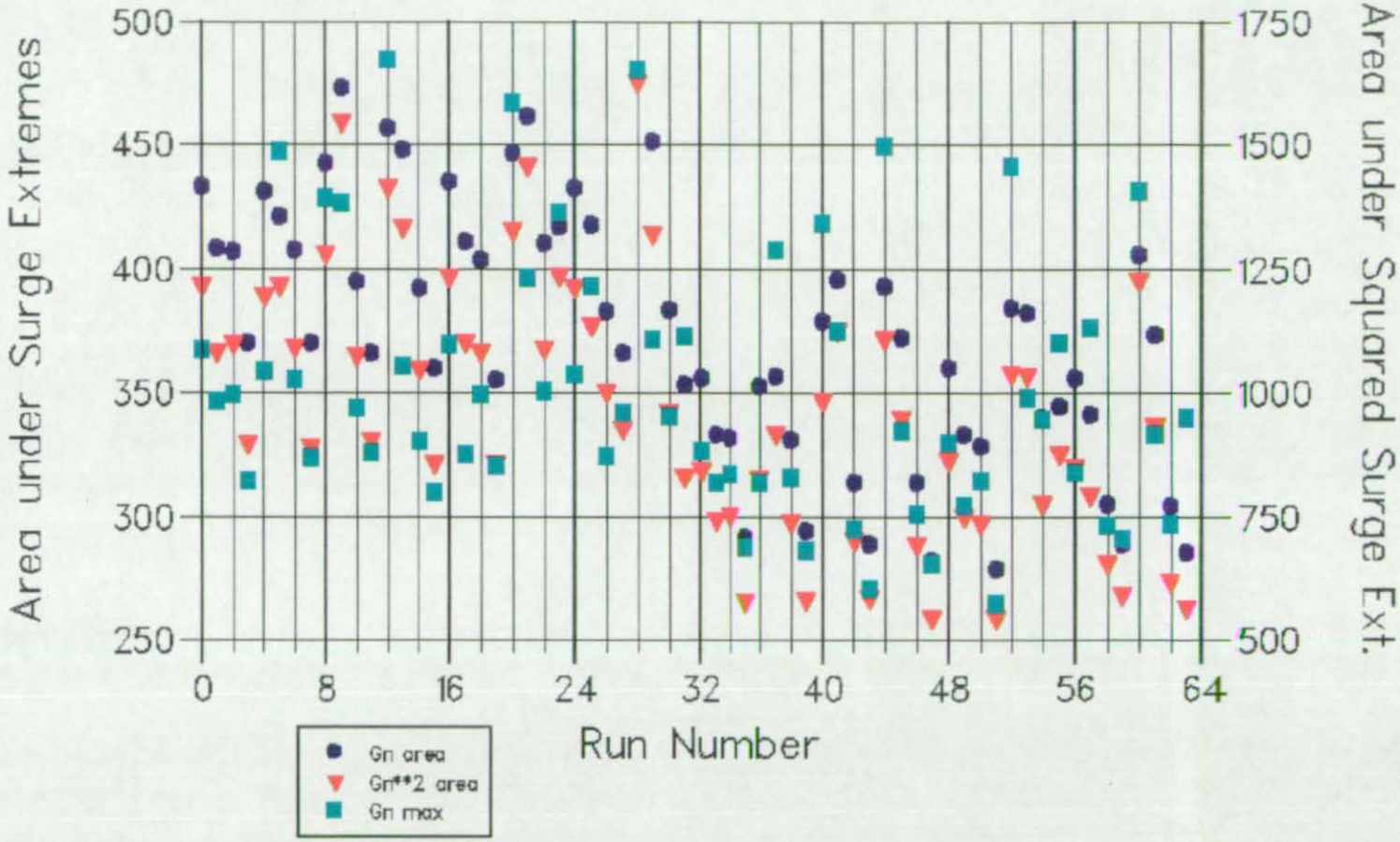

Figure 43: First 3 performance figures against run number (parameter combination see table). Blue dots: area under surge extremes, red triangles: area under squared surge extremes, green squares: absolute surge amplitude maximum

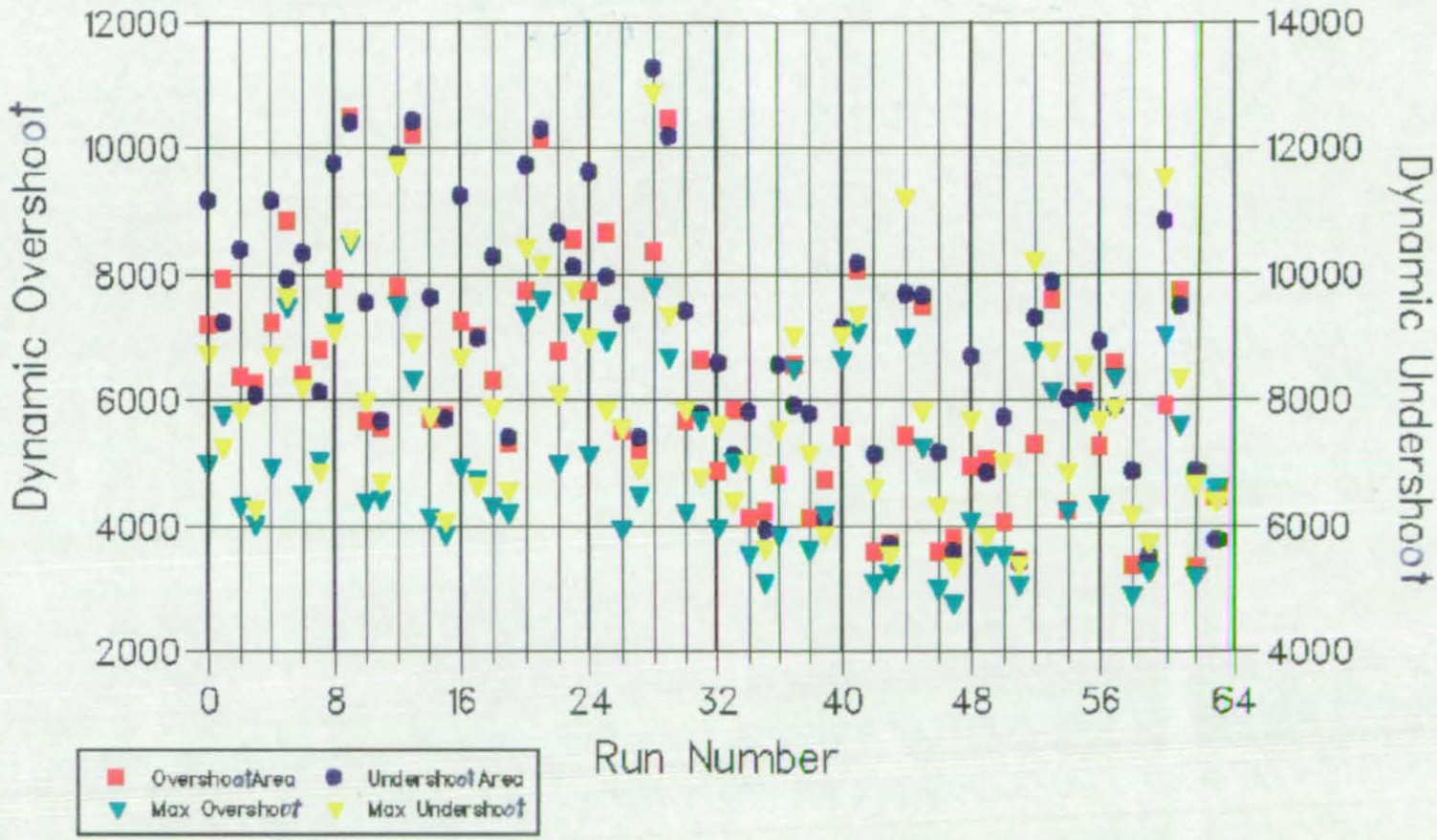

Figure 44: Performance figures 5, 6, 7, and 9 against run number (parameter combination see table). Red squares: area under overshoot, green triangle: maximum overshoot force, blue dots: area under maximum dynamic undershoot, yellow triangle: absolute maximum dynamic undershoot

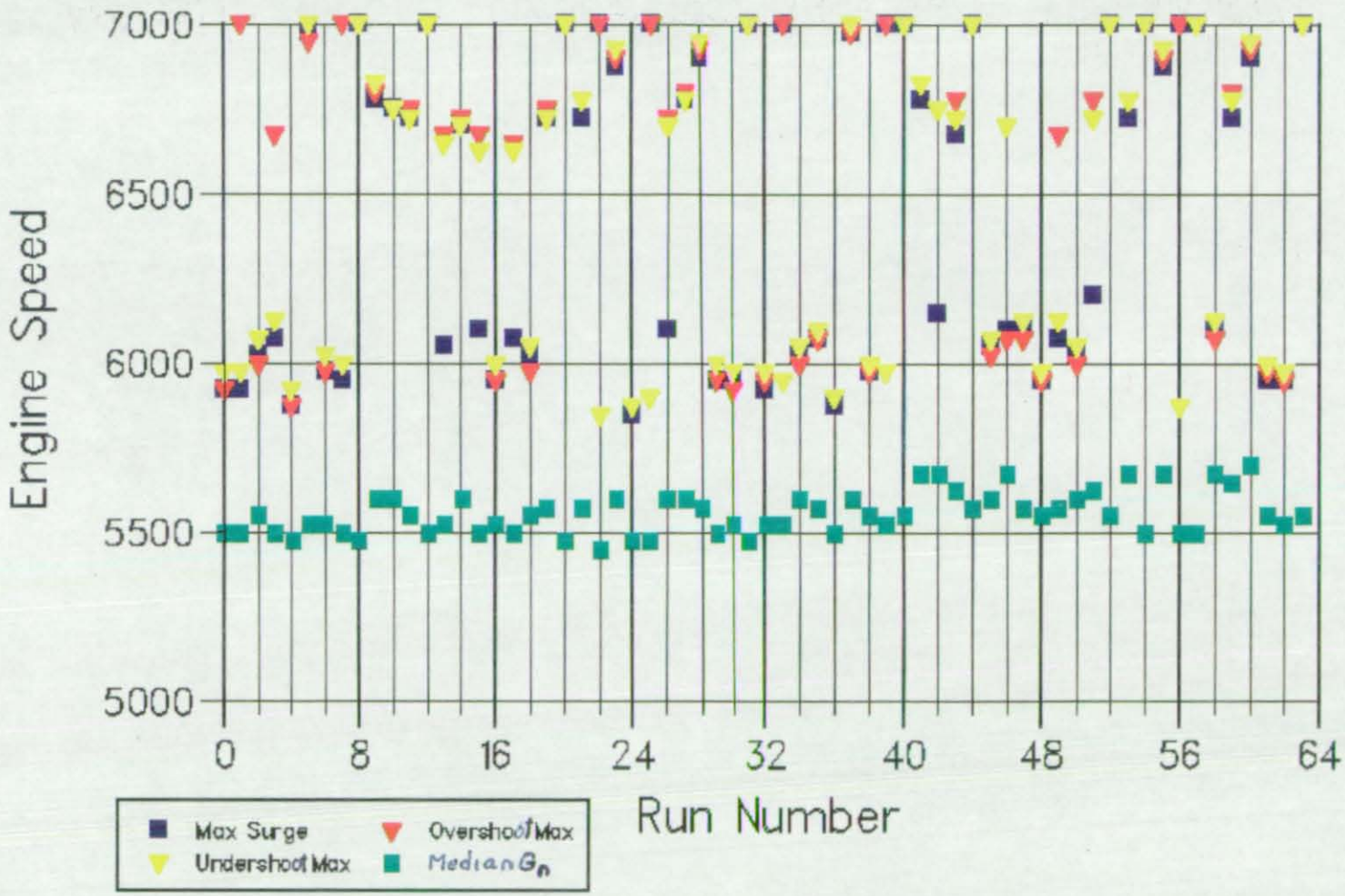

Figure 45: Speed locations for performance figures (performance figure 4 for 3, 8 for 7, 10 for 9, and 11) against run number (parameter combination see table). Blue squares: maximum surge, yellow triangle: maximum undershoot force, red triangle: maximum overshoot, green square: location of median speed

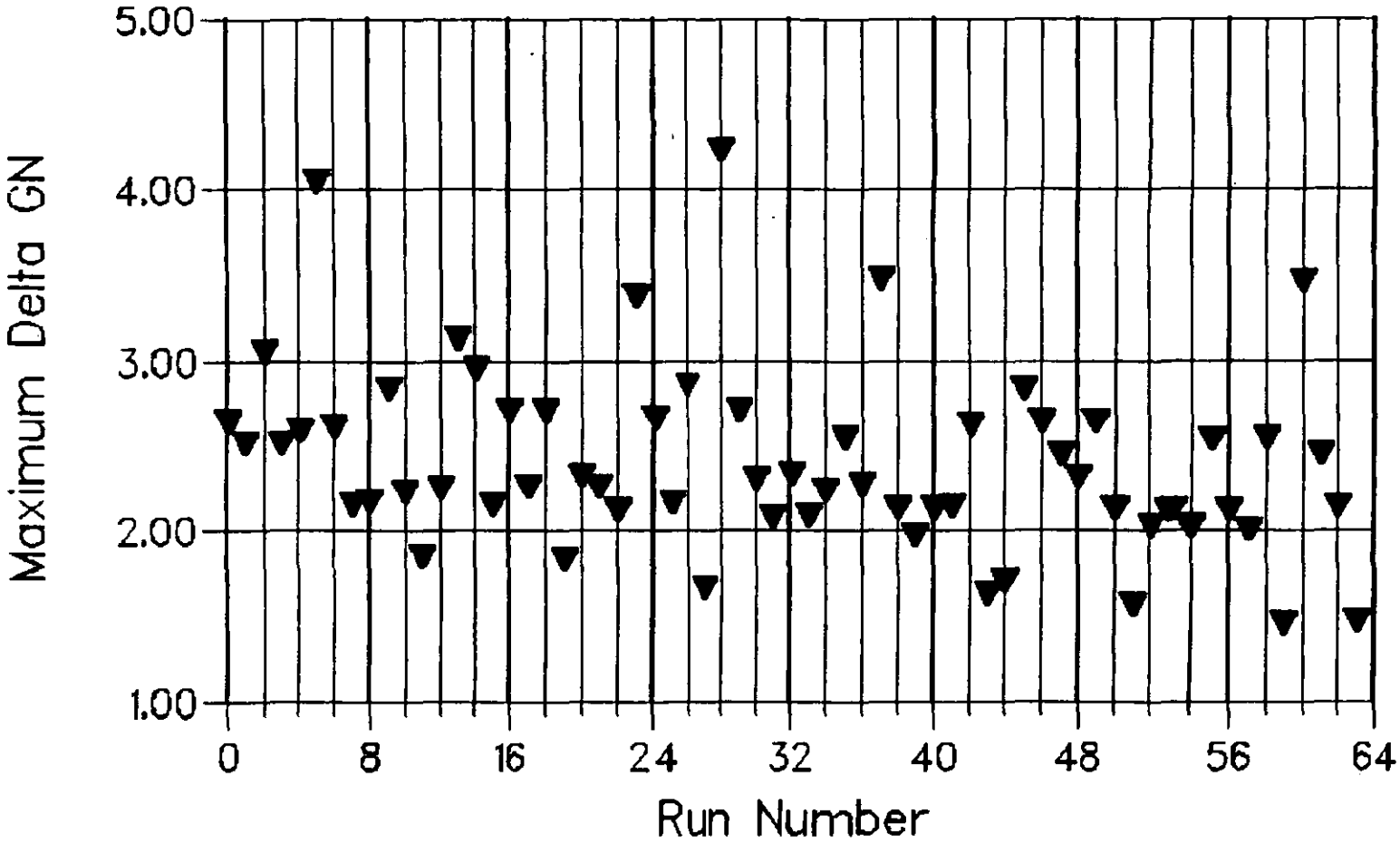

Figure 46: Maximum delta resonance against run number (parameter combination see table)

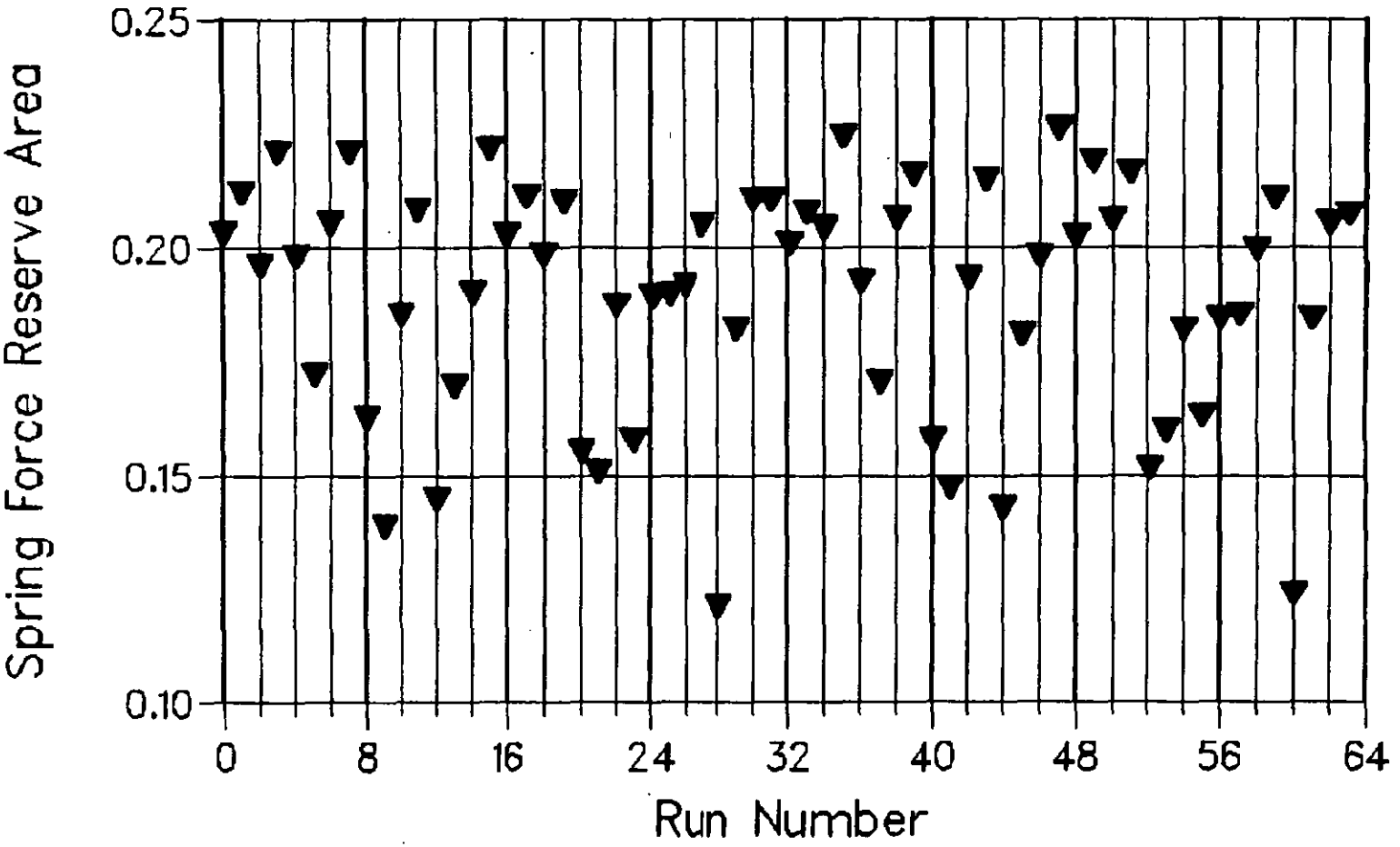

Figure 47: Spring force reserve area against run number (parameter combination see table)

9.6 Factorial Analysis of the Performance Figures

While the last section presented a survey of the various performance measures introduced to judge a particular design, the form of presentation of the results makes it difficult to pin specific responses down to specific parameters and to draw conclusions about these responses on the spring characteristic. In this section the results of processing the performance figures by statistical means will be presented.

To do this, the effects of the parameter changes and all parameter interactions on all performance figures have been calculated and a selection of them has been plotted against normal scores (The basics of a full factorial two level experiment and how to calculate the effects are outlined in the Appendix - Section 15.2). This enables the identification of parameters which have an important influence on each of the performance measures since they will stand out clearly at both ends of the graph. Since the underlying computer experiment is a full factorial in all parameters there are no confounding effects.

The formal analysis of the experiment has been carried out for all of the candidate performance measures introduced above. However, for most of them the conclusions were just a repetition of the ones gained from the others. Therefore the following presentation of the results will concentrate on three of the performance measures for cam 1 which allow one to cover the obtained insight. These performance figures are the sum of the maximum surge amplitude against speed (P_1), the speed location of the maximum surge amplitude (P_4) and the spring force reserve area (P_{13}).

Looking at the sum of the maximum surge in Figure 48 reveals that by far the most important influence on the area under the maximum surge amplitudes is due to parameter B. This is somewhat surprising since parameter B represents the slope of the frequency characteristic at installed height. At first glance one would have expected that parameter A which represents the total progressivity should be more important.

The significance of parameter B may perhaps be understood in terms of the excitation of the spring surge. From equation 6.2.1 it is known that the excitation in our model is given by valve acceleration. Broadly one can say that this excitation consists of the opening acceleration pulse, followed by an interval without significant excitation, the deceleration, and then another acceleration pulse (e.g. Figure 38). So to a coarse approximation there are two excitations per cam revolution with different long periods of free vibration in between. In the absence of damping this would mean that the increase in frequency during the valve lift does not help too much, once the excitation (the opening acceleration pulse) is over. The obvious importance of parameter B suggests that the frequency change should take place during the two principal excitation events in order to avoid large vibration amplitudes.

Having discussed the dominant influence of parameter B the next point in question is the observable importance of the interactions BD and CE (and to some extent the effect of C). The positive influence of the interaction BD can be understood by the same arguments as for parameter B alone. D represents the length of the tangent vector in point 1, thus influencing how long the slope of the frequency characteristic follows the slope in point 1. For its own parameter D seems to be meaningless but if the slope at installed height is at the large value, it is advantageous to follow this slope for a longer period.

The negative influence of parameter C and the CE interaction can be understood also from the above. Since parameter C represents the slope at valve open, a large value for this is by some degree coupled to a small progressivity at installed height, because of the requirement for a steady increase of spring frequency with lift. This is even more true if the characteristic follows this large slope what is represented by the CE interaction. The surprising fact is that all the other parameters and interactions really seem to have negligible effect on the spring surge mode amplitude.

The analysis above suggested a simple trend towards making the initial slope of the spring frequency characteristic as large as possible under the given spring design envelope. While this might be true to some extent, Figure 49 reveals an additional influence. This figure shows the effects for the location in the speed range for the surge mode extremes. Here one can see no obvious relationship between any dominant single parameter and the resonance location. The most important effect seems to come from the CD interaction, which is the combination of slope at valve open and tangent length at valve closed position. This combination influences mainly the shape of the characteristic in the middle of the lift. Another interpretation would be that there is not much change at all in the speed location, but it is known already from the previous section that this is not the case.

Figure 50 shows the analysis of what is probably the most important performance measure for the practical design (P_{13}), since the available spring reserve area is the key measure for the springs ability to perform its function of keeping all parts together. Although these effects are dominated by the slope at installed length again, this may be partly due to the usage of the kinematic valve acceleration. If the dynamic valve acceleration were taken, there should be a speed influence in the valve deceleration with local maximum and minimum amplitudes similar to the effects observed in the spring response. This will then couple the parameters and parameter interactions which influence the placement of the surge resonances in the speed range with the present performance measure of the spring force reserve area.

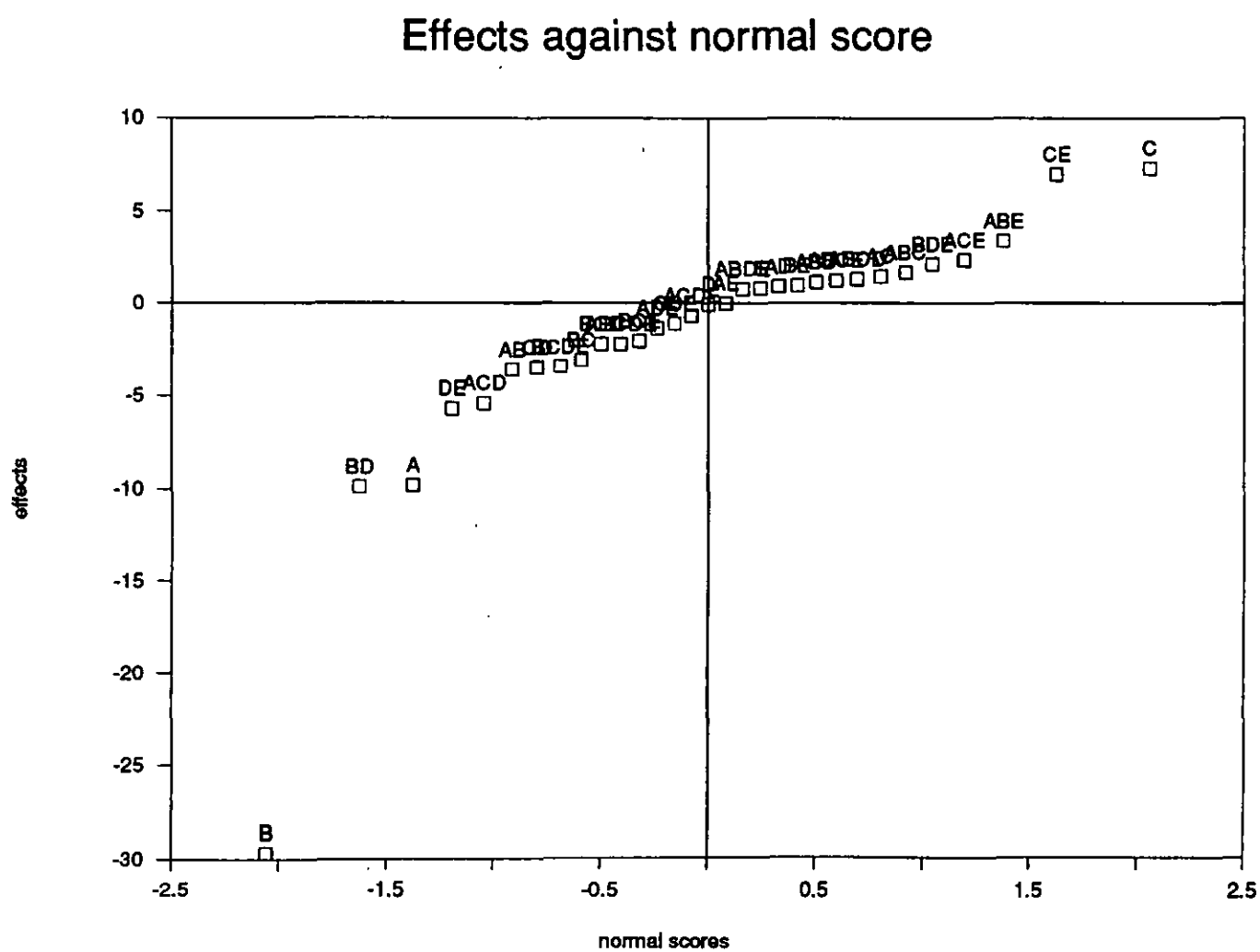

Figure 48: Effects against normal scores for the area under surge amplitude extremes (performance figure 1)

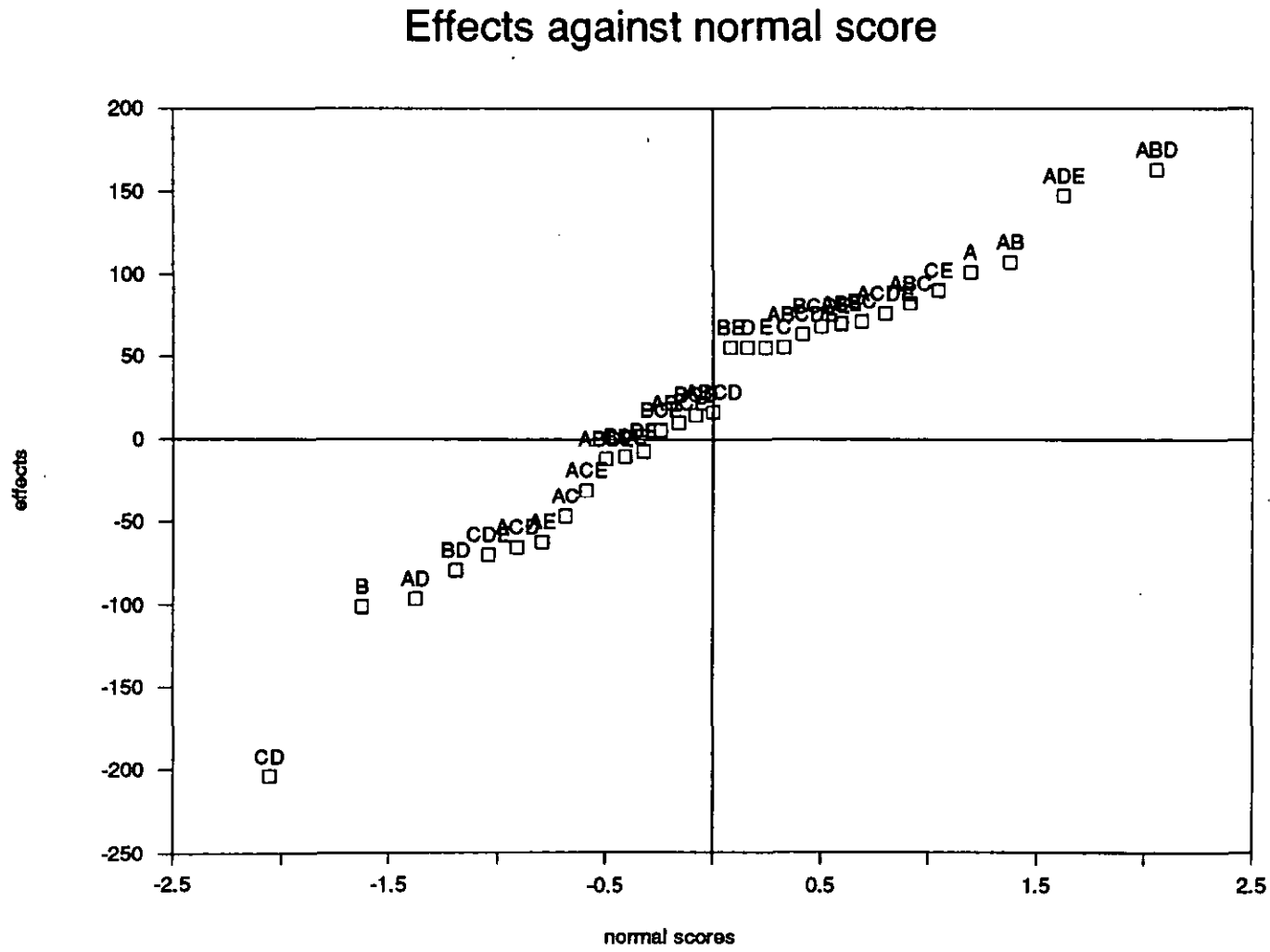

Figure 49: Effects against normal scores for the location of the maximum surge amplitude (performance figure 4)

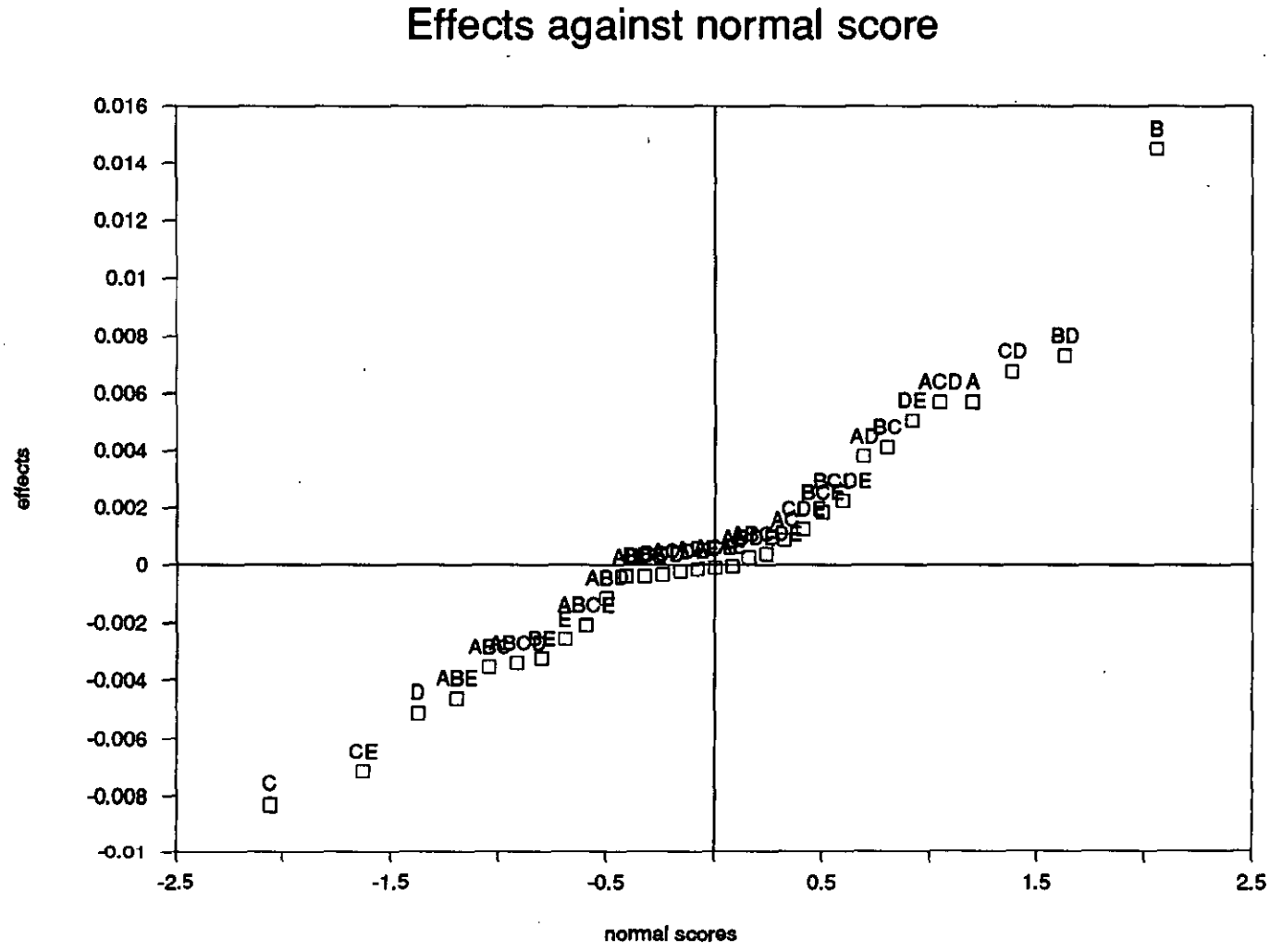

Figure 50: Effects against normal scores for the spring force reserve area (performance figure 13)

10

Valve Spring Optimization

In the last section, objective measures of the spring response have been introduced and the modal model for progressive springs has been employed for a basic study about the general effects of the springs frequency characteristic on these measures. In this section the analysis is taken a step further, by using the model results to optimize the spring response. Although the final step of such an optimization would have to be an actual manufacturing drawing, describing all the parameters necessary to produce the spring, the frequency characteristic is used as a simpler basis for the optimization (see Section 8). After this has been performed, deriving the spring design then requires additional work to find the spring layout for a given characteristic; this takes place outside the dynamic optimization loop.

In the last section, it has been emphasised that the optimal spring frequency characteristic is not the simple task of placing the frequency as close as possible to the stress limits of current spring technology and wire manufacturing technology. The "ideal" spring for a given valvetrain configuration will be a combination of overall limited amplitudes and specifically low amplitudes in a given speed range. To solve this task one may continue to work with the splines introduced in the last section. These splines have the advantage that their parameters can be more or less directly related to specific characteristics of the spring, compared to for example a polynomial representation of the frequency characteristic. This spline representation of the frequency characteristic thus allows one the definition of an optimization problem with a relatively low number of parameters. The target function for optimization may be taken as one (or a combination of several) of the performance figures defined in the last section. But before this is done, the question of the influence of dynamic valve acceleration on the spring response, which arose during the analysis and discussion of the factorial analysis, has to be investigated .

After this point has been clarified, general aspects of optimization, in terms of the target functions, constraints and the numerical algorithm used, need to be discussed before the main aim of the section, the formal spring optimization is carried out.

10.1 Influence of Dynamic Valve Acceleration

The profile from Figure 23 has been used to calculate the dynamic valve acceleration in a speed range from 3000 to 7000 rpm. For this purpose the model shown in Figure 5 has been used, but a static spring has been used instead of the dynamic one. This is because a dynamic spring submodel in the valvetrain model would superimpose a low frequency component on the results, as shown in Figures 8 to 10. If these results are used as an excitation of the spring, the low frequency part of them would excite the springs fundamental mode. Thus to some extent, even though they are expected to be small, the coupling effects between spring and valvetrain would reflect back again into the separated spring analysis.

The result for the valve acceleration against cam angle is shown in Figure 51. As can be recognized from this graph, there are significant dynamic effects in the results. How important they are for the spring response can be estimated by an analysis of the Fourier spectra of the results. Figure 52 shows a grid plot for the Fourier coefficient amplitude of the first 50 harmonics of the dynamic valve accelerations for each speed. Here dark blue stands for zero amplitude and bright yellow for high amplitude. One can now see, that the variation over speed is quite moderate for the low harmonics up to the 15th to 20th. This indicates that at least the lowest spring mode should be independent of the valvetrain dynamics.

Further verification can be gained from the comparison of the calculated spring response using the kinematic and the dynamic valve accelerations. Figure 53 shows this comparison. As one sees, the overall characteristic is nearly identical although the amplitude is slightly higher for the results from the dynamic accelerations, especially at higher speeds. Clearly the largest amplitude results from the fundamental mode and this mode is independent from the dynamic deviations of the profile; the high frequency oscillations in the dynamic acceleration cause an additional excitation of higher modes, which cause the increased overall amplitude at higher speeds, compared to the kinematically excited spring.

In all these arguments, one has to keep in mind that these findings are only valid for valvetrain configurations with a high fundamental natural frequency. An old pushrod design with 600Hz base frequency will surely show a significant coupling of spring and valvetrain vibrations, thus invalidating this separated analysis. Fortunately these types of valvetrains are ceasing to be important for modern high speed engines.

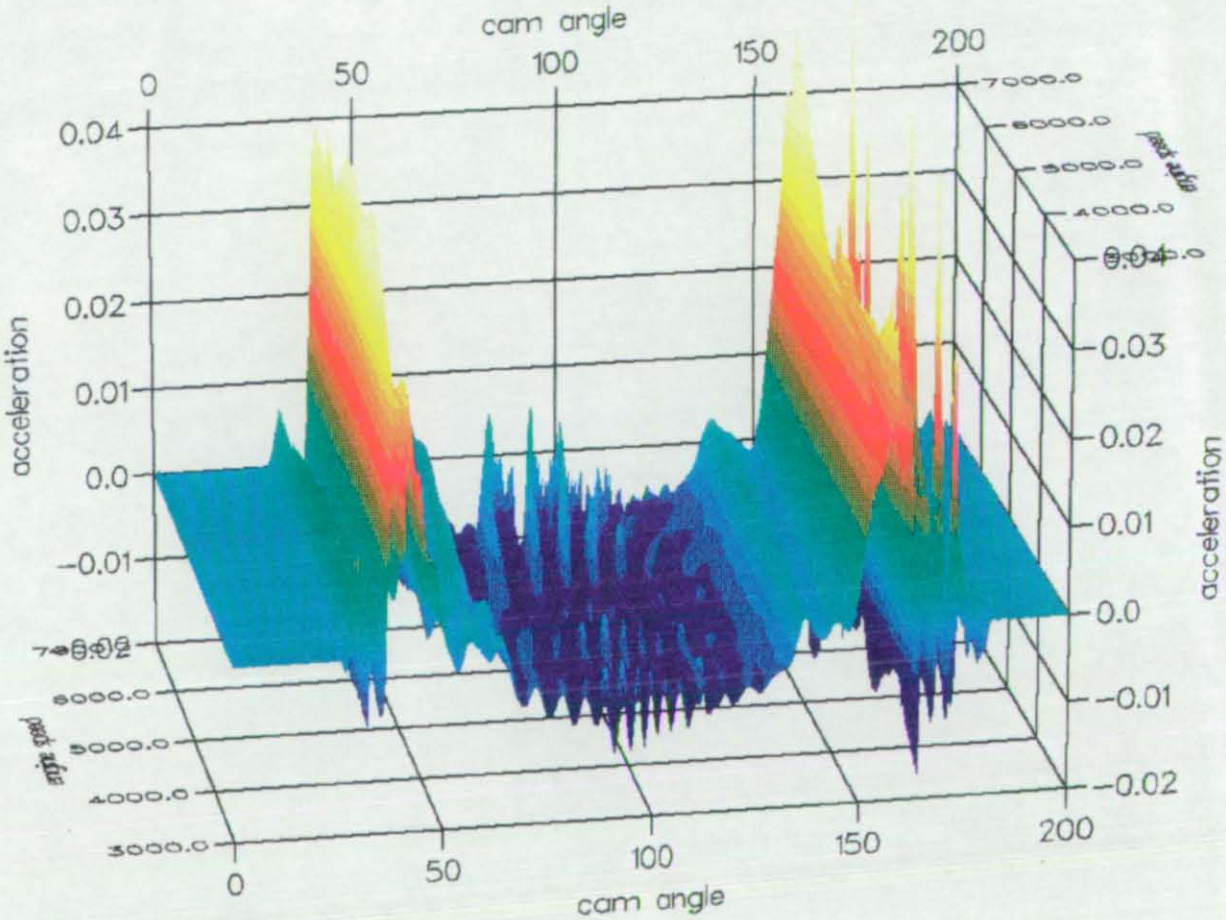

Figure 51: Dynamic valve acceleration for 3000 to 7000 rpm engine speed, simulated with the model from Figure 5b and excited by the cam profile from Figure 25

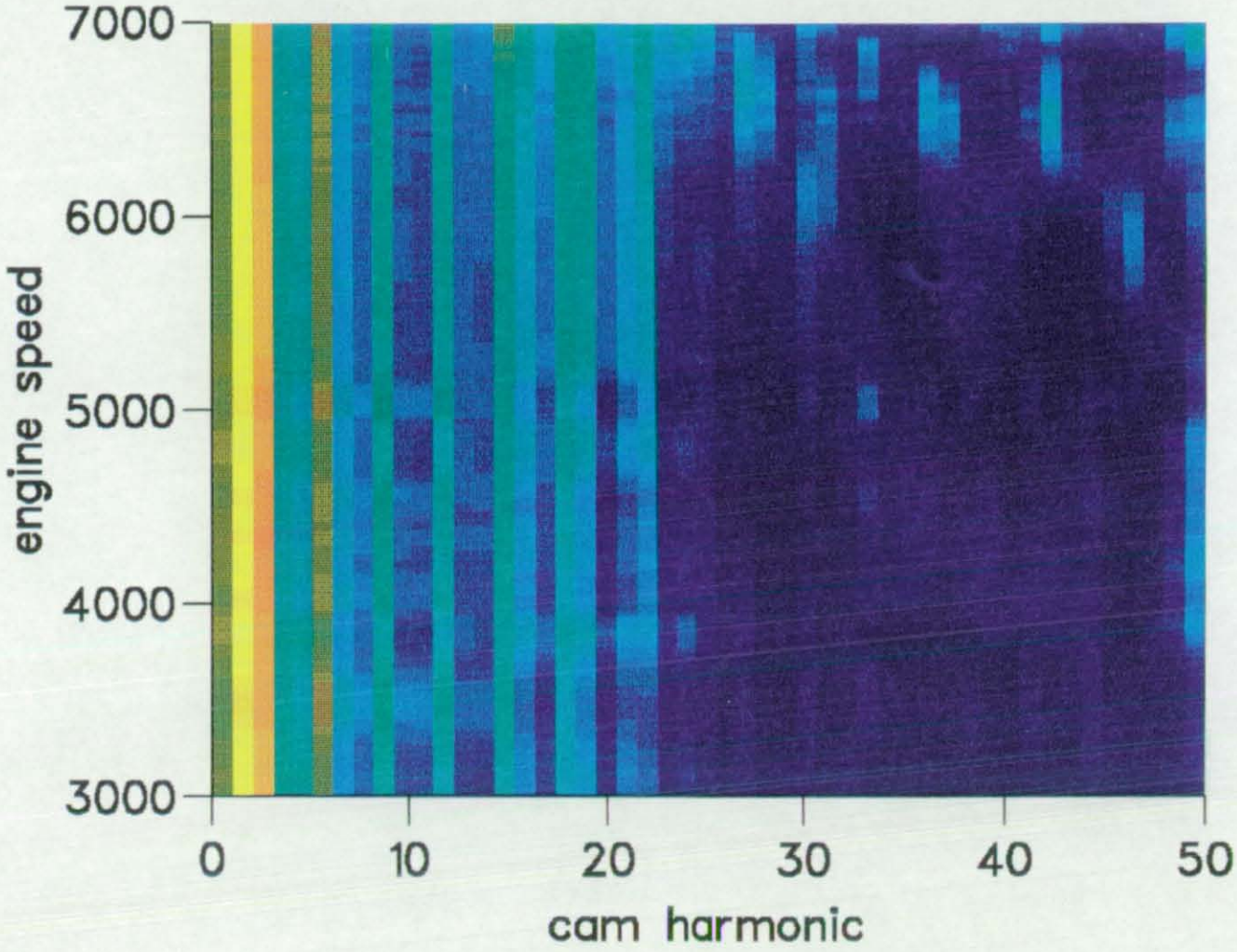

Figure 52: Grid plot of the first 50 coefficients for the Fourier series of the valve accelerations shown in Figure 51. Bright colours stand for high amplitude, dark colours for low amplitude

In view of the above argument, it is reasonable to assume that the factorial experiment (which used the kinematic acceleration of the two theoretical valve events) gives valid conclusions about the spring behaviour for stiff valvetrains. Nevertheless there is some sense in using dynamic accelerations for the spring optimization task. Although the coupling is obviously not that important, the phase relation of the spring and valvetrain vibrations may well be. This is due to the fact that the above discussion about the coupling effects in the system only applies to the part of the operating range of the valvetrain where the system is moderately linear. If one takes the cut-off speed range, one is in a situation where the spring force is just about sufficient to provide the deceleration forces. If now a minimum force from the spring vibration coincides with a minimum in the valve acceleration, the cam will lose contact, and this represents a major non-linear effect on the system. Depending on the valvetrain layout, this can have all sorts of negative effects on the valvetrain, even a total failure. But to get an indication of these effects, it is not necessary to attempt to use the full coupled valvetrain model for the optimization. Using the dynamic valve acceleration shown in Figure 51 as the excitation for the spring already represents the most important step in this direction. Taking the above defined performance measure P_{13} for the minimum spring force reserve area, this automatically weights the phase relation between the spring and the valvetrain vibrations.

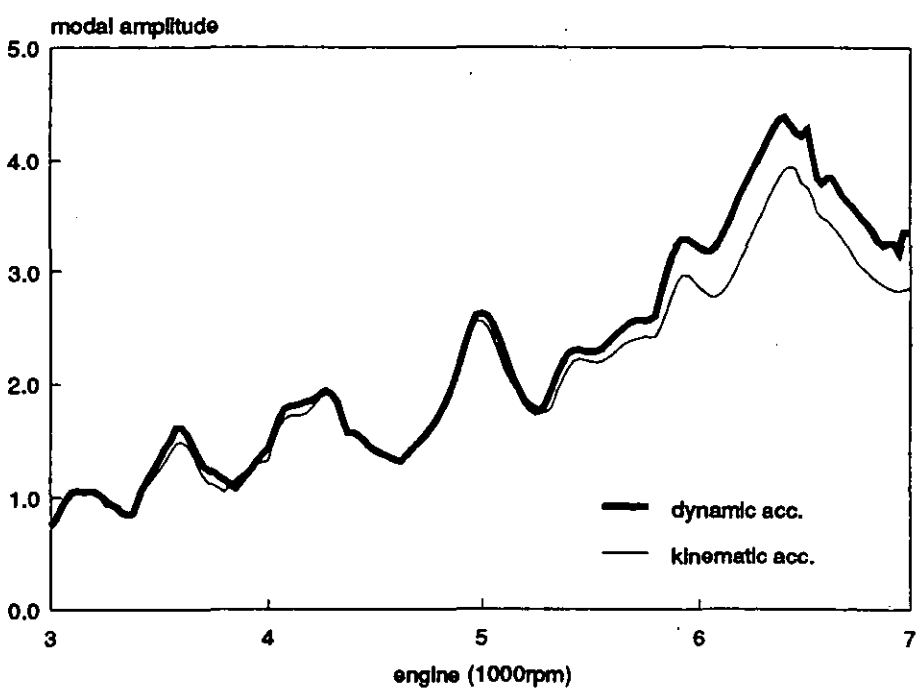

Figure 53: Comparison of modal amplitude against speed calculated using the dynamic valve acceleration and using the kinematic valve acceleration

10.2 General aspects of Spring Optimization

Generally, for an optimization task, a target function is formulated, which contains the quantities to be improved. If the target function is dependent on a set of parameters these can be varied to find extremes of the target function. In the present case, the target function depends on the valve spring characteristics, which can be parameterized as described above. As has been shown in the factorial experiment (Section 9) the parametric splines are useful for a flexible representation of the frequency characteristics with a very limited number of parameters.

Thus the task is a parameter optimization problem, where the control function is parameterized with splines. The spline parameters at the grid points define a set of design parameters $p_0,\ldots, p_n$ such that the control function u is defined by:

$$u = u(p_1, \ldots, p_n) \qquad /10.2.1/$$

As a result, one can modify the springs frequency characteristic by variation of the parameters.
Hence a target function l depending on u will also depend on $p_0,\ldots, p_n$

$$l = l(u(p_1, \ldots, p_n)) = l(p_1, \ldots, p_n) \qquad /10.2.2/$$

The task of the optimization routine is to iterate down to the point in the parameter space, that optimizes l. The function l can be formed by any combination of the performance figures from Section 9.4 plus any constraints to be taken into account.

The type of algorithm to be applied depends on the type of the function, the information available on the function and the time needed to evaluate the function to be minimised. In the case of the springs dynamic response, the evaluation of the function has to be performed numerically and not analytically. The cpu time needed for one function evaluation can be up to 2 minutes on a DEC 5000/200 workstation. Hence one may want to spend some effort in calculating the parameters for each step in the optimization procedure to avoid additional function evaluations. On the other hand there is no efficient way to calculate derivatives $\partial l/\partial p_n$.

With these considerations, the algorithm of choice was that of Powell's direction set method in multi-dimensions; the code was readily available (Press *et al* 1990) , and significant expertise was available via the work of Ernst and Hussmann (1992). This multidimensional

method uses an efficient one dimensional optimization algorithm as a working subroutine. This line optimization is carried out along an initial direction in the N-dimensional space of optimization parameters. The initial direction can be any vector in the space formed by the parameters, but since no better initial direction set is known for the problem, a Cartesian set of vectors is used for this study.

The optimization algorithm then successively determines more efficient direction sets depending on a strategy which takes numerically derived information on the gradient along the different directions in the initial set of vectors in the parameter space. The details of this algorithm are explained in the "Numerical Recipes" (Press *et al* 1990) and do not represent the core of the work presented here, since the algorithm is mainly used as a "black box" for the task of minimisation of the function. It could be exchanged easily by another algorithm if that were felt appropriate.

Appart from the algorithm being used for the optimization a further general aspect of optimization is the presence of constraints. Most practical engineering tasks involve constraints, and the present case clearly is a system with constraints on the optimization parameters, where one may distinguish two classes of constraints. These are engineering constraints and constraints resulting from the method of parameterization of the spring frequency characteristic. The engineering constraints are:

- Spring wire stresses

The static stress of the spring wire can be calculated by

$$\tau_v = v\frac{8D}{\pi d^3}F \qquad /10.2.3/$$

Where F is the spring force, D is the mean coiling diameter, d the wire diameter, and v is a correction factor which accounts for the stress concentration at the inner edge of the spring. This correction factor can be approximately calculated by

$$v \approx \left(\frac{D}{d}+0.2\right)\left(\frac{D}{d}-1\right) \qquad /10.2.4/$$

The resulting allowable maximum stress as well as the stress difference between the valve closed and valve open length of the spring is limited by the material properties. This stress can then be related back to the frequency characteristics of the spring.

From equation 5.1.10 one has for the frequency of the springs fundamental mode

$$\omega = \pi\sqrt{\frac{k}{m}} \qquad /10.2.5/$$

Furthermore from equation 5.2.1.1 follows for the springs mass

$$m = \rho A N 2\pi\bar{r} = \rho\pi\frac{d^2}{2} N 2\pi\frac{D}{2} \qquad /10.2.6/$$

and from equation 5.2.1.4 for the stiffness of a spring made from round wire

$$K \approx \frac{I_t G}{2\pi r^3 N} = \frac{\frac{\pi d^4}{32} G}{2\pi\left(\frac{D}{2}\right)^3 N} \qquad /10.2.7/$$

Hence the springs frequency depends also directly on the relation of wire diameter and coiling diameter. Basically, to reach a high frequency, a small wire diameter d (low mass) has to be coiled to a small diameter D (low mass and high stiffness). But this combination also increases the stress level for a given force F needed in the valvetrain. This stress consideration hence constrains the installed frequency and the valve open frequency of the spring, as well as the maximum difference of the two.

- Slope of frequency

The slope of the frequency characteristic needs also to be constrained. Clearly the slope may not be negative, since a spring with decreasing frequency with increasing lift just can not be realised. Such a characteristic would require coils to become active with decreasing spring length.

- Installation envelope

In a given engine only limited space is available to install the spring. This places constraints on the combination of wire dimensions, coiling diameter and number of coils. Since it has been shown above that the frequency of the spring depends directly on these key dimensions, this installation constraints relate again back to the allowable frequency envelope.

Two constraints resulting from the parametric splines being used are as follows:

- Minimum tangent vector length

If the tangent vector length gets too small, the parametric splines degenerate and the tangent vector direction has no longer any influence on the resulting characteristic.

- Maximum tangent vector length

Since the splines being used are parametric splines, there is no guarantee that they will always result in a valid function. If the tangent vector is too large, the resulting curve may form a loop, which means two frequency values for a given valve lift. The conditions under which this happens have been investigated and calculated in an earlier work by the author (Schamel 1987).

The sum of these constraints form a design space where one can search for a valid solution. In the worst case the remaining parameter space may be so small that in essence only one solution is possible which fulfils the constraints. Fortunately, for this study this was not the case and the design freedom may even be larger, at the early concept stage of a new engine.

For the numerical implementation of these constraints one has to consider one important aspect that proved to cause difficulty in the work of Hussmann (1992). Powell's method in the form provided by Numerical Recipes, is an optimization algorithm for unconstrained systems. One common way to take constraints into account in this type of algorithm, is to set up a cost function ("penalty function) which is added to the function which determines the quality of the response. If a parameter is in its allowed range, this cost or penalty function has to have a zero value. But when a parameter is violating the border of the allowed range, the penalty function has to impose a very rapid penalty increase.

In mathematical terms if the constraints, c_j, depend on the design parameters

$$c_j(p_{org_1}, \ldots, p_{org_n}) \qquad /10.2.8/$$

$$j = 1, \ldots, m$$

one is able to formulate penalty functions $pf_i(p_{org_1}, \ldots, p_{org_n})$

$$pf_{c_j}(p_{org_1}, \ldots, p_{org_n}) = a_j c_{diff_j}^2(p_{org_1}, \ldots, p_{org_n}) \qquad /10.2.9/$$

Here $c_{diff} = c_{limit} - c_j$ is the amount of violation of the constraint above the limit, $p_{org1}, \ldots, p_{orgn}$ are the design parameters as chosen by the optimization algorithm, and a_j is a scaling factor.

Taking any combination of the performance figures from Section 9.4 and the constraints, the target function l for the formal optimization can be formulated:

$$l = \sum_{targets} P_{targets}(p_{org_1}, \ldots, p_{org_n}) + \sum_{constraints} pf_{constraints}(a_{org_j}, p_{org_1}, \ldots, p_{org_n}) \qquad /10.2.10/$$

This way of handling the constraints proved to have a clear disadvantage. To ensure that the solution is not following a direction with very advantageous performance figures which violates the constraints, the scaling factor of the constraints has to be very large. The resulting rapid penalty increase when a constraint is violated more or less blocks the total direction in the parameter space which leads to the constraint violation, even if only one of the parameters in the direction set is causing the violation. This causes useful and efficient directions to be discarded.

To avoid this effect, a different method has been tried for this study. The advantage of the present application is, that most constraints depend only on one parameter p and not on a complex combination which would require the dynamic solution. Thus instead of placing a heavy penalty for a violation of the constraints, any parameter, set by the optimization algorithm, which exceeds the valid range, is flagged and reset to the allowed border value prior to the function evaluation. The amount of violation is then very softly penalised by a quadratic cost function and this penalty figure is added to the overall value of the function.

This can be expressed by a modified target function:

$$l = \sum_{targets} P_{targets}(p_{res_1}, \ldots, p_{res_n}) + \sum_{constraints} pf_{constraints}(a_{res_j}, p_{org_1}, \ldots, p_{org_n}) \qquad /10.2.11/$$

where

$$p_{res} = p_{org} \quad for \quad p_{min} < p_{org} < p_{max}$$
$$p_{res} = p_{min} \quad for \quad p_{org} < p_{min}$$
$$p_{res} = p_{max} \quad for \quad p_{org} > p_{max}$$
$$and$$
$$a_{res_j} \ll a_{org_j}$$

Hence for the performance figure contribution of the target function, the evaluation takes place for parameters in the valid range, while the penalty function accounts for the violation.

This procedure has a number of advantages. The filtering of the parameters prior to the calculation of the associated dynamic response prevents the optimization algorithm from seeing any benefit from the violation of this parameter. The penalty on this violation on the other hand ensures that in the long term, the algorithm will drive this parameter back into the allowed range. But the very soft penalty possible with this strategy, or in other words the small scaling factor a_j, allows the algorithm to follow a direction set, which violates one aspect, but may be very beneficial for other aspects.

To verify the above considerations, a practical test run has been carried out, using two program versions for the same task. In both cases the following parameters have been constrained:

Parameter	Physical Meaning	Lower Boundary	Upper Boundary
f_1	Frequency at installed height	400	600
f_2	Frequency at valve open position	-	1000
df/ds_1	Slope of frequency characteristic at 0mm valve lift	0	1500
Rf_1	Relative length of tangent vector at 0mm valve lift	0.2	3.0
Rf_2	Relative length of tangent vector at max valve lift	0.2	3.0

Table 5

In the first run, all of these constraints were monitored, and if violated costed by a heavy quadratic increase of the penalty function. In the second run the above described method of pre-filtering and soft punishment of the violation has been used. In Figure 54 the resulting spring force reserve area (P_{13}) against number of optimization steps is plotted. The blue dots show the progress for the hard implementation of the constraints and the red dots show the progress for the soft pre-filtering implementation. The interesting point is that the soft implementation not only progresses faster, but also finds a better final solution. The sharp block of a direction for the original constraint formulation seems to discard important directions, which can not be recovered afterwards. Note that the overall larger number of steps for the faster optimization is due to the termination tolerance being set to an extremely low value, to ensure that both runs would progress through any period of small changes with a potential significant gain afterwards. This did not happen and both runs could have been stopped after approximately 100 steps without a significant disadvantage for the final result.

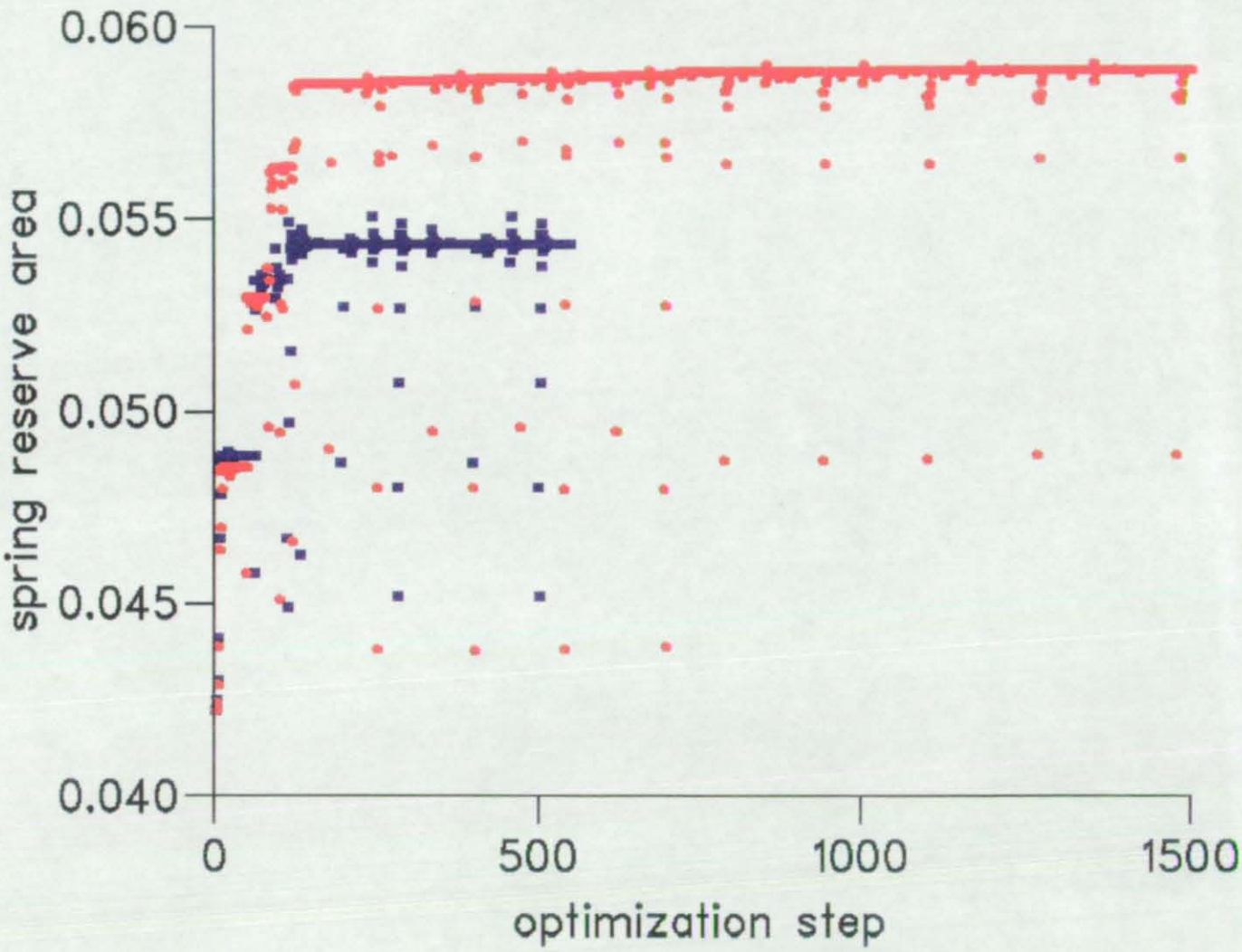

Figure 54: Spring force reserve area against optimization step for a "hard" implementation of constraints (blue squares) and a "soft" implementation of constraints (red dots)

10.3 An Initial Optimization Run

The above discussed algorithm may be used to optimize the spring frequency characteristic in respect to any of the previously introduced performance figures or any combination thereof. The allowed parameter range may be constrained to any range and the weighting factor for any of the components of the cost function may be specified separately. The initial value for each of the components of the cost function is normalised to 1, to ensure that the weighting factors have the same influence, independent of the units or the physical quantity of the component.

To see whether the general findings from the statistical study can be verified in the optimization procedure, an optimization attempt has been made, which allowed a very wide range of possible solutions, even if this range is unrealistic in terms of a real spring design. For this study the following parameters have been fixed:

Parameter	Unit	Physical Meaning
s_1	mm	displacement for base frequency (lift for installed height)
s_2	mm	displacement for maximum valve lift (10mm)

Table 6

This was necessary since the optimization was done only for one cam profile which obviously has to start with zero lift and which had a maximum lift of 10mm. The cam profile used is the actual one from the investigated 16 valve engine shown in Figure 23, which has been used for the correlation above and for determination of the dynamic valve accelerations from Figure 51.

The free optimization parameters where chosen as follows:

Parameter	Unit	Physical Meaning
f_1	Hz	installed height frequency (at s_1)
f_2	Hz	valve open frequency (at s_2)
df/ds_1	Hz/mm	slope for tangent vector in s_1 (rate of frequency change in point s_1)
df/ds_2	Hz/mm	slope for tangent vector in s_2 (rate of frequency change in point s_2)
Rf_1	-	relative length of tangent vector in point s_1
Rf_2	-	relative length of tangent vector in point s_2

Table 7

Hence one has a 6-dimensional parameter space for the optimization problem. For this initial run, the only constraint imposed was that the frequency had to increase monotonically with lift. For the other parameters there was no limit imposed. The target function was thus set up from two components, the first imposing a heavy penalty for a decrease of the frequency with lift, and a second component for the spring force reserve area (P_{13}, Section 9.4).

The initial values for the spline parameters were chosen to closely represent the frequency characteristic of the original spring for this engine, which has been used for the correlation shown in the Figures 31 to 34. A plot which compares the spline representation of this frequency characteristic with the one gained from the original polynomial representation, is shown against lift and cam angle in Figure 55. In addition, this plot shows the kinematic valve acceleration from this profile. Here one sees that the original spring has almost no increase in frequency at low lift where the positive acceleration period takes place.

In Figure 56 one can see the comparison of this initial characteristic with the one resulting from this sample optimization run. Clearly the optimization algorithm found a solution extremely biased towards an early frequency increase. This is totally consistent with the results from the statistical analysis. One can further see that the optimization lowered the fundamental frequency at zero lift, which one would not intuitively do to decrease spring vibrations. The end frequency at maximum lift was unchanged by the optimization.

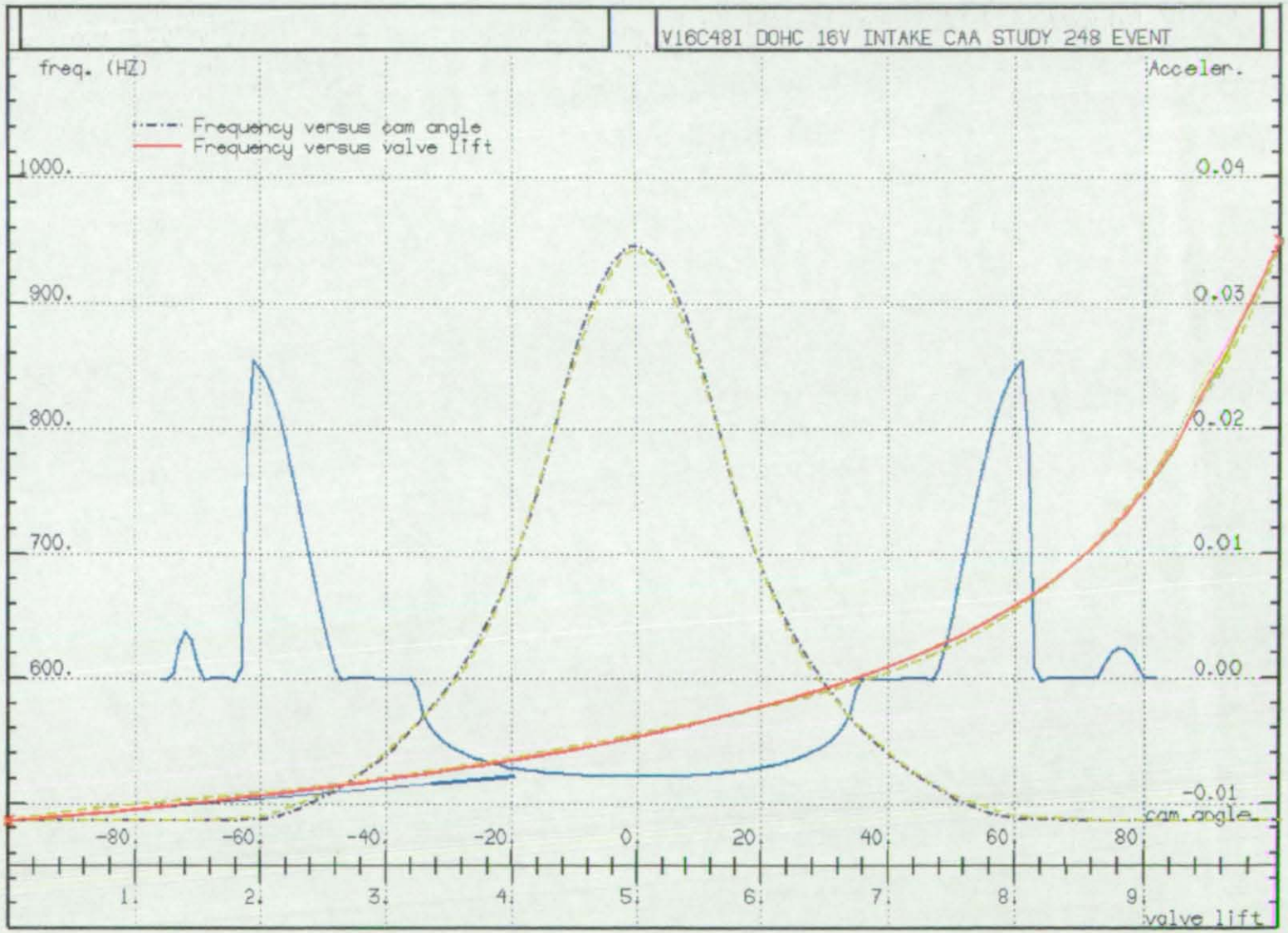

Figure 55: Comparison of frequency characteristic representation by the original polynomial representation (green curves) and the start set of optimization spline parameters

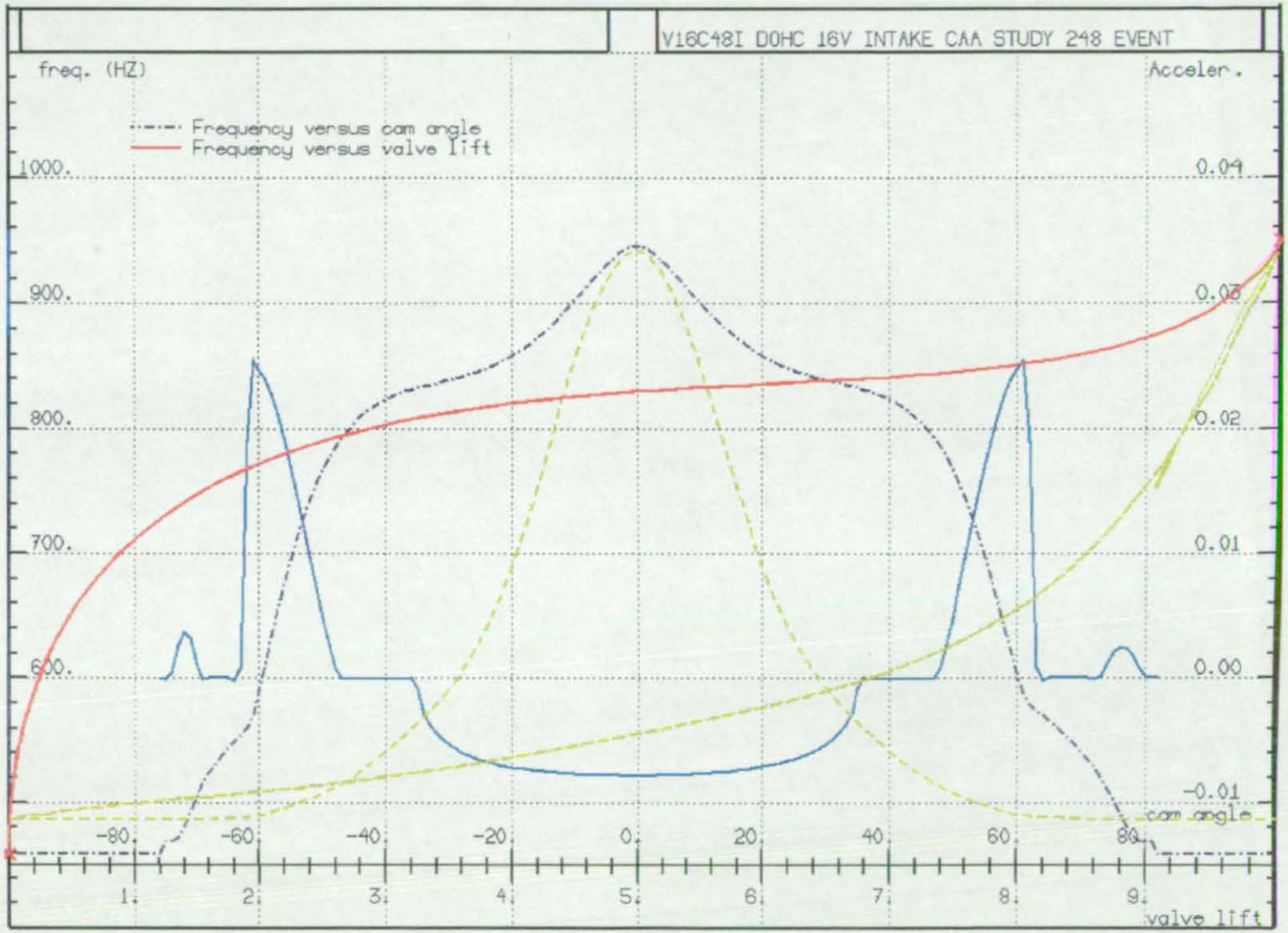

Figure 56: Comparison of frequency characteristic for the original spring and for the result from the first optimization run

These observations have a positive and a negative aspect. The positive side is, that there are obviously solutions of the problem which offer an overall advantage in terms of spring force reserve, without driving the spring characteristic to the extreme.

The negative aspect is, that one has to keep in mind that this run was carried out with a fully unconstrained system. The absolute optimum for this system with the given cost function should have been an infinitely high fundamental frequency correspondingly a zero-vibration amplitude, to give a spring force reserve area of 0.06395mm/deg^2 compared to 0.04571mm/deg^2 for this solution. Hence, instead of finding the global optimum the algorithm has found a local one. This is a well known problem for most optimization tasks. In practice one would have to restart the optimization from several different initial parameter values and either find that they converge to the same solution, or if not, take the best solution found.

The response against speed of the original spring and this optimization result is shown in Figure 57. Here one can see the extremes of the sum of the modal amplitude against speed, which is an indication of the amount of vibration in the spring, but which does not say anything about phase relationship. As it is shown, there is a clear and substantial reduction in amplitude for the optimization result. But it is interesting that the optimization has not moved the strong peak around 6500 rpm. In this speed range, the spring force begins to be critical and large spring vibrations carry the risk of contact loss in the valvetrain system.

It is useful to consider the time domain results for the spring force reserve (or the spring deceleration capacity, $a_S = F_S/m_{valvetrain}$). Figure 58 depicts the dynamic valve acceleration and the corresponding spring deceleration capacity for the original spring from 6100 to 6900 rpm. As can be seen, the phase relation of the first very strong negative acceleration vibration and the spring vibration is antiphase, which would lead to a serious and very early loss of contact, and which leads to a low (even negative value) for the total spring reserve area, which has been used for the cost function.

For the characteristic resulting from the optimization, the results are shown in Figure 59. Here one can see that the early increase in frequency leads to an in-phase vibration of valvetrain and spring force during the critical early deceleration period. If one looks at the 6500rpm result, it can be seen that a lower amplitude of the spring vibrations would lead to more loss of contact, because the vibration provides the force just in time. The conclusion is that although one would have expected that an unconstrained optimization would reduce or eliminate the vibration amplitude in the high speed area, the solution found, represents a reasonable local optimum.

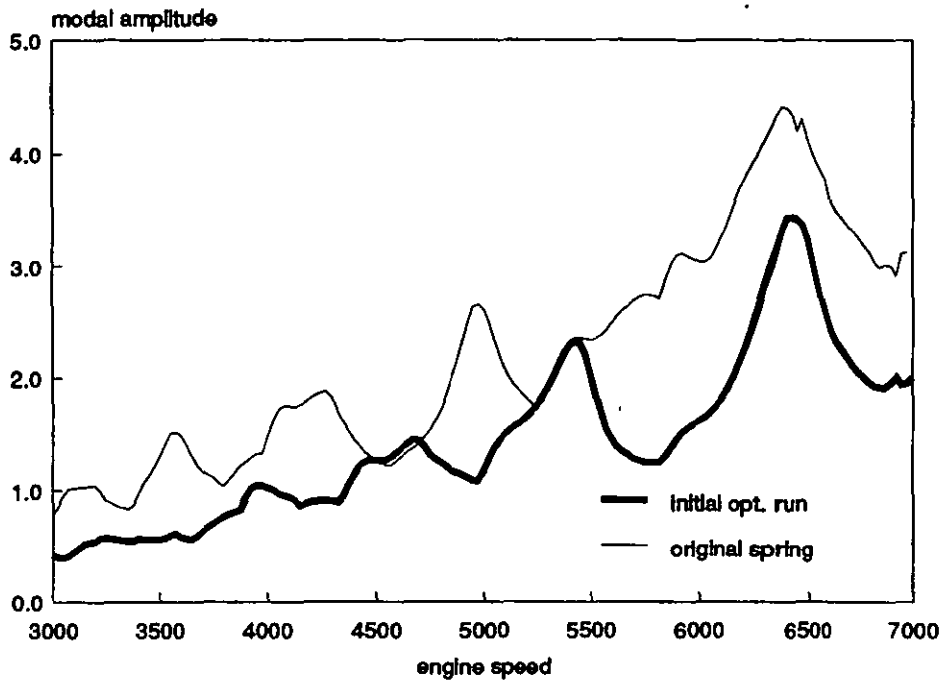

Figure 57: Comparison of modal amplitude against engine speed for the original spring and the result from the first optimization run

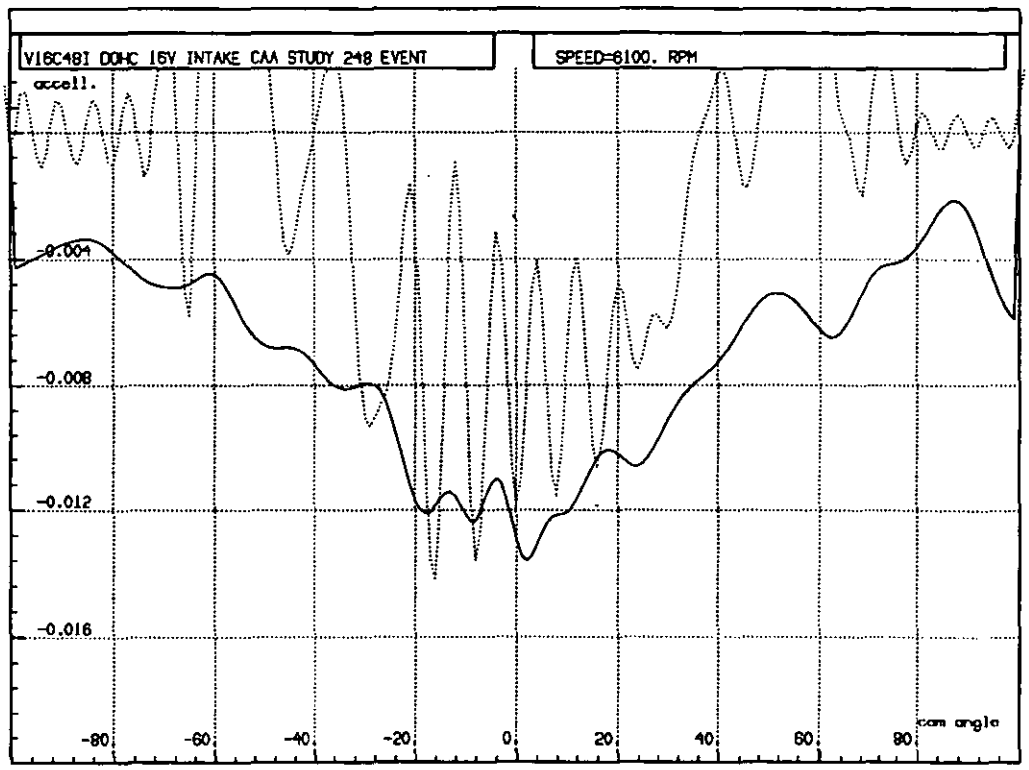
V16C48I DOHC 16V INTAKE CAA STUDY 248 EVENT
SPEED=6100. RPM
accell.
-0.004
-0.008
-0.012
-0.016
-80
-60
-40
-20
0
20
40
60
80
cam angle

(a)

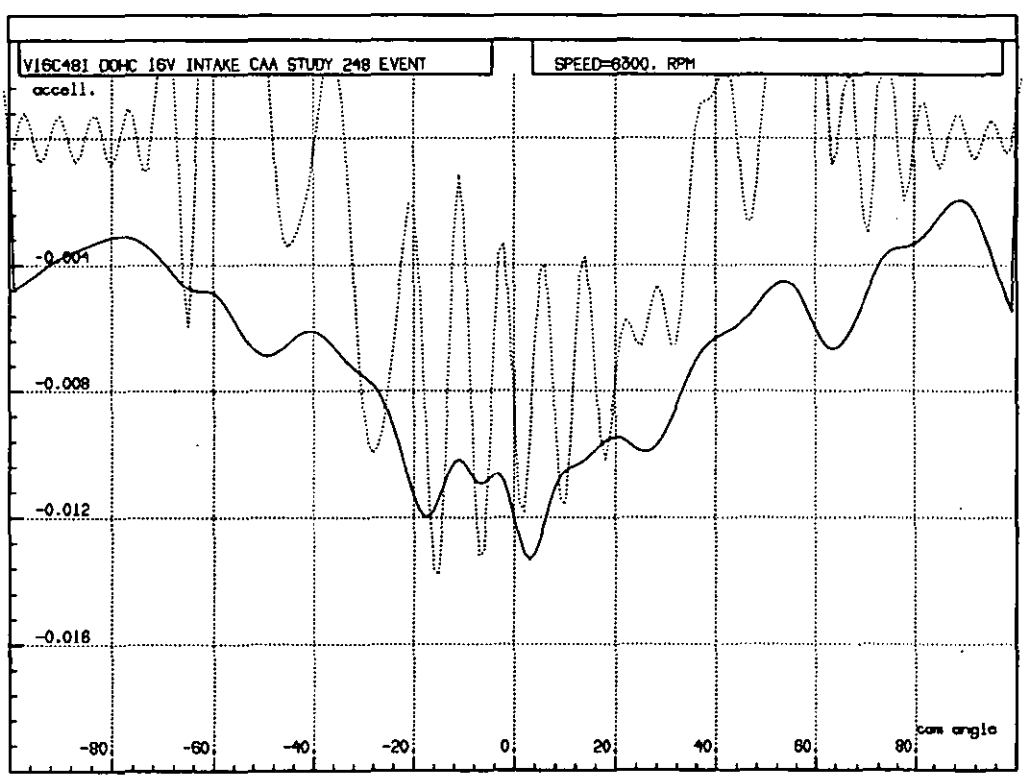
V16C48I DOHC 16V INTAKE CAA STUDY 248 EVENT
SPEED=6300. RPM
accell.
-0.004
-0.008
-0.012
-0.016
-80
-60
-40
-20
0
20
40
60
80
cam angle

(b)

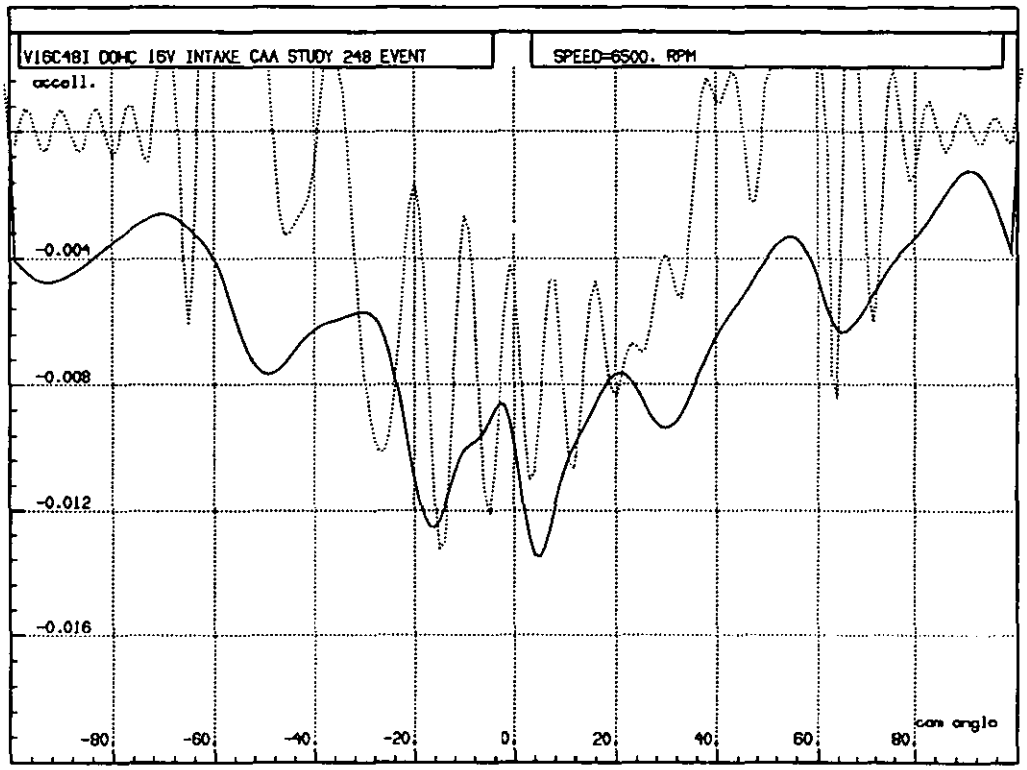
V16C48I DOHC 16V INTAKE CAA STUDY 248 EVENT
SPEED=6500. RPM
accell.
-0.004
-0.008
-0.012
-0.016
-80
-60
-40
-20
0
20
40
60
80
cam angle

(c)

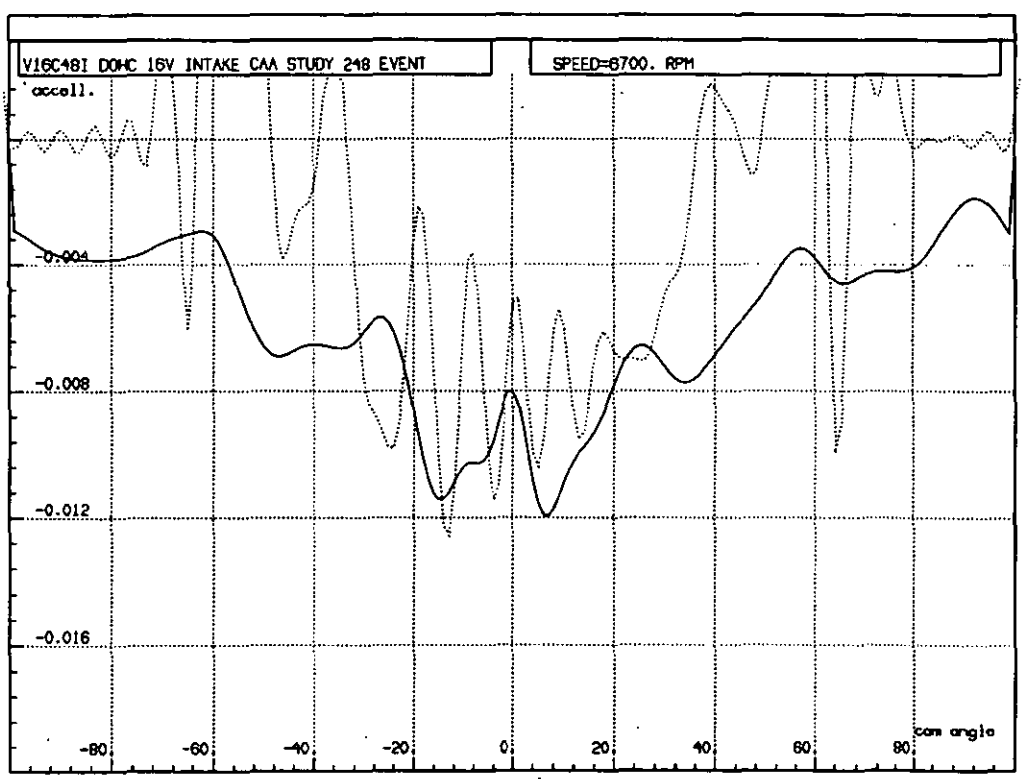
V16C48I DOHC 16V INTAKE CAA STUDY 248 EVENT
SPEED=6700. RPM
accell.
-0.004
-0.008
-0.012
-0.016
-80
-60
-40
-20
0
20
40
60
80
cam angle

(d)

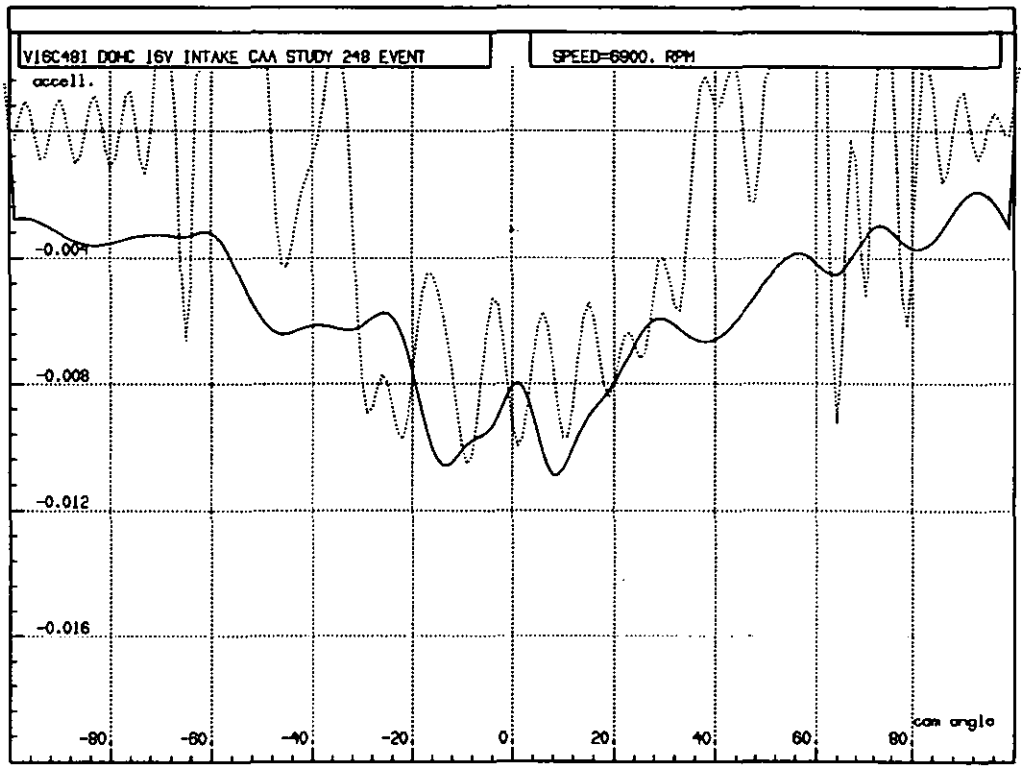

(e)

Figure 58: Dynamic valve deceleration and corresponding spring deceleration capacity (a measure of spring force reserve) for the original spring exited by the dynamic accelerations from Figure 51. (a) 6100rpm (b) 6300rpm (c) 6500rpm (d) 6700rpm (e) 6900rpm

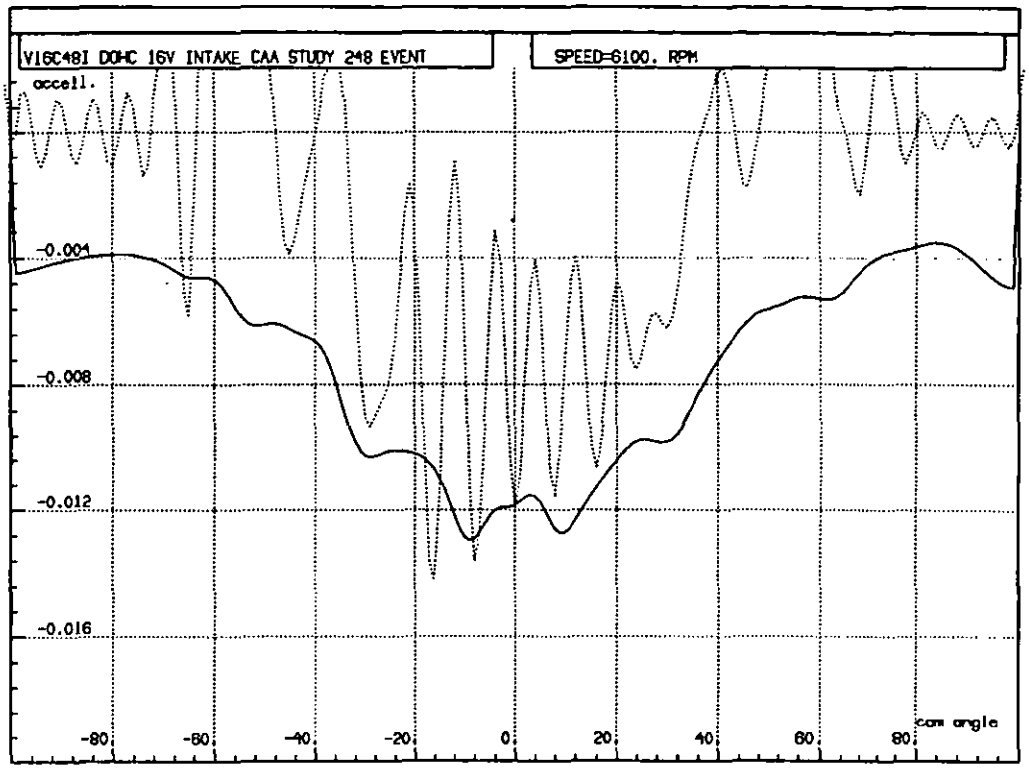
V16C48I DOHC 16V INTAKE CAA STUDY 248 EVENT
SPEED=6100. RPM
accell.
-0.004
-0.008
-0.012
-0.016
-80
-60
-40
-20
0
20
40
60
80
cam angle

(a)

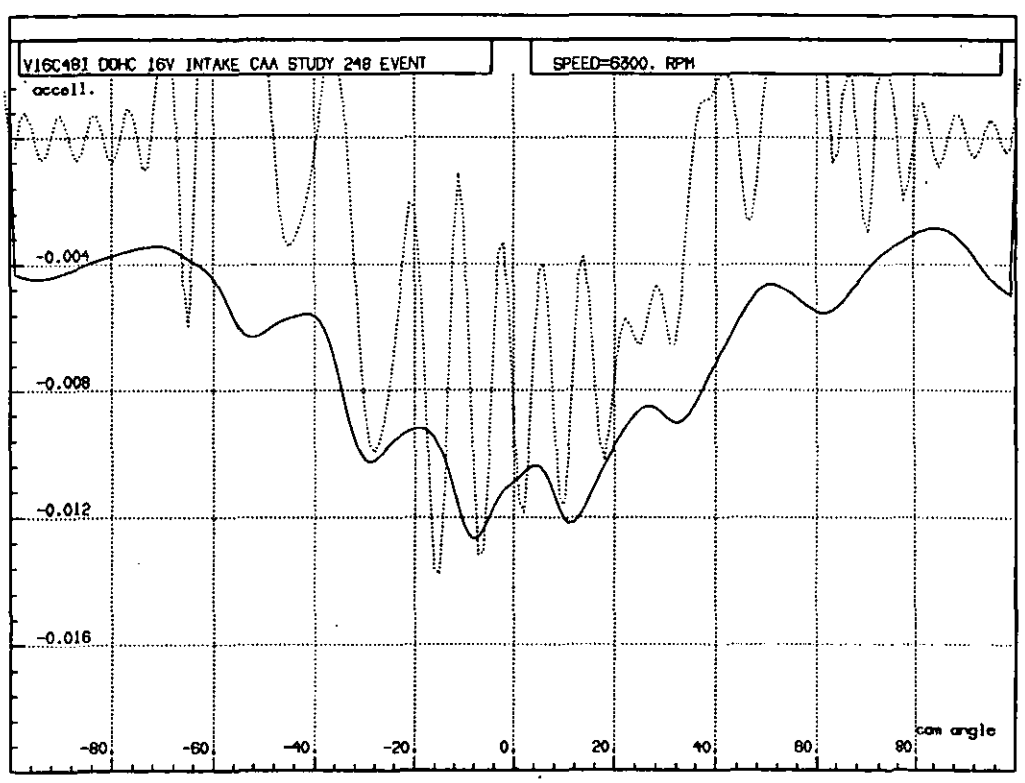
V16C48I DOHC 16V INTAKE CAA STUDY 248 EVENT
SPEED=6300. RPM
accell.
-0.004
-0.008
-0.012
-0.016
-80
-60
-40
-20
0
20
40
60
80
cam angle

(b)

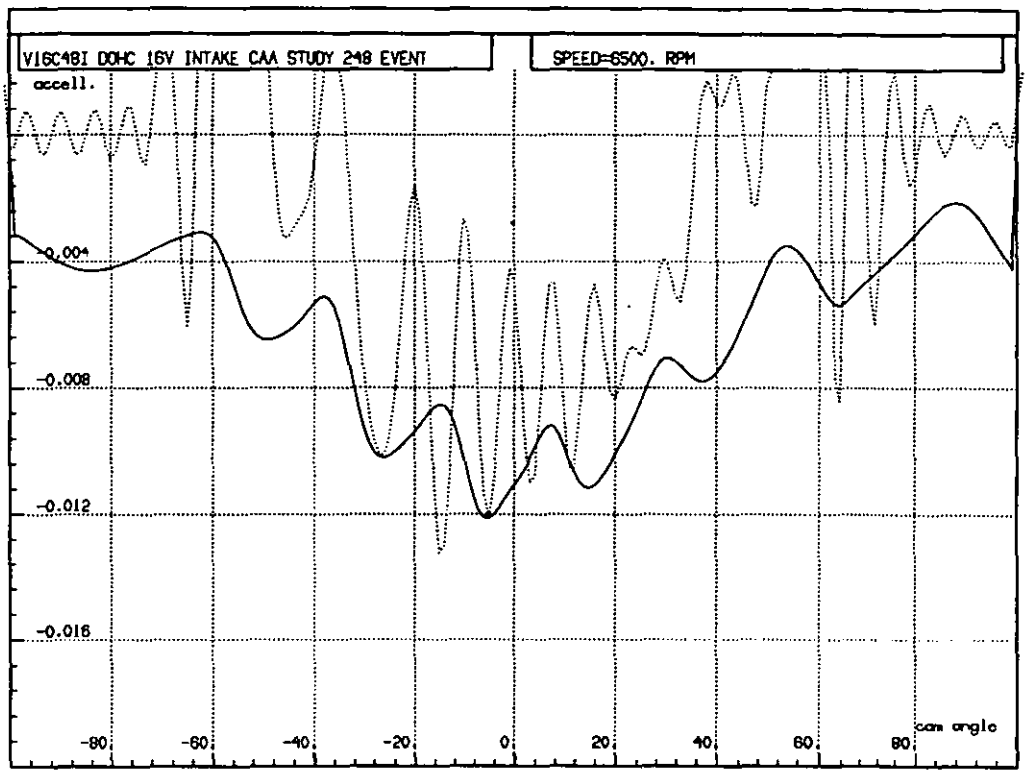
V16C48I DOHC 16V INTAKE CAA STUDY 248 EVENT
SPEED=6500. RPM
accell.
-0.004
-0.008
-0.012
-0.016
-80
-60
-40
-20
0
20
40
60
80
cam angle

(c)

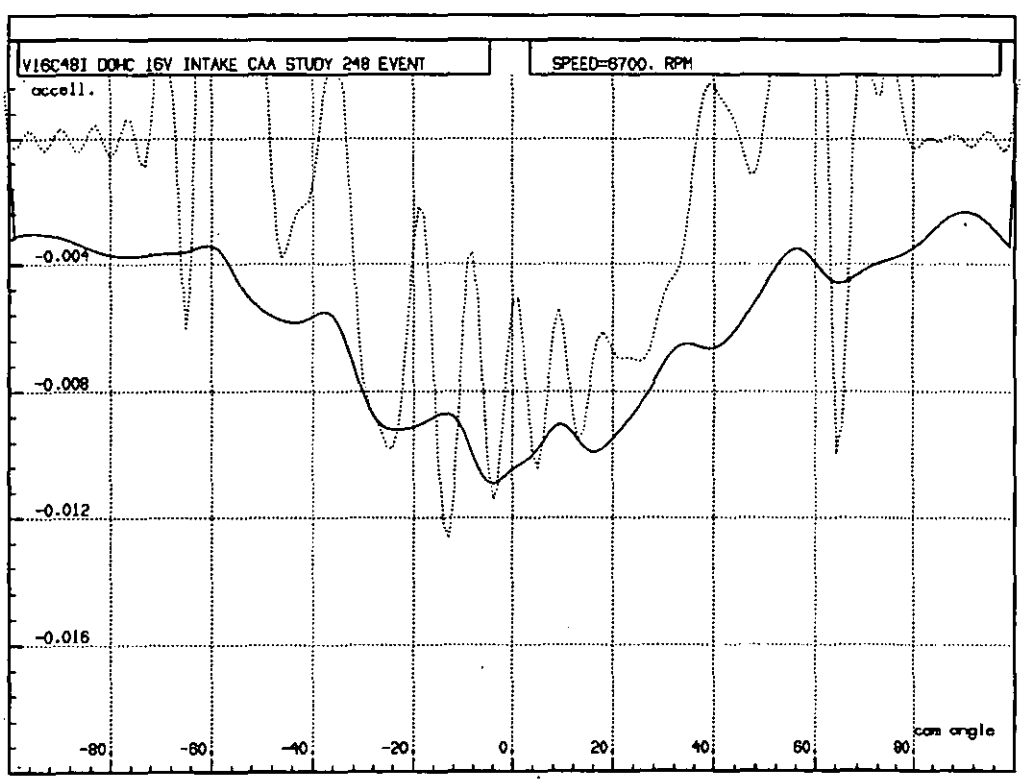
V16C48I DOHC 16V INTAKE CAA STUDY 248 EVENT
SPEED=6700. RPM
accell.
-0.004
-0.008
-0.012
-0.016
-80
-60
-40
-20
0
20
40
60
80
cam angle

(d)

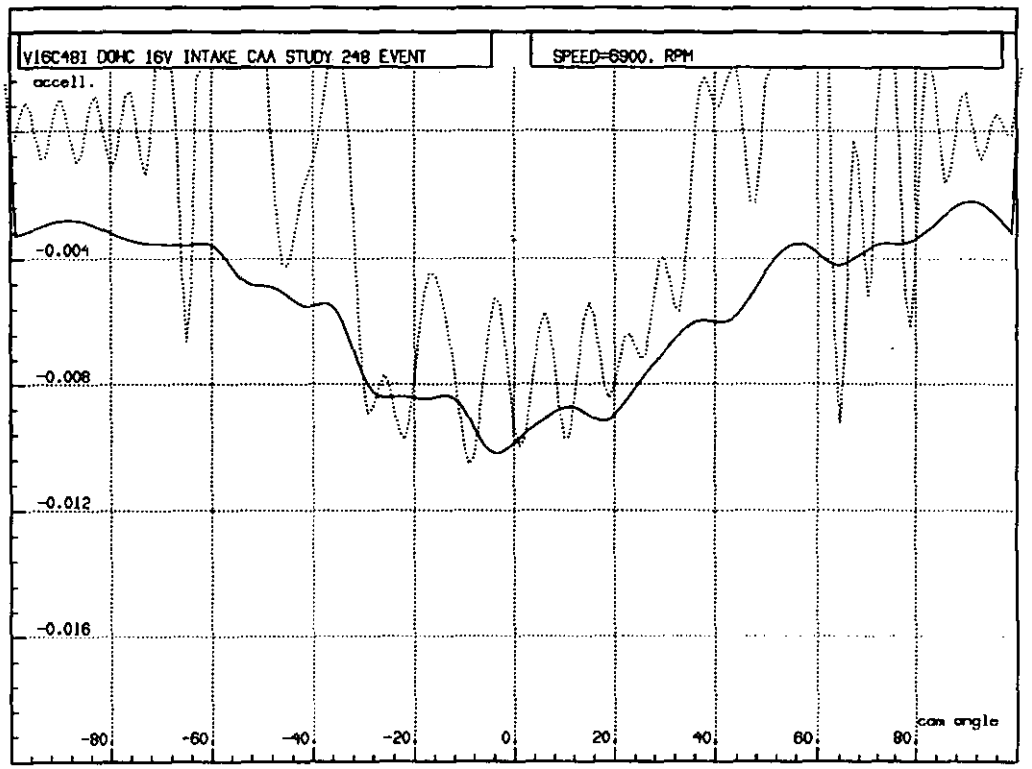

(e)

Figure 59: Dynamic valve deceleration and corresponding spring deceleration capacity for the frequency characteristic from the first optimization run exited by the dynamic accelerations from Figure 51. (a) 6100rpm (b) 6300rpm (c) 6500rpm (d) 6700rpm (e) 6900rpm

10.4 Spring Optimization under Realistic Constraints

The last section provided an interesting first optimization step, but the resulting frequency characteristic is far from that of any realistic spring. The almost infinite slope at zero lift would translate into a bending edge of the actual spring wire because the steep increase requires a large number of coils to become inactive all at once, hence they would have to have exactly the same pitch spacing. The directly adjacent coils on the other hand would have to have a much larger pitch spacing because they would have to stay active up to high lift.

But even if this characteristic could be achieved, there are additional practical considerations for a realistic spring design. The very early and extreme frequency increase means that the most part of the deformation is performed by a low number of active coils, which leads to very high stresses. Furthermore, in a practical application, the installed length space has significant tolerances associated with it. This means that the actual base frequency of a spring with the above derived characteristic would largely vary from engine to engine and partly also from valve to valve.

Earlier on, the limitation on the frequency characteristic by the stress of the wire material was discussed. But a general limit for every valvetrain configuration for the frequency range can not be given, since the required forces, the installation space, and the possible number on active coils vary in a wide range. Equally important is the fact that the allowed stress range depends very much on the material used, the manufacturing process and the material purity. Furthermore, using non round wire material and non cylindrical springs allows for additional design freedom to realise a frequency characteristic. In general, the more money one is willing to spend, the higher the stress limits one can achieve. Because of this, for the purpose of optimization, no fixed stress limit for the given design envelope has been chosen, but the frequency characteristic has been constrained instead. This allows more freedom to investigate afterwards whether a frequency characteristic obtained offers enough benefits to spend the extra costs to design such a spring.

To force the algorithm to a solution which results in a realistic spring, the parameters have been constrained as follows:

Parameter	Physical Meaning	Lower Boundary	Upper Boundary
f_1	Frequency at installed height	400	600
f_2	Frequency at valve open position	-	1000
df/ds_1	Slope of frequency characteristic at 0mm valve lift	0	10
df/ds_2	Slope of frequency characteristic at max (10 mm) valve lift	>0	-
Rf_1	Relative length of tangent vector at 0mm valve lift	0.2	3.0
Rf_2	Relative length of tangent vector at max valve lift	0.2	3.0

Table 8

These limits are based on hardware and mathematical considerations already discussed in Section 10.2; the reasoning is briefly summarised as follows:

Frequency at installed height:

This parameter has been constrained to limit the stress range of the resulting spring and to avoid a solution with the trivial answer of an infinite frequency.

Valve open frequency:

This parameter again has been constrained to limit the stress range and to prevent the trivial solution.

Rate of frequency change at installed length:

The lower boundary for this parameter avoids a decrease in frequency at installed length (which is impossible for a helical spring as explained before) while the upper limit guarantees that the rate of frequency change is not too high in the neighbourhood of the installed length, so that even under tolerance conditions the installed length frequency is close to the theoretical one.

Rate of frequency change at valve open:

This has been limited to be positive to avoid a decrease of frequency with lift.

Relative length of the tangent vectors:

The lower limit guarantees that the tangent vector has a minimum effect in the neighbourhood of the corresponding spline point; a zero length would cancel any effect of the slope at installed length. The upper limit ensures that the resulting spline forms a valid function.

The numerical values in Table 8 were set, somewhat arbitrarly, by reference to the standard hardware.

The constraints above can all be handled in the optimization by the efficient pre-filtering technique. There are two additional constraints which have to be taken into account by the cost function directly; these are the requirement for a monotone increase in frequency, and a limit on the maximum rate of frequency rise per mm valve lift. The maximum slope allowed for this optimization run was 1500Hz/mm.

All the above measures are only to ensure an envelope of valid characteristics; they give no indication of how an improved vibration response of the spring may be obtained. The measure used to perform this for the optimization run presented here is again the spring force reserve area, because of its unique combination of amplitude, phase, and speed location dependence. Hence all other parts of the cost function just have a zero contribution if the set of parameters fall into the allowed borders, and the spring force reserve area represents the function to be optimized. Since the algorithm used actually minimises the given function, and the requirement is to increase the spring force reserve area, the performance figure has simply been multiplied by a factor of -1. Hence the target function is:

$$l = \begin{array}{c} (-1)P_{13}(p_{res_1}, \ldots, p_{res_n}) + \\ \sum_{res} pf_{res}(a_{res_j}, p_{org_1}, \ldots, p_{org_n}) + \\ pf_{max/minslope}(a_{org_j}, p_{org_1}, \ldots, p_{org_n}) \end{array} \qquad /10.4.1/$$

The resulting frequency characteristic is shown in Figure 60, together with the original characteristic of the initial spring design. It can again be seen that the algorithm arrived at a maximal initial frequency increase, constrained by the slope and vector length at installed length. This time the algorithm has increased the base frequency, as one would expect to reduce spring vibrations. But it is worth mentioning that the algorithm did not push this to the allowed maximum of 600 Hz. The valve open frequency on the other hand has been placed at the maximum allowed value. The same is true for the maximum frequency increase of 1500Hz/mm.

A first impression of the quality of this result can be gained from the performance figure P_{13}. The end result for this optimization reached a spring force reserve area of 0.05888mm/deg^2 compared to 0.06395mm/deg^2 for the theoretical unconstrained maximum and 0.04571mm/deg^2 for the earlier unconstrained optimization run. Therefore this more realistic run reaches closer to the theoretical static spring result than the unconstrained run. For some reason the progress of optimization finds a better path down to the optimum. One possible explanation for this is the implementation of the soft constraints. The unconstrained run is allowed to use any parameter combination possible. This results very often in the violation of the only implemented hard constraint, the monotone increase in frequency. This obviously blocks off otherwise promising directions. The soft filtering constraints may avoid beforehand most of the combinations leading to this problem.

The resulting response over speed of the sum of the modal amplitudes is shown in Figure 61, in comparison to the response for the original base line spring. One can see that the amplitude is lower over the complete speed range, but the most significant reduction takes place in the critical speed range around 6500 rpm. The optimization algorithm has successfully placed a low response amplitude in the speed range where an out of phase spring vibration would be very risky for the valvetrain. This shows the benefit of using the performance figure for the spring force reserve area, with its ability to provide a speed dependent weighting of the spring vibrations.

The time domain spring force reserve results in Figure 62 show that the constraint on the frequency rise no longer allows the in phase vibration of valve and spring to the extent reached for the unconstrained run; consequently it seems to be more beneficial to have a low spring vibration amplitude in the critical speed range, rather than a large oscillation only partly in phase.

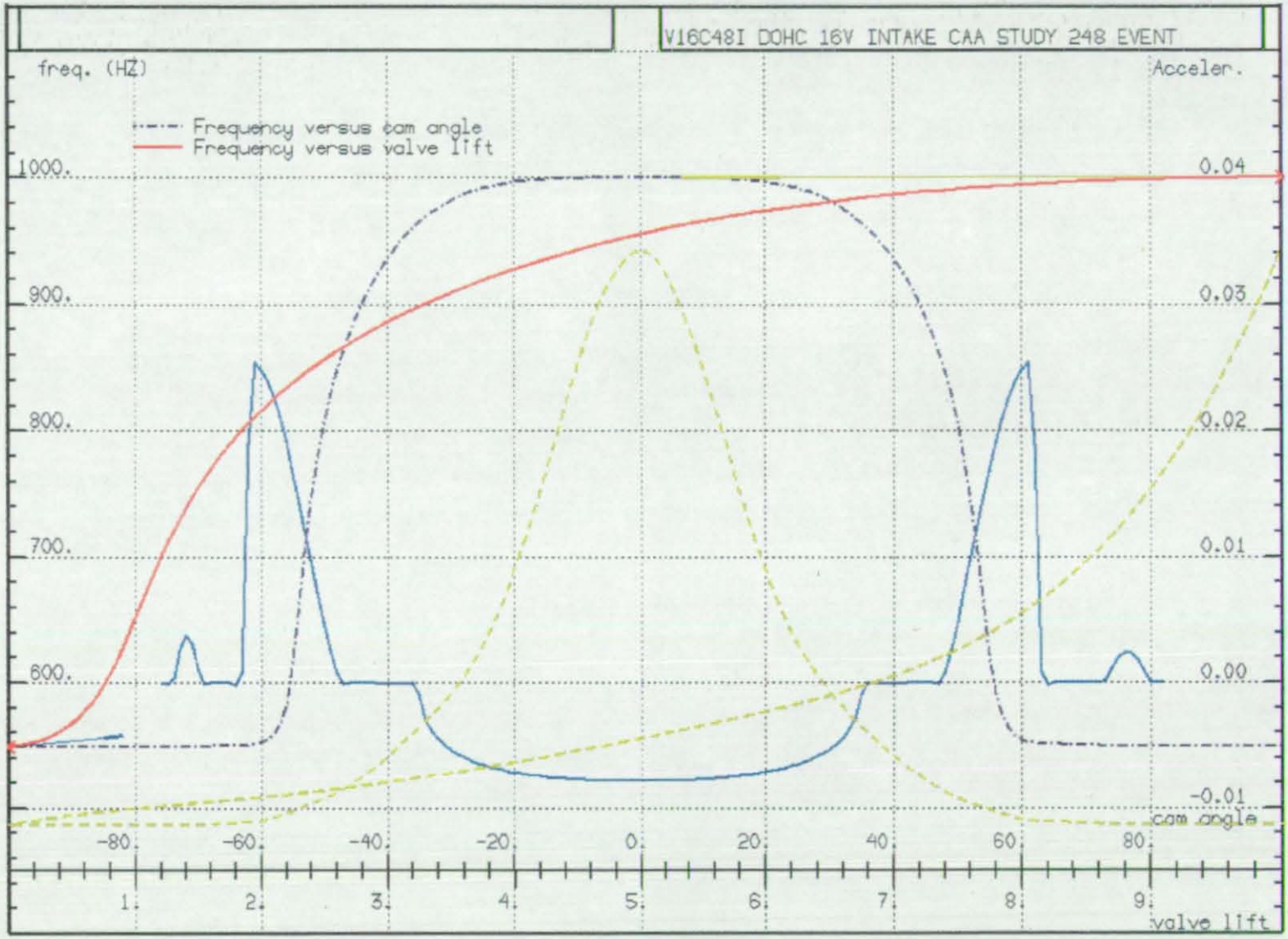

Figure 60: Comparison of frequency characteristic for the original spring and for the result from the final optimization run

Since the result for this run is extremely close to the theoretical optimum for a static spring, this frequency characteristic has been chosen to calculate the corresponding spring design. But before one proceeds to do so, there is one further aspect to be considered beforehand. Some of the benefits for this spring characteristic depend on the phase relation between spring and valve vibrations. Here is a critical point. While a stiff valvetrain has the advantage that spring and valvetrain vibrations are mainly decoupled, they have the disadvantage that there is significant scope for variation in the fundamental valvetrain frequency. Depending on oil temperature, installation length of the hydraulic lash adjuster, aeration, tappet body tolerances and bearing conditions for the camshaft the frequency may vary by more than 20%. Accordingly, the theoretically predicted phase of the valve vibrations can be quite different to the actual vibration in an arbitrary single valvetrain. Since a test of the resulting spring is envisaged, the influence of this effect shall be investigated before the decision for the above derived frequency characteristic is made.

For this purpose the result from the last run has been used to restart the optimization program. But this time the dynamic valve accelerations have not been used. Instead the kinematic valve accelerations are employed to excite the spring. All other settings where left unchanged. The resulting frequency characteristic of this restart is shown in Figure 63. There is relatively little change, as compared with the previous case which used the dynamic acceleration, but now the maximum frequency rise is no longer at the imposed limit. The rise in frequency no longer takes place so early and rapidly, since there is no more benefit from any phase relation aspects. But the general advantage of an early frequency rise still leads to a very similar shape.

The deterioration of the spring force reserve area for this characteristic is small. It drops from 0.05888mm/deg^2 to 0.05529mm/deg^2 which is still better than the result from the unconstrained run. A comparison of the maximum surge amplitude plot (Figure 64) reveals that this solution flattens out the response between 5700 and 6500 rpm, with only small deterioration of the overall response. This result verifies that the frequency characteristic found using the dynamic valve accelerations is close enough to the optimum for the quasi static valve acceleration, where the phase relation does not have any influence. The main conclusion is that overall performance is unlikely to be sensitive to valvetrain fundamental frequency, and it is natural to base the actual spring design on the optimization carried out with dynamic accelerations.

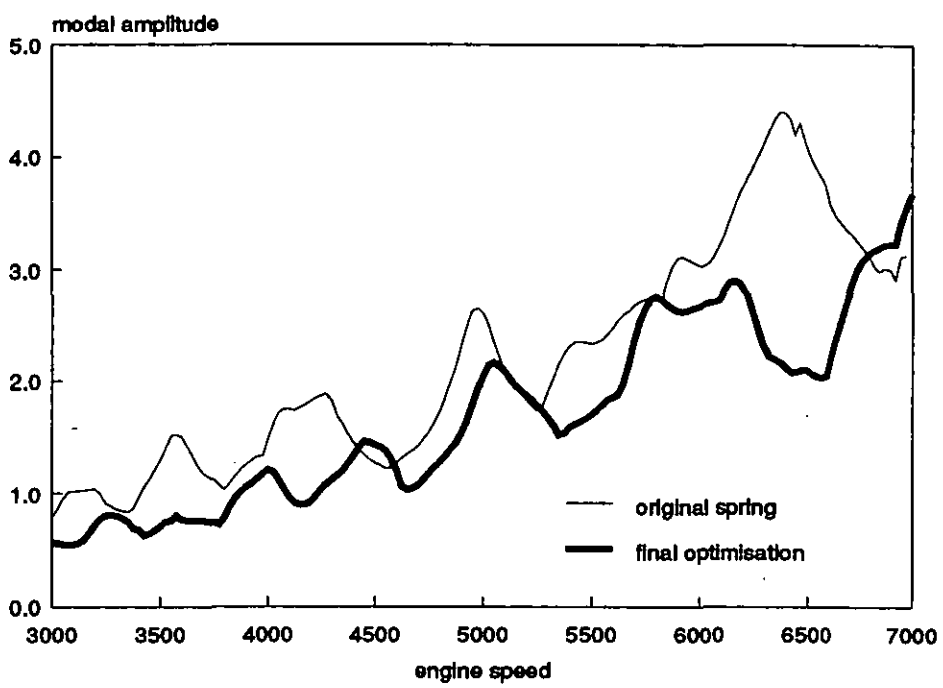

Figure 61: Comparison of modal amplitude against engine speed for the original spring and the result from the final optimization run

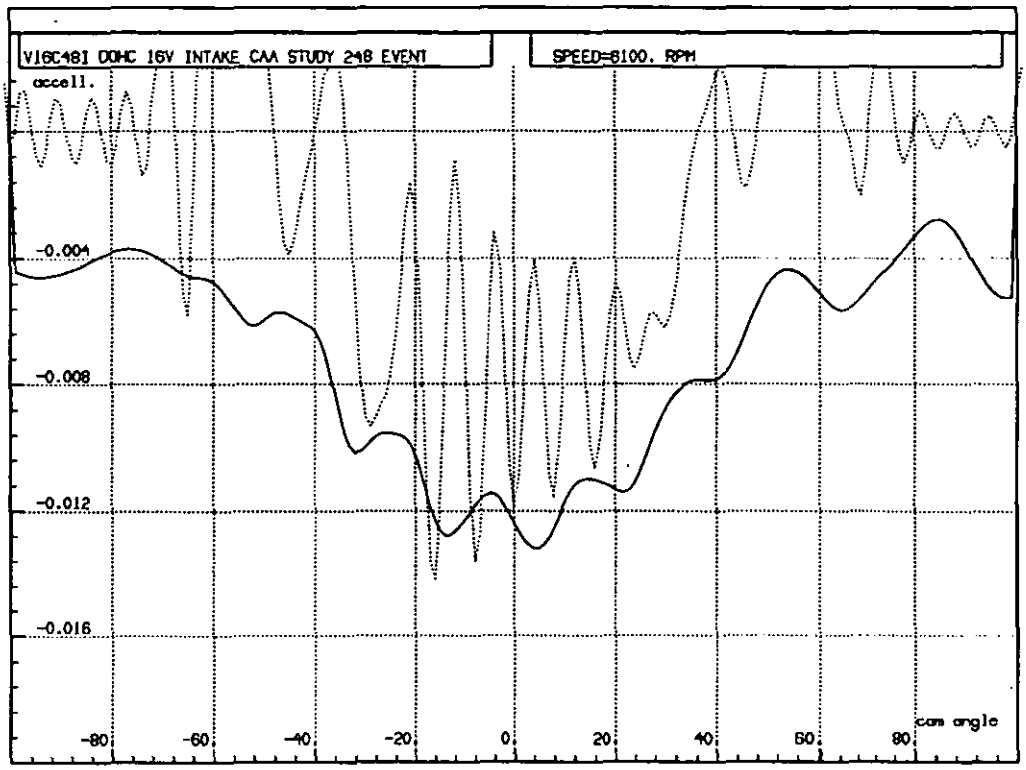
V16C481 DOHC 16V INTAKE CAA STUDY 248 EVENT
SPEED=8100. RPM
accell.
-0.004
-0.008
-0.012
-0.016
-80
-60
-40
-20
0
20
40
60
80
cam angle

(a)

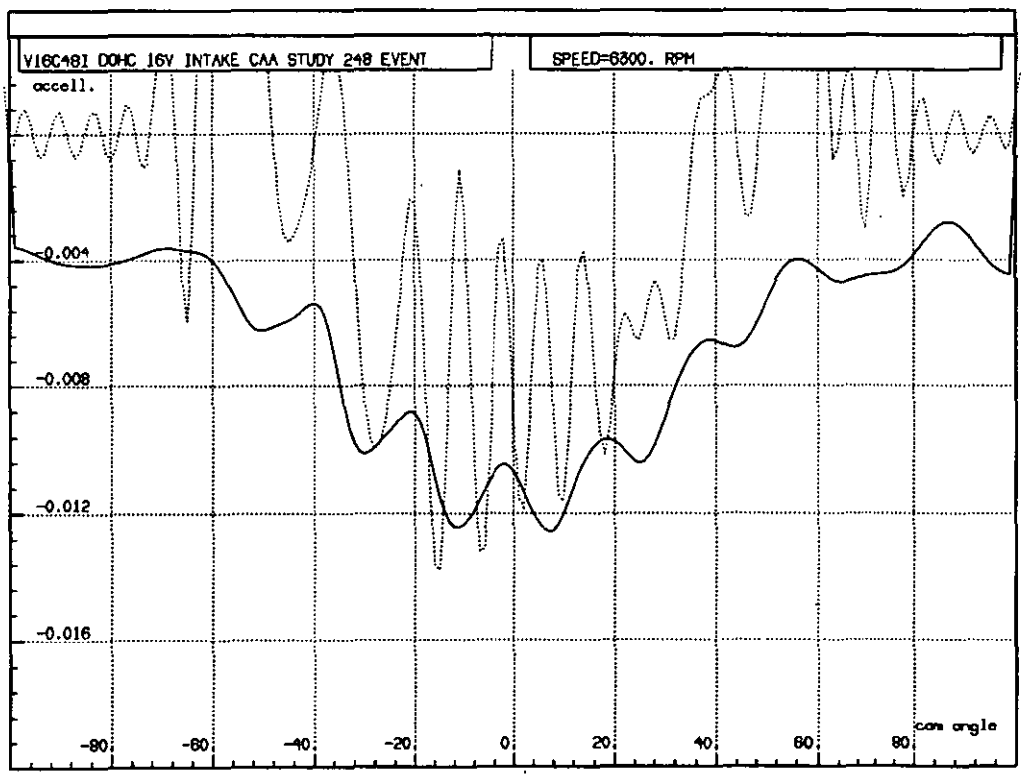
V16C481 DOHC 16V INTAKE CAA STUDY 248 EVENT
SPEED=6300. RPM
accell.
-0.004
-0.008
-0.012
-0.016
-80
-60
-40
-20
0
20
40
60
80
cam angle

(b)

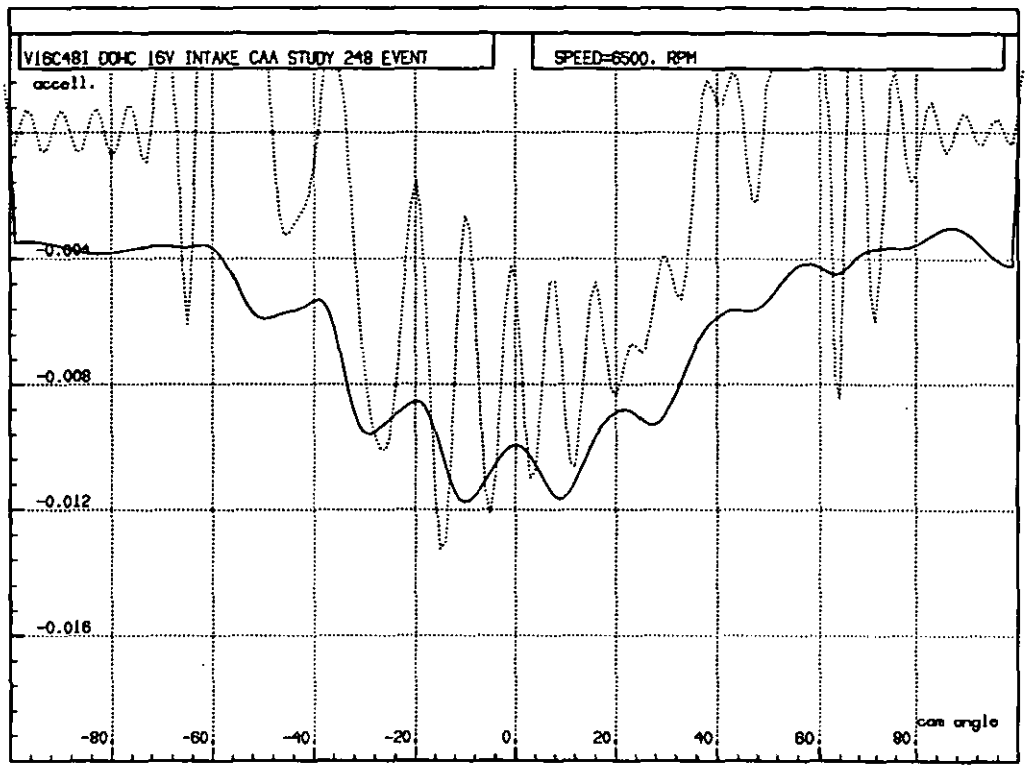
V16C48I DOHC 16V INTAKE CAA STUDY 248 EVENT
SPEED=6500. RPM
accell.
-0.004
-0.008
-0.012
-0.016
-80
-60
-40
-20
0
20
40
60
80
cam angle

(c)

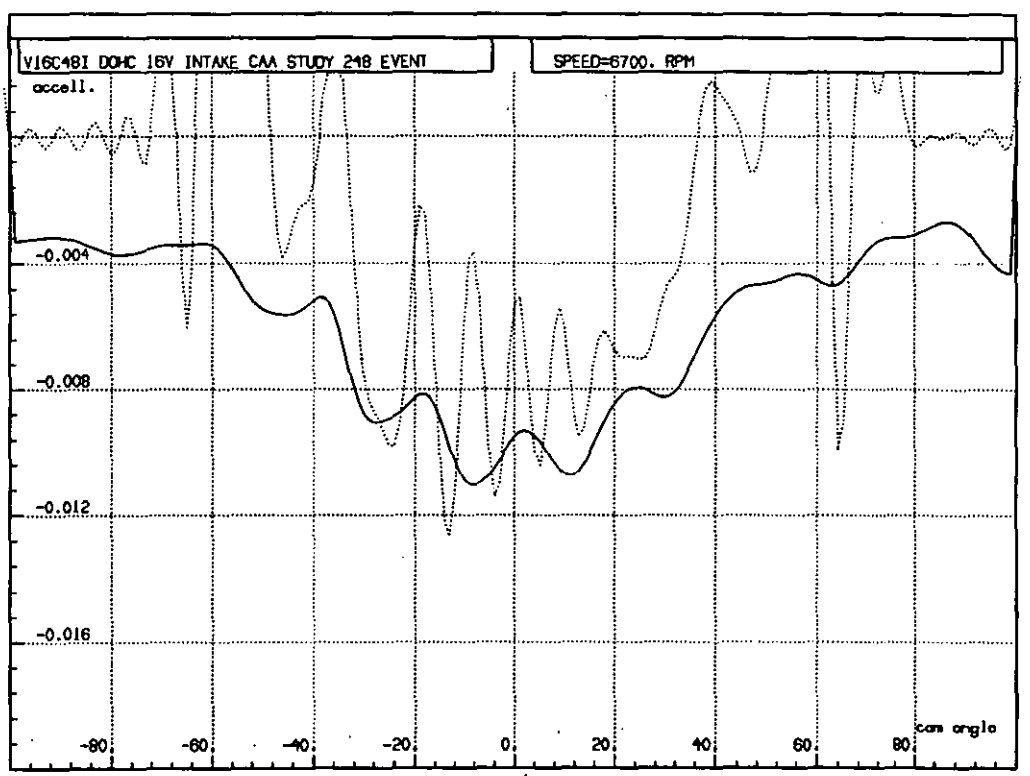
V16C48I DOHC 16V INTAKE CAA STUDY 248 EVENT
SPEED=6700. RPM
accell.
-0.004
-0.008
-0.012
-0.016
-80
-60
-40
-20
0
20
40
60
80
cam angle

(d)

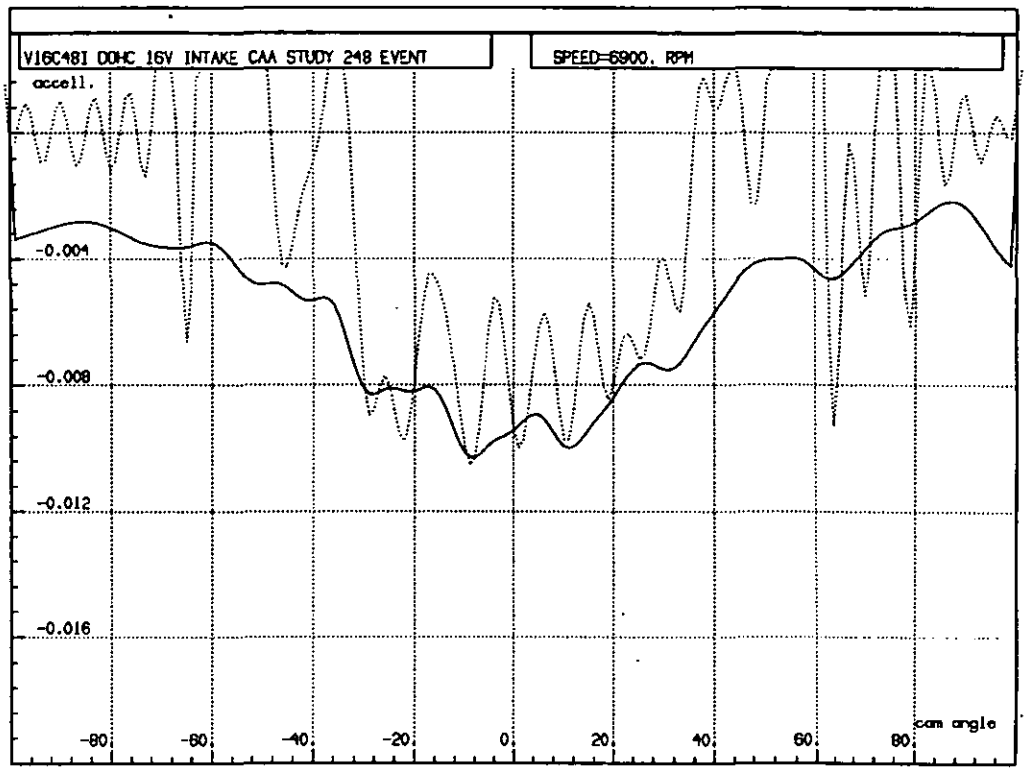

(e)

Figure 62: Dynamic valve deceleration and corresponding spring deceleration capacity for the frequency characteristic from the first optimization run exited by the dynamic accelerations from Figure 51. (a) 6100rpm (b) 6300rpm (c) 6500rpm (d) 6700rpm (e) 6900rpm

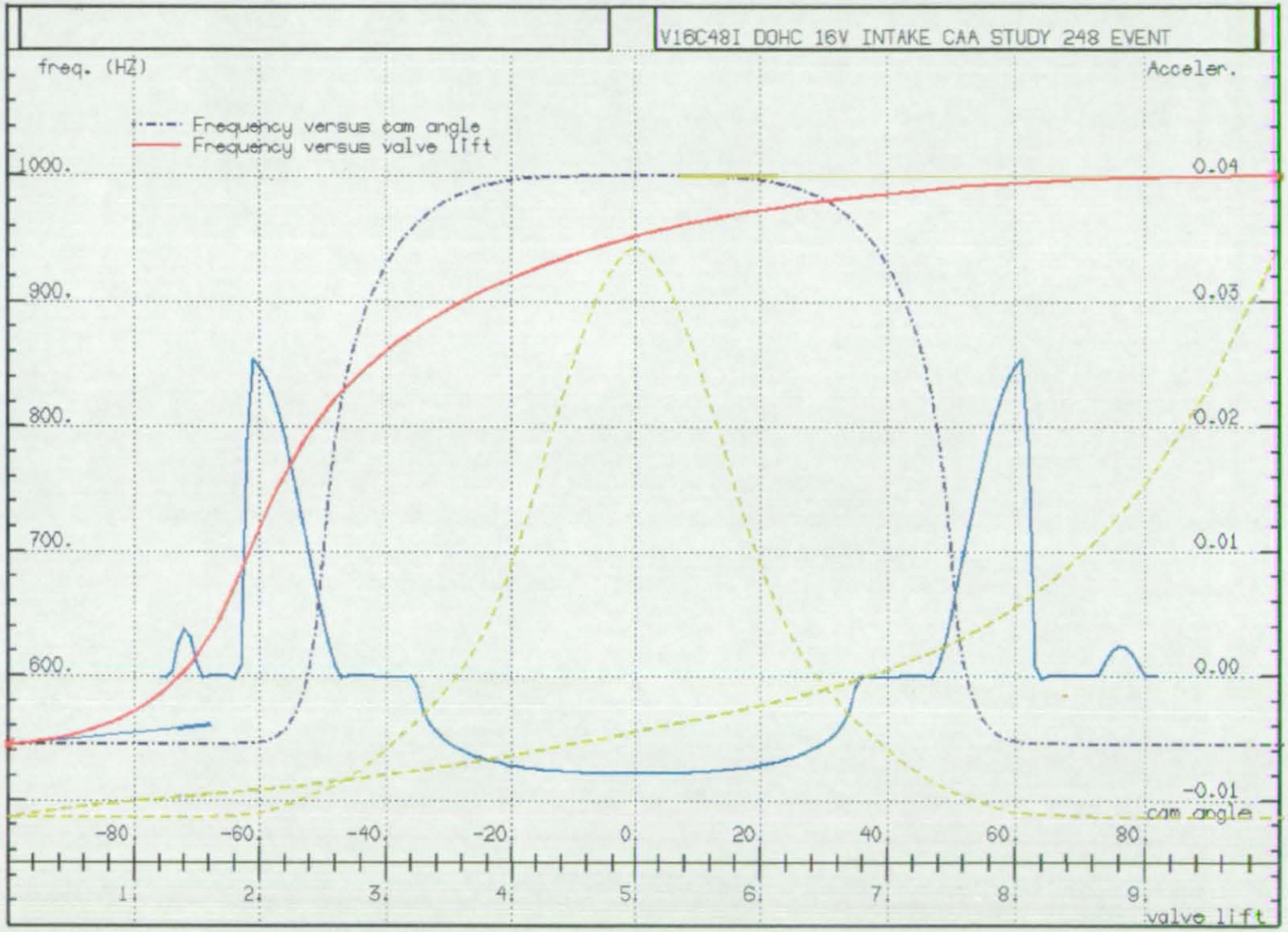

Figure 63: Comparison of frequency characteristic for the restart of the final optimization result using the kinematic acceleration as the forcing function

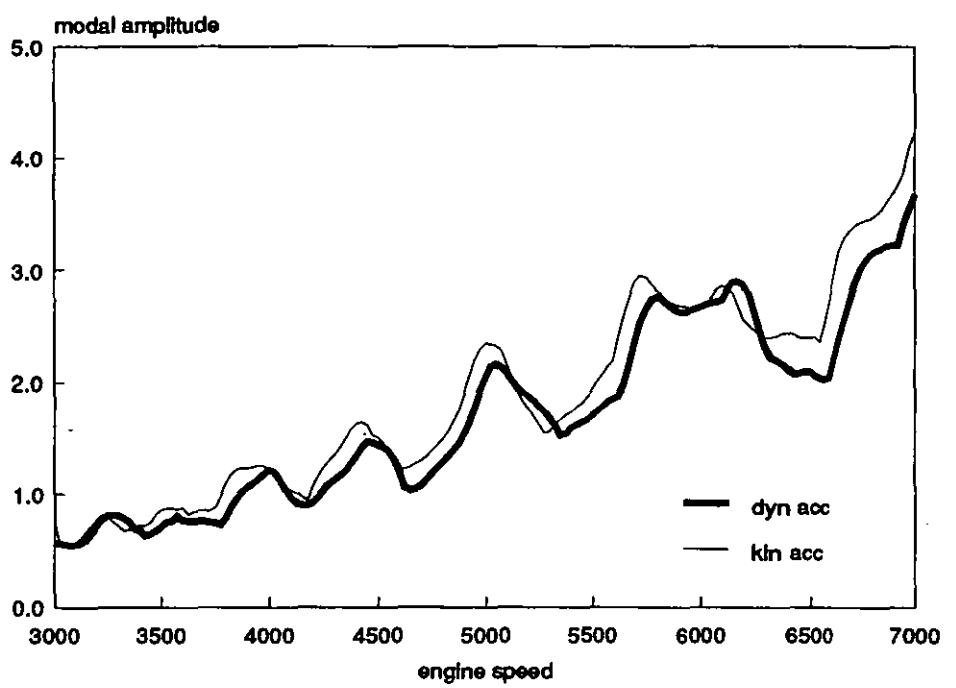

Figure 64: Comparison of modal amplitude against engine speed for the final optimization result and the restart result using the dynamic excitation for both frequency characteristics

10.5 Discussion

In the last section, three sample runs from the optimization program have been considered, which finally lead to a reasonable optimized frequency characteristic. Before presenting the method of evaluating the corresponding spring design in Section 11, a number of general observations from various other program runs are now summarised.

In the program runs above, the only real guidance for the optimization was the spring force reserve area. As mentioned before, optimization can be based on any other combination of the performance figures introduced in Section 9. One criterion considered, uses the total area under the spring surge extremes. The effect of this depends on the weighting compared to the spring reserve area. If the total area is dominant in the target function, the solution from the optimization simply moves to the borders of maximum allowed frequency and hence to a highly stressed spring. This is natural, since a frequency increase moves the response to higher speeds, leaving a smaller area in the investigated speed range. The usage of this figure thus normally does not give any additional benefits compared to the spring reserve area. Having said that, one case has been discovered where real benefit was obtained. In this case, a bad resonance was located just in the critical speed range. From the optimization using only the spring force reserve area it became apparent that a local minimum was located for an overall lower frequency characteristic. This solution had detrimental effects on the low speed range. Using a small contribution of the spring surge area helped to drive the solution to a characteristic in a slightly higher frequency range, with an overall improved response. In spite of this, for most of the runs so far, the spring force reserve area represented a highly satisfactory measure for the spring optimization.

Having discussed the response aspects of the spring optimization, it is useful to have a short look at the solution speed aspects. There are a number of different measures to improve the overall solution speed for the optimization run. The above described run for the chosen frequency characteristic required approximately 18 cpu hours on a DEC5000/200 workstation, taking the first two spring modes into account, with a speed range from 3000 to 7000 rpm, in steps of 25 rpm under the influence of dynamic valve accelerations. While this time might sound acceptable, it is definitely useful to speed up the process to enable the fast evaluation of alternatives, especially in view of the tendency to obtain local solutions rather than the final answer on the first attempt.

To speed up the process a number of possible measures are available.

- Reduced number of spring modes

The computational effort for a function evaluation linearly depends on the number of modes of the spring taken into account. Since the solutions for the higher modes are increasingly inaccurate anyway, it is useful to restrict the optimization to the first two modes. In some cases a first attempt may be made using only the first mode to get an initial idea about the right range.

- Reduced number of Harmonics for excitation and solution

The accuracy of the results depends on the number of harmonics used for the Fourier representation of the excitation and the response. How many of them are needed depends on the spring frequency, the speed range and the number of modes analysed. Since the number of harmonics determines the size of the matrix to be solved, the calculation speed has between linear and cubic dependence on the number of harmonics. Whether it is a linear dependence or a cubic one depends on the bandwidth of the matrix, for a constant frequency linear spring it would be linear because only main diagonal elements are non-zero in the resulting matrix.

- Reduced number of Harmonics used for frequency variation

As discussed before, the number of harmonics employed to represent the time dependent frequency variation of the spring, influences the band width of the resulting matrix. While this is an efficient way to reduce the cpu effort for a manual analysis of a single spring depending on the springs progressivity, it is not suitable to lower this value for the optimization since during the process there may be characteristics which can not be accurately represented by a low number of harmonics.

- Reduced speed range of the investigation

While for the above runs, a speed range from 3000 to 7000 rpm has been used to get a full range response plot, in a practical application this range can be reduced to the critical operating range of the engine which would be 4500 to 7000 rpm at most in this case. This would proportional reduce the cpu effort for each function evaluation.

- Reduced speed resolution

For the runs above, a speed resolution of 25 rpm has been used. In a practical application 50 rpm are most probably enough. A more coarse resolution carries the risk that the optimization would find a result, where no real improvement had taken place, but where the peak resonances just fall in between the evaluated speeds. Again any reduction in resolution results in a corresponding decrease of cpu-effort

- Selective time domain evaluation

Approximately 20 to 30 percent of the cpu time for each function evaluation is spent on the back-transformation of the Fourier coefficients into the time domain. Taking the spring force reserve area for example, only the deceleration phase of the profile has to be taken into account to calculate this quantity. So instead of carrying out the transformation into the time domain for the full 360° of cam angle, one can limit this step to ±40°, which again linearly decreases the cpu effort for this part of the solution procedure.

- Kinematic versus dynamic valve acceleration values

The usage of dynamic valve accelerations requires a less efficient order of assembly for the matrices at each speed point, which accounts for approximately 5% of the time needed for each function evaluation. So initial runs could be carried out with the kinematic accelerations and once a characteristic close to a satisfactory solution is obtained, a restart using dynamic accelerations may be carried out, which is then likely to be very efficient because the start point is close to the overall optimum.

11

Spring Design According to a Given Frequency Characteristic

The last section covered the derivation and application of a method to optimize the vibration response of a spring by means of the springs frequency against lift characteristic. The final step towards an optimized spring is to determine the corresponding physical spring design. In this section only a simplified example of this task will be looked at, since a full spring design program would be beyond the scope of this thesis.

Spring manufacturers have already extensive spring design programs to solve this task, but these programs do not take the frequency characteristic into account for the full lift range. Currently they determine only the frequency at installed length and at valve open length, but not the shape of the curve in between. During the progress of the work presented here, one of the manufacturers initiated the development of the necessary interfaces between their design program and those used in this study, to enhance the design capabilities for the future. Unfortunately, this tool was not available for the present study.

To overcome this shortfall, a simplified spring design task has been carried out specifically for this study, to enable the procurement of suitable test hardware. Since the number of variables are very large, this study used some constraints to narrow down the number of unknowns. Hence the design task has been restricted to a symmetrical, cylindrical, round cross-section wire spring. This choice significantly narrows down the number of open parameters to be determined for the required spring, and as we will see, also speeds up the solution process. In addition to this analytically motivated restriction, there are some additional constraints to be taken into account for the practical application.

For a new engine design, there is significant design freedom to establish the installed height of the spring, the outer and inner spring diameters, the number of coils employed and the bottom and retainer end diameters. For this study, the situation was different. Only a spring which fits into the current envelope of an existing engine, including the retainer, offered the opportunity to have the spring response tested on an engine rig. Thus the inner and outer diameters, the installed length, the maximum allowable solid length, and the bottom and retainer end diameters, were fixed.

The above restrictions have the advantage of making the design task relatively easy, but they have the drawback that the resulting spring suffers very high static stresses, which are just at the border of current material and manufacturing capabilities. It is generally true that a higher frequency spring requires higher wire stress values, if the rest of the design is fixed. But in an early stage of the development this effect can be partly counteracted by designing the right installation envelope and utilising a suitable wire cross-section.

The general approach for solving the spring design problem presented here, utilises the pre-processor program for the discrete spring model which has been shortly described above and in more detail in the MSc thesis by the author (Schamel 1991), which calculates

the frequency characteristic for a given nonlinear spring design. By allowing the spring definition to be modified as a set of free parameters, this program can be used to treat the spring design problem as an optimization task. The target for this optimization can then be defined in terms of the difference between the intended spring frequency characteristic and the one resulting from any set of spring design parameters.

The disadvantage is that the eigenvalue analysis performed in this discrete spring representation requires a substantial amount of cpu time, especially when the number of discrete masses is large enough to get a resonably fine frequency resolution. Here one can utilise the restriction made in the choice of cylindrical springs only. For such springs the frequency of the spring can be directly related to the spring mass and the spring rate as given in equation 5.1.10. The necessary information, mass and stiffness, at any given length is readily available in the pre-processor for the discrete spring model. Hence, instead of solving a large eigenvalue problem many times, the frequency characteristic can be solved efficiently by evaluation of equation 5.1.10 at any required length. Thus a fast tool to calculate the frequency characteristic for cylindrical springs is available.

The frequency characteristic depends on the design parameters of the spring, which, for a cylindrical round wire spring, are as follows

d	wire diameter
D	coiling diameter
N_t	total number of coils
L_0	free length
L_1	installed length (length at s_1)
L_2	valve open length (length at s_2)
F_1	force at installed length
F_2	force at valve open
	and the pitch spacing as a function of the coil number

These design parameters can now be adjusted by the same parameter optimization algorithm used above. The cost or target function can be set up by the difference of intended to achieved frequency characteristic.

$$l_{spr} = \sum_{i=1}^{n} (f_{required} - f_{achieved})^2 (n - i) \qquad /11.1/$$

Here n stands for the number of lift points where the frequency is evaluated and compared to the intended one from the optimization. The term $(n\text{-}i)$ is a weighting term to emphasize the frequency at low lifts, since the study so far has shown that the low lift portion of the spring characteristic is more important than the high lift portion. Thus any error due to a necessary compromise will accumulate more towards the higher lift portion of the spring characteristic.

The method is quite general; using a full eigenvalue computation of the discrete spring model, this approach would allow one to set up a spring design program, to calculate any spring design. However this would require the cost function to be enhanced by additional terms which have to control the preferences between the various possible spring design options to achieve the same frequency characteristic (due to the one-to many relationship mentioned in the introduction). Furthermore for such a general program, the number of parameters would be very large, and the target function evaluations would require an excessive amount of computational effort.

In the present restricted case it is feasible to narrow down the number of free parameters. Since the spring is to be designed to fit into an existing engine, with the same cam profile currently used, it is also required to have the same force levels. As noted in the statistical investigation (Section 9.2, Equation 9.2.1), this normalisation to the same stored energy is performed for each frequency characteristic during the optimization run. Hence not only the frequency characteristic has already been determined, but also the force against lift. From this force against lift one can also derive the rate against lift.

For the spring rate one also has

$$k = \frac{G}{8}\frac{d^4}{D^3 N} \qquad /11.2/$$

where G stands for the shear modulus, d is the wire diameter, and D is the mean coil diameter and N stands for the number of active coils.

Also for the spring mass

$$m = D\pi^2 N \frac{d^2}{4}\rho \qquad /11.3/$$

where ρ represents for the density of the spring material.

Using the above equations, it is now possible to establish the required number of active coils for the given mean spring diameter and wire diameter to give the intended installed height frequency (see equation 5.1.10). Because of the restriction that the spring has to fit to an existing retainer, and the solid height (defined by the total number of coils and the wire diameter), has to allow for the 10mm valve lift, the determination of these three parameters can be carried out using a simple trial- and -error process. A further practical restriction is that the spring supplier has only wire material available in steps of 0.1mm diameter, which requires an additional compromise. To speed up this process, Powell's algorithm has again been employed to determine the right combination.

Once these parameters (number of coils, wire diameter and mean coil diameter) have been established, the only remaining parameters to be modified to obtain the intended frequency characteristic, are the free length of the spring, and the pitch spacing. The restriction to symmetrical springs further cuts down the number of optimization parameters.

The approach described above has then been used to calculate this pitch spacing and the free length of the spring. For this purpose initially a very small number of points has been used at which the pitch spacing is specified. Subsequently this set of points is refined until finally a quarter coil representation is established.

The above procedure requires a number of tries and initial estimations at various stages, and is not meant to represent a final way to design a spring, but it outlines a technique which allows, after a number of enhancements also in the more general case, to find the spring design for any given frequency characteristic. Employing an optimization algorithm, rather than analytical steps at some of the stages, has the advantage that the various restrictions to be taken into account can be balanced for a good compromise. For example the fact that only discrete steps in wire diameter are practical requires to compromise other of the spring design parameters to ensure the intended frequency characteristic where it is most important. In the present case this has been done for the frequency characteristic at higher lifts.

Table 9 shows the key data resulting from the spring design optimization, sufficient to manufacture an actual spring. Figure 65 is a plot of the pitch spacing against coil number. The important points in this characteristic are the dwell periods in the pitch spacing at either ends of the spring. The area of almost constant pitch means that these parts of the spring become inactive almost all at once, which creates the intended sharp frequency rise at low lift. The comparison of the intended frequency characteristic from the spring response optimization with the one achieved by this spring design is shown in Figure 66. As one can see, the achieved characteristic is very close to the intended one.

This completes the description of the physical spring design. The work presented so far in this thesis concentrated mainly on analytical work to analyse and optimize a spring design. The final part of the work will concentrate on test verification. Therefore the data derived for the optimized spring design has at this point been given to one of the valve spring manufacturers to produce hardware samples of this spring. The intention was to verify the findings from the statistical analysis, and from the spring optimization. This could not be done quite as had been intended, since the spring manufacturer involved was not able to produce the spring to a sufficient amount of accuracy to really deliver the spring hardware described. The reasons for that as well as an analysis and test results from the hardware actually received will be discussed in the following section.

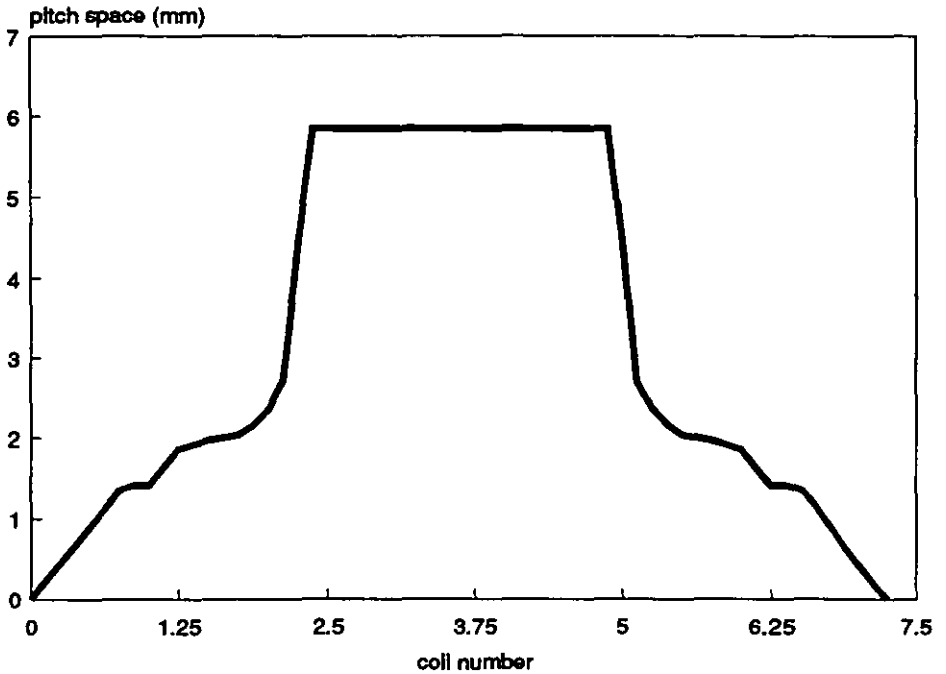

Figure 65: Space between one coil to the next coil for the spring designed to match the frequency characteristic from the optimization shown in Figure 60

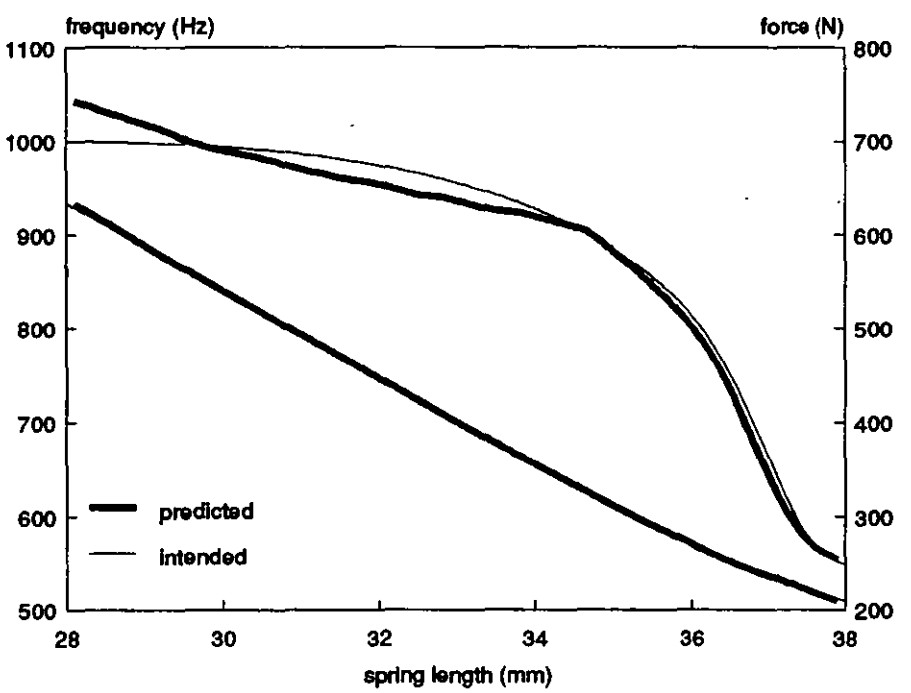

Figure 66: Comparison of intended frequency characteristic and the characteristic achieved by the designed spring

Length (mm)	Frequency (Hz)	Force (N)	Coil Number (-)	Pitch Space (mm)
37.9	555	210	0.000	0.00
37.5	567	220	0.750	1.31
37.1	607	232	0.875	1.37
36.7	700	244	1.000	1.37
36.3	773	259	1.250	1.81
35.8	819	277	1.500	1.92
35.4	857	296	1.750	1.98
34.9	890	316	1.875	2.10
34.7	905	326	2.000	2.29
34.4	910	336	2.125	2.63
34.2	915	346	2.250	4.33
34.0	920	356	2.375	5.69
33.7	925	367	2.500	5.69
33.5	925	377	2.750	5.69
33.3	930	388	2.875	5.69
33.0	936	399	3.000	5.69
32.8	941	409	4.250	5.69
32.6	941	420	4.375	5.69
32.3	947	431	4.500	5.69
32.1	952	442	4.750	5.69
31.9	958	452	4.875	5.69
31.6	958	463	5.000	4.33
31.4	963	473	5.125	2.63
31.0	969	493	5.250	2.29
30.6	980	511	5.375	2.10
30.2	986	529	5.500	1.98
29.9	992	545	5.750	1.92
29.6	998	560	6.000	1.81
29.3	1011	574	6.250	1.37
29.1	1017	586	6.375	1.37
28.8	1023	597	6.500	1.31
28.6	1030	611	7.250	0.00
28.3	1036	622		
28.1	1043	632		
28.1	1043	634		
Wire diameter (d):		3.3 mm		
Mean coil diameter (D):		21.0 mm		
Free Length:		47.8 mm		
Total number of coils (N_t):		8.25		
Approximate static stress:		1150N/mm^2		

Table 9

12

Measurement Results for the Optimized Valve Spring

In this section, the hardware actually received from a spring manufacturer will be examined and discussed. It turned out that the received hardware had major shortfalls in respect of the intended validation of the results from the analytical work. The first part of this section will discuss these shortfalls and compare measured results with corresponding simulations. In the second part, it will be shown how these shortfalls have been overcome to finally enable a meaningful experimental test of the theoretical findings.

12.1 Analysis of Received Hardware

Figure 67 shows the comparison of the original spring for the engine and a sample of the springs received according to the design calculated in the last section. One can clearly see the totally different nature of the pitch of the spring. For the original spring the differences in pitch are relatively small, causing the late progressivity observed in Figure 27. The hardware for the optimized spring shows the areas at the ends where only small space is available between coils, and this small space stays nearly constant for a while. This means that these coils are active for some range of spring compression and then suddenly these coils become inactive, causing a sharp rise in frequency. Then there is a sudden increase in the pitch spacing, associated with coils staying active towards high lifts, meaning that only moderate changes in frequency take place during the higher lift portion.

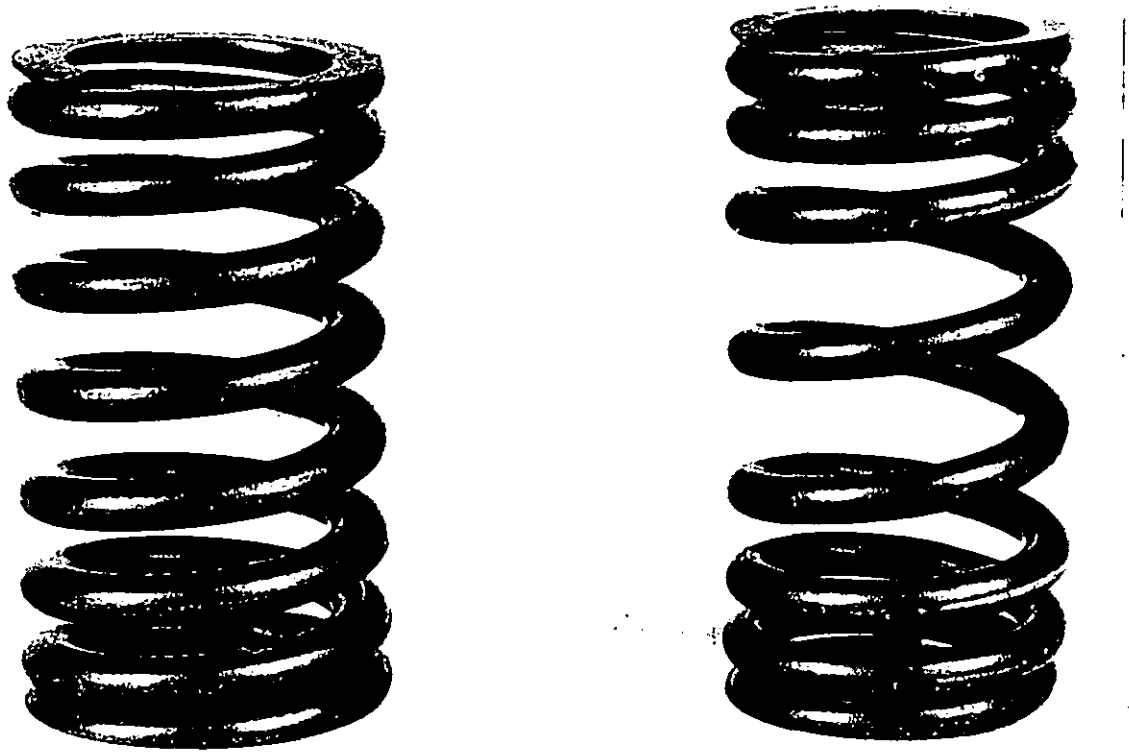

Figure 67: Comparison of original base line spring (left) and hardware for the optimized spring design (right)

Unfortunately, a detailed measurement of the pitch spacing revealed that the intended design was not matched as well as hoped. Figure 68 shows a comparison of the intended and the actually received pitch spacing. One can see that the intended symmetrical dwell in the pitch spacing around coil number 1.5 and 5.5 is not met, the main portions of these dwell areas seem to be shifted to lower pitch values and in addition the areas where a strict dwell can be observed are much shorter than designed.

The latter error is of less importance, as long as the pitch spacing around these dwells varies only moderately. The shorter strict dwell in the pitch spacing only means that there is only a short portion of the lift where the frequency stays constant. Since for a one-off test it is feasible to control the installation conditions of the spring, one would still be able to place the spring with the right installed frequency.

Also, as discussed before, the dwell in frequency was only a compromise to accommodate different installation conditions; the important effect is the early rise in frequency during the valve lift, which would take place with a moderate change in pitch spacing.

The fact that the end coils have an overall too low pitch spacing is much worse than the shorter dwell areas. This means that the coils become inactive too early during the spring compression. They are actually inactive at installed length of the spring. This causes the spring to have a fundamental installed frequency of 650Hz instead of the intended 555Hz. The comparison of the predicted frequency against spring length for the requested design and the received hardware is shown in Figure 69. Here it can be seen that the overall frequency characteristic is much higher than requested.

Nevertheless the received spring was tested. For this purpose the force transducer from the top of Figure 29 was used. In this case correlation was based not only the time domain results, because this only gives snapshots at certain speeds, and does not safely determine resonance areas and the overall response of the spring. To correlate the earlier analysis, and to verify the optimization results, a tracking analysis of the peak amplitudes of all orders against speed was performed. The measurement was carried out on a motored test rig, with the engine speed slowly increased from 1000 to 7000rpm engine speed (500 to 3500 rpm camshaft). The increase in speed was at a rate of only 10rpm/sec, to ensure that the valvetrain had time to maintain steady state. For example at 6000 rpm (engine) the rate of 10rpm/sec means that during a change of one rpm, 5 complete cam cycles take place, considered sufficient to reach steady state response.

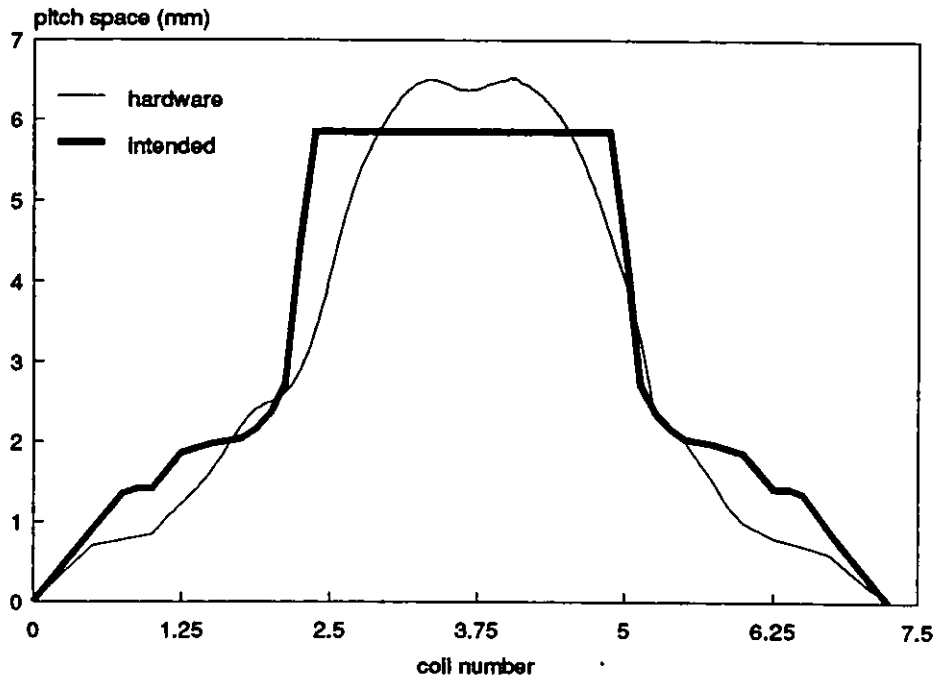

Figure 68: Comparison of the pitch spacing for the optimized spring design and the measured pitch spacing for the spring actually received from the spring supplier

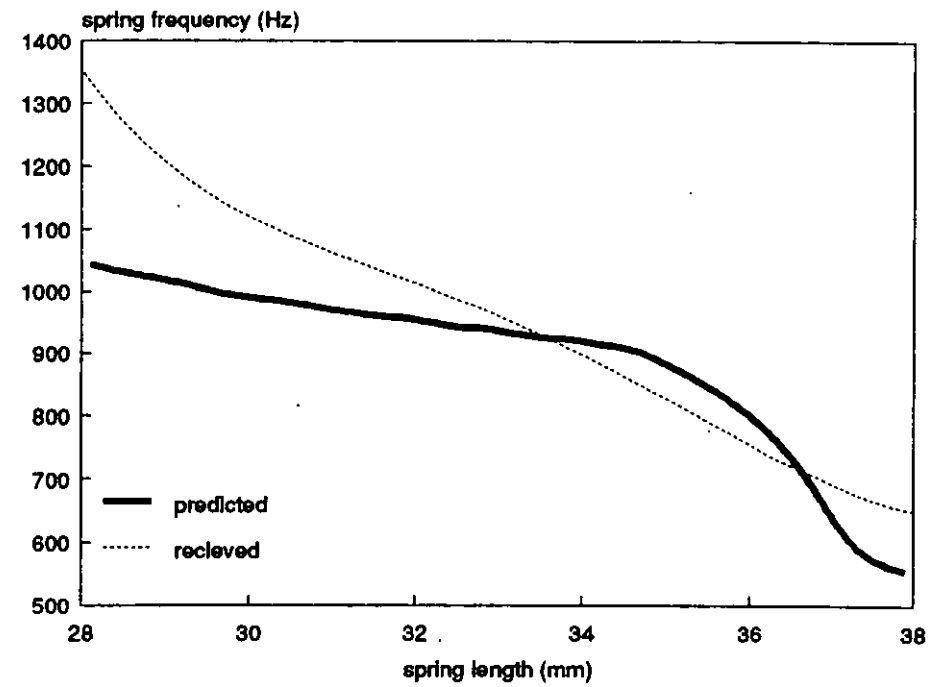

Figure 69: Comparison of the predicted frequency against spring length for the optimized spring design and received hardware with the pitch spacing from Figure 68

A further aspect for the measurement is the static component of the spring force. In the present case, the original spring had a maximum static force of 630N at maximum valve lift. The worst vibrations at high speeds have an amplitude of around ±125N. Hence if the full signal is used for the tracking analysis, the dynamic content is relatively small compared to the static contribution. To correlate and validate the findings above, the only point of interest is the dynamic component. Therefore a high pass filter has been applied to filter the signal prior to the tracking analysis. The corner frequency for this high pass was set to 400Hz to ensure that the dynamic component from the original spring (≥ 490Hz) fully passes the filter.

Furthermore, the clash events, evident in Figures 32 to 34, also need to be considered. First, the task is to correlate a model that does not have the capability to predict these events and hence would not follow the trace given by the envelope of the short peak force events. Secondly, these events are to some degree random in nature and an exact correlation would not even been possible between two different test measurements, when no averaging is performed over a number of cycles for each speed. To address both issues, a low pass filter has been used in series with the high pass filter. From previous analysis, it was known that the clash events have a frequency in the range of 5000Hz and above. On the other hand it is known that there is no realistic chance to correlate spring surge above the third spring mode. Since the investigated springs are all in the range of 1000Hz at maximum valve lift, the third order will reach up to 3000Hz. Correspondingly 3000Hz has been chosen as the corner frequency for the low pass filter.

The signal created by this filtering technique is qualitatively very similar to the spring surge mode extremes against speed. The spring surge extremes have been calculated according to the dynamic component in equation /5.1.20/ namely

$$G_{\Sigma} = \pi \sum_{n} n(-1)^{n} G_{n}(t) \qquad /12.1/$$

with units Nmm/N. Thus the factor relating the measured dynamic force component to the modal amplitude against speed is the spring rate.

Figure 70 shows the measured result, and Figure 71 the corresponding calculated values; one can see that there is a good correlation between these graphs. In particular, the speed location of the resonances are accurately predicted by the model. One has to keep in mind that in the context of this study it is not the goal to find a fully accurate three dimensional description of all dynamic effects taking place in a valve spring. The real challenge was to find a model, that is easy and fast enough to solve to allow an efficient analysis and optimization in terms of computer time, and yet predicting trends well enough to make

the findings useful and applicable to real hardware. In this context, the correlation between the two traces for each spring is fully satisfactory and would allow one to predict whether serious vibrations would have to be expected in a certain speed range.

One can also see model limitations for extremely large amplitudes. Comparing the last resonance peak around 3300 rpm camshaft speed, one sees that the measured peak is chopped off. The discrepancy probably arises from the existence of additional damping, as well as the restriction of torsional motion by the interference of coils. The modal model does not consider these effects. In practice, the real force peak for the measured result is much higher than the predicted modal one, since the additional damping takes place during very sharp high frequency impacts, as can be seen in Figures 32 to 34; since the signal has been filtered, these high frequency events do not show up on the measured trace.

12.2 Corrective Actions and Discussion

From the above, one can reasonably conclude that the correlation between the measured and predicted results is acceptable; however the main issue concerns the improvement gained by the optimized frequency characteristic. The measurement shows that the "optimized" spring has a much reduced vibration amplitude compared to the original spring. Unfortunately this is possibly because of the high installed frequency rather than the shape of the frequency characteristic. Hence this test was not really suitable to validate the findings from the statistical study and from the optimization, - the result that a higher frequency spring reduces vibration amplitudes is a trivial one.

A procurement of parts much closer to that intended was not possible, since with current manufacturing capabilities the received hardware represented the closest that was possible to manufacture. The reason for this is mainly the extremely different pitch spacing required. In principle the coiling of the spring towards the given design is possible. The problem arises from the necessary production steps after the coiling. When the springs are stress relieved and heat set after the coiling the original pitch spacing changes. In conventional springs, all coils give more or less equally and so the result is quite accurately predictable. In the case of this extremely varying pitch spring, the deformation during heat setting is very different. The coils with large pitch space are raised to higher stress levels during heat set and hence have a larger plastic deformation than the coils with small pitch spacing. The spring manufacturers are well aware of this effect and counteract it by making the rough pitch spacing larger for the coils that will encounter larger deformation. In this case this was obviously overdone, since the coils with insufficient pitch spacing are the end coils which should have a smaller deformation relative to the large pitch areas of the spring.

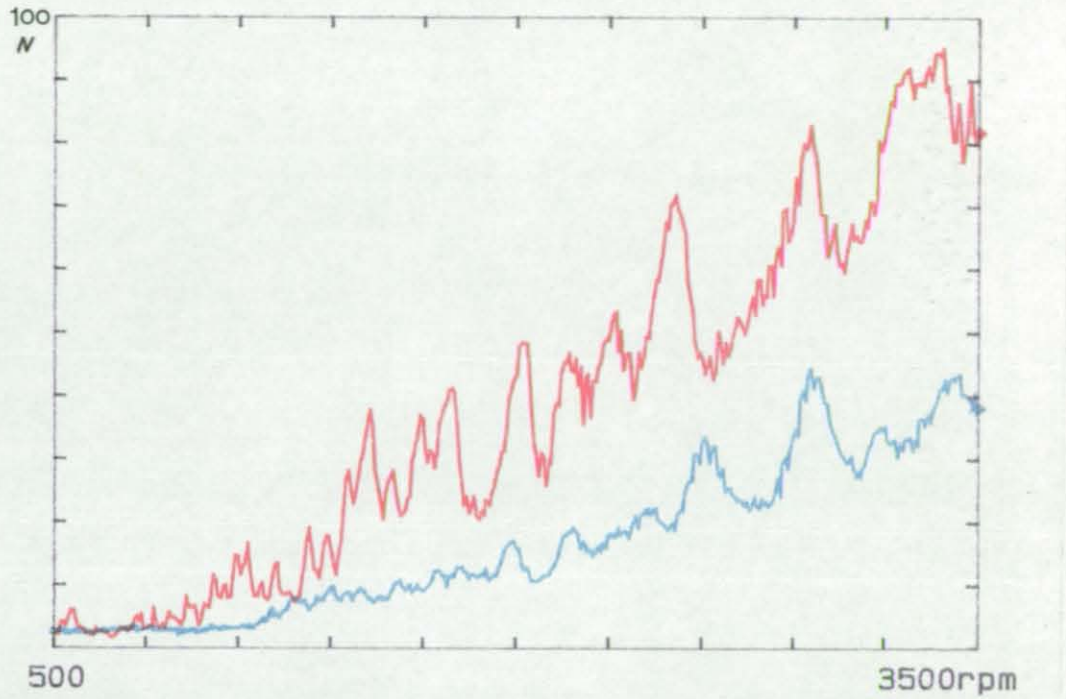

Figure 70: Measured dynamic response tracking analysis of the band pass filtered (400-3000Hz) spring bottom end force from 500 to 3500 rpm camshaft speed for the base line spring (red) and the received hardware (light blue)

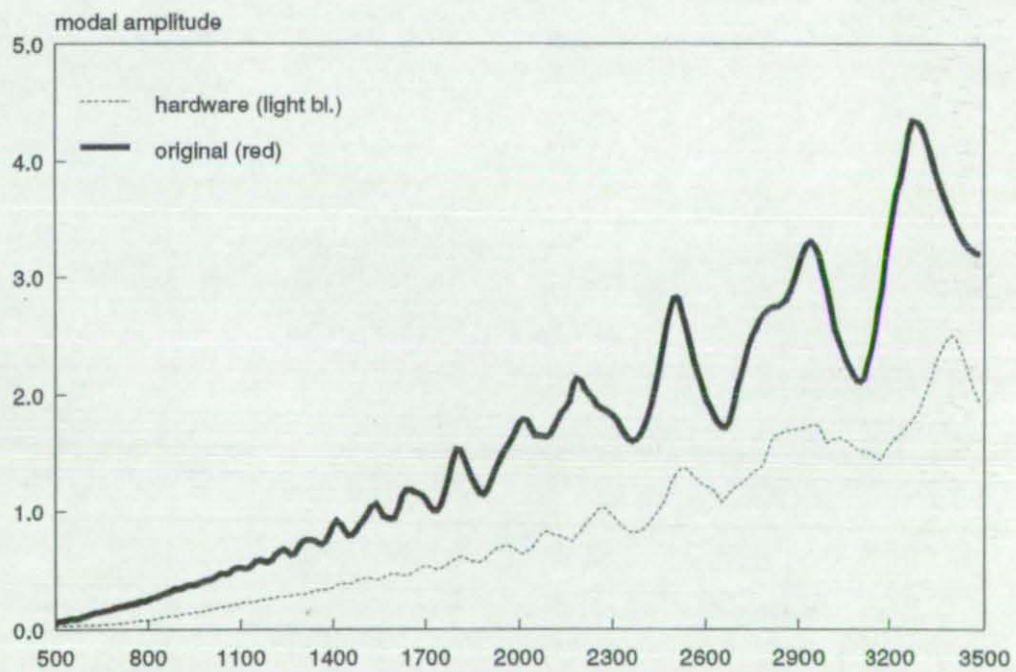

Figure 71: Predicted surge mode extremes against engine speed corresponding to the tracking analysis shown in Figure 70

For this study the above insight does not help to validate the intended frequency characteristic. To recover this information, a separate route has been followed. From the comparison of the pitch spacing in Figure 68 one can see, that the end coils do not have enough deformation space. To achieve the intended early frequency increase, these end areas have to be active at the installed condition. To achieve this the installed length of the spring would have to be increased. This of course lowers the spring forces, and hence carries the risk of early loss of contact, with resulting potential problems at high speeds. For a real application this would not be achievable without ordering corrected hardware. In this particular case the advantage is that only the spring response is of interest, and not that of the rest of the valvetrain. Furthermore, the discussed decoupling property of valvetrain and spring helps to recover the intended validation of the beneficial early frequency increase.

In fact, increasing the installed length of the spring is not possible since there is no space available; even if there was, it would require new retainers and specially prepared valves to accommodate the larger length. A second possibility is to grind the ends of the spring, thus effectively reducing the free length, which in turn reduces the amount of compression until the original installed length is reached. Using the pitch spacing shown in Figure 68, the analysis predicted that a reduction towards 560Hz instead of the original 650Hz could be achieved by grinding the ends 1mm shorter each. The resulting hardware in comparison to the received spring is shown in Figure 72.

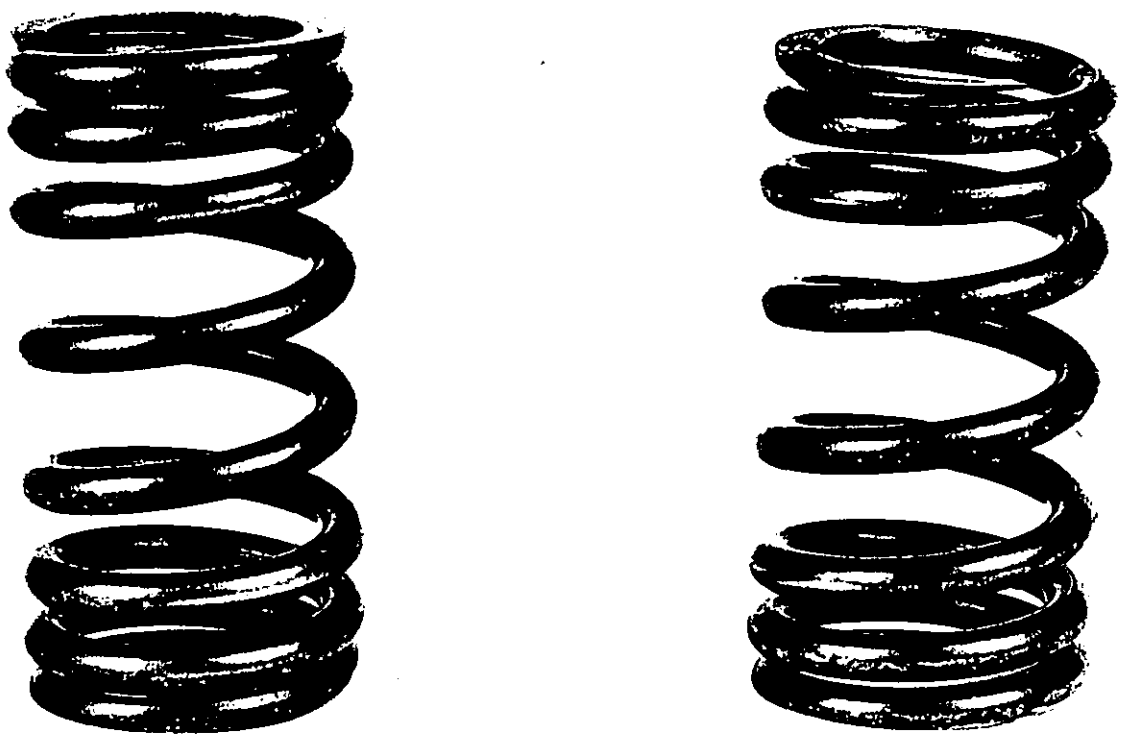

Figure 72: Comparison of the received hardware for the optimized spring (left) design and the modified spring by grinding off 1mm at each spring end (right)

Subsequent measurement revealed that the frequency went down to 563Hz according to a FFT analysis of the base circle portion of the measured time traces. These values are now much closer to the original intend of 555Hz and furthermore the frequency will at least increase to approximately 650Hz during the first 2 mm of lift. A comparison of the predicted corrected frequency characteristic from the ground spring with the originally intended optimized design is shown in Figure 73. One can see that the amount of early frequency increase is not as large as intended, but the obtained characteristic is much closer than the unmodified hardware, and is definitely closer to the intended design than to the original base line spring.

In Figure 74 one sees the resulting speed response for this spring together with the response of the base line spring, as well as the response from the unmodified hardware. The deterioration for the modified spring is very moderate, and definitely smaller than the increase of vibration that would be observed if a linear spring is lowered by 90Hz installed frequency.

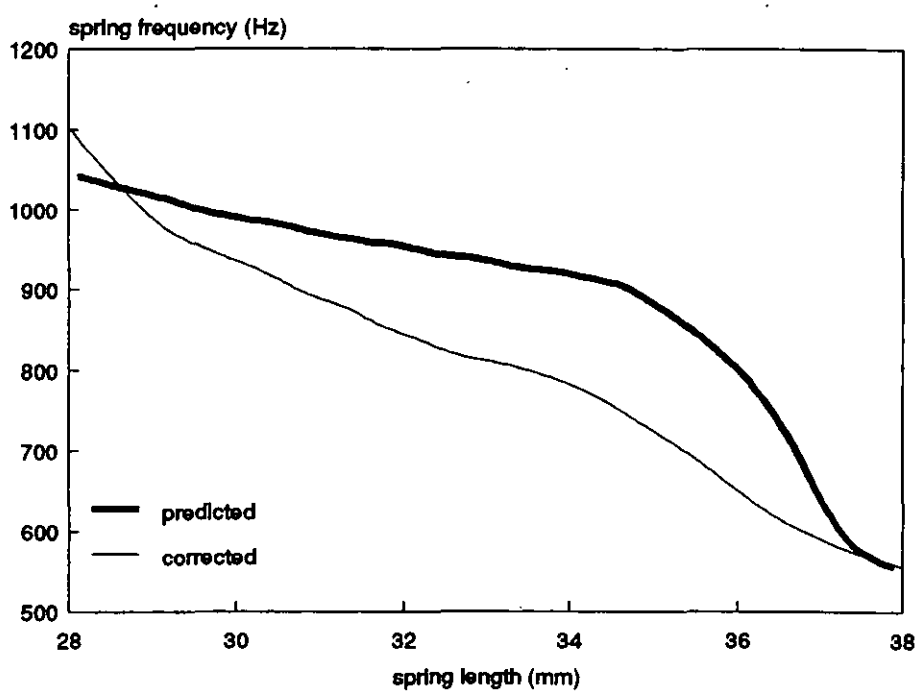

Figure 73: Comparison of the predicted frequency against spring length for the optimized spring design and the shortened spring by grinding the ends off

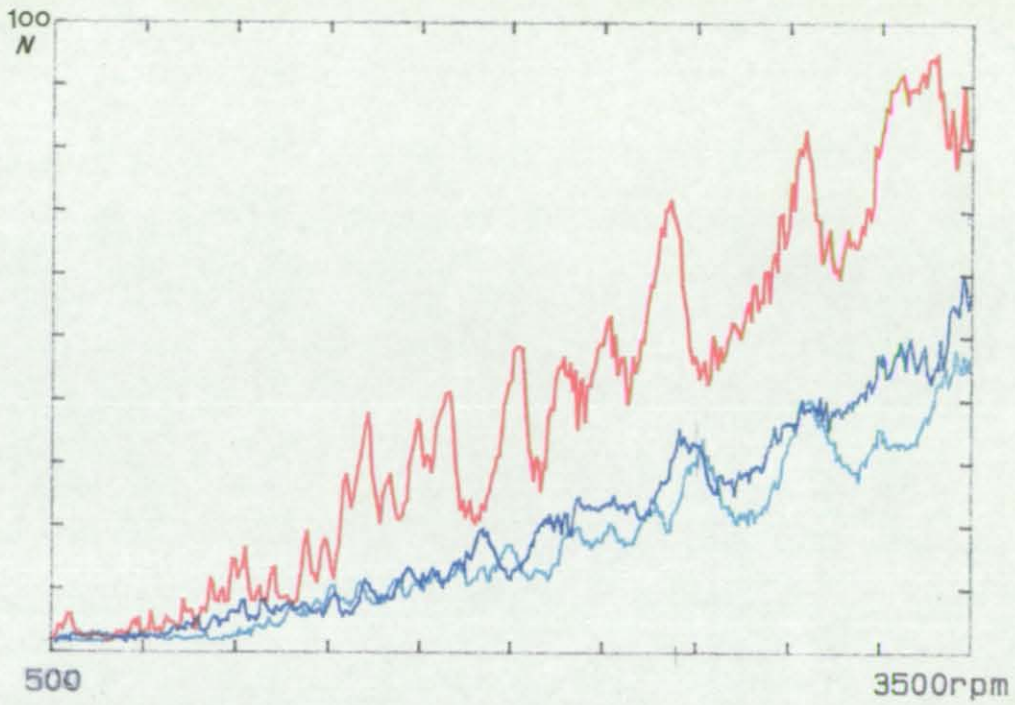

Figure 74: Measured dynamic response tracking analysis of the band pass filtered (400-3000Hz) spring bottom end force from 500 to 3500 rpm camshaft speed for the base line spring (red) the received hardware (light blue) and the ground spring (dark blue)

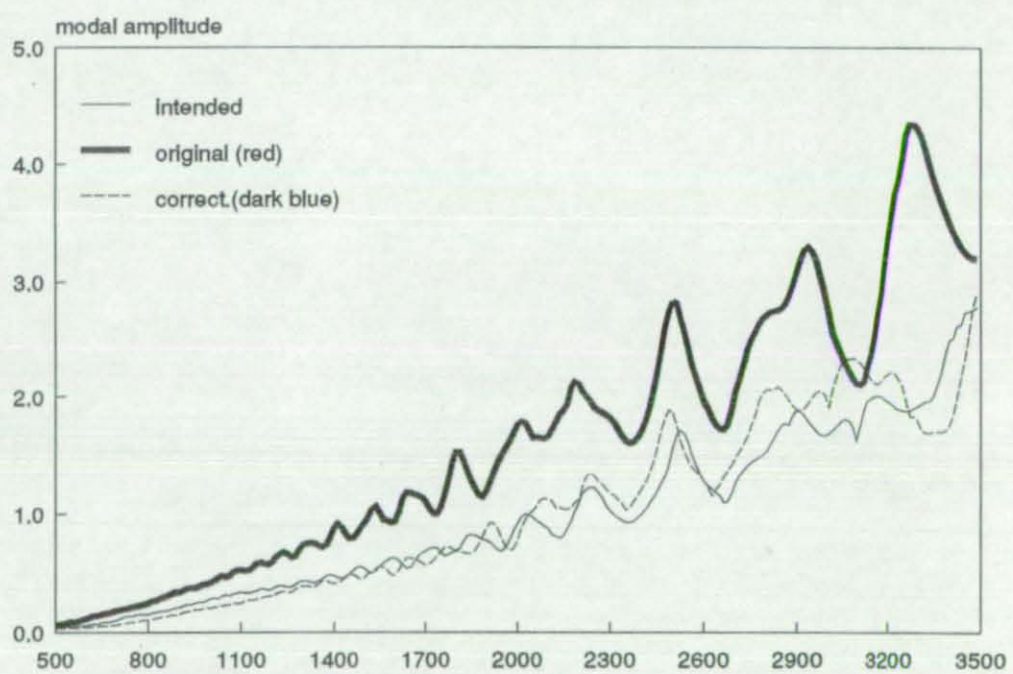

Figure 75: Predicted surge mode extremes against engine speed for the base line spring, the intended frequency characteristic and the frequency characteristic predicted for the shortened spring

Figure 75 plots the predicted responses for the base line spring, the spring with the intended frequency characteristic, and the spring with the adjusted frequency characteristic. As can be seen, they all match the measured traces acceptably well. It is difficult to say whether the intended or the shortened spring correlates better with measured data; this is not too surprising, since it has been seen from the analysis of the restart with the kinematic accelerations in Figure 64, that a moderate shift of the point where the frequency increase occurs has no dramatic effect on the response.

Overall it can be concluded that the above correlation verifies the findings from the statistical analysis and from the optimization. Two additional points are apparent from the results.

The first point arises from comparison of Figure 70 and 74. The trace of the received hardware is slightly different in these cases . Both traces are obtained from the same spring under the same boundary conditions, but during separate tests. In between, the cylinderhead had been disassembled, a new spring (the ground one) had been fitted to the neighbouring valve, and the cylinderhead had been assembled again. So the correlation of these two traces basically shows the repeatability of the spring behaviour. A direct comparison of the two is shown in Figure 76. Any closer correlation than the comparison shown would therefore be suspicious. The comparison shows that the "hash" like local variation is something that does not need to be considered at all, since it varies so much from measurement to measurement. This hash is either due to noise in the measurement equipment, or due to unpredictable random variations. But apart from this, the main resonances are well repeated, especially in the interesting speed range above 2500rpm camshaft.

At the top end of the speed range there is some difference between the two traces, one of them correlating better with the simulation; the other showing a later end of the resonance peak. Comparing it with the simulation in Figure 71 one recognizes that the peak around 2550rpm is slightly lower in speed than in the measurement, where it occurs at around 2600rpm. As previously mentioned the analysis predicted a frequency of 650Hz for the spring and the measurement showed the same, but the measurement had an error band of ±25Hz, which is equivalent to ±100rpm camshaft shift of the response curve. Shifting the calculation slightly upwards brings the last resonance in line with the blue measured trace, and also shifts the resonance around 2600rpm in line. This is an indication of the amount of variation and error that has to be accepted between prediction and measured behaviour. On the other hand, the magnitude of this error must be considered small when compared to the much more dramatic variations arising in realistic production.

The second point that needs some further discussion is associated with the damping model used for the valve spring model. Because of its mathematical simplicity and the lack of any obvious alternative, a standard viscous damping approach has been used in the form of a modal damping value. That this is not really adequate can be shown by comparison of the measured and calculated responses in Figure 70/71 and 74/75. Although the prediction of the locations of resonances is very good, and the prediction of trends for the optimized characteristics is satisfactory, the overall reduction of the vibration is significantly larger in reality than predicted by the model. This is almost certainly due to the damping in the system. There are several indications that this is the case. The first, more analytically motivated, is the shape of the resonance peaks. For the original base line spring the resonances are relatively narrow, compared to the resonances from the optimized spring. From basic theory of a single mass system, forced by a harmonic excitation, the frequency response is widened around the resonance in dependence on the damping level of the oscillator. This behaviour can be observed from the measured traces of the base line and the optimized springs.

If the possible damping mechanisms are considered in this context, the most likely one to produce higher levels of damping is the oil squeeze effect when coils close up. This takes place when coils are deactivated during compression in a progressive spring and is known to enhance the damping capabilities of progressive springs in comparison to linear valve springs. But the base line spring and the ground one both have roughly the same total progressivity, what means that roughly the same amount of coils are deactivated during compression.

It seemsthat this alone cannot be the explanation for the observed differences; however this simple argument is only valid for the static consideration of progressivity. In the dynamic case, it also matters where the progressivity takes place. For the base line spring, this oil film squeeze takes place in the vicinity of maximum valve lift and thus only influences a small fraction of a vibration cycle. For the optimized spring the vibration causes coils that have already closed up to open again and squeeze out oil again. The evidence of this effect can be seen in Figure 77.

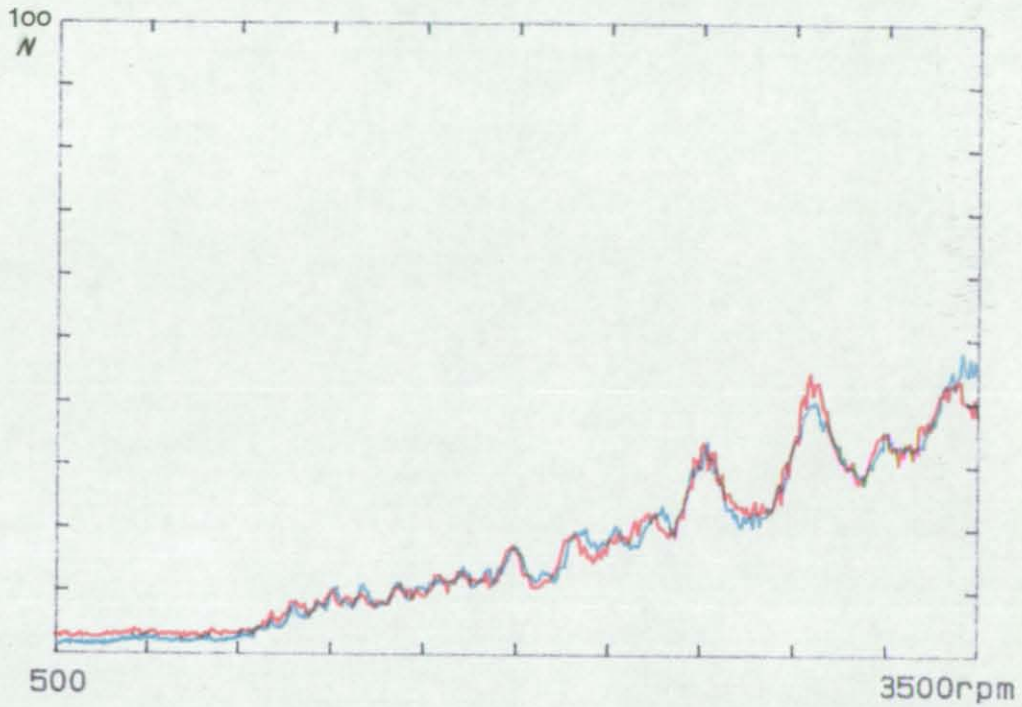

Figure 76: Repeatability of the measured dynamic response for the received hardware from two different tests under the same boundary conditions

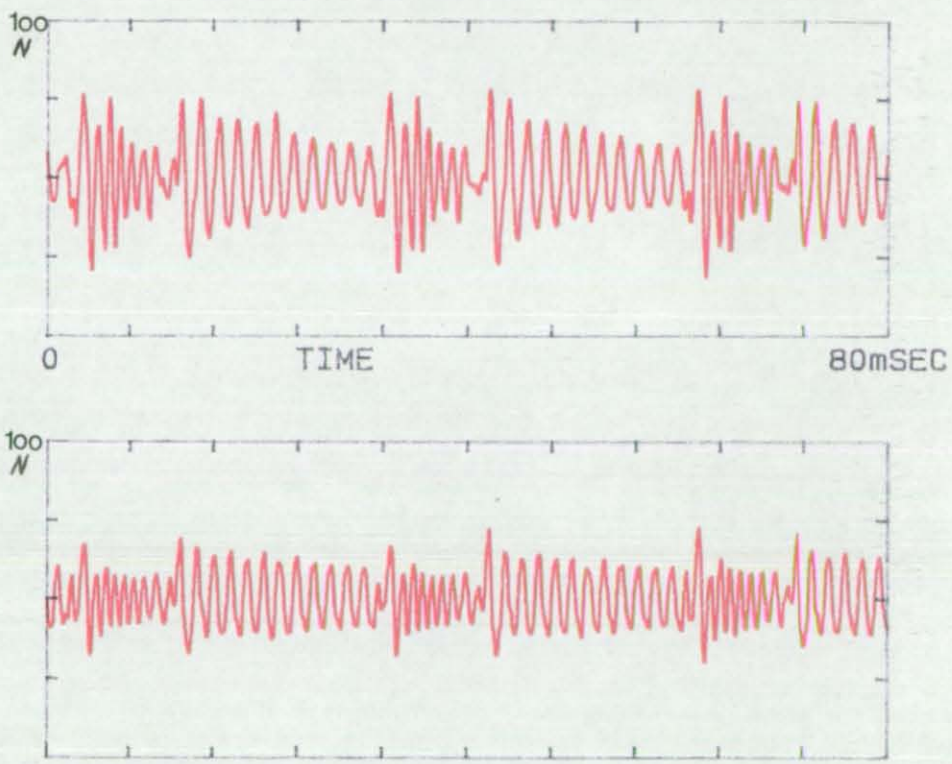

Figure 77: Measured dynamic response time domain results of the band pass filtered (400-3000Hz) spring bottom end force at 4100rpm. Top: ground spring, bottom original hardware received for the optimized design

Presented here is the comparison of the time trace of the filtered signal for the optimized spring as received (bottom) and for the ground one (top). One can see the areas where during the lift the frequency increases and the base circle periods with constant frequency. During the lift portion both springs have a considerable amount of damping, but during the base circle period the ground one has much larger damping than the other. The main difference of the two is that the ground one has coils which are very close to being deactivated statically as discussed before. These coils are able to alternately close up on both spring ends and cause damping during this process. This is the same effect that early progressivity causes during the valve lift.

The above explanation automatically implies that the damping is also amplitude dependent, since larger vibration causes more coils being near to the boundary to be either temporarily activated or deactivated. Evidence of this suspicion can be found by comparing the calculated and measured time traces for the ground optimized spring in Figures 78 and 79. Here one sees that at moderate speeds and surge amplitudes (5000rpm in Figure 78) the correlation is excellent, but at higher speeds with larger vibration amplitudes (6000rpm in Figure 79) the vibration is much more strongly damped during the lift portion (where the progressivity takes place), than during the base circle portion - where the correlation is again excellent. If this amplitude dependent damping becomes a very dominant factor, the time variant approach would have difficulty to take it into account. It might be possible to perform the calculation in two stages, one with an initial damping characteristic solely dependent on the frequency characteristic of the spring, and a second refinement stage where the original damping has been modified due to the amplitudes calculated in the first stage.

However, before one can think about including such mechanisms in the model, one first needs to undertake some principle measurement investigations to verify the above supposed mechanisms of damping. Because of the complexity of this task this has to be a subject for further study. However, since this damping effect obviously only causes an underestimate of the beneficial influence of certain frequency characteristics, the current model without this capability still allows a useful relative judgement of alternatives.

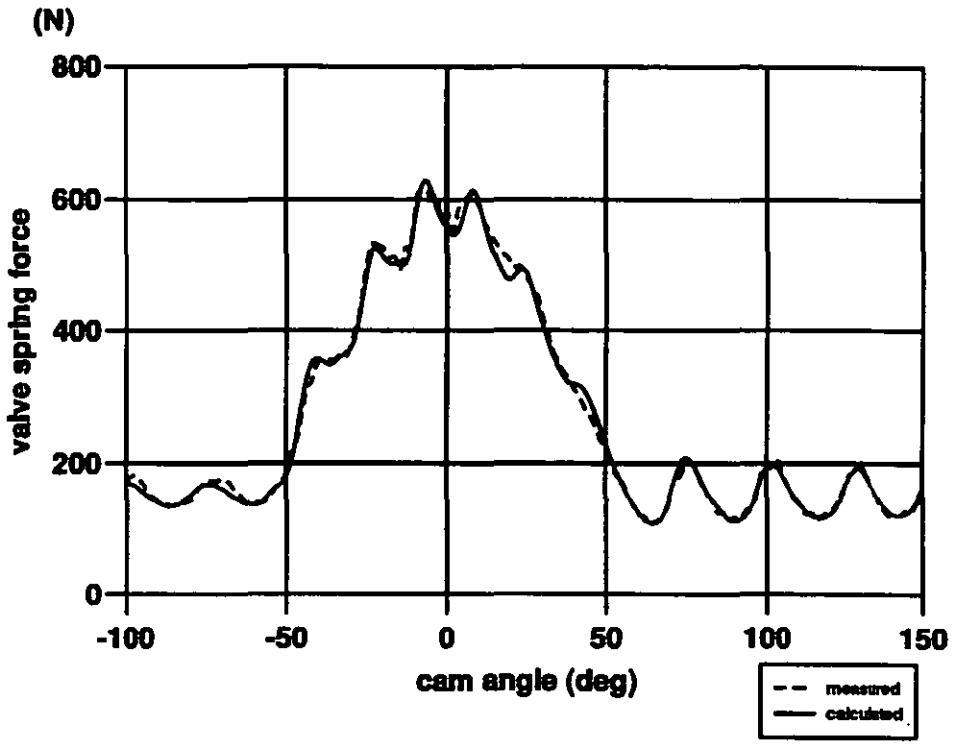

Figure 78: Comparison of measured spring force and simulated spring force for the ground optimized spring at 5000 rpm engine speed

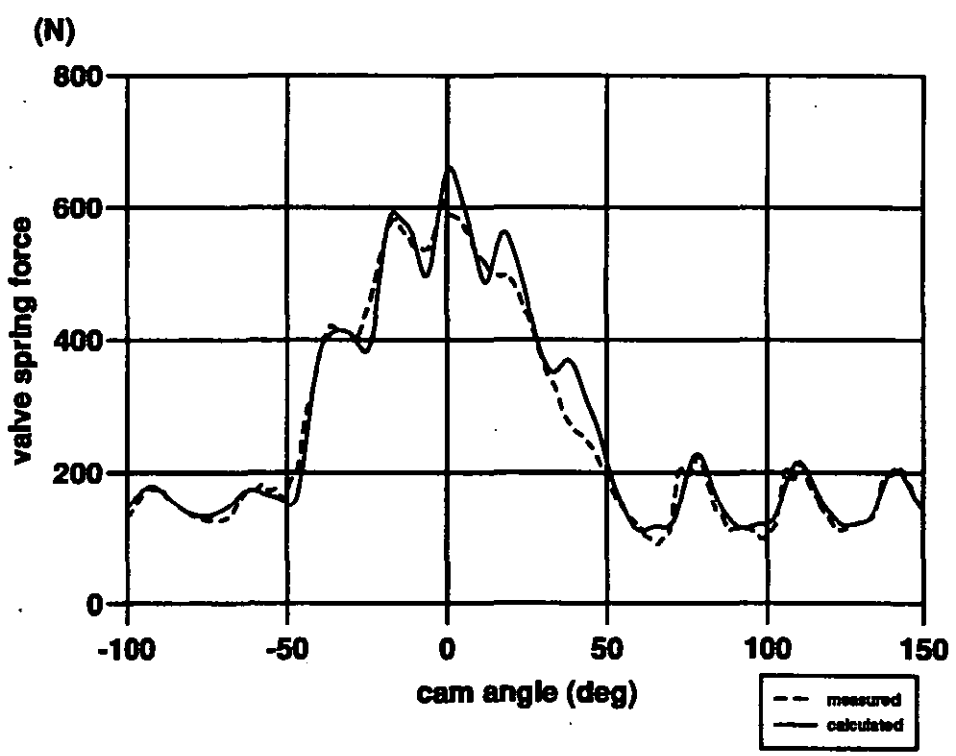

Figure 79: Comparison of measured spring force and simulated spring force for the ground optimized spring at 6000 rpm engine speed

13

Conclusions and Discussion

The main aim of this work has been the optimization of valve springs for vibration response. To achieve this, different modelling approaches, which had been used successfully in the past, have been reviewed. The drawbacks and merits of these models were discussed, leading to the conclusion that the available models were not suitable to match the requirements for optimization. Therefore an analytical model had to be developed to simulate the valve spring dynamic response. This is detailed and accurate enough to reflect trends correctly, and efficient enough to allow an automated design optimization.

This led to the development of a spring description which combines useful aspects of both the modal and discrete descriptions. The result is a modal description with properties that depend on the spring compression. Then it has been shown to be possible to approximate this non-linear modal model by a linear system with time variant coefficients. This was possible, since in modern stiff valvetrains, the lower spring surge modes are largely decoupled from the vibrations of the rest of the system. However, there was no method directly available which would have allowed a solution of this type of a system more efficiently than for the nonlinear case, since in time stepping integration it does not matter very much whether the system properties depend on spring compression or purely on time.

However, the linear time variant nature of the system allowed to develop a solution method which solves the response efficiently in the frequency domain. Since the properties are time variant and periodic in nature, and the base period of this variation is the same as for the excitation, it is possible to express the properties, the excitation and the solution as Fourier series with the same base period of one camshaft revolution. A similar approach was known for the linear case with constant coefficients where the response has been calculated for each order and each of the harmonics separately. This basically reduces the problem to the separated solution of the response of a single degree of freedom model to a single harmonic excitation for each of the modes and harmonics. The subsequent superposition of each of the harmonics and modes leads to the combined response of the spring. This is based on the fact that for a linear system with constant coefficients the frequency of the response will be equal to the frequency of the excitation.

For the case of varying coefficients the situation is different. Each exciting frequency results in a series of response frequencies, what is reflected by the product of Fourier series emerging in the equations for the modal model for progressive springs. This no longer allows one to solve each harmonic separately; however the fact that the product of two Fourier series is again a Fourier series led to a set of algebraic equations that may be solved for the complete response. This method is less efficient than for the linear case with constant coefficients, but is still very efficient compared to time domain integration. The application

of this method to the spring surge problem showed a degree of correlation that encouraged the application of the method to a more general investigation on valve spring dynamics and its optimization.

To establish the important characteristics of a valve spring, a statistical experiment was undertaken. To enable this investigation it was essential to express the important characteristics of the spring by a low number of parameters. It became clear that the key description of a springs response to camshaft excitation is the frequency versus lift characteristic. This was then represented by parametric splines of third order. These splines have the advantage that they offer a large degree of flexibility with a small number of parameters. The splines were thus used to represent a wide range of possible characteristics, with the variation of only five spline parameters at two levels each, leading to a full factorial two level experiment.

The formal analysis of the factorial experiment that was carried out, revealed that the dominant effect on spring response is defined by the degree of frequency change during the excitation period. It has been shown that this excitation mainly takes place at low valve lifts where the opening and closing acceleration pulses of the valve lift profile take place. This was somewhat surprising, since most of the current spring applications tend to have their main progressivity towards higher lifts. However, it became clear that the rapid change of spring frequency during the initial excitation avoids the build up of large resonant amplitudes. Late progressivity during the higher lift portions on the other hand only helps somewhat in damping, since more free vibration cycles take place in the same time period. Furthermore, it could be verified by the optimization procedure and the subsequent testing, that these findings where correct. One drawback of the new design was the difficulties arising during the manufacturing of the optimized spring design; this suggested that this type of spring is more vulnerable to manufacturing errors than conventional springs.

The immediate tangible outcome of this work is threefold:

1) A method has been developed to efficiently solve linear systems with periodically time variant coefficients with a low number of degrees of freedom. This method has been successfully applied to the problem of spring analysis and correlated with actual measurements.

2) The utilization of the developed model for a statistical analysis and formal numerical optimization led to a basic understanding of the important characteristics of the spring.

3) In the course of the study, a comprehensive set of computer programs has been developed, which allows the analysis and optimization of the valve spring frequency characteristic to a given valvetrain configuration. The development of a program which finds the corresponding spring design for the simplified case of a symmetrical cylindrical spring enabled the manufacture of a spring, validating the analytical findings.

However, two major open issues were discovered, where further analysis and work is recommended. One is in the area of further model development, the other is a manufacturing issue.

The main shortfall of the modelling approach is the inability to accurately predict the damping characteristics of a progressive spring. In a further step, it is planned to work on this and develop the necessary analytical models for the damping mechanisms to overcome this shortfall. However, at the current point in time, the lack of detailed and well controlled measurement investigations does not allow one to establish much more than the employed viscous damping model and to develop some experience about the magnitude of this damping for different spring designs. In terms of optimization and relative judgement of spring variants, this is not too much of an issue. A case where this might become important is if a choice is to be made between a high base frequency linear spring and a low base frequency spring with high progressivity. If both show a similar dynamic response under the analysis within the current modelling, one has to keep in mind for the final decision, that the progressive one will most probably behave better. One reason for this is the under-estimation of the damping influence in a progressive spring. Additionally there is a durability aspect in the comparison of linear to progressive springs that lead to the preference of progressive springs even for the same dynamic stress levels. For a linear spring, the dynamic stress peaks always act on the same fraction of the spring wire which leads to an corresponding spring life depending on the material. In the case of a progressive spring, the fraction of the coil that receives the maximum dynamic peak stress, moves up and down the wire during the valve lift (this effect is easily understood from Figure 30).

The above given arguments show that one must not blindly accept all results from the spring model, and at this stage the modelling and optimization shown above do not replace well founded engineering judgement. On the other hand, with a sufficient degree of understanding, the developed methodology and software tools should help to give a faster development of a well matched valvetrain design.

The second, more critical issue, is the manufacturing problem which arises in actually producing the required spring. As a sad conclusion, one must say that currently the very beneficial effects of early spring frequency increase is probably not feasible for mass production, since the degree of variation and the amount of error observed in the test hardware, would not be acceptable for a robust valvetrain system. This point has been discussed by the author with a number of major spring manufacturers. These manufacturers see the need for a development in this respect, and have taken first steps towards such a capability. One of them is currently investigating the change in pitch spacing caused in extremely progressive springs during heat treatment and hot setting. Another manufacturer expects to put a measurement device into service shortly, which allows him to measure the pitch spacing of the spring under mass production conditions - a key requirement to produce precision controlled spring frequency characteristics.

Although the application of the advantageous special designs is put on hold, until the manufacturing technology is developed, the analytical tools developed can help to achieve conventional spring designs "right first time". If a nearly linear spring or a conventional progressive one is considered, it is known that there will be certain areas of resonance and anti-resonances. Since these types of springs can be produced to a sufficient amount of accuracy, the developed software allows one to place these resonances at the right points in speed to avoid large spring vibrations at the maximum operating speed of the engine. This enables one to lower the nominal spring force level. Alternatively, if it is assumed that such a spring has been developed in the past by trial and error, the design of such a spring can be significantly speeded up.

The above discussion more or less summarises the total picture and the conclusions drawn out of this study in terms of valve spring dynamics and its implications on the spring design. However, the method developed to enable this study, the frequency domain solution of time variant linear systems, has additional potential in other engineering areas. Initial results from a simplified model of a complete valvetrain solved by this method are already available and promise to result in an extremely fast tool for initial investigations during camshaft design. Other areas of application for this method can be imagined, since many engineering problems have a periodic nature. An example is the time variant moment of inertia in a crank train, depending on the piston and con-rod position; further examples can be imagined in many cam driven mechanisms, where the properties change due to linkages with varying transmission ratio. However, serious investigations in this direction would be beyond the scope of this thesis.

14

References

14.1 **Akiba, Kishiro, and Toshiaki Kakiuchi (1988)**
A Dynamic Study of Engine Valving Mechanisms: Determination of Impulse Force Acting on the Valve
SAE Technical Paper 880389

14.2 **Assanis, D.N. and M. Polishak (1990)**
Valve Event Optimization in a Spark-Ignition Engine
Journal of Engineering for Gas Turbines and Power 7/1990, Vol 112/341

14.3 **Associated Spring (1987)**
Design Handbook, Engineering Guide To Spring Design
Associated Spring 1987, Bristol, USA

14.4 **Bakaj, L.F. (1988)**
Numerical Simulation of the Dynamics of an OHC Finger Follower Valvetrain with Hydraulic Lash Adjuster
Dissertation University of Karlsruhe, 1988

14.5 **Bensinger W.D (1968)**
Die Steuerung des Gaswechsels in schnellaufenden Verbrennungsmotoren
Springer Verlag, Berlin

14.6 **Chan, C., A.P. Pisano (1986)**
Optimal Valvetrain Lift Curve Design for Valve Train Cam Systems
Publication from Mechanical Engineering Department, University of California, Berkeley

14.7 **Chan , C. and A.P.Pisano (1986)**
Dynamic Model of a Fluctuating Rocker-Arm Ratio Cam System
Technical Paper, The American Society of Mechanical Engineers 86-DET-79

14.8 **Chen , F.Y. (1975)**
A Survey of the State of the Art of Cam System Dynamics
Mechanism and Machine Theory, 1977 Vol 12, pp 201-224

14.9 **Colombo, T. , V. Pagliarulo, U. Virgilio (1990)**
Computer Simulation of the Dynamic Behaviour of the Overhead Camshaft Valve Train Assembly with Hydraulic Lash Adjuster
SAE Technical Paper 905174

14.10 **Craig, R.R. (1981)**
Structural Dynamics
John Wiley & Sons, New York

14.11 **Dojoong, Kim and Joseph W. David (1990)**
A Combined Model for High Speed Valve Train Dynamics (Partly Linear and Partly Nonlinear)
SAE Technical Paper 901726

14.12 **Engeln-Müllges, G, F. Reuter (1986)**
Formelsammlung zur Numerischen Mathematik mit Standard-FORTRAN 77-Programmen
B.I.Wissenschaftsverlag 5. Auflage 1986

14.13 **Ernst, R., J. Meyer and W. Husmann (1992)**
An Optimization algorithm for Improving Cam Lobes Towards Reduced Valve Train Vibrations in Automotive Engines
Proceedings for ISATA Conference on Mechatronics, June 1992

14.14 **Ernst, R and A. Schamel (1993)**
Advanced Optimization Techniques in Valvetrain Design
To be published at the 1993 IPC-7 conference, Phoenix, Arizona

14.15 **Gordon, T.J. (1989)**
Notes on Statistical Methods
Loughborough University of Technology 1989

14.16 **Hammacher, J (1991)**
Investigation of Dynamic Valve Train Behaviour on an Electric Driven Test Rig
MSc Thesis, Loughborough U. of Technology, March 1991

14.17 **Hatch, C. and A.P.Pisano (after 1988)**
Modeling, Simulation, and Modal Analysis of a Hydraulic Valve Lifter with Oil Compressibility Effects
University of California, Berkeley, Department of Mechanical Engineering

14.18 **Heath, A.R. (1988)**
Valve Train Design For Multivalve Automotive Gasoline Engines
SAE Technical Paper 885133

14.19 **Hoschtalek, Manfred (1955)**
Valve Spring Calculations for high revving Combustion Engines (in German)
Motortechnische Zeitschrift

14.20 **Hsu, Wensyang (1989)**
Simulation of an Oscillating Automotive Finger-Follower Valve Train
University of California, Berkeley, MSc Thesis 12/1989

14.21 **Hussmann, A (1937)**
Vibrations in Helical Valve Springs (in German)
Ringbuch der Luftfahrttechnik, Reichsluftfahrtministerium

14.22 **Husmann, Wolfgang (1992)**
Implementation and Application of an Efficient Optimization Algorithm for the Improvement of Cam Profiles under Kinematic and Dynamic Considerations (in German)
Final Degree Thesis for Dipl.Ing (FH), Fachhochschule Cologne

14.23 **Jeon, H.-S., K.-J. Park and Y.-S. Park (1988)**
An Optimal Cam Profile Design Considering Dynamic Characteristics of a Cam-valve System
1988 SEM Spring Conference on Experimental Mechanics, Portland

14.24 **Kaiser, H-J., P. Phlips, A. Schamel (1989)**
Engine Noise Reduction by Camshaft Modifications in Multi-Valve Engines
2nd Aachen Colloquium Automobile and Engine Technology, October 1989

14.25 **Kaiser, H.-J. , A. Schamel (1993)**
Valvetrain Noise in Multi-Valve Engines - Optimization with the aid of CAE Methods and confirming Measurements (in German)
Seminar on Acustics in Internal Combustion Engines, Essen , March 1993

14.26 **Korakianitis,T. and G.I. Pantazopoulos (1991)**
Nonlinear Valve Train Dynamics
Washington University in St. Louis, Internal Combustion Engines Laboratory

14.27 **Koster, M.P. (1975)**
Technische Schwingungslehre
Springer Verlag, New York 1978

14.28 **Koster, M.P. (1975)**
Effect of Flexibility of Driving Shaft on the Dynamic Behaviour of a Cam Mechanism
Journal of Engineering for Industry, May 1975,P 595ff

14.29 **Kreuter, P. and G. Maas (1987)**
Influence of Hydraulic Valve Lash Adjusters on the Dynamic Behavior of Valve Trains
SAE Technical Paper 870086

14.30 **Kurz, Dietrich (1954)**
Entwurf und Berechnung ruckfreier Nocken (Design and Calculation of jerk free cam lobes)
ATZ Nr. 11/1954

14.31 **Lianchun, Long, Sui Yunkang and Teng Hongfei (1991)**
Dynamic analysis and optimization of internal combustion engine valve train
Computational Mechanics, Cheung, Lee&Leung 1991,pp727

14.32 **Lin, Yuyi, A.P. Pisano (1987)**
General Dynamic Equations of Helical Springs With Static Solution and Experimental Verification
Journal of Applied Mechanics, Vol 54, PP 910, December 1987

14.33 **Lin, Yuyi, A.P. Pisano (1988)**
The Differential Geometry of the General Helix as Applied to Mechanical Springs
Journal of Applied Mechanics, Vol 110, PP 831, December 1988

14.34 **Lin, Yuyi, A.P. Pisano (1989)**
Three-Dimensional Dynamic Simulation of Helical Compression Springs
Mechanical Engineering Department, University of California, Berkeley March 1989

14.35 **Mettig, H (1973)**
Die Konstruktion schnellaufender Verbrennungsmotoren
De Gruyter Lehrbuch 1973

14.36 **Mews, H (1992)**
The simulation of valvetrains
European Adams User Conference 1992, Munich

14.37 **Mook, H. (1986)**
A Mathematical Algorithm for the Optimization of Cams (in German)
Final Degree Thesis UNI- Kaiserslautern

14.38 **Muhr, Thomas H. (1993)**
New Technologies for Engine Valve Springs
SAE Technical Paper 930912

14.39 **Nagaya, K (1989)**
Nonlinear Transient Response of a High Speed Driven Valve System and Stresses in Valve Springs for Internal Combustion Engines
Transactions of the ASME, 7/1989, Vol 111/264

14.40 **Nakano, Y., S. Matsuoko and M. Matsuura (1983)**
Development of HLA for High Speed Motorcycle Engine
SAE Technical Paper 830090

14.41 **Newland, D.E. (1989)**
Mechanical Vibration Analysis and Computation
Longman Scientific & Technical, New York

14.42 **Niepage, Peter, Peter Grindel (1991)**
Valve Springs with Wire Cross-sections which deviate from the Circular Shape (in German)
IMechE 1992, Paper 925101

14.43 **Phlips, P, A. Schamel, J. Meyer (1989)**
An efficient Model for Valvetrain and Spring Dynamics
Transactions SAE 1989

14.44 **Phlips, P, and A. Schamel (1991)**
The Dynamics of Valvetrains with Hydraulic Lash Adjusters and the Interaction with the Gas Exchange Process
SAE Technical Paper 910071

14.45 **Pisano, A.P., F. Freudenstein (1983a)**
An Experimental and Analytical Investigation of the Response of a High-Speed Cam-Follower System. Part 1: Experimental Investigation
Journal of Mechanisms, Transmissions, and Automation in Design Vol 105/692

14.46 **Pisano, A.P., F. Freudenstein (1983b)**
An Experimental and Analytical Investigation of the Response of a High-Speed Cam-Follower System. Part 2: A Combined, Lumped/Distributed Parameter Dynamic Model
Journal of Mechanisms, Transmissions, and Automation in Design Vol 105/699

14.47 **Porot, P, J. Trapy (1993)**
A Numerical and Experimental Study of the Effect of Aeration of Oil on Valve Trains Equipped with Hydraulic Lash Adjusters
SAE Technical Paper 930997

14.48 **Press, William H., B.P. Flannery, S.A. Teukolsky, W.T. Vetterling (1990)**
Numerical Recipes, The Art of Scientific Computing
Cambridge University Press, Cambridge

14.49 **Priebsch, HH, W Hellinger, K Landfahrer, U. Mayerhofer (1992)**
Valve train dynamics and their contribution to engine performance
IMechE 1992, Paper 925101

14.50 **Saito, Y, Y. Miyamae and F. Tamura (1991)**
Analysis of Characteristics on Hydraulic Lash Adjuster
JSAE Vol 45 No. 12, 1991

14.51 **Schamel, Andreas (1987)**
Development of a Program for the Design and Optimization of Cam Lift Profiles under given Boundary Conditions (in German)
Final thesis for the degree of a Dipl. Ing. (FH), Fachhochschule Cologne

14.52 **Schamel, A, J. Meyer, P. Phlips (1988a)**
Numerical Simulation of the Dynamic Behaviour of Modern Valvetrains (in German)
VDI Conference on CAE methods in Automotive Engineering, Würzburg, Paper Nr 699, October 1988

14.53 **Schamel, A, J. Meyer, P. Phlips (1988b)**
Simulation of Valvetrain Dynamics
Ford International Technical Exchange, Detroit, Oktober 1988

14.54 **Schamel, A. (1991)**
Development of a Mathematical Model for the Dynamics of Nonlinear Valve Springs
Final thesis for the degree of a Master of Science, Loughborough University of Technology, June 1991

14.55 **Schamel, A. and J. Meyer (1992)**
The efficient application of ADAMS to the Simulation of Valvetrain Dynamics
Paper for the 1992 International ADAMS User Conference, Ypsilanti, Michigan

14.56 **Schamel, A., J. Hammacher, D. Utsch (1993)**
Modelling and Measurement Techniques for Valve Spring Dynamics in High Revving Internal Combustion Engines
SAE Technical Paper 930615

14.57 **Scherdel (1987)**
Federfibel
Scherdel GmbH 1987

14.58 **Seidlitz, Steve (1990)**
An Optimization Approach to Valve Train Design
SAE Technical Paper 901638

14.59 **Tümer, Turgut (after 1986)**
Nondimensional Analysis of Jump Phenomenon in Force-closed Cam Mechanisms
Mechnical Engineering Department, King Saud University, Saudi Arabia

14.60 **Wahl, A.M. (1963)**
Mechanical Springs
McGraw-Hill (1963)

14.61 **Yano, H and J. Yabumoto (1990)**
The Behaviour of Entrained Gas Bubbles in Engine Oil and the Development of Effective Gas-Oil Seperators
SAE Technical Paper 900812

15

Appendix

15.1 Table of Symbols

ψ	spring particle displacement
x	position along the spring
t	time
c	speed of wave propagation in the spring
L	spring length
k	active spring stiffness
m	mass of the active part of the spring
h	dynamic valve lift
F_0	spring preload
S	spring pre-compression in installed position
F	spring force
μ	dynamic deviation from static spring particle displacement
M	spatial component of spring particle displacement
ω	natural frequency of the spring in radians/sec
f	natural frequency of the spring in Hz
n	spring mode number
G	time component of the spring particle displacement
ω_{cs}	camshaft rotational frequency
φ	cam angle
m_i	i'th mass of discrete spring model
h_i	dynamic displacement of i'th mass
d_i	dynamic deviation displacement of i'th mass
s_i	kinematic displacement of i'th mass
c_i	viscous damping coefficient between mass *i* and *i-1*
k_i	stiffness between mass *i* and *i-1*
X_i	border deformation between mass *i* and *i-1* when clash force becomes active
F_{cl}	clash force between two spring masses
F_{cle}	elastic component of the clash force
F_{cld}	damping component of the clash force
N	number of spring coils
$\bar{r}$	mean coil radius of the spring
V	volume of spring material
A	sectional area of the spring wire
ρ	density of the spring material
G	shear modulus of the spring material
I_t	torsional moment of inertia
α	pitch angle
T	thickness of the spring wire
L_s	solid length of the spring

15.2 Full factorial experiments

In Section 9 of this thesis, statistical methods have been used to analyse the influence of the various parameters which describe the springs frequency against lift characteristic. Although the parameters being used are artificial spline parameters, the majority of them relates directly to the spring properties. Table 10 gives the list of these parameters and the corresponding labels used. In classical testing, these parameters could now be modified at several levels in a strategic manner, one at a time, to investigate all responses for all parameter levels. But if this is done for say 4 levels of each parameter, there are $4^6 = 4096$ parameter combinations which need to be tested. For real testing this would clearly be impossible.

Parameter	Physical Meaning	Label	Level 1	Level 2
f_2	Frequency at valve open position	A	750	1000
df/ds_1	Slope of frequency characteristic at 0mm valve lift	B	0	100
df/ds_2	Slope of frequency characteristic at max (10 mm) valve lift	C	25	200
Rf_1	Relative length of tangent vector at 0mm valve lift	D	0.5	2.0
Rf_2	Relative length of tangent vector at max valve lift	E	0.5	2.0
Cam 1/Cam 2	Cam profile used as excitation	F	Cam 1	Cam 2

Table 10

In the present case, the applied "test" is a computer program used to calculate the spring response corresponding to a given frequency characteristic. In this case performing all tests would not be impossible, since a single "test" only requires approximately 2 minutes cpu time, resulting in about 6 days cpu. Although this is not impossible, it would not be advisable. Furthermore the required time for the necessary analysis of the resulting amount of data would be extremely large. From publications about statistical methods (Gordon 1989) it is known that useful information can already be obtained from substantially smaller test programs. In contrast to varying the parameters at four levels, a two level experiment reduces the number of combinations down to $2^6 = 64$. For a real test, this would most probably still be too many, but for the computer experiment carried out in this work, it results in about 2 hours cpu time, and the analysis stays also in reasonable bounds. Thus any further reduction by means of a fractional factorial design is not required.

Varying each parameter at two levels can be denoted as a -1 (level 1) and a +1 (level 2) level for each of the parameters. If this is done in an orderly pattern for all parameter combinations we get the design matrix for the problem. In Table 11 this design matrix is given for the subset A to E of the parameters. In a real test one would have to randomise the order in which the tests are done, to prevent a systematical influence of test variations. In a computer experiment this is not necessary. So in this case the run number can be directly linked to the parameter combination. In the present case, the binary representation of the run number allows to identify the parameter combination used. Thus each row in Table 11 stands for one run and has results in all 13 performance figures defined in Section 9 associated with it. Table 3 and 4 gave these results and the corresponding parameter levels. The results have already been discussed in the main body of the thesis. At this place a short description shall be given how the effects of the parameters can be calculated.

The statistical model forming the basis of this investigation is

$$P_{1,..,13_{ijklm}} = \begin{array}{c} \mu + A_i + B_j + C_k + D_l + E_m + \\ (AB)_{ij} + (AC)_{ik} + \ldots\ldots + \\ (ABC)_{ijk} + \ldots.(ABCD)_{ijkl} + \ldots.. + (ABCDE)_{ijklm} \end{array} \qquad /15.2.1/$$

where μ is the mean, A,B,C,D,E are the main effects, AB, BC ..., are the second order interactions and so on up to the 5th-order interactions. Since the computer experiment is a full factorial there are no confounding effects for the interactions. Because of the simple linear nature of this statistical model, the resulting effects can be easily calculated from the contrast coefficients given in Table 11. For every column we can multiply the contrast coefficient (+ or -1) with the corresponding result for each of the performance measures ($P_{1\ to\ 13}$) separately and add the results up. This gives for each of the parameters and parameter interactions the effect of changing this parameter from level 1 (-1) to level 2 (+1).

Plotting these effects then against normal scores (normal probability plot) shows which of the parameters and parameter interactions are important since the most important ones will stand out at the left and right of the plot and should deviate substantially from an imagined straight line drawn through the majority of the effects. The underlying assumption is, that parameters with no or a small effect only cause random variations in the results what under ideal circumstances would put them on a straight line.

I	*A*	*B*	*C*	*D*	*E*	*AB*	*AC*	*AD*	*AE*	*BC*	*BD*	*BE*	*CD*	*CE*	*DE*	*ABC*	*ABD*	*ABE*	*ACD*	*ACE*	*ADE*	*BCD*	*BCE*	*BDE*	*CDE*	*ABCD*	*ABCE*	*ABDE*	*ACDE*	*BCDE*	*ABCDE*	RUN
1	-1	-1	-1	-1	-1	1	1	1	1	1	1	1	1	1	1	-1	-1	-1	-1	-1	-1	-1	-1	-1	-1	1	1	1	1	1	-1	0
1	1	-1	-1	-1	-1	-1	-1	-1	-1	1	1	1	1	1	1	1	1	1	1	1	1	-1	-1	-1	-1	-1	-1	-1	-1	1	1	1
1	-1	1	-1	-1	-1	-1	1	1	1	-1	-1	-1	1	1	1	1	1	1	-1	-1	-1	1	1	1	-1	-1	-1	-1	1	-1	1	2
1	1	1	-1	-1	-1	1	-1	-1	-1	-1	-1	-1	1	1	1	-1	-1	-1	1	1	1	1	1	1	-1	1	1	1	-1	-1	-1	3
1	-1	-1	1	-1	-1	1	-1	1	1	-1	1	1	-1	-1	1	1	-1	-1	1	1	-1	1	1	-1	1	-1	-1	1	-1	-1	1	4
1	1	-1	1	-1	-1	-1	1	-1	-1	-1	1	1	-1	-1	1	-1	1	1	-1	-1	1	1	1	-1	1	1	1	-1	1	-1	-1	5
1	-1	1	1	-1	-1	-1	-1	1	1	1	-1	-1	-1	-1	1	-1	1	1	1	1	-1	-1	-1	1	1	1	1	-1	-1	1	-1	6
1	1	1	1	-1	-1	1	1	-1	-1	1	-1	-1	-1	-1	1	1	-1	-1	-1	-1	1	-1	-1	1	1	-1	-1	1	1	1	1	7
1	-1	-1	-1	1	-1	1	1	-1	1	1	-1	1	-1	1	-1	-1	1	-1	1	-1	1	1	-1	1	1	-1	1	-1	-1	-1	1	8
1	1	-1	-1	1	-1	-1	-1	1	-1	1	-1	1	-1	1	-1	1	-1	1	-1	1	-1	1	-1	1	1	1	-1	1	1	-1	-1	9
1	-1	1	-1	1	-1	-1	1	-1	1	-1	1	-1	-1	1	-1	1	-1	1	1	-1	1	-1	1	-1	1	1	-1	1	-1	1	-1	10
1	1	1	-1	1	-1	1	-1	1	-1	-1	1	-1	-1	1	-1	-1	1	-1	-1	1	-1	-1	1	-1	1	-1	1	-1	1	1	1	11
1	-1	-1	1	1	-1	1	-1	-1	1	-1	-1	1	1	-1	-1	1	1	-1	-1	1	1	-1	1	1	-1	1	-1	-1	1	1	-1	12
1	1	-1	1	1	-1	-1	1	1	-1	-1	-1	1	1	-1	-1	-1	-1	1	1	-1	-1	-1	1	1	-1	-1	1	1	-1	1	1	13
1	-1	1	1	1	-1	-1	-1	-1	1	1	1	-1	1	-1	-1	-1	-1	1	1	-1	1	1	-1	-1	-1	-1	1	1	1	-1	1	14
1	1	1	1	1	-1	1	1	1	-1	1	1	-1	1	-1	-1	1	1	-1	1	-1	-1	1	-1	-1	-1	1	-1	-1	-1	-1	-1	15
1	-1	-1	-1	-1	1	1	1	1	-1	1	1	-1	1	-1	-1	-1	-1	1	-1	1	1	-1	1	1	1	1	-1	-1	-1	-1	1	16
1	1	-1	-1	-1	1	-1	-1	-1	1	1	1	-1	1	-1	-1	1	1	-1	1	-1	-1	-1	1	1	1	-1	1	1	1	-1	-1	17
1	-1	1	-1	-1	1	-1	1	1	-1	-1	-1	1	1	-1	-1	1	1	-1	-1	1	1	1	-1	-1	1	-1	1	1	-1	1	-1	18
1	1	1	-1	-1	1	1	-1	-1	1	-1	-1	1	1	-1	-1	-1	-1	1	1	-1	-1	1	-1	-1	1	1	-1	-1	1	1	1	19
1	-1	-1	1	-1	1	1	-1	1	-1	-1	1	-1	-1	1	-1	1	-1	1	1	-1	1	1	-1	1	-1	-1	1	-1	1	1	-1	20
1	1	-1	1	-1	1	-1	1	-1	1	-1	1	-1	-1	1	-1	-1	1	-1	-1	1	-1	1	-1	1	-1	1	-1	1	-1	1	1	21
1	-1	1	1	-1	1	-1	-1	1	-1	1	-1	1	-1	1	-1	-1	1	-1	1	-1	1	-1	1	-1	1	-1	-1	1	-1	1	-1	22
1	1	1	1	-1	1	1	1	-1	1	1	-1	1	-1	1	-1	1	-1	1	-1	1	-1	-1	1	-1	-1	-1	1	-1	-1	-1	-1	23
1	-1	-1	-1	1	1	1	1	-1	-1	1	-1	-1	-1	-1	1	-1	1	1	1	1	-1	1	1	-1	-1	-1	-1	1	1	1	-1	24
1	1	-1	-1	1	1	-1	-1	1	1	1	-1	-1	-1	-1	1	1	-1	-1	-1	-1	1	1	1	-1	-1	1	1	-1	-1	1	1	25
1	-1	1	-1	1	1	-1	1	-1	-1	-1	1	1	-1	-1	1	1	-1	-1	1	1	-1	-1	-1	1	-1	1	1	-1	1	-1	1	26
1	1	1	-1	1	1	1	-1	1	1	-1	1	1	-1	-1	1	-1	1	1	-1	-1	1	-1	-1	1	-1	-1	-1	1	-1	-1	-1	27
1	-1	-1	1	1	1	1	-1	-1	-1	-1	-1	-1	1	1	1	1	1	1	-1	-1	-1	-1	-1	-1	1	1	1	1	-1	-1	1	28
1	1	-1	1	1	1	-1	1	1	1	-1	-1	-1	1	1	1	-1	-1	-1	1	1	1	-1	-1	-1	1	-1	-1	-1	1	-1	-1	29
1	-1	1	1	1	1	-1	-1	-1	-1	1	1	1	1	1	1	-1	-1	-1	-1	-1	-1	1	1	1	1	-1	-1	-1	-1	1	-1	30
1	1	1	1	1	1	1	1	1	1	1	1	1	1	1	1	1	1	1	1	1	1	1	1	1	1	1	1	1	1	1	1	31

Table 11: Experiment design matrix for a full factorial in A,B,C,D,E

15.3 Program Modules

This section presents a brief overview and a short explanation of the key software modules used for the study presented in this thesis. Discussing the programs in any detail would be beyond the scope of this thesis because of the total size and complexity of the involved Fortran code. Figure 80 shows a sketch mentioning the main program modules and how they are linked together. The following list summarises the modules in sequential order where possible.

Pspring and CLASH

These two modules handle the discrete spring model. Input to these programs is the spring design information, as forces at installed and valve open height, length for free, installed, valve open and solid height. Wire dimensions and properties and coiling information.

CLASH uses this information to build a discrete description of the spring. This description is then combined with a generic valvetrain dynamics model. Generic valvetrain models are available for different types of valvetrains, as pushrod, finger follower, bucket tappet and so on. Output of this program is a valvetrain dynamics model specific for the spring design supplied to the program. Further output is a debug file which contains important information on the resulting spring model. The resolution of the model (i.e. the number of masses used) can be modified by the user.

Pspring does the same model set-up, but then uses the model to simulate a static compression of this model. In 20 steps from installed to valve open length, the spring model is compressed and an eigenvalue analysis is performed at each length to determine the frequency of the fundamental spring surge mode. This data is then output as a function of spring length, together with the spring forces and the coil numbers for the boundary of the active coils.

findpar

The program *findpar* uses the output from *Pspring* and establishes a parameterized description of the data. For the force and boundary data a polynomial description is used, while the springs frequency characteristic is represented by parametric splines. The coefficients for the polynomial fits can be calculated directly for a minimum error since the difference between the fit and the given data depends linear on the polynomial coefficient (Numerical Recipes, Press *et al* 1990). For the parametric splines an

optimization algorithm has been employed which automatically restarts until a sufficient accuracy for the fit is reached. The fit data is then output to a file which is used by three other modules (*ADAMS User subs, spring, OPTspring*).

ADAMS

ADAMS is a commercial code (Automatic Dynamic Analysis of Mechanical Systems) for rigid body dynamics. It is mainly used as a robust integrator for the strongly non-linear valvetrain models. For valvetrain specific features as the excitation, behaviour of hydraulic elements and complex kinematics a set of user written subroutines (*User Subs*) is linked to the package. This subroutine package also performs the calculation of the springs initial conditions according to the described Fourier approach for time variant problems. For this purposes the package uses the output from *findpar*. Output from *ADAMS* are time domain results which can be analysed in the *ADAMS* post-processor.
For the purpose of this study an interface has been written (*dynacc*), which transforms the time domain results for the dynamic valve acceleration into a set of Fourier coefficients for each speed. This can then either be used for the spring optimization program (*OPTspring*) or the stand alone spring analysis (*spring*).

spring

spring is the stand-alone analysis program for the dynamic spring surge response over engine speed, using the Fourier approach for time variant problems. The input required is the parameterised spring description from *findpar* and either the dynamic excitation from *dynacc* or kinematic valve lift data.
A special version of this program, which also included a subroutine to calculate the defined performance figures has been used for the statistical experiment.

OPTspring

This is the core spring optimization program. The evaluation of the spring response is done as in *spring*. Further required inputs are the weighting factors for the target function and the constraints, an initial description as a start point from *findpar*, a kinematic valve lift profile, and optionally dynamic valve acceleration data supplied by *dynacc*. Main output, beside several output files to monitor and analyse the optimization progress, is the frequency and force characteristic of the optimization result.

findDd

This module is a small routine to find the right wire diameter and coiling diameter for a cylindrical helical round wire spring for a given frequency, rate and number of active coils at installed length.

findPITCH

In *findPITCH* a previously described optimization strategy is used to establish the right pitch spacing and free length for a spring with the wire diameter and coiling diameter established by *findDd* and the frequency characteristic supplied by *OPTspring*. The main working subroutine of the program is very similar to *Pspring* but an analytical way to calculate the spring frequency is used for the special case of a cylindrical spring instead of the more generic eigenvalue analysis used in *Pspring*. Output of the program is all data needed to create a spring drawing for manufacturing purpose.

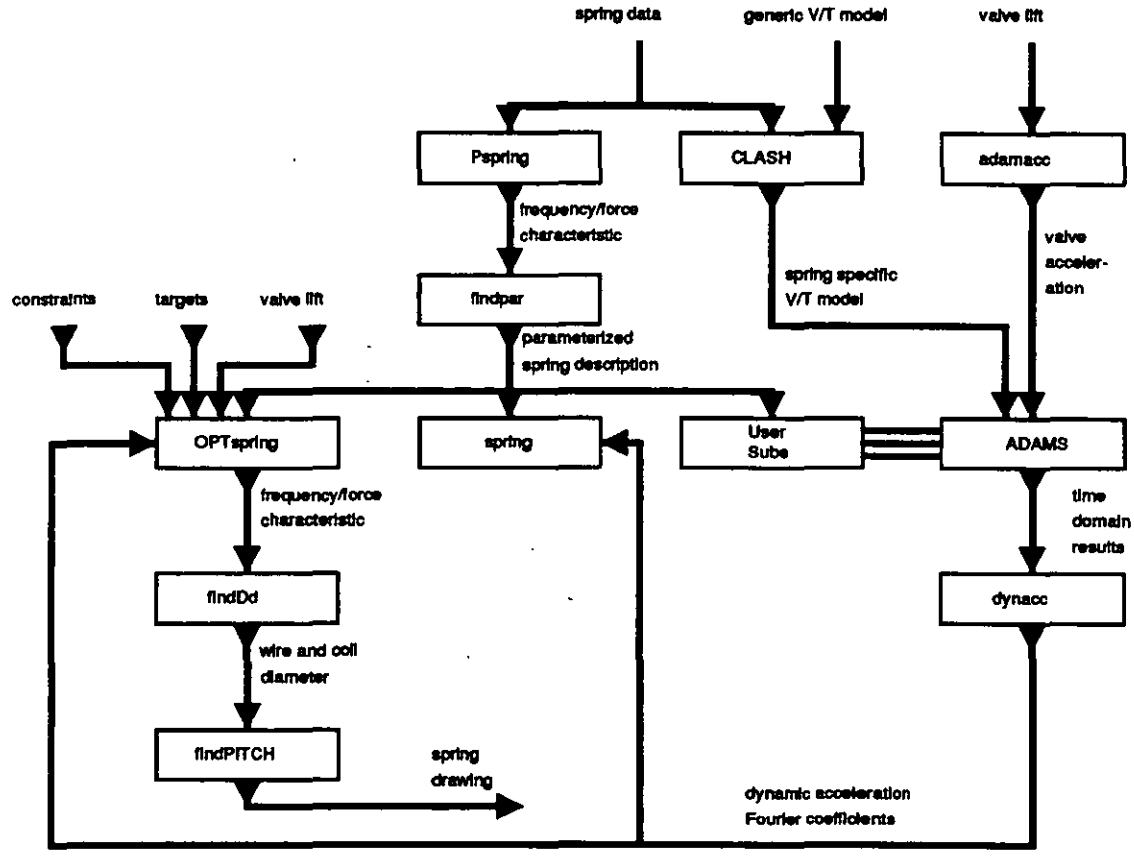

Figure 80: Sketch of the key program modules used for the CAE studies